Regulation of the redox homeostasis during polyglutamine misfolding in Huntington's Disease

by

Muhammad Umar Sajjad BSc (Hons)

A thesis presented for the degree of
Doctor of Philosophy
of the
University of Southampton
in the
Faculty of Medicine, Health and Life Sciences
School of Biological Sciences

September 2010

UNIVERSITY OF SOUTHAMPTON

ABSTRACT

FACULTY OF MEDICINE AND LIFE SCIENCES

Doctor of Philosophy

Regulation of the redox homeostasis during polyglutamine protein misfolding in Huntington's Disease

Huntington's Disease (HD) is one of many neurodegenerative diseases that are associated with protein misfolding, aggregation and oxidative stress. While several changes in the redox homeostasis have been shown to occur in HD animal models and HD brains, the formal relationships between intracellular protein misfolding that occurs in HD, redox dysregulation and cellular toxicity are unknown. Therefore, several cellular models of intracellular polyglutamine (polyQ) protein misfolding were established for mechanistic studies.

Various *in vitro* transient and stable cell expression systems expressing an N-terminal fragment of huntingtin (htt) (httExon 1, httEx1) with/or without a polyQ expansion and fused to fluorescent proteins were characterized. Mutant httEx1 (mhttEx1) constructs expressed in both neuronal and non-neuronal cell lines produced early polyQ aggregates and intracellular inclusion bodies (IBs) followed by cell toxicity that increased over time in time-course experiments. Using oxidation-sensitive probes, reactive oxygen species (ROS) were measured in polyQ-expressing cells using single, live-cell imaging analysis by confocal microscopy or population assays in order to explore the relationship between polyQ aggregation, ROS production and cellular toxicity. This study highlighted an early increase in ROS due to the expression of aggregation-prone mhttEx1 in both transient and stable cellular systems that coincided with polyQ aggregation, but preceded cell death. Suppression of ROS and toxicity was achieved by two antioxidant compounds (L-NAC and Trolox). Moreover, the use of MitoQ (Coenzyme Q10 covalently attached to triphenylphosphonium cation (TPP^+)) at nanomolar concentrations abrogated the increased ROS due to mhttEx1 suggesting a mitochondrial origin of ROS.

Given that molecular chaperones regulate the folding/misfolding of proteins and are involved in the regulation of the cellular redox homeostasis, the role of the redox-activatable chaperone DJ-1 in HD was investigated. Protein expression analysis in HD cell models, a rodent model of HD and human HD brain samples showed an up-regulation of DJ-1 protein expression compared to control samples. Oxidation of DJ-1 was also elevated in the human HD cortex. To test for a functional role of DJ-1 elevation and oxidation in HD, DJ-1 was overexpressed with wild-type or mhttEx1 in cell lines and mouse primary astrocytes. Overexpression of DJ-1 accelerated mhttEx1 aggregation and toxicity both of which could be suppressed by exposure of cells to mild oxidants suggesting that DJ-1, when redox-activated to a chaperone, modulates polyQ aggregation and toxicity. This hypothesis was tested by overexpression of mhttEx1 with a DJ-1 mutant lacking a critical redox activatable cysteine (Cys106). The C106S-DJ-1 mutant lost its ability to reduce polyQ aggregation and toxicity under oxidising conditions upon co-expression with mhttEx1 suggesting that DJ-1 indeed functions as a modulator of polyQ misfolding and toxicity.

Together this work suggests that ROS may be produced during polyQ aggregation and is involved in cellular toxicity. This study also shows that DJ-1 regulates both, polyQ aggregation and toxicity in cell models and given the increased DJ-1 expression *in vitro* and *in vivo* (human HD), this protein could be a potential target for HD therapy.

Contents

Declaration of Authorship

I, Muhammad Umar Sajjad declare that the thesis entitled “Regulation of the redox homeostasis during polyglutamine protein misfolding in Huntington’s Disease” and the work presented in the thesis are both my own, and have been generated by me as the result of my own original research. I confirm that:

this work was done wholly or mainly while in candidature for research degree at this University;

where any part of this thesis has previously been submitted for a degree or any other qualification at this University or any other institution, this has been clearly stated;

where I have consulted the published work of others, this is always clearly attributed;

where I have quoted from the work of others, the source is always given. With the exception of such quotations, this thesis is entirely my own work;

I have acknowledged all main sources of help;

where the thesis is based on work done by myself jointly with others, I have made what was done by others and what I have contributed myself.

Signed……..

Date ……

Acknowledgements

I deeply express gratitude to my supervisor Dr. Andreas Wyttenbach for being supportive and helpful during the last four years.

I would like to thank Dr. S. Hands for her continuous help and advice in the lab during the first three years of this project.

I would also like to thank Dr. V. O'Conner for advice and critical feedback, Dr. Rich Edward for helping me with computer programming and Dr. Hans Schuppe for confocal microscopy troubleshooting.

I would like to thank Dr. Shmma Quraishe (University of Southampton, UK) and Prof. Jennifer Morton (University of Cambridge, UK) for providing R6/2 mouse tissue samples and Dr. Lesley Jones (University of Cardiff, UK) and Dr. Richard Faull (University of Auckland, NZ) for the kind provision of human HD brain samples. Thanks also go to Neville Wright with help on the mass spectrometry and Prof. G. Bates (King's College, London) for providing S830 antibody and Dr Mike Murphy and Antipodean Pharmaceuticals, Inc (Auckland, NZ) for the provision of MitoQ.

I would like to thank Dr. Farida Hafiz for emotional support during difficult times.

I am grateful to the Gerald Kerkut Charitable Trust who provided most of the funding for this PhD and also to the School of Biological Sciences and the BestWay Foundation for some financial contribution. I would also like to thank my parents for their financial support toward this project.

I would like to thank Ben Samson for proof reading my thesis and his friendship and my colleagues from the School of Biological Sciences for being helpful and sociable.

I would like to especially thank my parents and siblings for their continuous support, love and encouragement during the last seven years.

Finally, I would like to dedicate this thesis to my parents.

Abbreviations

Aß	Amyloid beta
ABC	αB-crystallin
AD	Alzheimer's disease
AFM	atomic force microscopy
ALS	Amyotrophic Lateral Sclerosis
ANOVA	analysis of variance
APOE	apolipoprotein E
APS	ammonium persulphate
ASK1	apoptosis signal-regulating kinase
ATM/ATR	ataxia-telangiectasia mutated/ ataxia-telangiectasia and Rad3 related
ATP	adenosine triphosphate
BDNF	brain derived neurotrophic factor
BSA	bovine serum albumin
BSE	bovine spongiform encephalopath
CBD	Corticobasal degeneration
CBP	CREB-binding protein
CJD	Creutzfeldt–Jakob disease
CMA	chaperone mediated autophagy
CM-H2DCFDA	5-(and-6)-chloromethyl-2',7'-dichlorodihydrofluorescein diacetate, acetyl ester
CPE	cytopathic effect
CREB	cAMP- responsive element binding protein
CSF	cerebrospinal fluid
CSP	cysteine string protein
CsCl	Caesium chloride
Cu	copper
Cyt.*C*	cytochrome *c*
Da	Dalton
DAPI	4',6-diamidino-2-phenylindole
DHE	dihydroethidium
DMEM	Dulbecco's modified Eagle's medium
DNA	deoxyribonucleic acid
DNPH	dinitrophenylhydrazine
DRPLA	Dentatorubral-Pallidolusian Atrophy
E.coli	*Escherichia coli*
EAAC1	glutamate transporter
ECL	enhanced chemiluminescence
EDTA	ethylene-diamine-tetra-acetate
EGFP	enhanced green fluorescent protein
EOFAD	Early-Onset Familial Alzheimer disease
ER	endoplasmic reticulum
ERK	extracellular signal regulated kinase
ERRα	estrogen-related receptors alpha
ETC	electron transport chain
EV	empty vector

FAD	Familial Alzheimer disease
FALS	Familial Amyotrophic Lateral Sclerosis
FBS	fetal bovine serum
FCCP	carbonyl cyanide 4-(trifluoromethoxy) phenylhydrazone
FL-htt	full length huntingtin
FTD	Frontotemporal Dementia
FTDP	Frontotemporal Dementia with Parkinsonism
GAPDH	Glyceraldehyde 3-phosphate dehydrogenase
GAT	glutamine amidotransferase
GFAP	glial fibrillary acidic protein
GPx1	Glutathione peroxidise-1
GSH	glutathione
HAP1	huntingtin associated protein-1
HBSS	Hank's Buffer Salt solution
HD	Huntington's disease
HDAC	histone deacetylase
HEPES	4-(2-hydroxyethyl)-1-piperazineethanesulfonic acid
HIF	Hypoxia inducible factor
HIP1	huntingtin interacting protein-1
hOGG1	human 8-hydroxyguanine DNA-glycosylase
HRP	horseradish peroxidase
Htt	huntingtin
HttEx1	huntingtin exon1
Htt^{NT}	N-terminal htt domain
HSPs	heat shock proteins
IBs	Inclusion bodies
ICC	immunocytochemistry
i.d.	inner diameter
I*kB*	inhibitory kappa B
IKK	I*k*B kinase
$InsP_3R1$	inositol 1,4,5-trisphosphate receptor type 1
JNK	c-Jun N-terminal kinase (JNK)
L-NAC	N-acetyl-L-cysteine
L-NAME	L-nitro-arginine methyl ester
MAPK	mitogen-activated protein kinase
MAPKKK	mitogen-activated protein kinase kinase kinase
MEKK1	mitogen-activated protein kinase/extracellular signal-regulated kinase kinase kinase 1
Mfn	mitofusin
mGluR5	metabotropic glutamate receptor 5
Mhtt	mutant huntingtin
Mn	manganese
MOI	multiplicity of infection
MPTP	1-methyl-4-phenyl-1,2,3,6-tetrahydropyridine
mRFP	monomeric red fluorescent protein
mRNA	messenger ribonucleic acid
MSA	Multiple System Atrophy
MSNs	medium spiny neurons
mTOR	mammalian target of rapamycin

MTS	tetrazolium compound 3-4, 5-dimethylthiazol-2-yl-5-3-carboxymethoxyphenyl-2-4-sulfophenyl-2H-tetrazolium
NA	Nuclear abnormality
NADPH	nicotinamide adenine dinucleotide phosphate
NF-*k*B	Nuclear factor kappa B
NFTs	neurofibrillary tangles
NGF	nerve growth factor
NMDA	N-methyl-D-aspartate
NMDAR	N-methyl-D-aspartate receptor
NMR	Nuclear magnetic resonance
NO	nitric oxide
NOS	nitric oxide synthase
NP-40	Tergitol-type NP-40
NRF	nuclear respiratory factor
NRF-2	nuclear factor erythroid 2-related factor-2
NTs	neuropil threads
o.d.	outer diameter
OH8dG	8-hydroxy-2-deoxyguanosine
PBS	phosphate buffer saline
PD	Parkinson's Disease
PDI	protein disulfide isomerase
PET	Positron emission tomography
PFU	plaque-forming unit
PGC-1α	Peroxisome proliferator-activated receptor gamma coactivator 1-alpha
PiD	Picks disease
PI3K	phosphotidyl inositol 3-kinase
PMS	phenazine methosulphate
PolyQ	polyglutamine
PPARγ	Peroxisome proliferator-activated receptor gamma
PRNP	prion protein gene
PrP^{c}	normal cellular prion
PrP^{sc}	scrapie prion
PS-1	presenilin-1
PS-2	presenilin-2
PSA	puromycin sensitive amino-peptidase
PSD 95	postsynaptic density 95
PSP	Progressive Supranuclear Palsy
PYDH	pyruvate dehydrogenase
REST-NRSF	repressor element silencing transcription factor/neuron-restrictive silencing factor
RILP	REST-interacting LIM-domain protein
RBS	reactive bromide species
RCS	reactive chloride species
RNS	reactive nitrogen species
ROS	reactive oxygen species
SARKs	stress activated protein kinases
SBMA	Spinal and Bulbar Muscular Atrophy
SCA	Spinocerebellar ataxia
SDH	succinate dehydrogenase

SDS	sodium dodecyl sulphate
SDS-PAGE	SDS polyacrylamide gel electrophoresis
SNPS	single nucleotide polymorphisms
SOD	superoxide dismutase
SOH	sulfenic acid
SO_2H	sulfinic acid
SO_3H	sulfonic acid
SP-1	specificity protein-1
TAE	tris acetate EDTA
TBP	TATA binding protein
TBS	tris buffered saline
TCA	Tricarboxylic acid
TCID50	tissue culture infectious dose 50
TEMED	N, N, N, N-tetramethyl-ethylenediamine
Tfam	mitochondrial transcriptional factor
Tg	transgenic
thttEx1	truncated httEx1
TNF	tumour necrosis factor
Trx	thioredoxin
UCH-L1	ubiquitin carboxy-terminal hydrolase L1
UCP	uncoupling proteins
UPS	ubiquitin-proteasome system
TPP^+	triphenylphosphonium cation
Wt	wild-type
YAC	yeast artificial chromosome
Zn	Zinc

1 Introduction

1.1 Neurodegeneration is associated with protein misfolding

Neurodegeneration is the process by which neurons lose their structure and function and eventually die. There are a number of chronic diseases presenting with neuronal degeneration associated with protein misfolding and aggregation, also known as the "proteinopathies". The most commonly studied proteinopathies are Alzheimer's Disease (AD), Parkinson's Disease (PD), Amyotrophic Lateral Sclerosis (ALS), the prion disorders and the polyglutamine (polyQ) diseases (Cleveland and Rothstein, 2001; Kremer et al., 1990; Li and Li, 2004a; Mead, 2006; Prusiner, 1982; Ross and Poirier, 2004; Saper, 1999; Wenk, 2003). Below, the genetic aspects and some common pathological mechanisms of these proteinopathies, mainly in relation to protein aggregation and the occurrence of oxidative stress, are briefly introduced.

1.1.1 Alzheimer's Disease (AD)

AD is a progressive neurodegenerative disease and is classified into two major types, a common sporadic form and a group of rare familial forms of AD (FAD). FAD follows an autosomal dominant mode of inheritance. Mutations in several genes (APP, Presenilin-1 and Presenilin-2) are likely to be the cause of FAD (see Table 1.1). Genetic studies revealed that the APOE type-4 allele (ε4) is a key susceptibility factor for late onset FAD and sporadic AD (Jellinger, 2006). APOE encodes for a protein called apolipoprotein E (Table 1.1). The clinical symptoms of AD are memory loss, likely due to synaptic dysfunction, and impairment in cognitive domains that interfere with mood, reason and judgment (Laferla and Oddo, 2005). AD dementia progresses with time and the risk of suffering from it doubles every five years after the age of 65 (Jorm et al., 1987).

AD is characterized by the deposition of extracellular amyloid plaques and intracellular neurofibrillary tangles. Amyloid plaques are dense, round extracellular deposits. These deposits mainly consist of Amyloid beta (Aβ) peptides and these accumulates are found in the AD patient limbic brain regions and also in the cortical and subcortical areas (Laferla and Oddo, 2005). A genetic study revealed that Aβ-deposition is likely an

upstream, perhaps causative factor of AD compared to other genes (PS-1 and PS-2) involved in FAD and also regulates Aβ-metabolism (Scheuner et al., 1996).

Neurofibrillary tangles are intracellular aggregates and are composed of a hyperphosphorylated form of the microtubule-associated protein, tau (Grundke-Iqbal et al., 1986). Tau promotes microtubule assembly and stabilization (Lee and Rook, 1992). In pathological circumstances, tau's solubility is changed and it forms filamentous intracellular tangles due to abnormally hyperphosphorylated amino acid residues at many sites, including Ser202, Thr205, Ser231, Ser396 and Ser404 (Laferla and Oddo, 2005). These tangles are found within neuronal cell bodies. De et al., (2003) revealed that such intracellular protein aggregates are also found in other neurodegenerative disorders, for instance, Frontotemporal Dementia with Parkinsonism linked to chromosome-17 (FTDP-17), Picks disease, Progressive Supranuclear Palsy (PSP) and corticobasal degeneration (CBD). Interestingly, studies of animal models of AD showed a significant increase in oxidative damage to lipids, proteins and DNA within various brain regions (Manczak et al., 2006; Pratico et al., 2001; Smith et al., 1998). Post-mortem AD brain tissue also showed higher levels of isoprostanes in AD patients compared to control groups (Pratico et al., 1998). More recently, Bonda et al., (2010) asserted that there is a high level of lipid peroxidation, nitration, reactive carbonyls and nucleic acid oxidation in vulnerable neurons in AD. Hence AD is characterised by intra- and extracellular protein aggregation with a likely progressive dysfunction of the cellular redox homeostasis. Caspersen et al., (2005) showed that soluble Aβ is localised within mitochondria and associated with mitochondrial dysfunctions such as a decrease in oxygen consumption and impaired complex III and IV activities in a mouse model of AD. It has also been shown that Aβ oligomers were associated with the inner mitochondrial membrane and several mitochondrial alterations (Manczak et al., 2006). Many studies have investigated the role of Aβ aggregation and oxidative stress in cell models by mainly exposing either cell lines or primary cells to different forms of Aβ, or overexpressing Aβ or tau (Cente et al., 2006; Kadowaki et al., 2005; Li et al., 2008). These studies suggested that Aβ or tau are primary sources of ROS that leads to cellular toxicity. In addition to this, a study showed that H_2O_2 can directly be produced during the early stages of protein aggregation of amyloid peptides (Tabner et al., 2005). Hence there could be an association between protein aggregation and oxidative stress.

Table 1.1 Genes involved in the pathogenesis of AD and their encoded proteins with their function.

Locus	Genes with identified Mutations	Chromosomal Locus	Protein	Functions	Symptom	Age of onset
AD1 Early- onset Familial AD	APP 12 mutations	21q21	Amyloid beta A4 protein	Trans-membrane protein with unknown functions	Dementia	50s
AD2 Late- onset Familial AD	APOE	19q13.2	Apolipoprotein E	Cholesterol transportation, storage and metabolism.	Dementia	60s and older
AD3 (EOFAD)	PSEN-1 69 mutations	14q24.3	Presenilin-1	γ-secretase activity, cleaving the trans-membrane domain of APP after alpha and beta secretase cleavage occurs.	Dementia	Between 40s-50s
AD4 (EOFAD)	PSEN-2 5 mutations	1q31-q42	Presenilin-2	Aβ production and Notch signalling.	Dementia	50s

1.1.2 Parkinson's Disease (PD)

The pathological hallmark of PD is the production of intracytoplasmic proteinaceous inclusions called the Lewy bodies (Olanow et al., 2004). Clinically, patients with PD show cardinal symptoms of bradykinesia, postural instability, resting tremor and rigidity. Some PD patients also suffer from autonomic, cognitive and psychiatric disturbances. Symptoms in PD patients appear due to a significant loss of dopaminergic neurons in the substantia nigra pars compacta as a result of insufficient formation of dopamine to perform normal body functions (Fearnley and Lees, 1991; Hefti et al., 1980). The classical symptomatic pattern of PD starts with tremors, proceeds to muscle stiffness and rigidity followed by slowness and facial impassivity which then leads to balance and gait abnormalities. Genetic studies of PD highlight mutations in many genes (Table 1.2) which participate in the disease pathogenesis. In PD patients, there is compelling evidence for oxidative damage to different macromolecules, such as lipids and proteins (Alam et al., 1997a; Floor and Wetzel, 1998) and DNA (Alam et al., 1997b; Bogdanov et al., 2008; Zhang et al., 1999). Various studies showed a selective deficiency of mitochondrial complex I activity in the substantia nigra and peripheral tissue in PD patients compared to control groups (Mizuno et al., 1989; Schapira et al., 1989). In addition to this Beal et al., (2005) reviewed that mitochondrial dysfunction in PD leads to impaired ATP synthesis and causes an excess production of ROS. On the other hand, a neurotoxin (MPTP) mouse model and human PD patients showed an upregulation of the NADPH oxidase enzyme, which is a key source of ROS during inflammation (Wu et al., 2003). Furthermore, parkin and UCH-L1 (genes associated with FPD, see Table 1.2) are oxidatively and nitrosatively

modified and show decreased activity in PD (Choi et al., 2004; Chung et al., 2004; LaVoie et al., 2007; Yao et al., 2004). These alterations in parkin and UCH-L1 may contribute to the ubiquitin-proteasome system (UPS) dysfunction and, from there, result in the accumulation of damaged proteins that later form insoluble aggregates (Chung et al., 2004; Nishikawa et al., 2003; Yao et al., 2004). Hence oxidative and nitrosative stress and mitochondrial dysfunctions are likely to influence PD pathogenesis and protein aggregation has been suggested to be an initial factor that contributes to disease (reviewed in Beal, 2004; Chinta and Andersen, 2008; Ross and Poirier, 2004).

Table 1.2 Genes that cause FPD with associated phenotypes and pattern of inheritance (FPD, Familial Parkinson Disease; adapted from Beal, 2004; Chung et al., 2003; Moore et al., 2005).

Locus	Chromosome location	Gene	Inheritance pattern	Phenotype
PARK1 and PARK 4	4q21-q23	α-synuclein	Autosomal dominant	Early onset, dementia with Lewy body
PARK2	6q25.2-q27	Parkin	Autosomal recessive	Early onset with slow disease progression
PARK3	2p13	Unknown	Autosomal dominant and recessive	Classic PD and occasional dementia.
PARK 5	4p14	UCH-L1	Not clear yet	Classic PD
PARK 6	1p35-p36	PINK-1	Autosomal recessive	Early onset with slow disease progression
PARK 7	1p36	DJ-1	Autosomal recessive	Early onset with slow disease progression
PARK 8	12p11.2-q13.1	LRRK2	Autosomal dominant	Classic PD
PARK 10	1p32	Unknown	Not clear yet	Classic PD
PARK 11	2q36-q37	Unknown	Not clear yet	Classic PD
Unnamed	5q23.1-q23.3	Synphilin-1	Unclear	Classic PD
Unnamed	2q22-q23	NR4A2	Unclear	Classic PD

1.1.3 Amyotrophic Lateral Sclerosis (ALS)

ALS is the most common type of motor neuron disorder. It is characterized by progressive degeneration of the spinal motor neurons (lower motor neurons, LMN) and pyramidal motor neurons (upper motor neurons) (Cleveland and Rothstein, 2001). ALS is a subtle disorder in that symptoms are regularly overlooked. Early-stage ALS symptoms are twitching, limb muscle weakness and slurred speech whilst the advanced-stage symptoms are muscle weakness that leads to muscular atrophy (Walling, 1999). ALS is classified into three variants: I) Pacific type ALS that is usually associated with dementia, II) Familial ALS that is primarily autosomal dominant in its inheritance, III) Classic sporadic ALS (Table 1.3). As in other proteinopathies, ALS pathogenesis is associated with oxidative and nitrosative stress

that has been suggested to lead to mitochondrial dysfunction (reviewed in Bossy-Wetzel et al., 2004; Goodall and Morrison, 2006) showed that more than 90 mutations occur in the Cu/Zn superoxide dismutase (SOD1) gene and are the cause of a subset (~25 %) of familial ALS (Zhang et al., 2007). SOD1 is an important antioxidant enzyme that protects neurons from oxidative damage. Cytoplasmic IBs containing mutant SOD1, ubiquitin and neurofilaments are hallmarks of familial ALS. Boillee et al., (2006) suggested that accumulation of mutant SOD1 into aggregates participates in cellular dysfunction by damaging mitochondria, proteasomes and chaperones. Individuals with ALS also show high levels of glutamate in the serum which implies a failure of astrocytes to sequester glutamate from extracellular fluids suggesting a possible role for excitotoxicity during neuronal degeneration. Hence, as in AD and PD, protein aggregation occurs in ALS and SOD-1 misfolding is thought to initiate FALS pathology (Bruijn et al., 1997). SOD1 is also localised in the IBs found in the spinal cords of sporadic ALS patients suggesting a possible role of SOD1 in the sporadic forms of ALS which accounts for 80-90% of all ALS cases (Chattopadhyay and Valentine, 2009).

Oxidative stress is considered to be one of the key factors of ALS pathology and mouse models of ALS presented with mitochondrial impairment associated with increased ROS production (Martin et al., 2007; Warita et al., 2001). Furthermore, oxidative damage to lipids (Shibata et al., 2001), proteins (Ferrante et al., 1997) and DNA (Fitzmaurice et al., 1996) has also been reported in the CNS of ALS patients.

Table 1.3 Classification and genetics of amyotrophic lateral sclerosis (ALS).
AD, autosomal dominant; AR, autosomal recessive (Majoor-Krakauer et al., 2003).

Classification	Gene	Chromosomal Location	Inheritance pattern
Major Genes			
ALS1	SOD1	21q22	AD/AR
ALS2	ALSin	2q33-34	AR
ALS3		Unknown	AD
ALS4		9q34	AD
ALS5		15q12-21	AR
ALS6		18q21	AD
FTDP	TAu	17q	AD
FTD		9q21-22	AD
Susceptibility genes			
Neurofilament heavy chain	NF-H	22q12.2	
Neurofilament light chain	NF-L	8p21	
Peripherin	PRPH	12q12-13	
Glutamate transporter	EAAT2	11p13-12	
Glutamate receptor	AMPA	5p33	
Apolipoprotein E	ApoE	19q13.2	
Ciliary neurotrophic factor	CNTF	11q12.2	
Debrisoquine hydroxylase	CYP2D	22q13.1	
Apurinic apyrimidinic endonuclease	APEX	14q11-12	
Mitochondrial DNA	COX	-	
Manganese superoxide dismutase	SOD2	6q25	
P2 blood group	P2	22q11	

1.1.4 The prion disorders

Prion related encephalopathies include bovine spongiform encephalopathy (BSE) in cattle, scrapie in sheep, Creutzfelt-Jakob disease (CJD), Gerstmann-Straussler-Scheinker syndrome and Kuru in humans and are fatal neurodegenerative disorders (Melo et al., 2007). These disorders are characterised both in human and animals by cerebral neuronal loss, astrocytic gliosis, microgliosis, spongiform changes, and abnormal prion protein production and deposition (Aguzzi and Polymenidou, 2004; Pamplona et al., 2008; Prusiner, 1998; Soto and Castilla, 2004). In humans, prion disorders can be acquired by exposure to environmental factors or through genetic mutations in the prion protein gene (PRNP) (Mead, 2006; Prusiner, 1982; Ross and Poirier, 2004). Normal cellular prion protein (PrP^{c}) is changed into the abnormal (scrapie) conformation of prion protein (PrP^{sc}) due to the presence of the PrP^{sc} form of the protein. PrP^{sc} is infectious (Prusiner, 1982) and present in the diseased brain. Like many major neurodegenerative diseases, the prion diseases are therefore associated with protein misfolding that leads to protein aggregation. Protein misfolding in prion diseases is somewhat analogous to AD in that it can be present

both intracellularly and extracellularly (Ma et al., 2002; Ma and Lindquist, 2002). It is known that neuronal death in prion disease occurs via the induction of apoptosis. There are a number of studies that suggest that full length PrP^{sc} is toxic and known to be involved in mitochondrial dysfunction, oxidative stress, activation of caspases and impaired protein trafficking (reviewed in Melo et al., 2007). Studies of toxic prion fragments (PrP106-126) in both *in vitro* and in primary cell culture both suggest the involvement of increased oxidative stress in pathology (Agostinho and Oliveira, 2003; Turnbull et al., 2003). Similarly, mouse models of prion disease exhibit oxidative stress leading to neuronal damage (Guentchev et al., 2000). Guentchev et al., (2002) also reported oxidative damage to nucleic acids in human CJD patient brains that correlated with disease progression. More recently, Pamplona et al., (2008) performed mass spectrometry analysis to quantify oxidative modifications (protein oxidation, glycoxidation and lipoxidation) in the brains of CJD patients and their analysis showed that PrP^{sc} is itself prone to oxidative modifications.

1.2 The polyglutamine disorders

There are, at least, nine neurodegenerative disorders caused by the expansion of an unstable CAG repeat, coding for glutamine residues, located within the protein encoding regions. All of these polyQ disorders follow an autosomal dominant mode of inheritance except SBMA, which is X-linked (reviewed in Ross, 2002). These disorders are characterized by selective neuronal cell death in particular regions of the brain (see below). The genes involved in these diseases are different, but all of them encode a polyQ stretch. In all of the polyQ disorders, there is a striking threshold effect of a minimal polyQ length to cause disease. The exact length is different in each disease but, generally, is in the range of 35 to 45 (see Table 1.4 for exact ranges). In all cases, mutant proteins seem to undergo a conformational change and aggregate inside the cell to form IBs. The role of IBs in polyQ pathogenesis is controversial (Arrasate et al., 2004; Saudou et al., 1998). As the main focus of my studies is HD, I will discuss this disorder in more detail below.

Table 1.4 PolyQ disorders with associated genes and normal functions of the encoded proteins (Riley and Orr, 2006; Tarlac and Storey, 2003; Truant et al., 2006)**.**

Disease/Gene locus/Protein	**Phenotype**	**Normal protein functions**	**Protein subcellular Location**	**Normal allele CAG repeat**	**Mutant allele CAG repeat**
Huntington's disease (HD) 4p16.3 Huntingtin (348 kDa)	Psychiatric, cognitive and motor abnormalities	Involved in cytoplasmic anchoring, clathrin mediated endocytosis, vesicular trafficking, postsynaptic signalling and neuronal transport.	Nuclear and cytoplasmic	6 - 34	36-121
Spinocerebellar ataxia type 1 (SCA-1) 6p22-23 Ataxin-1, (87 kDa)	Gait ataxia, dysarthria and bulbar dysfunction	Involved in the regulation of gene expression in the nucleus. It is also capable of nuclear export. But exact function is unknown.	Nuclear	8 - 44	39 - 83
Spinocerebellar ataxia type 2 (SCA-2) 12q23-24 Ataxin-2, (40-150kDa)	Ataxia	It is proposed that ataxin-2 is involved in RNA metabolism and aiding protein-protein interactions within the cell.	Cytoplasmic	13-33	32-77
Spinocerebellar ataxia type type-3 (SCA-3) 14q24-31 Ataxin-3, (48 kDa)	Ataxia	Ataxin-3 functions as a polyubiquitin chain-editing enzyme	Cytoplasmic	12-40	54-89
Spinocerebellar ataxia type-6 (SCA- 6) 19p13 α_{1A} Ca^{2+} channels, (280 kDa)	Ataxia	Functionally, α_{1A} Ca^{2+} channels work with the N-type (CaV2.2) channels and are responsible for the Ca^{2+} entry that triggers neurotransmitter release at synapses	Cell membrane	4-17	20-30
Spinocerebellar ataxia type-7 (SCA-7) 3p12-21 Ataxia-7, (96 kDa)	Ataxia and retinal degeneration	Exact function of ataxin-7 is unknown but it is suggested that it may have a nuclear localization and could act at a transcriptional level.	Nuclear	4-35	37-306
Spinocerebellar ataxia type -17 (SCA-17), 2q13 TATA binding protein (TBP), (42 kDa)	Ataxia, dementia and rarely epilepsy	TBP is a key transcription factor involved in transcription by all three RNA polymerases.	Nuclear	29-42	47-55
Dentatorubral-pallidolusian atrophy (DRPLA) 12q Atrophin-1, (190 kDa)	Ataxia, epilepsy and dementia	It is suggested that atrophin-1 functions as a transcriptional co-repressor.	Cytoplasmic	6-36	49-84
Spinal bulbar muscular atrophy (SBMA) Xq11-12 Androgen receptor (AR), (99 kDa)	Proximal muscle atrophy, fasciculations and bulbar movement	AR functions as a transcriptional modulator. AR function in relation to disease is still unclear.	Nuclear and cytoplasmic	6-39	40-63

1.3 The genetics and neuropathology of HD

HD is an autosomal - dominant neurodegenerative disorder caused by a CAG repeat expansion in the Exon-1 of the *IT15* gene that results in a long polyQ stretch close to the amino terminal of the huntingtin protein (htt) (The Huntington's Disease Collaborative Research Group, 1993). It is unclear how mutant huntingtin (mhtt) protein elicits its neurotoxic effects, but there are several postulated mechanisms, such as transcriptional dysregulation (Gauthier et al., 2004; Zuccato et al., 2003), impairment of protein degradation pathways (Ravikumar et al., 2002; Seo et al., 2004), alterations of the energy metabolism (Browne et al., 2004) and oxidative damage (Brown et al., 1997; Polidori et al., 1999).

Individuals with 35 or less CAG repeats in htt do not develop HD and individuals having 36- 40 CAG repeats (intermediate mutation range) are more likely to present with HD whereas individuals with more than 40 CAG repeats invariably succumb to HD (Ho et al., 2001). The time of disease onset is inversely correlated with the number of CAG repeats. The higher the number of CAG repeats, the earlier the onset of the disease (see Figure 1.1). This process is called anticipation (Ranen et al., 1995). Moreover, it has also been shown that the age of onset varies in individuals having the same number of CAG repeat and this suggests that modifying factors exist (Andrew et al., 1993). Wexler et al., (2004) proposed that the age of onset of HD is influenced by a combination of additional genetic and environmental factors. So far, various studies have been performed to identify genetic modifiers in HD. These studies identified genes associated with pathways or processes involved in the pathogenesis of HD, including oxidative stress. Taherzadeh-Fard et al., (2009) identified 15 single nucleotide polymorphisms (SNPs) with functional relevance in the peroxisome proliferator-activated receptor-γ (PPARγ) coactivator-1α (PGC-1α) gene (see section 1.6.3 for further discussion on PGC-1α). They further analysed the modifying effects of the polymorphisms in PGC-1α on the age of onset in addition to the expanded CAG repeats identifying a polymorphism located within intron 2 that correlates with age of onset variability (Taherzadeh-Fard et al., 2009). Yet another study by an Italian group reported that the DNA base excision repair enzyme (hOGG1) polymorphism Ser326Cys is associated with higher CAG repeats and earlier age of onset (Coppede et al., 2009). This study complements the report by Kovtun et al., (2007) in which they showed that OGG1 initiates age-dependent CAG

expansion in somatic cells as a result of the process of removing oxidized base lesions. Gusella and MacDonald (2009) reviewed other genetic modifiers from different pathways involved in HD and these genes are involved in 1) glutamatergic transmission, 2) gene transcription, 3) stress response and/or apoptosis 4) lipoprotein metabolism, 5) axonal trafficking and 6) folate metabolism. But at the same time these authors also criticise the modifier studies mentioned above due to the small numbers of volunteers involved in these studies, problems with methodology used and in some cases these studies were not linked to genetic variations of a particular mechanism by which delayed age of onset could be explained, for example in the case of PGC-1α (Gusella and MacDonald, 2009).

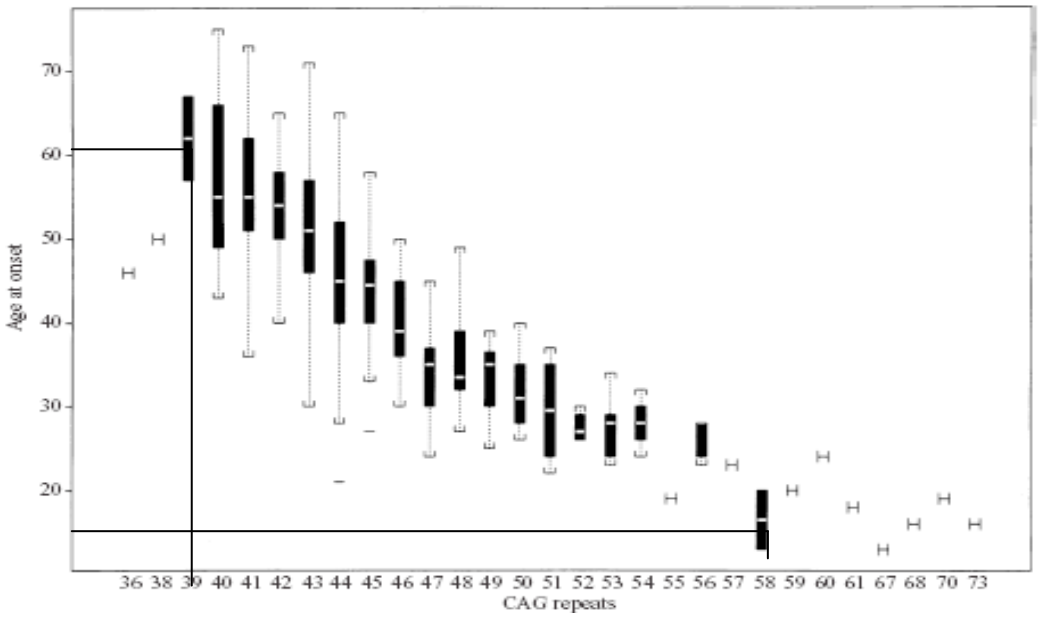

Figure 1.1 Relationship between the number of CAG repeats and age of onset of disease. For example, an individual having 39 CAG repeats has shown disease onset at the age of around 60 years whereas, an individual with 58 CAG repeats has disease onset at the age of 10 years (Ho et al., 2001; Ranen et al., 1995).

HD is fatal after 15-20 years of onset, whereas juvenile cases progress more rapidly and death usually occurs 7 to 10 years after onset (reviewed in Gusella and MacDonald, 1995; Ho et al., 2001). Furthermore, in juvenile cases, the signs and symptoms are different and include bradykinesia, rigidity and dystonia whilst chorea may be completely absent (reviewed in Ho et al., 2001; Squitieri et al., 2006).

A relatively selective neurodegeneration of the striatum and deep layers of the cerebral cortex is the most prominent feature of HD. In advanced stages (Vonsattel Grade 3 and 4) of HD other brain regions are also affected such as the hippocampus,

the hypothalamus, the cerebellum, the amygdala and some thalamic nuclei (Li and Li, 2004a). Also, the lateral tuberal nucleus of the hypothalamus is severely atrophied in HD (Kremer et al., 1990). In HD, spiny projection neurons are the most susceptible to death. Medium-sized spiny neurons (MSNs) constitute 95% of all striatal neurons and innervate the substantia nigra and globus pallidus and these neurons also contain encephalin, dynorphin and substance P (Gerfen et al., 1991). In the cerebral cortex large neurons of layer VI are affected. These neurons project mainly to the thalamus, claustrum and other parts of the cortex (Li and Li, 2004a). In the HD patient brain, axons of MSNs have been suggested to degenerate early and there is a decreased density of encephalin-immunoreactive fibres in the lateral globus pallidus and substance P immunoreactive neuropil in the substantia nigra (Reiner et al., 1988; Richfield et al., 1995). In juvenile HD similar brain regions are affected as in adult onset HD. In addition to this, loss of neurons consisting of Purkinje cells and granular cells of the cerebellum as well as atrophy of various brain regions such as the hippocampus, dentate nucleus, globus pallidus, and neocortex has been also reported in juvenile HD (Byers et al., 1973). In addition pathology is much more severe in juvenile cases compared to adult onset HD (Nance and Myers, 2001).

1.4 The functions of huntingtin

Htt is a 348 kDa multi-domain protein and it has polymorphic glutamine/proline rich domains at its amino-terminal. Htt is localised in the nucleus, cell body, dendrites and nerve terminals (synapses) of neurons (DiFiglia et al., 1995; Gutekunst et al., 1998; Jones, 1999). It is also associated with many cell organelles, such as the Golgi apparatus, the endoplasmic reticulum and mitochondria (Gutekunst et al., 1995; Gutekunst et al., 1998). Htt participates in many cellular functions, for instance, it co-localises with microtubules interacting directly with β-tubulin and forms part of the dynactin complex, which suggests a role in vesicle transport and cytoplasmic anchoring (Caviston et al., 2007; Li and Li, 2004b). Many studies have shown that htt interacts with other proteins and/or has further potential roles in clathrin mediated endocytosis, neuronal transport processes, postsynaptic signalling and is involved in neuronal survival after apoptotic stress (see Table 1.5 for some important htt interacting proteins) (reviewed in Landles and Bates, 2004; Smith et al., 2005). Goehler et al., (2004) demonstrated that htt is part of an extensive interaction network using yeast two-hybrid screening. They showed that htt potentially binds to 186

proteins, 165 of which were previously unknown and they confirmed 32 of these interactions with independent binding experiments. Clearly there is much more work to be done on the physiological functions of htt.

Table 1.5 Proteins that interact with htt, their normal functions and the effect of the CAG repeat mutation on their functions (adapted from Smith et al., 2005).

Protein	Binding region in htt	Functions	Effect of CAG mutation
β-tubulin	Unknown	structural protein	no effect
CSP	probably N-terminal	inhibits N-type Ca^{2+} channel	required for interaction with mhtt
Endophilins	exon 1, proline-rich region	involved in endocytosis	enhances binding
HAP1	N-terminal	vesicle trafficking	enhances binding
HIP1	N-terminal	clathrin mediated endocytosis	decreased interaction
HIP1-related/ HIP12	binds to HIP1	links actin to clathrin	similar to HIP1
InsP3R1	amino acid 1-158	calcium release channel	enhances binding
PACSIN 1	N-terminal, proline rich region	involved in endocytosis	enhances binding
PSD-95	N-terminal, proline rich region activity	regulates NMDA receptor	decreased binding

1.5 Huntingtin cleavage and aggregation

Mutant htt is known to be proteolytically cleaved which profoundly influences its aggregation intracellularly and both of these mechanisms will be discussed in more detail below.

1.5.1 Huntingtin cleavage

Proteolytic cleavage of mhtt takes place both in the cytoplasm and the nucleus (reviewed in Ross, 2002). Proteolytic N- terminal fragments with expanded CAG repeats are assumed to form a compact β- pleated sheet structure (Perutz, 1994), as shown in Figure 1.2 and tend to aggregate more readily than full length htt in both *in vitro* and cell models (Li and Li, 1998). It is well established that N-terminal fragments of htt are more toxic and have a higher propensity to aggregate than full length mutant protein (Davies et al., 1997; DiFiglia et al., 1997; Gutekunst et al.,

1999; Hackam et al., 1998; Hodgson et al., 1999). Numerous studies showed that human htt protein contains cleavage sites for caspase-1, 3, 6, 7 and 8 and an aspartic endopeptidase (Gafni et al., 2004; Gafni and Ellerby, 2002; Hermel et al., 2004; Kim et al., 2001; Lunkes et al., 2002; Wellington et al., 1998; Wellington et al., 2000; Wellington et al., 2002). Ona et al., (1999) has suggested that up-regulation of the caspase-1 gene is an early event in the symptomatic stage of HD. Mhtt protein translocates to the nucleus leading to overexpression of caspase-1 that may activate caspase-3 and cause apoptosis. Furthermore, caspase-8 and 9 activation and the release of cytochrome *c* are also seen in HD (Ciammola et al., 2006). In HD cell models, inhibition of caspases has been shown to reduce mutant htt toxicity (Kim et al., 1999 and Wang et al., 1999). Graham et al., (2006) reported that inhibition of caspase-6 to cleave mhtt in the YAC transgenic mouse model of HD provides neuroprotection. This mouse model was previously known to present with HD like symptoms upon caspase activation and htt cleavage (Wellington et al., 2000). FL-htt is cleaved into many cleavage products, and one prominent fragment found in both transgenic mice and human brain is htt Exon 1 (httEx1). HttEx1 comprises the N-terminal htt domain (htt^{NT}) containing the first 17 amino acids of the protein, the polyQ tract and two oligoproline stretches (11 and 10 prolines) separated by a 17 amino acid proline rich region (Dehay et al., 2007; Kim et al., 2009). Htt^{NT} is known to form an amphipathic alpha-helical membrane binding domain and disruption of this domain is associated with reduced aggregation and elevated toxicity by disrupting intracellular Ca^{2+} homeostasis (reviewed in Hands and Wyttenbach, 2010). In addition to this, the polyproline region adjacent to the polyQ region has been shown to influence htt aggregation and toxicity (reviewed in Hands and Wyttenbach, 2010). Thus many studies suggest that httEx1 is a relevant peptide/protein model to study, as its use models key features of HD (Aiken et al., 2004; Apostol et al., 2003; Mangiarini et al., 1996).

1.5.2 Huntingtin aggregation

Aggregation is the process during which abnormal association of misfolded proteins or parts of proteins form larger insoluble structures (Ross and Poirier, 2005). Wacker et al., (2004) has proposed two different mechanisms by which this occurs (discussed below). Understanding these mechanisms of aggregation is crucial as it is a matter of considerable debate in the scientific literature as to which polyQ aggregates are

neurotoxic or neuroprotective. Hands et al., (2010) reviewed that all monomers, soluble intermediate, and insoluble aggregate species may have toxic properties whilst others claim that some of them are not as toxic as others.

Max Perutz (1994) proposed that expanded polyQ repeats interact with each other through a polar zipper mechanism and hence contribute to aggregate formation. A polar zipper is a set of anti-parallel β-sheets which are strongly held together by hydrogen bonds between main chain and side chain amides. Perutz demonstrated that a proportion of polyQ peptides do indeed adopt a β-structure as shown in his atom model of poly (L-glutamine) (Figure 1.2).

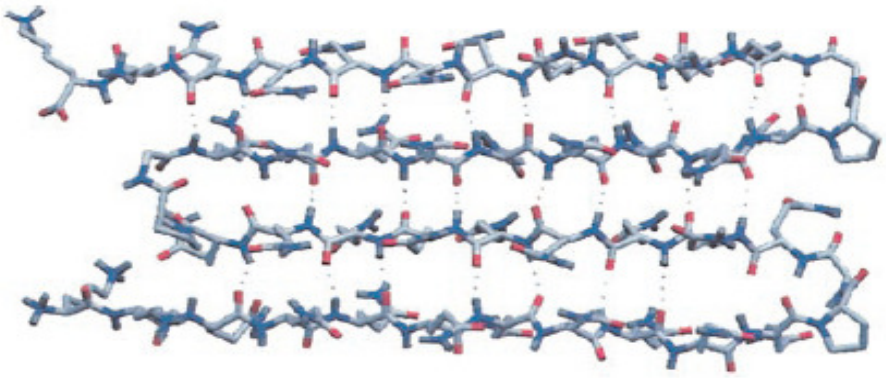

Figure 1.2 Structure of two paired anti-parallel β-strands of poly (L-glutamine) linked together by hydrogen bonds (blue dots) between main chain and side chain amides (adapted from Perutz, 1994; Ross et al., 2003)**.**

Computational structural biology models imply that aggregated mutant polyQ can form secondary structures including parallel β-sheets, anti-parallel β-hairpins comprising two β-strands and a single β-turn, compact random coils consisting of four anti-parallel random coils (Lathrop et al., 1998; Starikov et al., 1999). Later on, X-ray studies showed compact β-sheets comprised of four anti-parallel β-sheets and a parallel β-helices that contains 20 residues per turn (Perutz et al., 2002a; Perutz et al., 2002b).

Wacker et al., (2004) showed that mhtt fragments with expanded polyQ repeats form spherical and annular oligomeric assemblies in the test tube and these assemblies are similar in size and shape to those which are formed by Aβ and α-synuclein. Based on studies using httEx1, Wacker and colleagues proposed two models of how misfolded polyQ proteins cause assembly into fibrils (Figure 1.3).

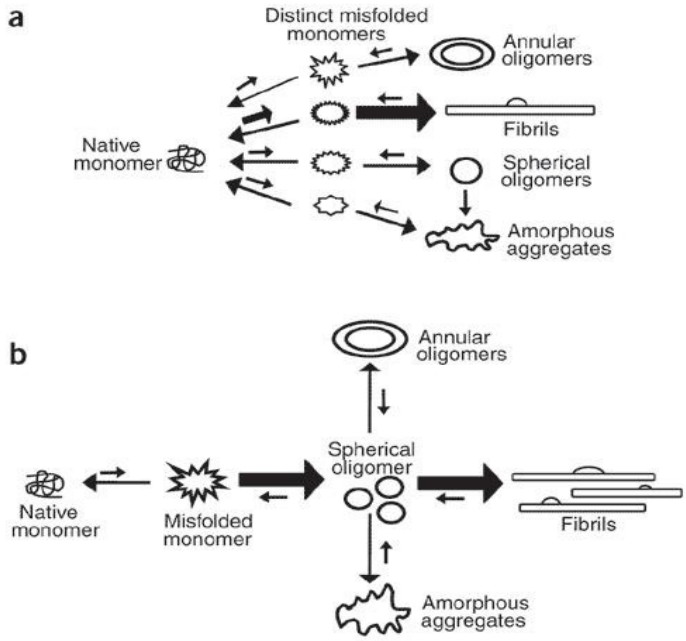

Figure 1.3 Models for the protein assembly of expanded polyQ protein into amyloid like fibrils. (A) The first model shows that monomers may exist in many diverse misfolded conformations and only one altered conformation is on-pathway for fibril formation. **(B)** The second model shows that only spherical oligomeric structures are major on-pathway intermediates for fibrils formation (taken from Wacker et al., 2004).

The first model (Figure 1.3A) proposes that multiple misfolding conformations of polyQ monomer coexist and give rise to a range of off-pathway assemblies, for example, annular, spherical, and/or amorphous oligomers. In this model, only one conformation of misfolded polyQ monomer participates in fibril formation whereas metastable off-pathway structures such as annular, spherical and amorphous structures compete with and decrease the likelihood of on-pathway conformation as a result of monomer addition to fibril nuclei. This model suggests that misfolding of monomeric polyQ conformations leads to the formation of fibrils.

The second model (Figure 1.3B) suggests that a misfolded conformation of polyQ monomers self-associates to form spherical structures and these then serve as on-pathway intermediates for fibril formation, whereas metastable off-pathway intermediates (annular and amorphous oligomers) compete with, and decrease the likelihood of, on-pathway interaction that ultimately leads to fibril formation. More recently, an elegant study performed by Legleiter et al., (2010) reported that mhtt fragments or synthetic polyQ peptides form spherical oligomers leading to fibril

formation in a polyQ length and concentration dependant fashion *in vitro*, in an immortalized striatal cell line as well as in the brain homogenate from a mouse model of HD. They also confirmed these oligomeric-like structures in the HD brain using EM analysis.

1.5.2.1 Toxicity associated with different forms of aggregated mhtt

As mentioned previously, mhtt forms three main aggregation intermediates: monomers, oligomers (spherical, annular and amorphous) and fibrils. The role of these different intermediates in aggregation-associated toxicity is not clearly defined in the literature. Yang et al., (2002) suggested that soluble htt monomers do not cause toxicity. Chen et al., (2002) further revealed that the nucleation seed for aggregate formation is the monomer itself (Figure 1.3). Furthermore, Dunah et al., (2002) proposed that mhtt interferes with gene transcription and soluble monomeric polyQ species cause cell toxicity.

It has been reported that spherical and annular polyQ oligomers may mediate the sequestration of transcription factors and participate in HD pathogenesis and that chaperones diminish the effect of toxic species or oligomers by prevention of transcriptional factor sequestration (Sugars and Rubinsztein, 2003; Wacker et al., 2004). Hence it is likely that polyQ oligomerisation and ensuing further aggregation contribute to several pathological mechanisms that operate during HD pathogenesis (Legleiter et al., 2010). Olshina et al., (2010) performed sedimentation velocity analysis *in vitro* and in cell models of HD, and showed that within cells there was no change in the oligomeric population or in their size distribution in proportion to total htt over time of polyQ expression, while continuous conversion of monomers to IBs was observed. Their study suggests that oligomers are the rate limiting intermediate for IB formation and have the potential to cause toxicity.

Protein aggregates are present in the regions of the brains that degenerate in HD, for example the basal ganglia and cortex (reviewed in Ross and Poirier, 2004). It is believed that the neurons containing aggregates behave differently from the neurons that degenerate. The neurons that degenerate (MSNs) belong to the striatum, whereas IBs are mostly observed in the interneurons and these are not susceptible to degeneration (Kuemmerle et al., 1999). This suggests that IB formation could play a

protective role in the neurons and may be produced in response to toxic monomeric or oligomeric mhtt species. However, it has also been reported that htt aggregates are preferentially formed in the striatal projection neurons and cause toxicity (Li et al., 2001). Hence it is controversial whether htt aggregates are neurotoxic or neuroprotective. More recently, Gong et al., (2008) performed live cell time-lapse microscopy to study aggregate formation and its relationship to cell death in PC12 cells. They showed that cells that form larger aggregates survive longer than cells that form small or no microscopically visible aggregates supporting the toxic precursor hypothesis.

1.5.2.2 Role of molecular chaperones in htt aggregation

Protein misfolding does not just occur in disease, but also takes place in normal tissue and under stress conditions such as thermal stress, oxidative stress, in the presence of chemicals and during irradiation (reviewed in Soo et al., 2008). The body has compensatory mechanisms to refold or degrade abnormal proteins. As well as the protein degradation pathways described in section 1.6.1 (see below) heat shock proteins (HSPs) exist which act as molecular chaperones. HSPs provide protection against protein aggregation, help folding of newly synthesised proteins and re-fold damaged proteins (Barral et al., 2004; Hartl, 1996). They are also known to sequester severely damaged proteins for degradation (Barral et al., 2004; Gething and Sambrook, 1992; Hartl, 1996). HSPs are classified into different families according to their molecular size or function. High molecular weight HSPs include HSP 40, 60, 70, 90 and 100 and small molecular size HSPs (sHSPs) with the size range of 15-30 kDa and some of these will be discussed in section 1.7.1 in more detail. The high molecular weight HSPs are ATP dependent whilst the sHSPs function in an ATP independent fashion (Barral et al., 2004).

Many studies suggest that HSP40 and HSP70 chaperones are effective modulators of polyQ aggregation and associated cell death in mammalian cell systems and in *in vivo* systems such as in worms (*Caenorhabditis elegans*) the fruit fly (*Drosophila melanogaster*) and mice (*Mus musculus*). Similarly, a yeast model of HD showed that overexpression of Sis1 (yeast HSP40 homologue of human hDJ-1) and HSP70 enhance mhttEx1 aggregation whereas overexpression or deletion of HSP104 rescues mhttEx1 induced aggregation (Krobitsch and Lindquist, 2000). Numerous studies

also suggest that chaperones such as HSP40, HSP60, HSP70 and HSP100 are co-localised with polyQ protein aggregates and enhanced chaperone levels are not only associated with aggregation suppression, but also increased IB formation (Carmichael et al., 2000; Cummings et al., 1998; Krobitsch and Lindquist, 2000; Wyttenbach et al., 2000; Wyttenbach et al., 2001). Wyttenbach et al., (2002) revealed that HSP27 protects neuronal and non-neuronal cells against polyQ cytotoxicity without suppressing polyQ aggregation. In this study, polyQ cell toxicity was linked to cytochrome c release and participation of the mitochondrial death pathways. HSP27 was suggested to provide protection to cells against ROS, produced at a higher rate in cells expressing an abnormal number of polyQ repeats (Q74) compared to cells expressing control polyQ repeats (Q25) (Wyttenbach et al., 2002). Hence it is clear that chaperones are able to modulate both polyQ aggregation and a potentially altered redox-state due to expression of expanded polyQ stretches. For further information on the involvement of HSP and sHSP in the pathology of polyQ disorders the reader is referred to reviews by Wyttenbach (2004) and Sajjad et al., (2010).

1.6 Pathological mechanisms of HD

There are a number of mechanisms that have been proposed to participate in HD pathogenesis and these are 1) impairment of protein degradation pathways, 2) altered vesicular transport 3) transcriptional dysregulation, 4) dysfunctional bioenergetics and 5) alterations in redox homeostasis leading to oxidative stress. These pathways will be discussed below. Figure 1.4 summarizes how the potential roles of mhtt are related to the pathogenesis of HD.

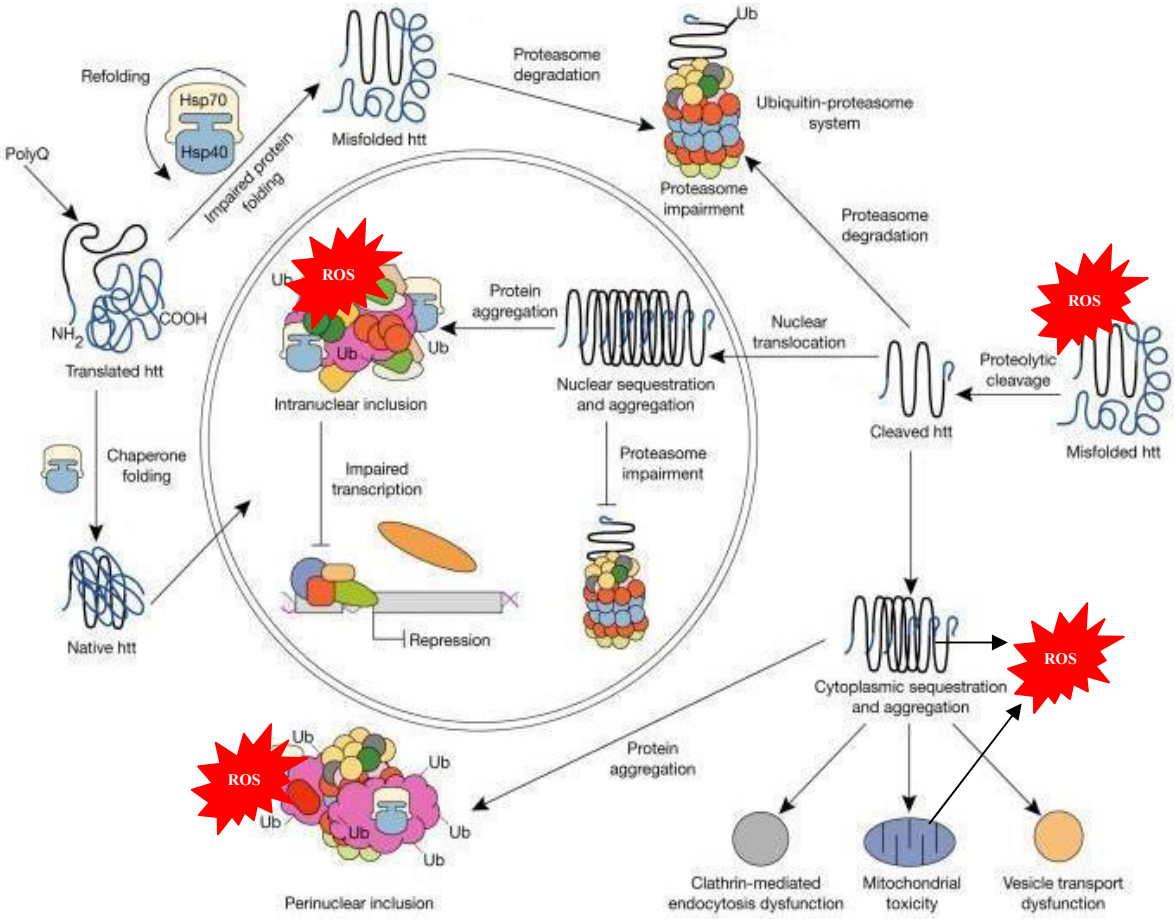

Figure 1.4 A cell model for HD. This model shows the possible effects of mhtt on different cell organelles and their contribution in the pathogenesis of HD (modified from Landles and Bates, 2004)**.**

1.6.1 The role of protein degradation pathways in HD

There are two major protein degradation pathways, the ubiquitin proteasome system (UPS) and the autophagy-lysosomal pathways that are involved in normal and abnormal protein clearance in mammalian cells (Rubinsztein, 2006). The UPS is a system located in the cytoplasm and nucleus of all cells containing multiple parts that serve to identify and then degrade damaged proteins. Proteins are targeted by the UPS through covalent conjugation with multiple molecules of ubiquitin and these tagged proteins are then degraded by the 26S proteasome as shown in Figure 1.5 (Korhonen and Lindholm, 2004). Protein conjugation involves three different enzymes, E1 (UPS activating enzyme), E2 (ubiquitin conjugating enzyme), and E3 (ubiquitin ligases).

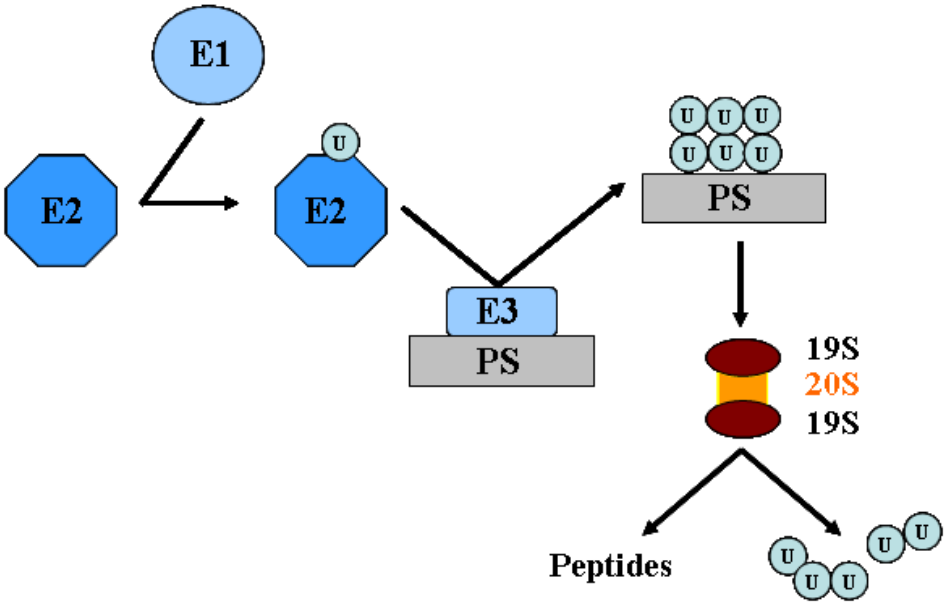

Figure 1.5 The ubiquitin-proteasome system (UPS). The UPS consists of ubiquitin, U; ubiquitin activating enzyme, E1; ubiquitin conjugating enzyme, E2 and ubiquitin ligase, E3; catalytic core of 26S proteasome, 20S; regulatory particle, 19S and protein substrate, PS (adapted from Korhonen and Lindholm, 2004).

The UPS is a diverse system because there are several E2 and E3 enzymes that bind to different target proteins. The main component of the UPS system is the 26S proteasome that comprises a 20S core subunit and two 19S regulatory particles (Figure 1.5). The UPS also contains deubiquitination enzymes that regulate the function of the proteasomes by reloading the cellular ubiquitin. The UPS participates in many cellular processes, such as cell cycle control, DNA repair, transcription, regulation of protein trafficking and cell signalling by modifying the substrate protein through attaching a monoubiquitin and polyubiquitin chain (Korhonen and Lindholm, 2004). Alterations in the UPS system may be involved in the pathogenesis of many neurodegenerative diseases such as AD, HD, PD and SCAs (reviewed in Ciechanover and Brundin, 2003). It has been shown that the UPS is impaired due to mhtt and its components (particularly ubiquitin) aggregate with mutant proteins (e.g., mhtt in the case of HD, α- synuclein in PD) and form IBs.

Venkatraman et al., (2004) reported that eukaryotic proteasomes can only cleave single glutamine-glutamine bonds instead of cutting polyQ stretches. Therefore, eukaryotic proteasomes release undigested polyQ peptides when degrading polyQ

protein. Lecker et al., (2006) suggested that some of the peptidases are capable of degrading undigested proteasomal polyQ fragments but enzymes that cleave polyQ stretches have limited degradative activity. For example, puromycin-sensitive amino-peptidase (PSA) can degrade polyQ fragments of up to 30 glutamines long (Bhutani et al., 2007). In addition to this, UPS impairment has been reported in cellular models of HD (Bence et al., 2001; Bennett et al., 2005; Verhoef et al., 2002) and within the synapses of neurons cultured from N-terminal fragment mice model (R6/2) and full length htt knock-in mice (Wang et al., 2008). Furthermore, human HD post-mortem brain tissue and skin fibroblasts provided evidence for UPS inhibition (Bennett et al., 2007; Seo et al., 2004). A study by Diaz-Hernandez and colleagues in (2006) suggested that mhtt filaments can interact with the 19S regulatory caps of the 26S proteasome and may contribute toward the impairment of proteasomal activity. On the other hand, two studies also showed accumulation of polyubiquitinated proteins in R6/2 transgenic mice model without UPS impairment (Bett et al., 2009; Maynard et al., 2009). Ding et al., (2002) also reported that UPS activity was not impaired in an HD cell model, but in some studies enhanced UPS activity was reported even in the presence of IBs (Bett et al., 2006; Diaz-Hernandez et al., 2003; Mitra et al., 2009). All of this suggests the existence of a controversy as to the impairment of the UPS in HD model systems and in patients. Hence it is vital to further study the UPS degradation mechanism in an HD context.

Beside the UPS, autophagy is the other important mechanism for removal of mutant proteins and cell organelle turnover (reviewed in Mizushima and Klionsky, 2007). Autophagy is a cytosolic degradation pathway that involves the targeting of superfluous and damaged organelles and proteins to lysosomes. Aggregated and soluble forms of mutant proteins are cleared after the induction of autophagy which provides protection to the cell against mutant protein toxicity (reviewed in Moreau et al., 2010). Autophagy is well characterised in yeast, whereas it is less well understood in the mammalian cell system.

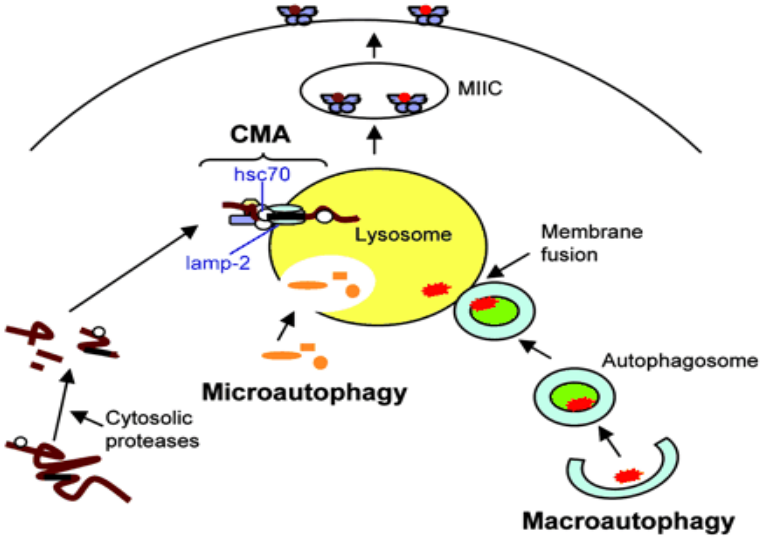

Figure 1.6 Morphology of the autophagy pathway in yeast. There are three autophagy pathways: macroautophagy, microautophagy and chaperone-mediated autophagy. Macroautophagy functions via the formation of a cytosolic double membrane vesicle which stores bulk cytoplasm containing damaged proteins and/or organelles. Autophagosomes, fuse with this vesicle and produce a single membrane autophagic body which then degrades its contents with hydrolases. In the case of microautophagy, the sequestration events occur at the vesicle surface. In chaperone-mediated autophagy (CMA) specific cytosolic proteins are translocated across the lysosomal membrane through the lamp2A receptor on the lysosomes (adapted from Crotzer and Blum, 2005).

Autophagy is activated only under starvation conditions in yeast, while it is constitutively activated in mammals (Ravikumar and Rubinsztein, 2006). Autophagy is centrally regulated by mammalian target of rapamycin (mTOR). Under starvation conditions Tor kinase is inactivated itself, but activates autophagy. Membranes of mitochondria and/or ER, non-specifically sequester cytoplasm containing abnormal protein and form autophagosomes (Figure 1.6) that fuse with lysosomal vacuoles where abnormal protein is degraded by the action of vacuolar hydrolases (Hailey et al., 2010; Wang and Klionsky, 2003). Autophagy can be inhibited at the stage of autophagosome formation or at the fusion of autophagosome with the lysosomal vacuole in response to chemical stimuli. Pharmacological inhibition of autophagy at different steps interferes with the clearance of mhtt fragments which then enhances aggregation formation and increases toxicity (Ravikumar et al., 2002). In *Drosophila* and mouse models expressing mhtt activation of autophagy with rapamycin and the

rapamycin ester CCI-779 significantly reduced aggregation and toxicity (Ravikumar and Rubinsztein, 2006).

However, an alternative explanation for this reduction is the inhibition of protein synthesis by mTOR, a key negative regulator of autophagy (King et al., 2008b; Wyttenbach et al., 2008). mTOR is sequestered in mhtt aggregates in various model systems and in patients brain and this causes an induction of autophagy that is associated with reduced mhtt aggregation load (reviewed in Sarkar et al., 2009). More recently, Bauer et al., (2010) performed a study causing the specific recruitment of CMA in a HD cell model and in R6/2 mice showing that this led to the selective degradation of mhtt without changing the levels of normal htt. They then further showed that CMA induction ameliorates the HD-like phenotype seen in the R6/2 model (Bauer et al., 2010) suggesting that the application of a chemical modulator of CMA may well be therapeutic in HD. Interestingly, a recent study suggested that antioxidant (thiol and non-thiol based) compounds block autophagy and impair both basal and induced autophagy activity and enhance protein aggregation in cell model of HD and PD (Underwood et al., 2010). In fly and zebrafish models of HD, antioxidant treatment aggravated disease phenotypes and this effect was rescued upon autophagy induction with rapamycin. Therefore, this study suggests that antioxidant compounds' protective effects were compromised due to their anti-autophagy properties (Underwood et al., 2010).

Autophagy and the UPS are both important for cellular homeostasis. However, the induction of autophagy may well be the preferred route towards an HD therapy, as autophagic mechanisms degrade not only proteins, but also other damaged cellular organelles, such as mitochondria, endoplasmic reticulum and peroxysomes (Mizushima and Klionsky, 2007).

1.6.2 The relationship between mhtt and vesicular transport

Wild-type htt interacts with trafficking motor proteins and clathrin-interacting proteins, such as huntingtin interacting protein-1(HIP-1) (Kalchman et al., 1997; Legendre-Guillemin et al., 2002; Wanker et al., 1997), huntingtin interacting protein-related (HIP1-R) (Engqvist-Goldstein et al., 1999; Legendre-Guillemin et al., 2002)

and huntingtin associated protein 1 (HAP1) (Li et al., 1995; Smith et al., 2005). There are a number of other proteins that also interact with htt as shown in Table 1.5.

Htt interacts with its associated proteins (HIP-1, HAP1and HIP-1R) and participates in endocytosis and axonal trafficking. Wild-type htt, together with HAP1, enhances microtubule based trafficking of an important neuronal growth factor, brain derived neurotrophic factor (BDNF) (reviewed in Trushina and McMurray, 2007). Mhtt has a high binding affinity for HAP1 compared to wild-type htt and, as a result, mhtt binds strongly to HAP1 and interferes with BDNF trafficking by competing with HAP1 for microtubule binding. Hence, HD pathology may be initiated in the cortex where mhtt reduces BDNF production for striatal neurons, leading to striatal degeneration (Zuccato et al., 2001; Zuccato et al., 2003).

More recently, Smith et al., (2009) used various biochemical approaches to show that mhtt binds strongly with microtubular β-tubulin, as compared to wild-type htt and suggested that mhtt physically blocks microtubule dependent transport by directly recruiting monomer, microaggregates or larger aggregates to the microtubules. This idea of axonal blockage is consistent with another study where Sinadinos et al., (2009) showed that mhtt causes axonal vesicles to accumulate and aggregate within larval motor neuron axons in a *Drosophila* HD model expressing mhttEx1. This accumulation did not alter vesicle velocity but there was a significant increase in the number of times vesicles stalled. There are a few studies on human post-mortem brain tissues from pre-symptomatic patients which show axonal dysfunction (Albin et al., 1992; Sapp et al., 1997) and these results are consistent with other studies on animal models of HD (Gunawardena et al., 2003; Li et al., 2001; Trushina et al., 2004).

A study by Li et al., (2010) showed that mutant htt caused an impairment of neuronal glutamate/cysteine transporter (EAAC1) trafficking and, as a result, impaired uptake of cysteine which then reduces neuronal glutathione levels potentially leading to an impaired redox homeostasis. This report suggested that impaired endosomal recycling of EAAC1 was due to impaired Rab11 activity and previously they have also shown that mhtt inhibits guanine nucleotide exchange on Rab11 in brains of young HD knock-in mice (Li et al., 2009). Mhtt is also known to have less binding affinity for

HIP1, compared to wild-type htt (Kalchman et al., 1997). HIP-1 is a key component of the endocytotic pathway (reviewed in Hyun and Ross, 2004) and endocytosis is impaired in the striatal neurons of HD mice (Trushina et al., 2006). However, the mechanistic link between mhtt, HIP-1 and endocytosis is yet to be established.

The evidence mentioned above establishes the presence and importance of transport impairment in cell models, HD animal models and patients with HD. Transport defects due to the presence of misfolded protein are a common pathology between most major neurodegenerative diseases (reviewed in De Vos et al., 2008; Nixon, 2005) and this is a burgeoning field of research.

1.6.3 Transcriptional dysregulation and HD

Mhtt interferes with the transcriptional machinery leading to abnormal interactions with nuclear activators or co-repressors, such as p53, Sp1, CBP and TAFII130 (Dunah et al., 2002; Steffan et al., 2000). Mhtt has a higher binding affinity to the transcription factors than wt htt, thus potentially causing toxicity (Dunah et al., 2002). Another study showed that mhtt binds to short polyQ stretches present in many transcription activators or co-repressors but particularly, CREB binding protein (CBP), which contains a homopolymeric stretch of 19 glutamines (Kazantsev et al., 1999). Mhtt alters CBP conformation and removes it from its normal site of survival-promoting actions within the cell and, as a result, causes toxicity. It has been shown that transcriptional factors such as p53, CBP, TBP and Sp1 are recruited into intranuclear aggregates (Dunah et al., 2002; Steffan et al., 2000; van Roon-Mom et al., 2002). Preisinger et al., (1999) proposed a sequestration hypothesis by which expanded polyQ protein has the potential to interact with any protein that contains short stretches of glutamine-rich regions in the cell. They highlighted that transcription factors and translational co-repressors have homopolymeric glutamine stretches which would be vulnerable to aggregate with mhtt and this theory was later supported by several of the above mentioned studies.

Several studies implicated altered cAMP- responsive element (CRE) mediated transcription *in vitro, in vivo* and in patients with HD (Kita et al., 2002; Luthi-Carter et al., 2000; Nucifora, Jr. et al., 2001; Steffan et al., 2001; Wyttenbach et al., 2001). The activation of CRE allows the transcription machinery to work and participate in

several neuronal survival pathways (Lonze and Ginty, 2002). The transcription factor, cAMP- responsive element binding protein (CREB) binds to CRE, which is the cellular promoter in many genes including the encephalin gene. Figure 1.7A shows the transcriptional activation achieved by phosphorylation of CREB by protein kinase A which then permits the recruitment of CBP. CBP has intrinsic histone acetyltransferase activity that allows the subsequent recruitment of TAF_{II}^{130}, after remodelling of chromatin into an open structure, followed by transcriptional activity. After recruitment of transcription factors, polymerase II is phosphorylated and then initiates transcription. It is known and outlined schematically in Figure 1.7B that mhtt disrupts CRE-mediated transcription by either directly interacting with both the glutamine activation domain and acetyltransferase domain of CBP or by sequestering CBP (Luthi-Carter et al., 2000; Nucifora, Jr. et al., 2001; Steffan et al., 2000; Steffan et al., 2001; Wyttenbach et al., 2001). In addition to this, Shimohata et al., (2000) showed that a transcription coactivator (TAF_{II}^{130}) also binds to polyQ stretches and suppresses CREB dependant transcriptional activation.

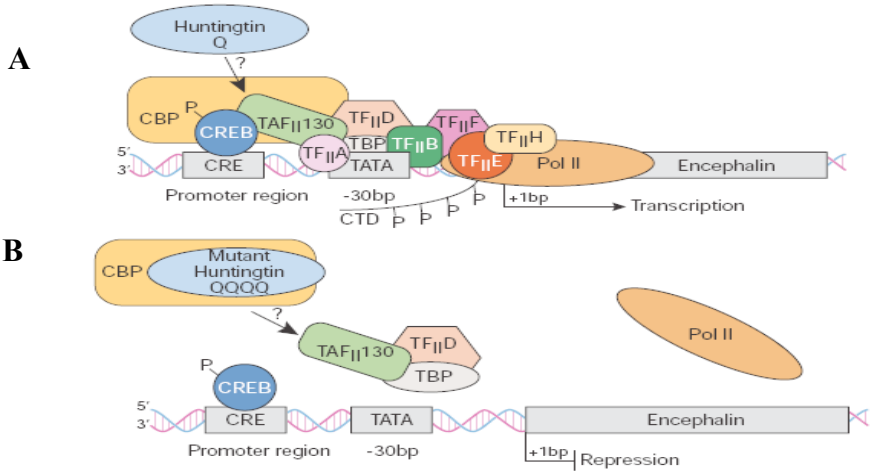

Figure 1.7 Impact of wild-type htt and mhtt on the transcriptional machinery of the encephalin gene. (A) Wild-type htt participate in the transcription activation whereas **(B)** reveals that mhtt interrupts CRE-mediated transcription and as a result impairs the transcriptional machinery (adapted from Landles and Bates, 2004) .

Another well-studied and relevant example of transcriptional dysregulation in HD is related to the production of BDNF. BDNF transcription has been reported to be altered in HD cell models, animal models (full length, YAC72 and N-terminal fragment model, R6/2) and HD patients (Gauthier et al., 2004; Trettel et al., 2000; Zhang et al., 2003; Zuccato et al., 2001; Zuccato et al., 2003). BDNF is made in the

cortex and transported to the striatum by cortico-striatal afferents. BDNF is an essential survival factor for striatal neurons (Altar et al., 1997). Zuccato et al., (2001) showed that wild-type htt upregulates the expression of the BDNF gene via BDNF promoter II, whereas the presence of mhtt was associated with low levels of BDNF. Later on they showed that BDNF production is sustained by normal htt interacting with Repressor Element-1 Silencing Transcription Factor/Neuron-Restrictive Silencer Factor (REST-NRSF) in the cytoplasm and preventing REST-NRSF from translocating to the nucleus efficiently. Mhtt fails to maintain its interaction with REST-NRSF and this causes an increase in nuclear REST-NRSF levels. Nuclear REST-NRSF binds to a promoter region and recruits Sin3A. Sin3A is a regulatory protein with histone deacetylase activity for remodelling chromatin into a closed architecture, which prevents gene transcription. One of the genes regulated by Sin3a is BDNF, hence, its impaired transcription in HD (Zuccato et al., 2003). In addition to this, a recent study showed that htt indirectly interacts with REST by forming a complex with dynactin p150glued, REST-interacting LIM-domain protein (RILP) and addition of HAP1 into the complex retain the REST-NRSF in the cytoplasm (Shimojo, 2008).

Yet another prominent example of transcriptional dysregulation in HD concerns the impairment of PGC-1α (McGill and Beal, 2006). PGC-1α is thought to be a key regulator of mitochondrial biogenesis and respiration via the integration of several transcription factors, NRF-1, NRF-2 and the nuclear hormones receptors, PPARα, PPARδ, ERRα and TR (reviewed in Lin et al., 2005). Some of these factors, such as NRF-1, NRF-2 and ERRα, regulate the expression of several nuclear-encoded mitochondrial genes, which encode cytochrome c, complex I to IV and mitochondrial transcriptional factors (Tfam) (Kelly and Scarpulla, 2004; McGill and Beal, 2006). Many studies have suggested that PGC-1α transduces physiological stimuli in certain metabolic pathways. For instance, it is known to function as a co-activator of the UCP-1 gene that regulates adaptive thermogenesis in brown adipose tissues (Puigserver et al., 1998), fiber-type switching in skeletal muscle (Lin et al., 2002) β-oxidation of fatty acids and gluconeogenesis in liver (Herzig et al., 2001; Rhee et al., 2003; Yoon et al., 2001). PGC-1α is a potent suppressor of ROS and induces production of ROS scavenging enzymes, SOD1, SOD2 and GPx1 (St-Pierre et al., 2006). PGC-1α seems to lose its function in neurodegenerative disorders (Figure 1.8).

PGC-1α knockout mice exhibit impaired mitochondrial function, show a hyperkinetic movement disorder and striatal degeneration (Lin et al., 2004). Studies have shown a marked down-regulation of PGC-1α mRNA expression in a STHdh^{Q111} striatal HD cell line, in striatal neurons from a HD knock-in mice model and post-mortem tissue from HD patients brain (Cui et al., 2006; Weydt et al., 2006).

HD mice (N171-82 model) tend to exhibit reduced food intake and impaired energy metabolism (Weydt et al., 2006). Alterations in the transcriptional regulation of PGC-1α may well play a central role in these energetic deficits. Brain slice cultures from HD murine brain showed impaired mitochondrial oxygen consumption rates compared to slices of healthy control groups. Hence it was suggested that altered PGC-1α function may well be a link between impaired transcription and mitochondrial dysfunction in HD (Weydt et al., 2006).

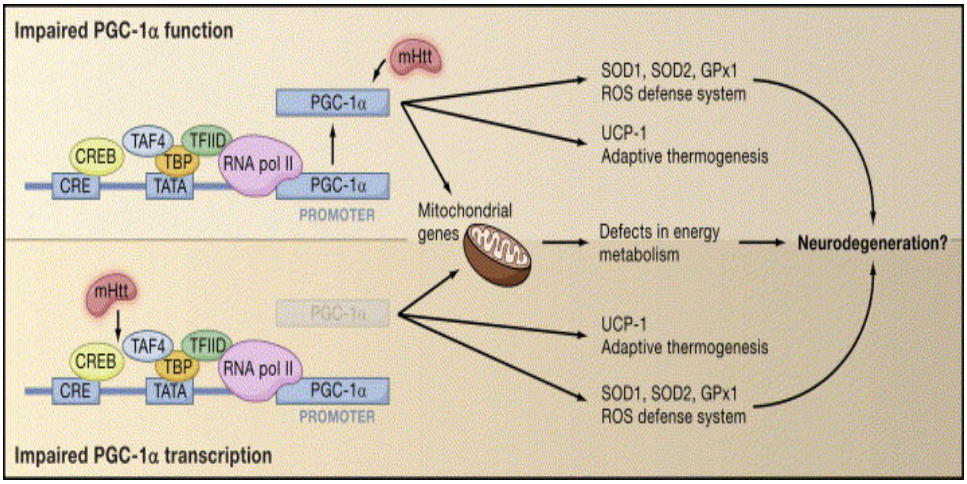

Figure 1.8 Mhtt impairs PGC-1α functions and its transcription. (A) Mhtt interferes with the ability of PGC-1α to switch on its downstream target genes such as those involved in ROS defense and adaptive thermogenesis. Mhtt is known to obstruct PGC-1α's coactivator properties. **(B)** Furthermore, mhtt binds to the CREB/TAF4 complex within the PGC-1α promoter and impairs its transcription (adapted from McGill and Beal, 2006)**.**

1.6.4 Bioenergetics and HD

1.6.4.1 Biochemical pathways and bioenergetic defects

Bioenergetic defects are hypothesized to be an important feature of HD. HD patients suffer weight loss despite sustained caloric intake and this weight loss does not correlate with chorea (Aziz et al., 2008; Trejo et al., 2004). Nuclear Magnetic Resonance (NMR) spectroscopic and Positron Emission Tomography (PET) studies

revealed that glucose metabolism is impaired and, as a result, lactate levels in the cortex and basal ganglia are elevated in HD patients and reduced production of ATP occurs in muscles (Andrews and Brooks, 1998; Jenkins et al., 1993; Kuhl et al., 1985; Kuwert et al., 1990). Koroshetz et al., (1997) showed that the abnormal level of lactate can be rescued by a metabolic cofactor, coenzyme Q10. Another NMR study showed an increase in pyruvate contents in the cerebrospinal fluid (Nicoli et al., 1993). Furthermore, cortical biopsies of HD patients show abnormal mitochondrial morphology (Goebel et al., 1978).

Biochemical studies of HD post-mortem brain also show abnormalities in major components of the tricarboxylic acid (TCA) cycle and ETC in different brain regions (Figure 1.9). Firstly, pyruvate dehydrogenase (PYDH) is one of the TCA cycle enzymes and it catalyzes oxidative decarboxylation of pyruvate to form acetyl-CoA that enters into the TCA cycle for complete oxidation to CO_2 and H_2O (Figure 1.9).

PYDH activity is reported to be decreased in the basal ganglia and hippocampus with reduced striatal oxygen consumption in HD individuals (Butterworth et al., 1985; Sorbi et al., 1983). Secondly, putamen and caudate of HD advanced grade (Vonsattel 3 and 4) patients brain show decreased activity of ETC complexes II, III and IV (Browne et al., 1997). Succinate dehydrogenase (SDH) is the main component of complex II and plays a central role in the respiratory chain consisting of four nuclear encoded subunits, Fp (70kDa), Ip (30kDa) and two smaller subunits SDH-D and SDH-C. It is known that both Fp and Ip subunits levels are significantly reduced in the striatum of HD patients (Benchoua et al., 2006). This suggests that reduced activity of complex II in the HD striatum is possibly due to reduced expression of complex II (Benchoua et al., 2006). Tabrizi et al., (1999) has also shown impaired complex II activity in post-mortem brain of HD patients. Browne et al., (2004) reviewed that HD patients brain may well exhibit a selective loss of complex II or III activity. Lastly, GAPDH is another metabolic enzyme reported to participate in the pathogenesis of HD because mhtt has a tendency to bind to this enzyme and as a result decrease its glycolytic activity (Mazzola and Sirover, 2001). The various points in which mhtt has been proposed to interfere with glycolysis and the TCA cycle are outlined in Figure 1.9.

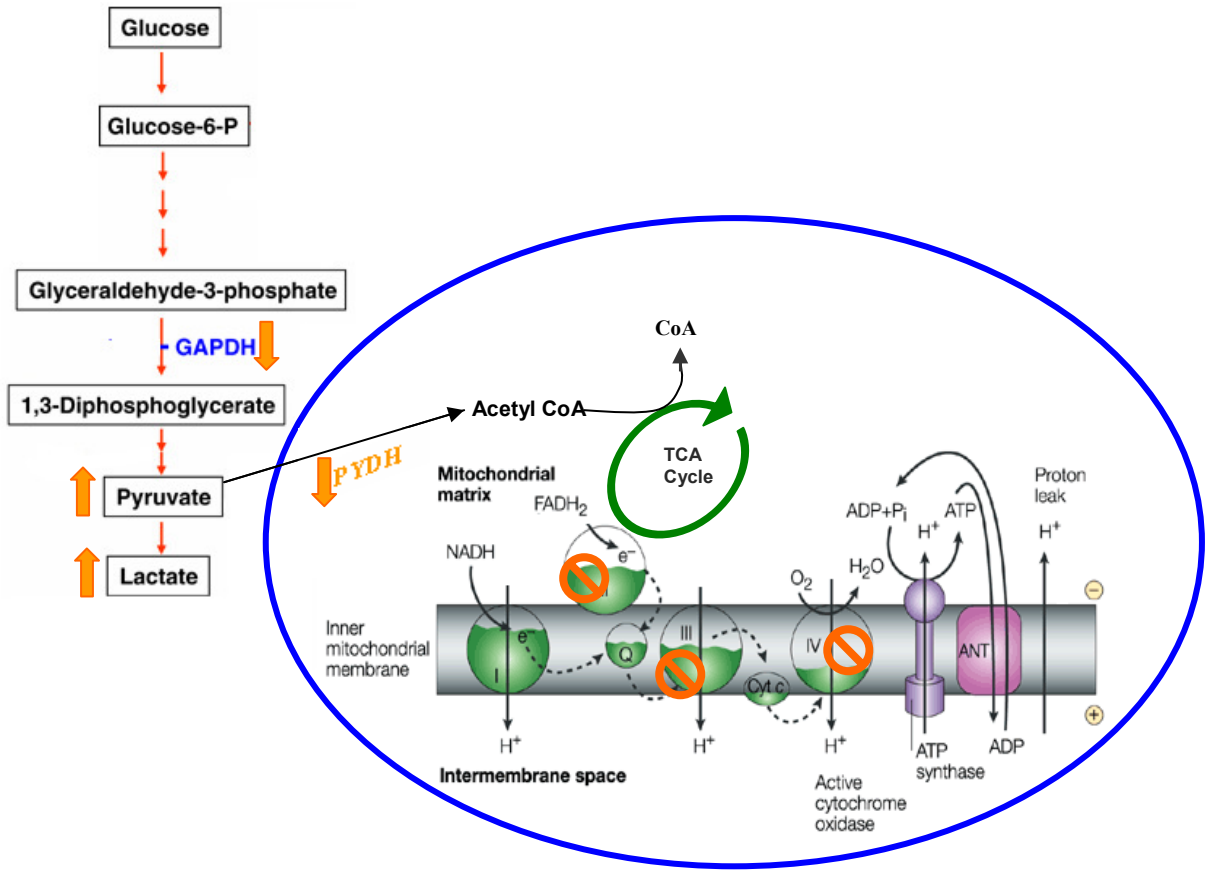

Figure 1.9 Mhtt impairs glucose metabolism and the ETC. In the case of HD, glucose metabolism is impaired and enhances lactate production. Browne et al., (2004) suggested that impaired components of the TCA cycle and the ETC impair ATP production. Orange arrows represent an increase or decrease in enzymatic activity of components of glycolysis and orange signs represent inhibition of ETC components (modified from Moncada and Erusalimsky, 2002).

1.6.4.2 ER, mitochondrial dysfunction and the role of Ca^{2+}

Abnormal bioenergetics and transcription, as outlined above, probably impact indirectly on mitochondrial physiology and calcium metabolism leading to excitotoxicity in HD. Glutamate-mediated excitotoxicity is thought to play an important role in the pathogenesis of HD. For example, infusion of an agonist (quinolinic acid) of the N-methyl-D-aspartate (NMDA) subtype of glutamate receptor mimics HD pathology (Beal et al., 1986; Ferrante et al., 1993; Schwarcz et al., 1983 Young et al., 1988). NMDA receptor-mediated toxicity and mitochondrial impairment are thought to be linked by a number of mechanisms. The most important link between these two relates to abnormal mitochondrial Ca^{2+} homeostasis (Panov et al., 2002) that may be disrupted via a direct interaction of mhtt fragments with mitochondria.

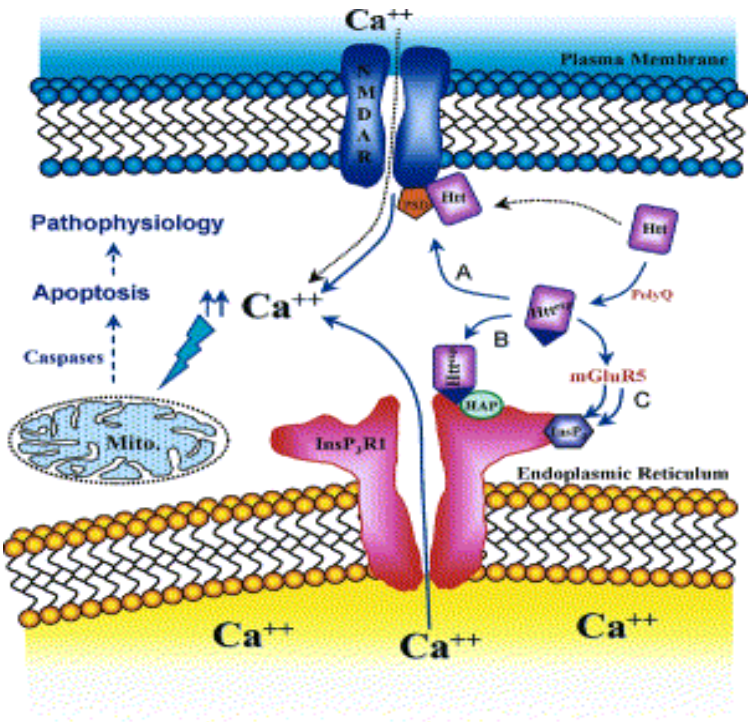

Figure 1.10 The role of mhtt in the pathogenesis of HD in relation to intracellular Ca^{2+} levels which is regulated by $InsP_3R$ and NMDAR. Mhtt forms a strong complex with $InsP_3R$ and HAP1A and impairs intracellular Ca^{2+} homeostasis that leads to cell death (adapted from Varshney and Ehrlich, 2003).

Another way by which mhtt could alter Ca^{2+}signalling is by modification of Ca^{2+} channels (Tang et al., 2003). Mhtt forms a stronger complex with the inositol (1,4,5)-triphosphate receptor ($InsP_3R$) and HAP1A compared to wild-type htt and enhances the sensitivity of the $InsP_3$ receptor at the ER (Tang et al., 2003). Mutant htt has been found to enhance the production of $InsP_3$ through mGluR5 stimulation and increase the intracellular calcium levels in neurons, thus potentially leading to the initiation of the apoptotic pathways (Varshney and Ehrlich, 2003). Intracellular Ca^{2+} is also regulated by NMDAR in addition to $InsP_3R$ (Figure 1.10). Wild-type htt interacts with NMDAR and enhances intracellular calcium levels. Mutant htt increases NMDA receptor sensitivity more so than wild-type htt, possibly due to its abnormal interaction with PSD95, NR1A or NR2B complex (reviewed in (Varshney and Ehrlich, 2003). The mechanisms outlined above could all lead to a high level of intracellular Ca^{2+}, which can activate cell death enzymes, such as caspases and calpains.

1.6.5 Abnormal redox homeostasis and oxidative stress in HD

Many of the above mentioned pathological mechanisms are expected to contribute to an abnormal redox homeostasis and produce oxidative stress in HD. It is well established that there is an alteration in the redox homeostasis in *in vitro* models, animal models and human HD brain (see below, section 1.6.5.4). As free radicals are the key subject of my investigations, it is important to understand their chemistry, which will be introduced below. Furthermore, some potential roles of ROS in neuropathology and cell signalling is also summarized.

1.6.5.1 The chemistry of free radicals

A free radical is any species capable of independent existence that carries one or more unpaired electrons (Thannickal and Fanburg, 2000). There are many classes of radicals that exist in biological systems. Oxygen centred radicals are called Reactive Oxygen Species (ROS), nitrogen centred radicals are called Reactive Nitrogen Species (RNS), Bromide centred radicals are called Reactive Bromide Species (RBS) and chloride centred radicals are called Reactive Chloride Species (RCS). Radicals can be formed by losing or gaining an electron from a non radical. For example, loss of an electron:

$$A \longrightarrow e^- + A^{\cdot +}$$

or gain of an electron:

$$B + e^- \longrightarrow B^{\cdot}$$

Radicals can be formed by homolytic bond fission whereby the cleavage of covalent bonds takes place and one electron from a bonding pair stays on each atom:

$$H\text{-}O\text{-}H \longrightarrow H^{\cdot} + OH^{\cdot}$$

Heterolytic bond fission can form a radical whereby the cleavage of bonds transfers both electrons on one atom:

$$H\text{-}O\text{-}H \longrightarrow H^+ + OH^-$$

ROS exists as: 1) oxygen radicals that carry a lone pair of electron and/or 2) non-radical derivatives of oxygen (see Table 1.6). Some ROS are more toxic than others. Superoxide anion radicals and hydrogen peroxides for example react with certain

biological molecules (see Figure 1.12) and produce more reactive forms of ROS that cause damage to DNA, lipids and proteins, whereas hydroxyl radicals cannot diffuse from its site of formation because of their extreme reactivity and therefore they can cause serious damage to any molecule around them.

Table 1.6 A classification of Reactive Oxygen Species

Radicals	Non-radicals
Superoxide, $\mathbf{O_2^-}$	Hydrogen peroxide, $\mathbf{H_2O_2}$
Hydroperoxide, $\mathbf{HOO^\cdot}$	Peroxynitrite, $\mathbf{ONOO^-}$
Hydroxyl, $\mathbf{OH^\cdot}$	Peroxynitrous acid, **ONOOH**
Peroxyl, $\mathbf{ROO^\cdot}$	Nitrosoperoxycarbonate, $\mathbf{ONOOCO2^-}$
Alkoxyl, $\mathbf{RO^\cdot}$	Hypochlorous acid, **HOCl**
Carbonate, $\mathbf{CO3^-}$	Hypobromous acid, **HOBr**
Carbon dioxide, $\mathbf{.CO2^-}$	Ozone, $\mathbf{O_3}$
Singlet, $\mathbf{O_2\ 1\sum g+}$	Singlet oxygen, $^1\Delta\mathbf{g}$

1.6.5.2 The role of free radicals in neuropathology

Excessive production of ROS in an uncontrolled fashion significantly damages cellular macromolecules such as lipids, proteins and DNA which then cause different pathologies (Halliwell and Gutteridge, 2007). These processes of oxidation will be discussed below.

Initiation of lipid peroxidation starts due to the addition of hydrogen atom abstraction from a methylene (-NH_2-) group by reactive species which results in a carbon radical being formed. Different types of ROS affect lipids differently, for example, ozone directly oxidizes lipids by forming ozonides (Cortesi and Privett, 1972). Once carbon radicals are formed then in the next stage, and a process called propagation, starts. During this stage, carbon radicals are arranged in such a way that it forms conjugated dienes that stabilise carbon radicals. These carbon radicals then react with molecular oxygen present in the cell and produce a peroxyl radical (-$ROO^\cdot$). This continuous chain reaction produces more radicals followed by radical collision that form non-radical species. Lipid peroxidation is a well-established phenomenon in many

neurodegenerative diseases (reviewed in Barnham et al., 2004), including HD, as discussed earlier in this chapter.

Protein carbonylation can be promoted by ROS and it can happen directly or indirectly. For example, direct protein oxidation (primary protein carbonylation) of protein side chains, arginine and proline via metal-catalysed oxidation form glutamic semialdehydes, whereas lysines form aminoadipic semialdehydes and the hydroxyl group of threonine side chain oxidised and introduced carbonyl group (RR'C = O) (Stadtman, 1990). Carbonyl groups of reactive aldehydes or ketones then react to 2, 4-dinitrophenylhydrazine (DNPH) and produce hydrazine derivatives (DNP). These DNPH products are produced by secondary protein carbonylation. This happens when aldehydes were added to protein side chain residues produced during lipid peroxidation.

Proteins can also be oxidised and modify their structures in such a way that this is an essentially harmless event. For example, S-glutathionylation, S-nitrosylation and methionine sulfoxidation can protect cells both by their irreversible oxidation and their ability to act as redox regulators (Dalle-Donne et al., 2005a; Dalle-Donne et al., 2005b; Levine et al., 2000). Wong et al., (2008) suggested that protein carbonylation may be an important factor for modulation of signal transduction pathways which are linked to disease pathogenesis. Protein carbonyls are often observed in human neurodegenerative diseases, such as AD, PD, ALS (reviewed in Barnham et al., 2004) and HD (Browne et al., 1999). Under physiological conditions, proteins are produced and degraded all the time through an organised system (quality control mechanism), whereas unfolded or mildly damaged protein are sent to the UPS where they are ubiquitinated and degraded in the cytoplasm by the 26S proteasome (see section 1.6.1). Oxidatively damaged proteins tend to aggregate and these aggregates cannot be cleared by the 26S proteasome and may eventually impair UPS function (reviewed in (Dalle-Donne et al., 2006).

Oxidative DNA damage can cause gene mutations that lead to genetic instability. This instability has been proposed to lead to a number of different pathologies including cancer, heart diseases and ageing (reviewed in Ames, 1983; Harman, 1981). Under physiological conditions, DNA is quite stable, whereas under oxidative stress

conditions, ROS can cause DNA strand breakage and/or modification of DNA bases or deoxyribose (reviewed in Demple and Harrison, 1994). DNA oxidation can take place in the presence of both ROS or RNS, but approximately 1% of the oxygen consumed by the human body directly participates in ROS production, derived from molecular oxygen (Halliwell and Gutteridge, 2007). Wardman et al., (1996) has proposed that DNA can by oxidised by ROS using Fenton reactions where metals, particularly iron, catalyse hydrogen peroxide and generate the highly reactive hydroxyl radical ($OH^{\cdot}$). $OH^{\cdot}$ can bind to guanine at C4, C5 and C8 of its purine ring. The addition of $OH^{\cdot}$ at position 8 of the guanine's purine ring produces a C-8 OH adduct radical that can further oxidise and produce 8-hydroxyguanine. Hydroxyl anion radicals can also oxidise other DNA bases. Cheng et al., (1992) performed complementary bacteriophage plaque color assays to analyse mutagenic specificity of 8-hydroxyguanine *in vivo* and showed that 8-hydroxyguanine mutagenic replication of a template causes G to T and A to C substitutions.

Mitochondrial DNA undergoes damage in the same manner as nuclear DNA. Richter et al., (1988) reported that mitochondrial DNA damage was several fold greater than nuclear DNA damage in isolated and γ-irradiated rat livers. This difference between the levels of oxidative damage in nuclear versus mitochondrial DNA is thought to be due to the following reasons: 1) mitochondria are the primary source of ROS, 2) mitochondria have a relatively poor DNA repair mechanism and 3) mitochondria have a weak antioxidant defence system. Hence, numerous studies also showed mitochondrial DNA damage in the CNS in AD (Mecocci et al., 1994; Wang et al., 2005), PD (Alam et al., 1997b; Swerdlow et al., 1996) ALS (Wiedemann et al., 2002) and HD (Polidori et al., 1999).

1.6.5.3 The role of ROS in cell signalling

Uncontrolled or high sustainable levels of ROS are detrimental in living systems, whereas low levels of ROS are essential for the regulation of many physiological responses. For example, it is well established that ROS levels regulate oxygen sensing, angiogenesis, vascular tone as well as cellular differentiation, migration and growth (reviewed in Martinon, 2010).

Hence, redox signalling is an essential component of cellular functions. Signal transduction can occur via ROS, similar to stimuli such as growth factors transducing signals through protein tyrosine (or serine/threonine) kinases/phosphatases, the small G protein Ras, phospholipases, phosphatidylinositol kinase (PI3K), Ca^{2+} and various transcription factors (reviewed in Kamata and Hirata, 1999). Intracellular ROS can also be generated by various stress stimuli (oxidative stress, heat shock, cytokines, UV-radiation and anti-cancer drugs) and this activates mitogen-activated protein kinase (MAPK) pathways such as the c-Jun N-terminal kinase (JNK) pathway (Cui and Douglas, 1997; Guyton et al., 1996; Lo et al., 1996; Verheij et al., 1996; Wilmer et al., 1997), p38 MAPK pathway (Aikawa et al., 1997; Han et al., 1998; Huot et al., 1997; Moriguchi et al., 1996; Purdom and Chen, 2005) and the extracellular signal regulated kinase (ERK) pathway (Aikawa et al., 1997; Purdom and Chen, 2005; Sigaud et al., 2005). Each individual MAPK pathway has a different role in cell function (see Figure 1.11). For example, ERK is usually associated with the regulation of cellular proliferation in response to growth factors whereas p38 and JNK are associated with apoptosis in response to cell stress signal transduction. Xia et al., (1995) demonstrated that withdrawal of nerve growth factor (NGF) from rat pheochromocytoma (PC12) cells leads to the activation of JNK and p38 (JNK and P38 are also collectively called the stress activated protein kinases (SARKs)) and inhibition of ERKs which then lead to the induction of apoptosis. Dugan et al., (1997) showed that NGF withdrawal in neuronal cells presented with elevated levels of ROS and this increase was rescued upon NGF treatment. They further reported that NGF blocks ROS production in neurons via activation of the MAPK pathway. In addition to this, apoptosis signal-regulating kinase (ASK1) is a member of the MAPKKK family and activates JNK and p38 MAPK signalling pathways in response to oxidative stress (Hsieh and Papaconstantinou, 2006; Ichijo et al., 1997; Saitoh et al., 1998). Saitoh et al., (1998) performed a yeast two hybrid screen and identified that ASK1 forms an inactive complex with thioredoxin (Trx), where upon treatment with various stimuli, particularly H_2O_2, dissociate the ASK1-Trx complex and fully activates ASK1. They showed that Trx acts as a negative regulator of the ASK1-JNK-p38 pathways. On the other hand, Guyton et al., (1996) showed that treatment of various cell types with H_2O_2 stimulated many members of the MAPK family but that ERK2 was highly activated. Their study showed MAPK regulation was specific to H_2O_2 and that ERKs play an essential role in the cell survival after oxidant injury.

The signalling network between the different MAPK kinases is a good example to illustrate how the cross talk between pro- and anti-apoptotic signalling pathways determine whether a cell survives or dies in relation to ROS. It seems that low levels of ROS promote cell survival by activating anti-apoptotic pathways (AKT and ERK1/2) whereas upon high exposure of ROS, apoptotic pathways (ASK1 and SAPKs) are activated and promote apoptosis (Matsuzawa and Ichijo, 2005).

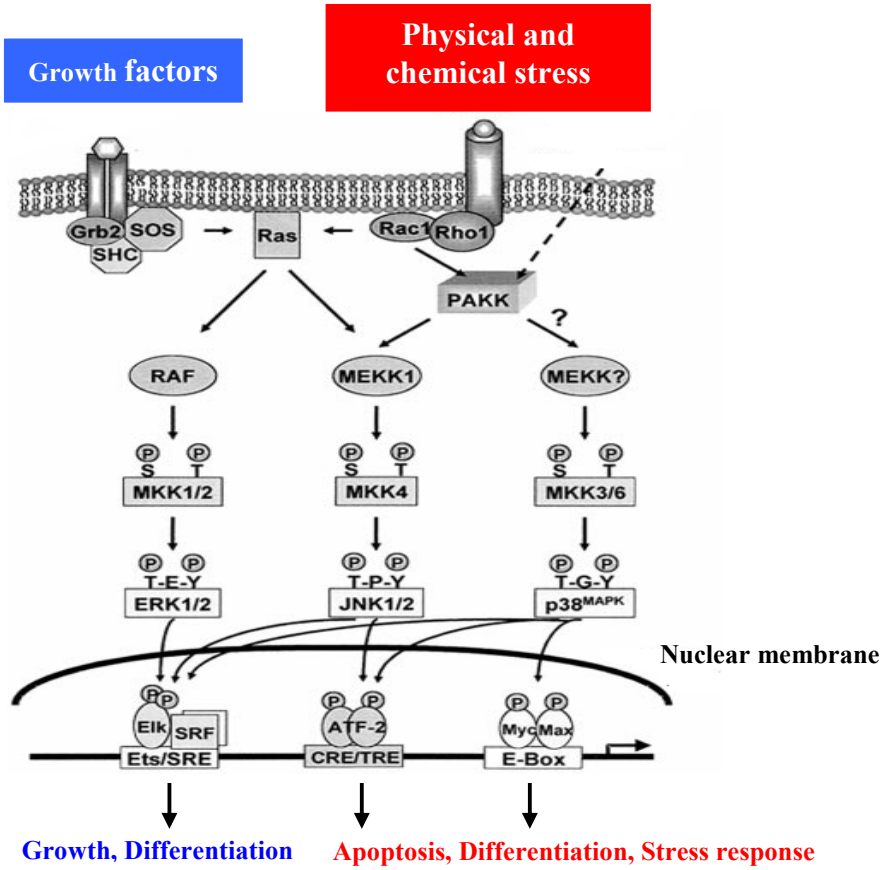

Figure 1.11 Outline of MAPK signalling pathways. ERK, JNK and p38 are three main subgroups of MAPKs. ERK is associated with cell growth and differentiation and is activated in response to growth factor and/or mild oxidative stress whereas JNK and p38 (SAPKs) are activated under increased stress stimuli such as oxidative stress, radiation, heat shock and anti- cancer drug therapy and are associated with cellular apoptosis (modified from Allen and Tresini, 2000; Matsuzawa and Ichijo, 2005).

In addition to these signalling pathways, various ROS sensitive transcriptional factors exist such as NF-*k*B, AP-1, specificity protein 1 (SP1), hypoxia inducible factor (HIF), p53, nuclear factor erythroid 2- related factor-2 (Nrf-2) and histone deacetylase 2 (HDAC2). These transcription factors are involved in the cellular pathways responsible for immune system and inflammatory responses, rapid gene

reprogramming, proliferation, survival, differentiation, growth, apoptosis, cell migration transformation, carcinogenesis, cell cycle arrest, antioxidant defence, memory and synaptic plasticity (reviewed in Lukosz et al., 2010).

ROS-mediated signal transduction during the oxidative stress response takes place by directly modulating redox sensitive transcriptional factors and kinases as mentioned above. This can occur via modification of reactive cysteines. Cysteine-rich redox sensitive proteins change in the presence of ROS and function as signalling molecules. Cysteine residues of a protein can be modified or inactivated in two different ways: 1) Protein oxidation causes an addition of one oxygen molecule at the active site of cysteine to form sulfenic acid derivates that leads to enzymatic inactivation, and this modification can be reversed under reducing conditions; 2) further oxidation leads to recruitment of one or two molecules of oxygen at the active site of the cysteine/s and as a result the formation of sulfinic or sulfonic acid occurs, respectively. This modification generally results in a permanent inactivation of the particular protein (reviewed in Groeger et al., 2009).

A classical example of how oxidative modification of protein/s can actively participate in signalling pathways in both prokaryotes and eukaryotes emanates from studies on the bacterial strain *S. typhimurium*. Christman et al., (1985) reported that *S. typhimurium* became resistant to acute oxidative stress after pre-exposure to mild oxidative stress. They identified a gene called OxyR that controls nine proteins, including five antioxidant enzymes (catalase, glutathione reductase, NAD(P)H dependant alkyl hydroperoxide reductase and MnSOD), which were consistently upregulated in a H_2O_2 resistant strain. Christman et al., (1985) also demonstrated that OxyR associates with heat shock proteins under heat shock conditions. OxyR has 6 cysteines and Kullik et al., (1995) demonstrated that one or two of these six cysteine residues are involved in OxyR activity. This study was further supported by Zheng et al., (1998) who showed that these cysteine residues form disulphide bonds that activate OxyR. Once OxyR is activated by H_2O_2, it acts as a transcriptional factor. Interestingly, there are several redox sensitive molecular chaperones that may have active signalling roles (see below, section 1.7).

1.6.5.4 Mechanisms of intracellular ROS production and evidence for redox abnormalities in HD

ROS are generated within the cell by several reactions, but perhaps mainly within the mitochondria by endogenous enzymatic reactions, (summarized in Figure 1.12 (reviewed in Sheu et al., 2006). Given that mitochondria are also central to the regulation of cell death and survival, mitochondrial ROS production is likely also crucial for redox signalling between this organelle and the the cell (reviewed in Hamanaka and Chandel, 2010). The proteins involved in the mitochondrial ETC are well-known to contribute to the production of ROS.

For example, the leakage of electrons from the ETC reacts with molecular oxygen and participates in the production of mitochondrial ROS, particularly superoxide anion radicals (Carreras et al., 1997). However, the TCA cycle enzymes, α-ketoglutarate dehydrogenase and the PYDH complex also produce superoxide anion radicals and H_2O_2 (Starkov et al., 2004). Mitochondrial superoxide anion radicals poorly penetrate through mitochondrial membranes therefore, mitochondrial MnSOD is known to catalyse superoxide anion radicals to produce H_2O_2 that passes through the mitochondrial membrane easily. Furthermore, mitochondrial monoamine oxidase produces H_2O_2 (Cohen and Kesler, 1999). There are other enzymes which participate in mitochondrial ROS production, not mentioned in Figure 1.12, for example, glycerol-3-phosphate dehydrogenase (GPDH), dihydroorotatic- and cytochrome b3 reductase (reviewed in Lin and Beal, 2006).

Xanthine oxidase and cytochrome P450 reductase are the main enzymatic sources of cytoplasmic, non-mitochondrial ROS and peroxysomal acyl-CoA oxidases also participate in H_2O_2 production (Sheu et al., 2006) . NADPH oxidase and cytochrome P450 membrane associated enzymes are further sources of ROS whereas cyclooxygenase and lipoxygenase in the presence of ROS participate in lipid-peroxidation (Figure 1.12, Sheu et al., 2006). Cytoplasmic Cu/Zn SOD actively participate in the conversion of cytosolic superoxide anion radicals to H_2O_2 which can react with Fe^{2+} to form hydroxyl radicals via the Fenton reaction (Figure 1.12). Fe^{2+} is produced in the cell by the action of superoxide anion radicals that oxidise the family of dehydratases at their active site. These enzymes contain [4Fe-4S]-clusters and upon oxidation they release Fe^{2+}. In addition to this, hydroxyl anion radicals can also

be generated through the metal catalysed Haber–Weiss reaction (Curtin et al., 2002). Myeloperoxidase can use intracellular H_2O_2 and halides to form hypohalous acids. In relation to cell damage and cell death, RNS also play a role in that nitric oxide synthase catalyses L-arginine to produce nitric oxide (NO) which may react with superoxide anion radicals to form peroxynitrite (Curtin et al., 2002).

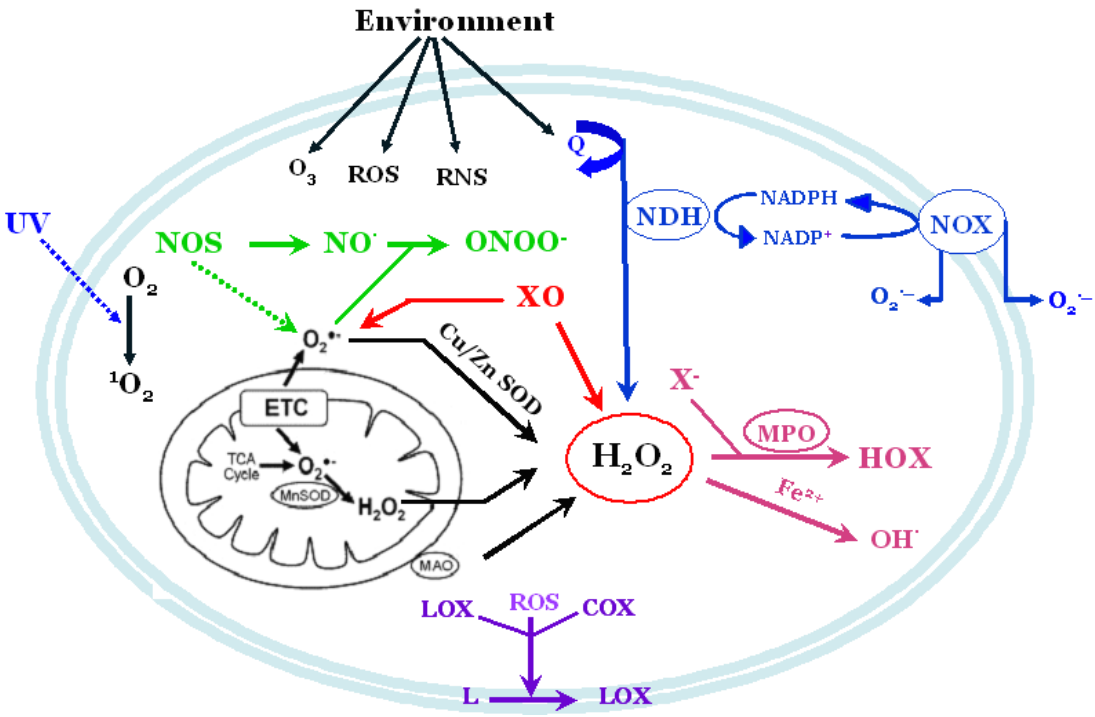

Figure 1.12 Different chemical reactions inside the cell that participate in the production of ROS. Intracellular ROS can be generated from the mitochondrial electron transport chain (ETC) and various enzymes that are associated with the cytoplasm, and plasma membrane of the cell (see text for details; modified from Sheu et al., 2006).

Hence there are many sources of intracellular ROS. A prolonged increase in the production of any such cellular RNS/ROS, for example due to increased mitochondrial activity brings an inherent risk of cellular damage (St-Pierre et al., 2006). In order to maintain cell integrity it is therefore necessary to detoxify increased ROS. ROS scavenging enzymes, such as glutathione peroxidase, glutathione transferases, glutathione reductase, catalase, Mn SOD and Cu/Zn SOD provide the first line of defence against ROS (Abid et al., 2004; Sheu et al., 2006; Warner et al., 1996; Zhang et al., 2002). These enzymes are mainly located in the mitochondria, peroxysomes, but also distributed within the cytoplasm. In addition to enzymatic components of the antioxidant defence system, there are some non-

enzymatic components including α-tocopherol, ascorbate, coenzyme Q10, cytochrome c and glutathione (reviewed in Browne and Beal, 2006a; Trushina and McMurray, 2007).

The second line of defence against ROS are the uncoupling proteins (UCPs) located in the inner mitochondria membrane. They are present in both mammals and plants and belong to the family of anion mitochondrial carriers (Rousset et al., 2004). UCPs decrease the electrochemical potential across the inner mitochondrial membrane and, as a result, shorten the half-life of many reactions in the ETC which then reduces ROS generation (Arsenijevic et al., 2000; Echtay et al., 2002).

The brain contains a high level of polyunsaturated fatty acids, which are more prone to lipid peroxidation because they hold multiple double bonds that lie between methylene groups and these groups possess reactive hydrogen. The brain is also known to have a poor antioxidant defence system compared with other body organs. For example, catalase and glutathione peroxidase have limited activity in the brain in comparison to other organs of the body (Halliwell, 1992).

So, what is the evidence for oxidative stress in HD? Mhtt is known to induce ROS in cellular models of HD. Wyttenbach and colleagues showed that mhtt caused an increased ROS production in neuronal and non-neuronal cells (Wyttenbach et al., 2002). Another *in vitro* study suggested an upregulation of genes responsible for scavenging radicals (genes of the antioxidant Nrf2-ARE pathway) in the presence of mhtt, as a protective mechanism (van Roon-Mom et al., 2008). Moreover, Giuliano et al., (2003) showed ATM/ATR-dependant DNA damage in a stable cell system of HD that could be related to ROS. More recently, Li et al., (2010) showed elevated levels of ROS in primary neurones prepared from embryos of HD knock-in mice (HD human Q140 model). They further showed that this increase was due to low levels of intracellular glutathione, an essential antioxidant.

In addition to cell models, Perez-Severiano et al., (2004) found increased levels of ROS in the brains of the R6/1 HD mouse model. This increase was observed in all ages and hence the authors suggested that ROS formation leads to onset of the disease phenotype and later on to lipid peroxidation. Bognadov et al., (2001) reported

increased levels of 8-hydroxy-2-deoxyguanosine (OH8dG) in the urine, plasma and striatal microdialysates of the R6/2 mouse. They also reported increased concentration of OH8dG in isolated brain DNA of transgenic mice at 12-14 weeks of age. OH8dG is a hydroxyl radical damaged guanine nucleotide, excised from DNA by the endonuclease repair enzyme (Mariani et al., 2005). In addition, Cevedo-Torres et al., (2009) reported increased levels of mtDNA damage in the striatum and cortex of 7-12 weeks old R6/2 mice. It has also been shown that SOD activities increased in young transgenic HD mice, but decreased in older mice, signifying perhaps that early SOD up-regulation represents a compensatory mechanism to protect cells against oxidative stress (Santamaria et al., 2001). Furthermore, genetic modifier screens and genomic studies in yeast, mammalian cells, invertebrate models (*Drosophila*) and transgenic mice in HD and other polyQ models show gene- and protein expression changes due to polyQ expanded proteins typically occurring during oxidative stress (Bahadorani and Hilliker, 2008; Giorgini et al., 2005; Hands et al., 2010b; Kita et al., 2002; Luthi-Carter et al., 2002; Perluigi et al., 2005; Wyttenbach et al., 2001; Wyttenbach et al., 2002).

Oxidative stress can cause significant DNA damage by breaking DNA strands, exacerbates lipofuscin accumulation and increases immunohistochemical staining of oxidatively damaged products in the human HD striatum and cortex (Browne et al., 1997; Polidori et al., 1999). Brown et al., (1997) showed a significant increase in OH8dG levels in the HD caudate. Human post-mortem studies demonstrated increased levels of 3-nitrotyrosine, a product of peroxynitrite-mediated protein nitration, in HD striatum and cerebral cortex (reviewed in Browne and Beal, 2006b). Furthermore, levels of hemeoxygenase and malondialdehyde (a marker for oxidative damage to lipids) is also increased in the HD brain (Browne et al., 1999). Klepac et al., (2007) reported elevated levels of lipid peroxidation and low reduced intracellular glutathione levels in asymptomatic HD gene carriers compared to their age and sex matched controls. This study suggests that oxidative stress occurs well before onset of the disease phenotype and possibly this elevated ROS may overload the cellular antioxidant defence system early during HD, hence causing irreversible oxidative damage. However, a study by Alam et al., (2000) has shown that oxidative stress might not cause as excessive damage to lipid, protein or DNA in HD, as compared to AD and PD, perhaps suggesting that the redox-alterations in HD are less severe or of

a different nature. Overall, studies on oxidative stress in the HD brain and HD cell- and animal models strongly support the hypothesis that an imbalance in redox-metabolism with increased ROS production occurs due to polyQ expanded htt. The mechanisms of abnormal ROS production however remain unknown.

1.7 Redox sensitive molecular chaperones and HD

Chaperone proteins are part of a protective mechanism against many cellular stresses, including the prevention of protein misfolding and aggregation (Hartl, 1996) and oxidative stress (Jakob et al., 1999; Morrow et al., 2000; Wyttenbach et al., 2002). As outlined in section 1.5.2.2, chaperones help other proteins to fold into their native forms and/or prevent protein aggregation (Hartl, 1996). However, there are some chaperones that are redox sensitive and their chaperone activity is only activated after exposure to oxidants (Jakob et al., 1999; Shendelman et al., 2004). Hence it is possible that during HD and indeed other proteinopathies involving oxidative stress, such redox chaperones may be activated and play a role during protein aggregation, signalling processes and the defence against oxidative stress.

1.7.1 Chaperones involved in redox-reactions and their modulation

Some chaperones of sHSP family, and others, are indeed modulated and/or activated by ROS (Graumann et al., 2001; Mehlen et al., 1996; Mehlen et al., 1997; Wyttenbach et al., 2002). There are two mechanisms that exist by which redox-chaperones function: a) by a change in the oligomerisation state (e.g. HSP25 and ABC) and b) via activation/modulation of specific cysteines through oxidation (e.g. HSP33, PDI and DJ-1). Both mechanisms will be introduced below.

HSPB1/HSP25 (human HSP27) is one of the members of the stress protein family and is ubiquitously expressed in most cells of the human body (Evgrafov et al., 2004). It is involved in the regulation of redox homeostasis and also stabilising mitochondria in cells (Arrigo, 2001; Concannon et al., 2003; Wyttenbach et al., 2002). A study by Wyttenbach et al., (2002) showed that transient overexpression of HSP27 suppresses polyQ mediated toxicity and polyQ-induced free radicals in cellular models of HD. Furthermore, Liu et al., (2007) reported that ABC provides early protection against H_2O_2-induced apoptosis in C2C12 cells by interacting with cytoplasmic p53 and prevents its translocation to the mitochondria.

HSPB5/αB-crystallin (ABC) expression levels are normally upregulated under stress conditions such as temperature and oxidative stress (Alge et al., 2002; Klemenz et al., 1991; Yaung et al., 2007). Increased levels of ABC are indeed present in neurodegenerative diseases such as AD, PD, Alexander's disease and Creutzfeldt-Jacob disease (reviewed in Horwitz, 2003) and typically found in glial cells. Mehlen et al., (1996) reported that overexpression of ABC increased the glutathione levels providing protection against TNF-α induced intracellular ROS. In addition to this, ABC binds to Cu^{2+} with close to a picomolar affinity range that leads to an increase in its chaperone activity as well as inhibition of ascorbate oxidation hence inhibiting the production of ROS (Ahmad et al., 2008).

sHSPs have the propensity to be phosphorylated in the presence of various stimuli, particularly during oxidative stress (reviewed in Gaestel, 2002). HSP27 and ABC are phosphorylated at three different serine residues (15, 78, 82, and 19, 45, 59 respectively) forming dimers or small oligomers whereas the unphosphorylated molecules form large oligomeric structures with the size range of 200 - 800kDa. It is these larger oligomers that provide cytoprotection by not only providing chaperone activity (holding of misfolded protein in a folding competent state), but also by modulating intracellular glutathione levels (Arrigo, 1998; Arrigo et al., 2007; Mehlen et al., 1997).

HSP33 is a classic redox-regulated molecular chaperone known to perform redox sensing using cysteines with a high affinity zinc motif (Graf and Jakob, 2002; Jakob et al., 1999). The zinc centre in HSP33 is folded in a stable domain and it is highly resistant to proteases. Under oxidising conditions, two intramolecular disulfide domains are formed and zinc is released. As a consequence, the process of HSP33 chaperone activity starts. *In vitro* studies suggest that HSP33 provides resistance against oxidative stress by acting as a chaperone (Graumann et al., 2001). Protein disulfide isomerase (PDI) is another example of a redox dependent molecular chaperone that contains four thioredoxin-like domains and two of these contain redox active CXXC motifs. Tsai et al., (2001) reported that PDI binds to a polypeptide chain under reducing condition and not in an oxidation state. They further suggested that PDI changes its affinity for substrate during the cycles of oxidation and reduction of its disulphide bridges.

Similar to HSP33, DJ-1 (yeast HSP31-34) is a chaperone that is regulated by ROS via cysteine oxidation (Lee et al., 2003; Wilson et al., 2003). Overall there is limited evidence on the expression and potential role of the above mentioned chaperones in HD. However, while some studies examined the roles of sHSPs and HSP33 in HD (Browne et al., 1999; Carra et al., 2008; Wyttenbach et al., 2002) a potential role of DJ-1 during HD has not been investigated, despite it being intensely studied in the context of PD (Anderson and Daggett, 2008; Bonifati et al., 2002; van Duijn et al., 2001; Waragai et al., 2006) and less so for AD (Choi et al., 2006) (see below).

1.7.2 Expression and function of DJ-1 in the CNS

DJ-1 is a redox dependent molecular chaperone that is widely expressed in the human body and ubiquitously expressed in the brain (Bonifati et al., 2003b; Shendelman et al., 2004). In human brain it is reported to be mainly expressed in astrocytes under physiological conditions (Bandopadhyay et al., 2004) whereas in the murine brain, DJ-1 is expressed in neurons as well as in astrocytes (Kotaria et al., 2005). DJ-1 is activated as a chaperone under oxidative stress conditions providing cytoprotection (Bandopadhyay et al., 2004).

DJ-1 has sequence homology with many other proteins that contain a ThiJ domain (chaperones, catalases, proteases and ThiJ kinases) as well as with members of the intracellular protease Pfp family (Figure 1.13). It is a 189 amino acid protein and was originally identified as an oncogene (Nagakubo et al., 1997). Later on, many other functions for DJ-1 were identified, for example, it acts as a regulatory subunit of an RNA-binding complex (Hod et al., 1999), is involved in androgen receptor signalling (Takahashi et al., 2001) and in male infertility (Klinefelter et al., 2002). In addition, it has also been suggested that DJ-1 has protease activity (Olzmann et al., 2004) and chaperone activity (Lee et al., 2003). A review by Da Costa et al., (2007) has described the involvement of DJ-1 with many cellular processes, such as the oxidative stress response, protein quality control, anti-apoptotic signalling, transcriptional regulation and translational control.

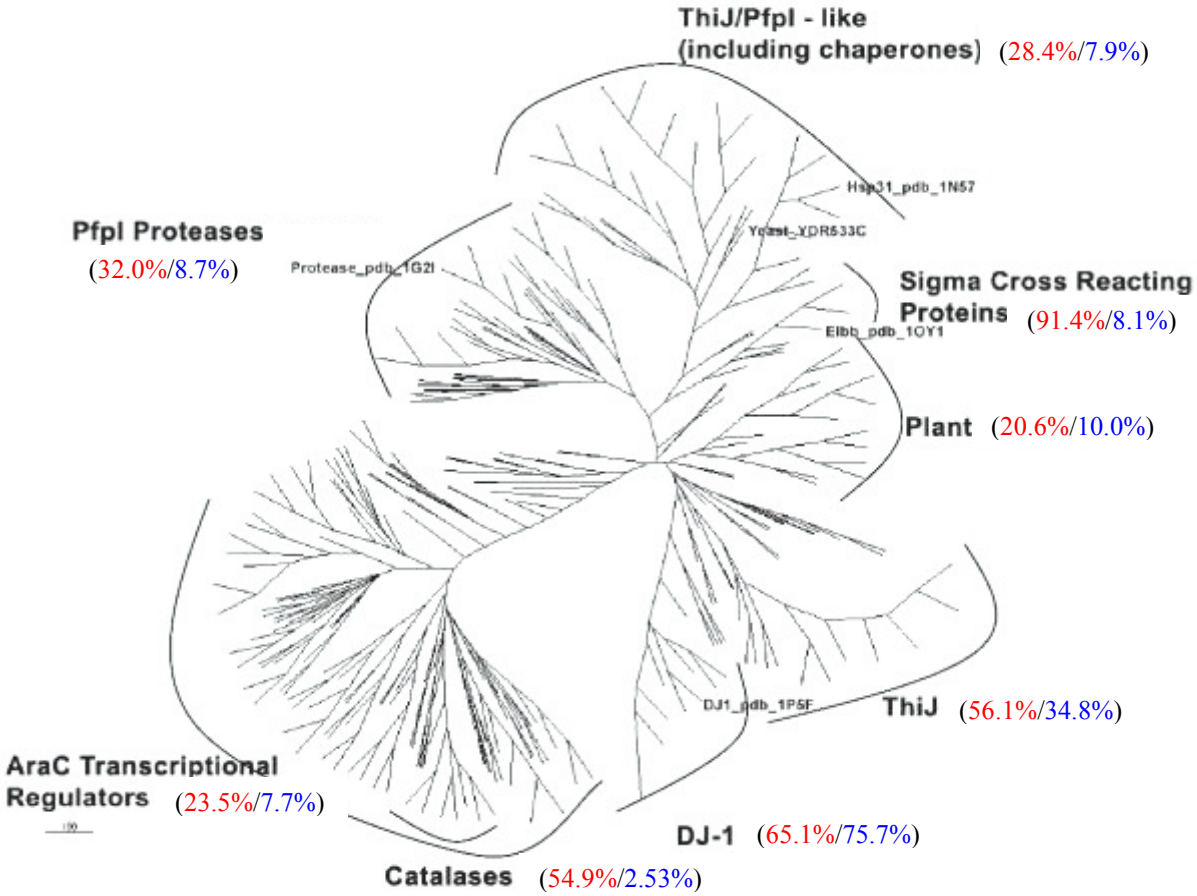

Figure 1.13 Cladogram of the DJ-1/ThiJ/PfpI superfamily.
Consensus maximum likelihood tree with branch distances corresponding to level of bootstrap support. Sequence homology between members of DJ-1/ThiJ/PfpI superfamily, the DJ-1 cluster is more similar to ThiJ subgroups as compared to others. Percentage values in parentheses represent proportion identities; the first (red) number identity % similarity within the group and the second (blue) number identity similarity with human DJ-1 (adapted from Bandyopadhyay et al., 2004).

1.7.3 Structural analysis and redox-activation of DJ-1

The structure of DJ-1 has been extensively studied and it is known to be a dimer (Honbou et al., 2003; Tao and Tong, 2003; Wilson et al., 2003) (Figure 1.14). DJ-1 has an overall α/β sandwich structure, arranged similar to the Rossmann fold- present in the members of the glutamine amidotransferase (GAT) superfamily (Cookson, 2003; Honbou et al., 2003; Horvath and Grishin, 2001; Huai et al., 2003; Tao and Tong, 2003; Wilson et al., 2003). All of these studies showed a similar overall folding pattern with slight variations. For example, Wilson et al., (2003) reported that the polypeptide chain fold of DJ-1 consists of a six stranded parallel β-sheets sandwiched

by eight α-helices with a β-hairpin on one end and a three stranded anti-parallel β-sheet at the other end. Huai et al., (2003) crystallized DJ-1 at 1.6A° resolution and reported that monomeric DJ-1 contains eight α-helices and eleven β-strands. Tao and Tong (2003) solved the DJ-1 crystal structure at 1.8A° resolution also showing 11 β-strands and 8 helices. In addition, Honbou et al., (2003) refined the DJ-1 structure at 1.95A° resolution stating that DJ-1 is a monomer composed of seven β-strands and nine α-helices in total. According to Honobou et al., (2003) an additional α-helix exists at the C-terminal of DJ-1 that is not present in other family members, except HPII, a bacterial catalase that has a similar fold of a domain. This additional helix is known to contribute in the dimer interface of DJ-1 whereas it role in the protein is unknown. Cysteine 106 (Cys106) is conserved in all of the ThiJ and DJ-1 family (Bandypadhyay et al., 2004).

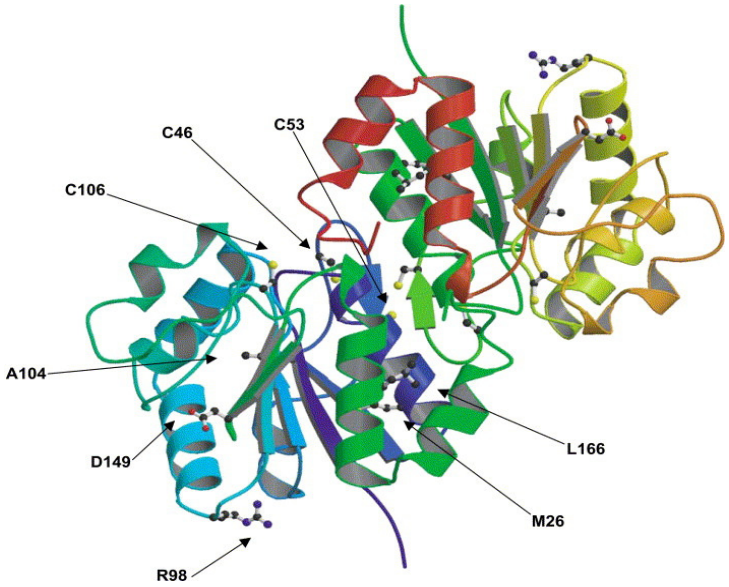

Figure 1.14 A ribbon structure of the DJ-1 dimer. Highlighted are the reactive cysteines, Cys46, Cys53 and Cys106 and mutation sites (L166, M26, R98, D149 and A104) that are associated with PD (Takahashi-Niki et al., 2004).

The crystal structure of DJ-1 exhibits three highly reactive cysteines, Cys46, 53 and 106, that are thought to participate in scavenging ROS under oxidising conditions (Figure 1.14) (Lee et al., 2003; Wilson et al., 2003). Under oxidative stress, cysteine forms three different species, cysteine sulfenic (-SOH), -sulfinic ($-SO_2H$) and -sulfonic acid ($-SO_3H$) and each of these cysteine species provide different structural and chemical properties to the protein (Blackinton et al., 2009b). Kinumi et al., (2004) showed that DJ-1 shifts its isoelectric point to an acidic form when cells were

treated with hydrogen peroxides. Many studies have shown that Cys106 was the most sensitive cysteine residue to hydrogen peroxide mediated oxidation compared to Cys46 and Cys53 (Andres-Mateos et al., 2007; Blackinton et al., 2009b; Ito et al., 2006; Kinumi et al., 2004). This is because Cys106 is known to have a low pK_a value of 5.4 and makes the highly reactive cysteine thiolate anion at physiological pH (Witt et al., 2008). On the other hand, a study by Ito et al., (2006) performed a mutagenesis analysis where all three cysteines were replaced (C46A, C53A and C106S), and showed that Cys46 and Cys53 of DJ-1, but not Cys106 were susceptible to S-nitrosylation in *in vitro* experiments as well as in SH-SY5Y cells. They also highlighted that an alanine substitution of Cys46 diminishes DJ-1 dimerization which is an essential feature of this protein (Ito et al., 2006). Many other studies suggest that replacement of Cys106 with other amino acids results in a loss of the protective activity associated with DJ-1 in *in vitro* and *in vivo* models (Aleyasin et al., 2010; Canet-Aviles et al., 2004; Meulener et al., 2005a). On the other hand, Canet-Aviles et al., (2004) showed that partial oxidation of Cys106 (cysteine-sulfinic acid) was required to exert its protective effect. Later on, Blackinton et al., (2009b) further explored the functional role of Cys106 when oxidized. They substituted glutamic acid residues with a series of amino acids to test whether changes in hydrogen bonding alter the oxidative propensity of Cys106. They observed a partial oxidation of Cys106 with two mutations, E18N and E18Q when treated with mild oxidants whereas the E18D substitution completely impaired Cys106 oxidation activity abolishing DJ-1's protective function (Blackinton et al., 2009b). Hence, they suggested that the formation of Cys106-sulfinic acid is an important modification that regulates the protective function of DJ-1 against oxidative stress. Based on the above mentioned studies, it appears that Cys106 acts as a redox switch that activates the DJ-1 protein against oxidative stress to function as a redox sensitive molecular chaperone.

1.7.4 DJ-1 and its association with neurodegenerative diseases

1.7.4.1 Loss of DJ-1 function in PD

Mutations in the DJ-1 gene are associated with rare autosomal recessive early onset PD (see Table 1.2). These single missense homozygous mutations (L166P and M26I) were observed in two European families (Bonifati et al., 2002; Bonifati et al., 2003a; Bonifati et al., 2003b; van Duijn et al., 2001). In addition, one family showed a large homozygous genomic deletion encompassing exons 1-5 which is also associated with

PD. Initially it was thought that the L166P mutation of DJ-1 may alter its cytoplasmic distribution as well as the partial sequestration to mitochondria and hence leads to a reduced DJ-1 stability making it non functional (Bonifati et al., 2003b; Macedo et al., 2003; Miller et al., 2003). Later on, multiple molecular dynamics simulation studies by Anderson and Daggett (2008) on both wild-type and L166P mutant DJ-1 at physiological temperature predicted significant structural effect/s of the L166P substitution. They showed that the L166P mutant may disrupt the α1, α5, α6 and α8 helices and critically the secondary structure of DJ-1 needed for protein stability and dimerization (Anderson and Daggett, 2008). Hence, L166P DJ-1 seems unable to form a dimer and function as a chaperone both *in vitro* and *in vivo* (Anderson and Daggett, 2008).

1.7.4.2 Expression and oxidation of DJ-1 in neurodegenerative diseases

A study by Waragai et al., (2006) quantified levels of DJ-1 in the CSF of the sporadic form of PD patients and age matched healthy controls. They showed increased levels of DJ-1 in the patients CSF compared to the control group (Waragai et al., 2006). Later on, they quantified plasma levels of DJ-1 in the sporadic PD patients, dementia with Lewy bodies and healthy age matched controls using immunoblotting and ELISA approaches. They showed that DJ-1 levels are significantly upregulated in the patients compared to control groups. They suggested that DJ-1 plasma levels can be used as a biomarker for PD (Waragai et al., 2007). A study by Choi et al., (2006) supported the above mentioned studies and showed that DJ-1 is associated with the sporadic form of PD as well as with AD. They performed immunoblotting and mass spectrometry analysis on PD and AD brain samples to show that DJ-1 expression was significantly increased. They also revealed that DJ-1 protein in the diseased brains was irreversibly oxidized by carbonylation as well as by methionine oxidation to sulfone. This study also identified 10 different types of DJ-1 isoforms both, oxidised acidic isoforms and basic isoforms - forming dimers that accumulated in the cortex of both AD and PD brains (Choi et al., 2006).

In contrast, Nural et al., (2009) found a significant reduction in DJ-1 levels in both the substantia nigra and the cortex of rapidly autopsied patients diagnosed with the sporadic form of PD as compared to a healthy age-matched control group. These

results were complemented by another study by Hong et al., (2010) also showing a significant reduction in the levels of DJ-1 and α-synuclein in patients with sporadic PD. Together therefore, the expression analysis of DJ-1 in PD is currently a matter of debate.

Morimoto et al., (2010) examined the role of DJ-1 in ALS. This study showed in a transgenic mouse model of ALS (G93ASOD1) that high levels of PINK1 and DJ-1 were present in spinal motor neurons using biochemical and histochemical approaches (Morimoto et al., 2010). Another study by Yamashita et al., (2010) also showed DJ-1 up-regulation in SOD1 transgenic mice. This study also analysed CSF collected from sporadic ALS patients and showed that DJ-1 levels were significantly higher in patients compared to healthy control group (Yamashita et al., 2010).

Perhaps the most comprehensive analysis of DJ-1 expression in α-synucleinopathies and tauopathies was performed by Neumann et al., (2004). Neumann and colleagues reported that neuronal tau IBs were immunopositive for DJ-1 in Picks disease (PiD), corticobasal degeneration (CBD), progressive supranuclear palsy (PSP) and AD. Moreover, they have observed DJ-1 glial immunopositive IBs in CBD, PSP and multiple system atrophy (MSA). Finally, DJ-1 is also associated with acute neurodegeneration, such as stroke. It has been reported in the literature that DJ-1 was upreglated in the CSF and plasma of patients within 3 hours of stroke onset (Allard et al., 2005).

Given the potentially important role of DJ-1 during chronic neurodegeneration and the evidence showing a significant increase in oxidative damage in HD brains (see 1.6.5.4) it would therefore be of interest to examine whether DJ-1 plays a role during polyQ pathology.

1.8 Aims

The mechanism(s) of protein misfolding and aggregation that lead to cellular toxicity and subsequently to neurodegeneration during proteinopathies are still unclear. However, one mechanism that likely participates in the pathogenesis of these disorders is oxidative stress as outlined in the introduction. There are many studies examining how extracellular protein aggregation is associated with oxidative stress (mainly studied in AD) (see section 1.1.1). However, it is unknown how intracellular protein aggregation causes abnormal redox homeostasis. Therefore, the aim of this thesis is to identify mechanisms involved in causing abnormal redox homeostasis associated with intracellular protein aggregation and toxicity using HD as a model disease.

As these processes have not been examined in cell systems in which the testing of cause-and effect relationships would be most amenable, my first aim was to establish several HD cell systems to model and characterise polyQ aggregation and toxicity in time course experiments. The second aim was to investigate how polyQ aggregation and toxicity relate to the production of ROS and whether it was possible to identify the potential intracellular sources of ROS. The third aim was to explore a potential role for the redox-sensitive chaperone DJ-1 in HD by analysing its expression levels in the human brain and CNS of mouse models of HD and investigate whether DJ-1 could alter polyQ aggregation and toxicity in cellular models of HD.

2 Materials and Methods

2.1 Preparation and analysis of DNA

2.1.1 Transformation of *E.coli* cells

The first step in *E.coli* transformation was to prepare the growth plates. To this end 500ml of LB agar (Tryptone 10g/L, Yeast extract 5g/L, NaCl 5g/L and Agar 15g/L) was melted, cooled down to 40-50ºC and then a 1:1000 dilution of ampicillin (100mg/ml stock concentration) was added. 20ml of LB agar media containing ampicillin was poured into petri dishes (100mm X 15mm) using aseptic techniques. 25µl of DH5α (Invitrogen, UK) cells were thawed on wet ice and gently mixed with a pipette tip. 1µl of plasmid (10-500ng) was added to DH5α cells and then kept on ice for 30 minutes. Cells were heat shocked for 15 seconds at 37ºC in a water bath. Cells were then incubated on ice for 2 minutes and then 0.9ml of pre-warmed sterilised LB media was added and incubated again at 37ºC in a water bath for 45 minutes. 100µl of media containing cells were streaked out on a plate and incubated overnight at 37ºC.

2.1.2 Purification of DNA

DNA was produced as follows: a single colony was picked from a freshly streaked ampicillin resistant plate and added to a starter culture of 5ml LB media containing 5µl of ampicillin (100mg/ml stock concentration). The culture was incubated for 6-8 hours at 37ºC on a shaker. 100µl of starter culture was then added to a flask containing 100ml of sterilised LB media with ampicillin and then incubated overnight at 37ºC on a shaker. Bacterial cells were harvested by spinning at 6000 x g for 15 minutes at 4ºC. The QIAGEN EndoFree maxi plasmid purification kit was then employed to extract the DNA as described below. The pellet was re-suspended in 10ml of buffer P1 containing RNase A. Subsequently, 10ml of buffer P2 was added and mixed thoroughly by vigorously inverting the tube 5-6 times and then incubating it at room temperature for 5 minutes. 10ml of ice cold buffer P3 was then added to the lysate, and mixed instantly and thoroughly by inverting tube 5-6 times. The lysate was then poured into a barrel of the QIAfilter cartridge and incubated at room temperature for 10 minutes. Following this the plunger was gently inserted into the QIAfilter Maxi Cartridge and the lysate was filtered into a 50ml tube. 2.5ml of buffer ER was added to the filtered lysate, mixed by inverting the tube and incubated on ice for 30 minutes. The QIAGEN-tip 500 was equilibrated by applying 10ml of buffer QBT, and the column was allowed to empty by

gravity flow. The filtered lysate was poured to the QIAGEN-tip and allow it to enter the resin by gravity flow. The QIAGEN-tip was washed with 2 x 30ml buffer QC and the DNA was eluted with 15ml of buffer QN. Eluted DNA was precipitated by adding 10.5ml of isopropanol, mixed and centrifuged instantly at 5000x g for 1 hour at 4ºC. The supernatant was carefully removed and the DNA pellet was washed with 5ml of endotoxin-free 70 % ethanol and centrifuged again at 5000x g for 30 minutes. Supernatant containing ethanol was carefully decanted and DNA pellet was dried for 5-10 minutes at room temperature. The DNA pellet was resuspended with 200µl of DNA-grade water. The DNA was also purified by using a sample miniprep kit (Stressgen, UK). DNA purified with a miniprep kit is not endotoxin-free.

2.1.3 Agarose gel electrophoresis

Agarose gel electrophoresis was used to confirm the integrity of the DNA purified as described above. 1% agarose gels were made by dissolving 0.6g of agarose in 60ml 1x Tris acetate (TAE) buffer (TAE was prepared from 50X stock (100ml/L 0.5M EDTA (pH 8.0), 2M Tris Base, 57.1ml/L Glacial Acetic acid, made up to 1 L with dH_2O) by heating in a microwave (at 40% power for 5-10 minutes). The molten agarose was allowed to cool and 3µl of ethidium bromide (10mg/ml, Fisher Scientific, UK) was added. Gels were poured into the electrophoresis chambers and gel combs were installed and were allowed to set. Electrophoresis tanks were filled with 1x TAE buffer and gel combs were taken off. Wells in the gels were washed carefully by pipetting 1x TAE buffer up and down. Samples were mixed with 6X loading dye (30% (v/v) glycerol, 60mM Tris-HCl (pH 7.5), 60mM EDTA, 0.36% (w/v) XCFF and 3.6% (w/v) Tartrazine) to achieve 1X final concentration. Samples were loaded into the wells along with a molecular marker (1Kb DNA ladder, Invitrogen, UK) in order to determine the size of DNA bands. Gels were run at 65mV for 20-40 minutes.

2.1.4 Restriction digest assay

Purified DNA was analysed by using a restriction digest approach in order to confirm httEx1Q25/Q97 insertions. 20µl of restriction digest complex was prepared by using the following amounts of buffers and enzymes.

For Q25/Q97

- 0.5µl of BamHI
- 0.5µl of Kpn I
- 10µl of DNA (0.5-1µg)
- 2µl of buffer (multicore)
- 0.2µl of BSA
- 6.8µl of dH_2O

The restriction digest was incubated overnight at 37ºC in a water bath. A 1% agarose gel was prepared and the restriction digest was run and compared with the appropriate DNA ladder (appendix 1). Plasmids were also analysed by commercial DNA sequencing (Eurofins, UK).

2.1.5 DNA constructs for expression in mammalian cells

Several plasmids were prepared as outlined above (section 2.1.2) and then used for transfection in mammalian cells (see below). The names and origin of all plasmids used are given in Table 2.1 (with the exact sequences in the appendix 2, as indicated in the table). Plasmids of each DNA preparation were sequenced before use.

Table 2.1 List of plasmids used for transfection experiments

Plasmids	**Origin**	**References**	**Sequence**
HttEx1Q25/Q72/Q97-EGFP	Drs. A. Tobin and G. Lawless University of California, Los Angeles	Wyttenbach et al., (2002)	see appendix 2
HttEx1Q25/Q72/Q97-mRFP	Dr. S. Hands University of Southampton	Unpublished	see appendix 2
Wt DJ-1	Dr. A. Khoshnan California Institute of Technology, Pasadena, California	Unpublished	see appendix 2
C106S-DJ-1	Prof. Hiroyoshi Ariga Hokkaido University, Japan	Takahashi-Niki et al., (2004) and Ooe et al., (2006)	see appendix 2
PcDNA3.1 (Empty Vector, EV)	Dr. S. Hands University of Southampton	Invitrogen, UK	-

2.2 Tissue culture

2.2.1 Trypsinisation, splitting and cell seeding

Supplemented cell media (see Table 2.2 for media composition of each cell type), 1x phosphate buffered solution (1.06mM KH_2PO_4, 155.17mM NaCl, 2.97mM Na_2PO_4-$7H_20$, PBS, GIBCO, UK) and trypsin/EDTA (0.05%, GIBCO, UK)) were pre-warmed at 37ºC. Media in the T75 cm^2 flask (Greiner, UK) containing cells (HeLa/PC12) was replaced with 10ml of PBS (without calcium and magnesium). PBS was removed and 0.8ml of trypsin/EDTA was added. The flask was subsequently incubated at 37ºC and observed after 2-3 minutes to see if the cells had dissociated from bottom of the flask. When the cells were dissociated, 10ml of supplemented media (see below) was added and cells collected in a 15ml falcon tube and spun at 1500 rpm for 5 minutes at 20ºC. The supernatant was removed and the cell pellet was resuspended with 1ml of supplemented media**.** 100µl (~10^4 cells) of cells suspension was added to a T75 cm^2 flask containing 15ml of supplemented media and then the flask was incubated at 37ºC. Cells were maintained at 37ºC (see Table 2.2 for detail) and split once a week to keep the culture stock available for each cell line.

For cell seeding, cells were trypsinised as mentioned above. For cell counting, 10µl of cells suspension was diluted into 90µl of supplemented media and the number of cells per ml was calculated by using a haemocytometer. Subsequently, a volume of cell suspension was calculated to obtain the required numbers of cells per well for 6 well or 24 well plates (see Table 2.2 for number of cells seeded per well for each cell line).

Table 2.2 Media compositions and growth conditions of various cell lines and astrocytes for transfection experiments.

Cell lines	Media composition	Maintenance conditions	Number of cells per well (transfection)	
			6 well plate	24 well plate
HeLa/ HEK293F cells	DMEM (Sigma, UK) 10% FBS, (Sigma, UK) 2mM L-glutamine (Sigma, UK) 100U/ml Penicillin and 100µg/ml Streptomycin (Sigma, UK)	37ºC, 10% CO_2 and 95% humidity	200,000 cells	30,000 cells
PC12-Tebufenozide inducible cells	DMEM (Sigma, UK) 25mM Hepes (Sigma, UK) 5% FBS (Sigma UK) 5% Horse serum (GIBCO, UK) 2mM L-glutamine (Sigma, UK) 100U/ml Penicillin and 100µg/ml Streptomycin (Sigma, UK) 100µg/ml G418 (Invitrogen)	37ºC, 5% CO_2 and 95% humidity	700,000 cells	120,000 cells
PC12-Ponasterone A inducible cells	DMEM (Sigma, UK) 5% FBS (Sigma UK) 10% Horse serum (GIBCO, UK) 2mM L-glutamine (GIBCO, UK) 100U/ml Penicillin and 100µg/ml Streptomycin (Sigma, UK) 100µg/ml G418 (Invitrogen, UK)	37ºC, 5% CO_2 and 95% humidity	700,000 cells	120,000 cells
PC12-naïve/ PC12-Tet-on inducible cells	RPMI 1640 (GIBCO, UK) 5% FBS (Sigma, UK) 10% Horse serum (GIBCO, UK) 4.5g/L D.glucose (Sigma, UK) 2mM L-glutamine (Sigma, UK) 10mM Hepes (Sigma, UK) 1mM Sodium pyruvate (Sigma, UK) 100U/ml Penicillin and 100µg/ml Streptomycin (Sigma, UK) 75µg/ml Hygromycin (Invitrogen, UK)* 100µg/ml G418 (Invitrogen)	37ºC, 5% CO_2 and 95% humidity	700,000 cells	120,000 cells
Mouse Primary Astrocytes	DMEM (Sigma, UK) 10% Hybond FBS (Hyclone, USA) 2mM L-glutamine (GIBCO, UK) 100U/ml Penicillin and100µg/ml Streptomycin (Sigma, UK)	37ºC, 5% CO_2 and 95% humidity	200,000 cells	40,000 cells

* Hygromycin and G418 were not used for PC12 naïve cells

2.2.2 Mouse astrocyte primary culture

P0 mouse cortices were dissected and the meninges were removed. Cortices were cut into small cubes (<1mm^3), suspended in 20ml of DMEM (maximum of 5 brains) and subsequently vortexed at maximum speed for 90 seconds in a 50ml centrifuge tube (Greiner Bio One) and then the cell suspension was sieved through a 40µm cell strainer (BD Falcon). Cell filtrate was mixed with DMEM supplemented by 10% Hybond FBS (characterised serum, Hyclone) and 100 U/ml penicillin with 100 µg/ml streptomycin (Sigma, UK) and seeded in a 1x T75cm^2 laminin (Sigma, UK) coated flask. Flasks were coated with 20mg/ml of laminin in 1x PBS for one hour and then the solution was removed and one flask per cerebrum was used instantly. 24 hours after seeding, the cells were washed twice with 1x PBS (GIBCO, UK) and the media was replaced. Cell media was changed every 4 days and cells reached confluency after 9-12 days. Confluent flask lids were sealed with parafilm, and shaken for 15 hours at 180 rpm in a 37ºC heated incubator. After 15 hours the media was removed and cells were washed with 1x PBS. Cells were then trypsinised with 0.025% trypsin/EDTA (GIBCO, UK) and seeded in a 6 well and/or 24 well poly-L-lysine coated plate with/ without coverslips (40,000 cells per well for 24 well plate and 200,000 cells per well for 6 well plate). These secondary cultures were then used after 3-4 days of seeding for transfection- and other studies (final age of astrocytes were normally between 15-20 days). Astrocyte cultures were characterised by Ben Samson and his results showed that >80% of cells were GFAP positive and >99% cells were connexion-43 positive (two astrocyte-specific marker proteins) hence suggesting a high astrocyte purity. These cultures did not show any microglial contamination as immunocytochemical (ICC) analysis using an antibody detecting CD68 immunoreactive cells (FA-11, Serotec, UK) did not detect microglia along side ICC analysis of microglial cells as a positive control (obtained from supernatants of cultures shaken over night after the primary culture) (Ben Samson, personal communication). Furthermore, no oligodendrocytes could be detected using an antibody detecting CNPase (Abcam, UK), a cytoplasmic, oligodendrocyte specific marker protein (Ben Samson, personal communication).

2.2.3 Transfection procedures

One day before transfection, a six well plate was seeded with the appropriate number of cells (see Table 2.2) per well with 2ml of supplemented DMEM for 6 Wells and 0.5ml of supplemented DMEM for 24 well plates. After 24 hours a 50-80% cell confluency

was achieved and HeLa/ PC12 cells were transfected (astrocytes were transfected after 3-4 days of seeding with a 70-80% confluency) by using the following amounts of DNA and lipofectamine (Invitrogen, UK) per well:

- DNA lipofectamine complex for transfection
  - For 6 well plate, Dilute 2µg DNA in 100µl of OPTI-MEM
    Dilute 4µl of lipofectamine in 100µl of OPTI-MEM
  - For 24 well plate, Dilute 0.6µg DNA in 25µl of OPTI-MEM
    Dilute 1.2µl lipofectamine in 25µl of OPTI-MEM

Diluted DNA and lipofectamine were combined, mixed and incubated for 15 minutes (Lipofectamine 2000 was used for PC12 cells and primary astrocytes). Supplemented media was removed from the cells and replaced with 0.8ml of pre-warmed OPTI-MEM (GIBCO, UK) per well in the 6 well plate (0.45ml per well for 24 well plate) pre-warmed at 37ºC in the water bath. The 0.2ml of lipofectamine-DNA complex was added per well in the 6 well plate (50µl of lipofectamine and DNA complex was used per well for the 24 well plate) and mixed gently by rocking the plate. Cells were then immediately incubated at 37ºC with 95% humidity and 5-10% CO_2 for 5 hours. After 5 hours of incubation, 1ml of DMEM supplemented with 20% FBS, L-glutamine, penicillin and streptomycin was added per well in a 6 well plate (0.5ml per well for 24 well plate) to achieve a final FBS concentration of 10%. After 24 hours of transfection, the media was replaced. The same procedure was used for the cells seeded on coverslips.

2.2.3.1 Co-transfection procedures

Cells were seeded and grown as described in the previous sections. These cells were co-transfected as follows:

- For 6 well plate, Dilute 2µg (0.5µg of httEx1Q25/Q97-mRFP with 1.5µg of DJ-1/empty vector) DNA in 100µl of OPTI-MEM
  -Dilute 4µl of lipofectamine in 100µl of OPTI-MEM
- For 24 well plate, Dilute 0.6µg (0.15µg of httEx1-Q25/Q97 with 0.45µg of DJ-1/empty vector) DNA in 25µl of OPTI-MEM
  -Dilute 1.2µl lipofectamine in 25µl of OPTI-MEM

Diluted DNA and lipofectamine volumes were then mixed, incubated and applied to cells as mentioned in the previous section. For some DJ-1 overexpression experiments in both HeLa cells and astrocytes, cells were treated with 5μM of Antimycin A or 100μM of H_2O_2 after the 5h incubation period in order to oxidise DJ-1 cysteines (e.g. Cys106) for 19 hours and fresh media was then replaced at 24 hours after co-transfection. Cells were fixed with 4% paraformaldehyde at 48 and 72 hours after co-transfection.

2.2.4 Cell death and Inclusion Body analysis

Transfected cells on coverslips were washed with 1x PBS and fixed with 4% para-formaldehyde after 24, 48 and 72 hours. Cells were stained with 1μg/ml of Hoechst (Sigma, UK) for 5-10 minutes and subsequently washed with dH_2O and coverslips (TAAB Laboratory and Microscopy, UK) were then mounted on glass slides with Fluoromount G (Southern Biotech, USA). IBs were scored by counting the total number of transfected cells with one or more IBs and this was performed in parallel to the toxicity assay. Cellular toxicity was quantified by scoring the proportion of cells with nuclear abnormalities in comparison to total number of cells expressing the transgene of interest. A cell was considered "dead" when a clear abnormal nuclear morphology was present. This was the case when cells showed either a fragmented nucleus (typical for apoptosis) or a highly condensed, shrunken nucleus as also found during necrotic types of death (Wyttenbach et al., 2000). Every experiment was performed in duplicates and 100-200 cells/coverslip were counted from 5-6 randomly chosen visual fields using a Zeiss Axioplan-2 epifluorescent microscope, unless otherwise stated.

2.2.5 CellTitre 96 AQ_{ueous} Non-Radioactive Cell Proliferation / Toxicity assay (MTS Assay)

In certain experiments involving 96 well plates the MTS assay was performed to determine toxicity. The CellTitre 96 AQ_{ueous} Non-Radioactive Cell Proliferation Assay kit (Promega) determines the number of viable cells. This assay employs a tetrazolium compound (3-(4, 5-dimethylthiazol-2-yl)-5-(3-carboxymethoxyphenyl)-2-(4-sulfophenyl)-2H-tetrazolium, inner salt; MTS) and an electron coupling reagent (phenazine methosulphate; PMS). The MTS solution and the PMS solution were thawed at room temperature and then 1ml of PMS solution was transferred to the 20ml of MTS solution bottle. MTS/PMS mixture was aliquoted into the 1.5ml eppendorf and

stored at -20ºC. The MTS is bio-reduced by cells and forms a soluble product called formazan, which is quantified by measuring its absorbance at 490 nm in an Optima plate reader (BMG Labtech).

In experiments involving the MTS assay cells were treated with 1mM H_2O_2 for 5 hours (HeLa cells) or 10mM H_2O_2 for 1 hour (Astrocytes) as a positive control. For adenovirus experiments, at 24, 48 and 72 hour of infection, 20µl of MTS/PMS solution was added into each well of the 96 well assay plate containing cells in 100µl of supplemented DMEM. Plates were then incubated at 37ºC with 95% humidity and 10% CO_2 for 1 hour followed by absorbance reading at 490 nm using a BMG plate reader.

2.3 Immunocytochemistry

Transfected cells were fixed with 4% paraformaldehyde for 15-20 minutes at room temperature and then washed 3 x 5 minutes with 1x PBS. 400µl of 0.2% Triton X100, 1% BSA (blocking agent) and 1x PBS was added to each well for 20-30 minutes in order to permeabilize cells, after which an additional blocking step with 1% BSA in 1x PBS-T was performed. Subsequently, cells were incubated with primary antibodies (see Table 2.3 for list of primary antibodies and concentrations used) for 1 hour at room temperature. Cells were then washed 2-3 times with 1x PBS. Cells were then incubated with the appropriate secondary antibody (1:500) for 1 hour at room temperature in the dark and then washed again 2-3 times with 1x PBS. Cell nuclei were then stained by incubating the cells in 1 µg/ml of Hoechst for 5 minutes. Cells were then washed again with dH_2O and allowed to dry. Finally slides were labelled and coverslips containing cells were mounted with Fluoromount G (Southern Biotech) and allowed to settle down for 12 hours at room temperature and then stored at 4ºC in the dark until analysis. All cell counting experiments (including nuclear morphology and IBs) were performed by using standard fluorescent settings on a Zeiss axioplan2 epifluorescent microscope.

Table 2.3 List of antibodies used for immunocytochemistry

Antibody	Supplier	Dilution	Species
Primary antibodies			
Anti-ACTIVE Caspase-3	Promega, UK	1:500	Rabbit
Anti-Cytochrome C	BD Bioscience, UK	1:500	Mouse
Anti-DJ-1 antibody	Cell Signaling, USA	1:200	Rabbit
Anti-DJ-1 antibody	Neuromics, USA	1:200	Rabbit
1C2 antibody	Chemicon, UK	1:500	Mouse
EM48 antibody	Chemicon, UK	1:500	Mouse
Anti-GFAP antibody	Cell Signaling, UK	1:1000	Mouse
Anti-Connexin 43 antibody	Sigma	1:1200	Rabbit
Anti-CD68 (FA-11) antibody	Serotec	1:250	Rat
Anti-CNPase antibody	Abcam	1:200	Mouse
Secondary antibodies			
Anti-mouse Alexa Flour-488	Invitrogen, UK	1:500	Donkey
Anti-rabbit Alexa Flour-555	Invitrogen, UK	1:500	Donkey
Anti-rabbit Alexa Flour-488	Invitrogen, UK	1:500	Goat
Anti-rat Alexa Fluor-555	Invitrogen, UK	1:500	Goat
Anti-mouse Alexa Fluor-488	Invitrogen, UK	1:500	Rabbit
Anti-rabbit Alexa Fluor-555	Invitrogen, UK	1:500	Goat
Anti-mouse Alexa Fluor-555	Invitrogen, UK	1:500	Goat

2.4 Confocal microscopy

A Zeiss LSM 510Meta Axioscope-2 confocal microscope was used for the following experiments: 1) Live cell imaging for ROS analysis was performed with a 40X water dipping objective and microscope settings were kept constant between cells expressing httEx1Q25-EGFP/mRFP and httEx1Q97-EGFP/mRFP in all experiments. 2) Cell samples fixed with 4% paraformaldehyde were imaged by sequentially scanning between z-stacks and LSM image browser software was used for image construction (40x and 63x oil immersion objectives). For all confocal imaging detection gains were

adjusted between experiments whereas the pin hole was set to 1 airy unit and the offset value was adjusted to 0.1% for each wavelength. (see Table 2.4 for excitation and emission spectrum ranges of fluorescent proteins and dyes used).

Table 2.4 Excitation and emission ranges of fluorescent proteins and dyes used

Fluorescent proteins/dyes	Excitation (nm)	Emission (nm)
EGFP	488	530
mRFP	543	580
DAPI	355	450
DCF	488	530
DHE	543	580
MitoTracker orange	554	576
MitoTracker deep red	644	665

2.5 Statistical analysis

Two way repeat measure analysis of variance (ANOVA) and Bonferroni post-tests were used for toxicity, dot blot and httEx1Q25/Q97-EGFP/mRFP transgene expression comparison analysis over time and comparisons deemed significant if $P<0.05$ (Graph Pad prism (version 5.0)). An unpaired (1-tailed) t-test was performed for IB formation data, cytochrome *c* release and activated caspase-3 counting data, ROS comparison (using redox sensitive dyes) between cells expressing httEx1Q25-EGFP/mRFP and httEx1Q97-EGFP/mRFP over time and DJ-1 expression analysis of different brain regions of the R6/2 mouse model and HD patients brains ($P<0.05$, Excel 2003). In addition to this, ROS data was plotted as a cumulative distribution analysis by using the computer languages, "Python" and "R" with the help of Dr. R. Edward (School of Biological Sciences, University of Southampton, UK). Graphs were plotted in R (see appendix 3 for programme code).

A paired t-test (two tailed) was performed on percentage aggregation and toxicity analysis comparisons of HeLa cells co-transfected with DJ-1/EV and httEx1Q25/Q97-mRFP (unless otherwise stated) whereas one sample t-tests were performed on percentage changes in toxicity and aggregation for both HeLa cells and astrocytes.

Similarly, one sample t-tests were performed on Western blot analysis of DJ-1 transgene expression levels in cells models of HD (Graph Pad prism (version 5.0).

2.6 Adenovirus infection

2.6.1 Infection of HeLa cells with httEx1Q25/Q97 expressing adenovirus

The AdEasy system was used for the construction of httEx1Q25/Q97-EGFP/mRFP recombinant adenoviruses. These viruses were made by assembling the httEx1Q25/Q97-EGFP/mRFP cassettes into the transfer vector and subsequently transferred into the adenovirus genome by homologous recombination. This was done by A. Wyttenbach and S. Hands (Hands et al., 2010b; King et al., 2008a).

For cell infection, cells were trypsinised, as mentioned previously, and appropriate numbers of cells in suspension were calculated by using the haemocytometer. Adenovirus was then added into HeLa cell suspensions at a dilution of 1:6000 for httEx1Q25-mRFP and 1:1000 for httEx1Q97-mRFP from a concentrated glycerol stock with a known previously determined particle titre (these concentrations were used according to a bioassay performed by A. Wyttenbach and S. Hands in the lab), incubated for 5 minutes at 37ºC and then plated out into the wells (see Table 2.5 for number of cells and volume for infection used). Plates were swirled every 10-20 minutes for 1 hour and the media was replaced after 24 hours of infection. For most experiments however, adenovirus titre concentrations were determined for new virus preparations as described below and infected by multiplicity of infection (MOI) as outlined in the text.

Table 2.5 The number of cells and volume for infection used, based on plate size.

Virus Infection (in suspension)	No. of cells per well	Volume for infectio
6 well plate	50000	1500µl
24 well plate	10000	300µl
96 well plate	10000	200µl

2.6.2 Infection of astrocytes with httEx1Q25/Q97 expressing adenovirus

Astrocytes were cultured as mentioned above and adherent cells were infected 3-4 day after seeding (see Table 2.6 for cell numbers). HttEx1Q25/Q97-mRFP expressing adenoviruses at MOI 10-20 were (see section 2.7.4 for MOI calculations) diluted to the required infection volumes for each plate as mentioned in the Table 2.6. Cells were then incubated with supplemented media containing adenoviruses and gently rocked on a shaker for 1 hour at 37ºC. Cells were then topped up with additional supplemented media and incubated at 37ºC, 5% CO2 and 95% humidity. After 24 hours of incubation media was replaced.

Table 2.6 Number of astrocytes and volume for infection used, based on plate size.

Virus Infection (Adherent cells)	No. of cells per well	Volume for infection	Top up media volume after 1 hour of infection
6 well plate	200,000	1000µl	1000µl
24 well plate	40,000	300µl	200µl
96 well plate	40,000	50µl	50µl

2.7 Purification and characterisation of adenovirus

Several adenovirus preparations were used in this study that were prepared and plaque purified. All adenovirus preparations were then bio-assayed for comparative studies (for both EGFP and mRFP tagged httEx1, see below).

2.7.1 Materials

For purification of Adenovirus the following solution were made up and pH equilibrated:

Heavy CsCl	42.23g CsCl in 57.77ml of 10mM Tris pH 8.0
Light CsCl	22.39g CsCl in 77.61ml of 10mM Tris pH 8.0
Equilibration buffer	10mM Tris pH 8.0, 1mM $MgCl_2$

2.7.2 Production of high titre adenovirus

HEK293F cells were grown and split 1:5 three days prior to infection of adenovirus from an existing stock into two 75cm^2 flasks (10µl of viral stock was used). Cells were 70% confluent on the day of infection. After 24 hours of infection cells with viral

particles were collected and frozen by using liquid nitrogen and stored at -80ºC. Cells containing viral particles were thawed and quickly frozen and thawed again, a total of three times. Cells were then spun at 4500g for 15 minutes at 20ºC and the supernatant was collected. Supernatant containing crude virus was used to infect six 150mM plates. Each plate was infected with virus in 20ml of DMEM standard growth media (described above), but containing only 5% FBS. Cells showed a cytopathic effect (CPE) after two days of infection and were then collected by washing off from the dish with a serological pipette. A cell pellet was collected by spinning at 1500 rpm for 10 minutes. The cell pellet was resuspended in 0.5ml of 100mM Tris pH 8.0 followed by three times freeze and thaw cycles in liquid nitrogen and the 37ºC water bath. Supernatant was collected after centrifuging at 2200 g for 15 minutes at 4ºC.

2.7.3 Purification of adenovirus using a CsCl gradient

10ml of light CsCl (see above) was pipetted in a 39ml Beckman tube followed by a layer of 10ml of heavy CsCl (see above) at the bottom of the tube. Cell supernatant was carefully added to the top of the CsCl gradient followed by a spin at 20000 rpm overnight at 4ºC in a SW28 rotor. A clear band of virus appeared after the overnight spin and it was carefully recovered by using 19 gauge (g) needle and 5ml of syringe. Equal volume of 10mM Tris pH 8.0 was then added to the banded virus followed by addition of another CsCl gradient in a 12ml Beckman tube (4ml of light CsCl was pipetted in a 12ml Beckman tube followed by a layer of 4ml of heavy CsCl at the bottom of the tube). Virus was then spun at 20,000 rpm for 10 hours in a SW40 rotor. The viral band was collected by using 19 g needle and a 2ml syringe. CsCl was removed from the viral prep by using a NAP-5 column (Amersham Biosciences, Sweden) that was equilibrated by using 30ml of equilibration buffer. Purified virus was loaded on the column and viral fractions were collected immediately in 1ml fraction. 10 viral fractions were collected and absorbance at 260 nm was measured for each fraction using the NanoDrop spectrophotometer. NanoDrop absorbance readings indicated concentrated viral fractions and these were pooled and 10% glycerol was added. Adenovirus was aliquoted to 15µl aliquots and stored at -80 °C. The multiplicity of infection (MOI) was calculated by using the tissue culture infectious dose 50 (TCID50) method (see section 2.7.4). Viral recombinant activity was also measured for all viruses, as described below.

2.7.4 Tissue Culture Infectious Dose (TCID50) method

One adenovirus was prepared as described in section 2.7 and five additional adenoviral preparations were obtained by A.Wyttenbach (see Table 2.7). Although all six adenoviruses were characterised and used for experiments in this study, only relevant data were obtained from httEx1Q25/Q97-mRFP expressing adenoviruses and are shown in the result section. The tissue culture infectious dose for each of these preparations was determined based on the development of the cytopathic effect (CPE) in HEK293F cells using end-point dilutions in 96 well plates. For example, to determine the TCID 50 and MOI, HEK293F cells were seeded in a 96 well plate and infected the following day by using a dilution series (10^{-6}–10^{-13}) of each adenovirus as described in the AdEasy manual (see appendix 4 as an example).

MOI was then calculated:

Ratios of positive cells per well

Dilution	**Ratio**
10^{-13}	0/10 = **0**
10^{-12}	0/10 = **0**
10^{-11}	0/10 = **0**
10^{-10}	1/10 = **0.1**
10^{-9}	3/10 = **0.3**
10^{-8}	8/10 = **0.8**
10^{-7}	10/10 = **1**
10^{-6}	10/10 = **1**

100% of the wells at a dilution 10^{-7} were positive, and 0 % of the wells at dilution 10^{-11} were positive, therefore the titre was determined by using the KÄRBER statistical method:

For 100µl of dilution,

$$\text{The titre is } T = 10^{1 + d\,(S - 0.5)}$$

Where

d = Log 10 of the dilution (= 1 for a ten-fold dilution).

S = the sum of ratios (ratios were started from 10^{-1} dilution)

= 1+1+1+1+1+1+1+0.8+0.3+0.1+0+0+0

According to the method emitted dilutions (like 10^{-1}–10^{-5}) were included in the calculation as ratios of 1

$$T = 10^{1 + 1\,(8.2 - 0.5)}$$

$$T = 10^{9.7}$$

To transform TCID50/ml in PFU/ml

$$T = 1 \times 10^{9.7}$$

It is established that the titre as measured by TCID50 is 0.7 Log higher than the titre by a standard plaque assay (this has been established by Quantum Biotechnologies, Canada)

$$T = 1 \times 10^{9.7 - 0.7}$$

$$T = 1 \times 10^{9.0}$$

MOI of 1 = No. of cells per well / PFU/ml x 1000

MOI of 1 = 150,000 cells / $1 \times 10^{9.0}$ x 1000

MOI of 1 = 0.015µL

Table 2.7 TCID50, PFU/ml and MOI values for six different httEx1 adenovirus preparations.

Types of Adenovirus	TCID50/ml	PFU/ml	MOI of 1
httEx1Q25-mRFP	$10^{10.6}$	$1 \times 10^{9.9}$	0.0189µl
httEx1Q97-mRFP	$10^{9.8}$	$1 \times 10^{9.1}$	0.119µl
httEx1Q25-EGFP	$10^{9.9}$	1×10^{9}	0.094µl
httEx1Q97-EGFP	$10^{9.7}$	1×10^{9}	0.015µl
httEx1Q25-NLS	$10^{9.2}$	$1 \times 10^{8.5}$	0.47µl
httEx1Q97-NLS	$10^{9.5}$	$1 \times 10^{8.8}$	0.24µl

2.7.5 Replication positive activity bioassay

Once all of above mentioned adenovirus MOI values were calculated the next step was to test whether these had recombinant replication activity or not. Therefore, each virus was screened for recombinant replication activity by using E1 and E3 deficient HeLa cells. Ideally, all of the recombinant adenoviruses should be deficient of E1 and E3 regions in their genome therefore they should not replicate in E1/E3 deficient cells. For this purpose, HeLa cells were seeded in six T75 cm^2 flasks (50-60% confluent) for each virus. After 24 hours of seeding, MOI of 1 for each virus was used to infect HeLa cells and media was replaced after 24 hours of infection. Cells were allowed to grow for four

days to complete their lytic cycle followed by trypsinization and collection of 10ml of supernatant media by centrifugation at 1500 rpm for 5 minutes. At the same time, HeLa cells (50-60% confluent) were seeded one day prior to trypsinization of the initial batch of infected cells. These cells were incubated with 5ml of supernatant and 5ml of fresh media for another 4 days. This procedure was repeated two more times. After a few repeats, each flask infected with different adenoviruses was observed under a fluorescent microscope to see whether they were green or red to show replication positive activity (this effect can also be observed under bright light microscope with determination of the formation of a CPE). As out of the six adenovirus preparations only httEx1Q25-EGFP showed replication positive activity, this preparation was again plaque purified for large scale virus preparation as described below.

2.7.6 Plaque purification

Plaque purification is a process whereby infection of cells begins with one virus particle followed by multiple cycles of complete infection when the released virus particles infects surrounding cells. Plaques are then formed and are visible in a monolayer with 100% confluency covered by an agarose layer (see Figure 2.1).

HEK293F (1×10^5 cells/well) cells were seeded in a 6-well plate. Cells were incubated at 37ºC for 24 hours to achieve a 80-90% confluent monolayer. Adenovirus was serially diluted by $10^{-4} – 10^{-9}$ in 1.5ml. Cell media was removed and 0.2ml of diluted adenovirus was added to each well. Plates were shaken every 15 minutes for 1 hour to spread the virus evenly over the monolayer and were kept at 37ºC. While cells were incubating, 5ml of 5% agarose (2.5 g of tissue culture graded SeaPlaque agarose in 50ml DPBS (pH 7.4)) was melted and then cooled to 44ºC. 45ml of pre-warmed supplemented HEK293F cell media was mixed with 5ml of 5% agarose. After 1 hour of incubation, viral inoculum was removed and 2ml of 0.5% of agarose solution per well was used to overlay the infected cell monolayer to prevent virus progeny from spreading to neighbouring plaques. Plates were incubated at 37ºC in a humidified 5% CO_2 incubator for 10 days, once the agarose had set.

2.7.6.1 Isolation of plaques

Cells were observed under the light and/or fluorescent microscopes to determine newly formed plaques. P200 filter tips were used to pick plaques containing adenovirus and these were transferred to a 24 well plate (one plaque/well) containing 500µl of

HEK293F supplemented media. These plaques were then incubated at 37ºC for 24 hours to elute the virus. At the same time, a 24 well plate was seeded with HEK293F cells (1 x 10^5 cells/well). After 24 hours of seeding, media was removed and 100µl of eluted virus of a single well was added and incubated for 90 minutes at 37ºC in a humidified chamber followed by addition of 900µl of supplemented media into each well. Cells were incubated again at 37ºC and 5% CO_2 for 5 days. At day 5, a complete cytopathic effect was observed and cells were collected and centrifuged at 1500 rpm for 5 minutes. Cells were then resuspended in 0.5ml PBS and lysed with three consecutive freeze-thaw cycles followed by brief centrifugation to pellet debris. Supernatant was collected and stored at -80ºC for scaling up production of adenovirus.

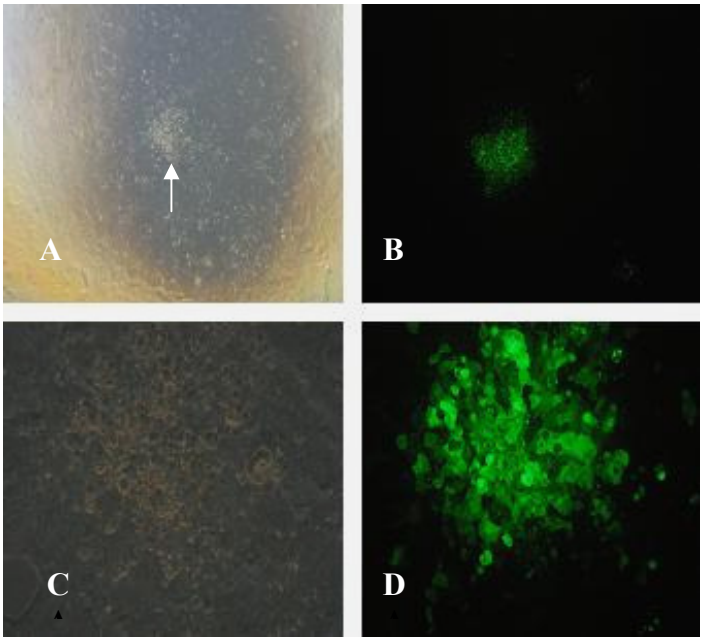

Figure 2.1 HEK293F forming plaques of httEx1Q25-EGFP.
Example of a plaque (white arrow) at bright field **(A)** and under fluorescent light **(B)** at 20x magnification and **(C)** and **(D)** show the same plaque at 63x in both conditions.

2.8 Protein extraction and Western blot analysis

2.8.1 Cell lines and astrocyte protein extraction

Protein was extracted from cells seeded and transfected as mentioned previously. DMEM was replaced with 1ml of fresh supplemented DMEM in each well and a cell scraper was used to scrape off the cells, which were then added to a 1.5ml of eppendorf (on ice). Cells were centrifuged at 4ºC for 8 minutes, at 3000 rpm. Supernatant was removed with a pump and then 1ml of ice cold PBS was added without disturbing the

pellet. Cells were centrifuged again at 4ºC for 4 minutes, at 3000 rpm. The supernatant was removed again and pellet was resuspended in 65µl of lysis buffer (1mM Tris-HCl (pH 7.5), 0.5% (v/v) NP-40, 0.2M NaCl, 0.2M EDTA, 0.5M NaF, 1M ß-glycerol phosphate, 0.2M Na-orthovanadate and 1M benzamidine). The lysis buffer for DJ-1 (cell lines and astrocytes) experiments consisted of 65.2mM Tris-HCl (pH 6.8), 2% (w/v) SDS and 10% sucrose and complete protease inhibitor cocktail. The lysate was incubated on ice for 20 minutes and then stored at -20ºC until required.

2.8.2 Protein extraction from R6/2 transgenic and wild-type mouse brain tissues

17 weeks old R6/2 tg and wt littermates were sacrificed and decapitated. Brains were removed and snap-frozen with liquid nitrogen followed by storage at -80ºC. These procedures were performed by Drs. A. Wyttenbach, V. O'Connor and S. Quraishe at the University of Cambridge where these mice were kindly provided by Prof. A. J. Morton (Department of Pharmacology). Different brain regions (cortex, cerebellum and striatum) were dissected from frozen brains on ice under a dissecting microscope and homogenised instantly in 10% w/v buffer (20mM Hepes and 100mM KCl (pH 7.4) with complete protease inhibitors). Protein samples were then stored at -20ºC until required. This protein extraction was performed by Dr. S. Quraishe at the University of Southampton and samples provided for analysis.

2.8.3 Protein extraction from human HD and control brain tissues

Pre-dissected brain regions (cortex and cerebellum) of human HD patients and control groups were kindly provided by Drs. Richard Faull (University of Auckland, NZ) and Lesley Jones (University of Cardiff, UK). Protein was extracted in pre-cooled 0.5ml tubes containing tissue which were half full of impact resistant Lysing D beads (Q-Biogene) and 400µl of ice cold lysis buffer (40mM ß-glycerolphosphate, 1mM EDTA, 1mM NaF, 50mM Tris-HCl (pH 7.5), 1% (v/v) NP-40, 120mM NaCl, 1mM Benzamidine, Antifoam (1:1000, Sigma, UK) and complete protease inhibitors). Sample group of 12 tubes were then processed in a fast preparation machine for 30 seconds (speed rotation setting of 4). Samples were than allowed to extract at 4ºC for 5 minutes followed by 3 minutes spin at 6000rpm. Samples of each tube were then split into 3-4 100µl aliquots and subsequently supernatant aliquots and beads containing tubes were frozen in dry ice and stored at -80ºC followed. These procedures were performed by Dr. A. Wyttenbach.

For DJ-1 Western analysis, human samples were extracted again by mixing soluble fraction and beads containing tissue chunks followed by the addition of 2% SDS. Samples were then boiled at 95ºC for 4 minutes followed by a quick centrifuge spin at 6000rpm for 3 minutes to remove any SDS insoluble material and beads. Similarly R6/2 tg and wild-type extracted protein samples (see above) were also re-extracted using 2% SDS. Protein concentrations were quantified using the Bio-Rad protein assay (see section 2.8.4) before storage at -20ºC.

2.8.4 Bio-Rad protein assay

Cell lysates were further diluted (1:4) to assay for protein concentration using the Bio-Rad D_c protein assay method (Bio-Rad, UK). Quantification was done against a bovine serum albumin (BSA) standard curve (0.031mg/ml – 2mg/ml). A 96 well plate was used to test all samples. A general protocol was used as provided with Bio-Rad D_c protein assay kit. Samples absorbance was read at 680nm. Equal loading of protein samples was calculated by using this assay prior to running on a SDS-polyacrylamide gel electrophoresis (SDS-PAGE).

2.8.5 SDS-Polyacrylamide Gel electrophoresis (SDS-PAGE)

The Atto protein gel system (Atto Bioscience and Biotechnology, Japan) was used for casting and running SDS-PAGE gels. 12% resolving gels and 5% stacking gels were used. The amounts of reagents used to make gels are given in the Table 2.8 below.

Table 2.8 SDS-PAGE gel recipe.
APS = ammonium persulphate, TEMED = N, N, N, N-tetramethyl-ethylenediamine and SDS = sodium dodecyl sulfate

12% resolving gel	5% stacking gel
3ml of 30% acrylamide	0.83ml of 30% acrylamide
2ml Tris, pH 8.8	0.63ml Tris pH6.8
80µl 10% SDS	3.4ml water
2.92ml water	50ul of 10%SDS
100µl of 10% APS	50µl of 10% APS
10µl TEMED	5µl of TEMED

TEMED was used to polymerise gels and was added just before pouring the resolving and stacking gel. Firstly, resolving gels were poured and overlaid with water until the gels polymerised. The water was removed completely by using Whatman's paper. Secondly, stacking gels were poured onto the resolving gels. Gel combs were inserted immediately after pouring the stacking gels and allowed to polymerise. Gel seals were taken off and washed carefully with distilled water and were placed into a gel tank containing 1 x running (Laemmlli) buffer (5mM Tris (pH 8.3), 192mM glycine, 0.1% SDS) and gel combs were removed. Loading wells were washed by pipetting running buffer in and out. 5x Sample buffer (10% SDS, 50% Glycerin, 25% ß-mercaptoethanol, 312.5mM Tris (pH6.8), 0.005% Bromophenol blue dye) was added to the samples to achieve a 1x concentration (15µg of total protein was loaded in each well, unless otherwise stated). Samples were then heated at 94ºC for 2 minutes and spun at 13000 rpm for 2 minutes at room temperature prior to loading. Samples and 10µl of pre-stained protein marker (Cell Signaling) were loaded into the wells. Gels were run at 30mA until the dye passed through the stacking gel. The current was subsequently increased to 60mA and gels were allowed to run until the dye exited the resolving gels.

2.8.6 Coomassie staining

Gels were soaked with 50ml of Coomassie blue stain (50% methanol, 10% acetic acid and 0.25% coomassie blue in dH_2O) for 1 hour at room temperature to visualise protein. Subsequently, gels were destained in destaining buffer (10% methanol, 10% acetic acid and 80% dH_2O) until bands appeared clearly. Gels were then scanned at 700nm to visualise and quantify total protein content in each lane by using an Odyssey Infrared Scanner (Li-COR, Biosciences) and Odyssey v1.2 software. Intensity values from boxed area for each lane were quantified by subtracting background pixel intensity value from the pixel intensity of the lane. Lanes were normalised to one another based on calculated intensity values and the ratios were used to normalise the measured intensity for each antibody labelled protein band (Gray et al., 2009).

2.8.7 Semi-dry protein transfer

Whatman's blotting paper and nitrocellulose membranes were soaked in transfer buffer (39mM glycine, 48mM Tris base, 0.037% SDS and 20% methanol). Each gel was layered between blotting papers and a nitrocellulose membrane as shown in Figure 2.2.

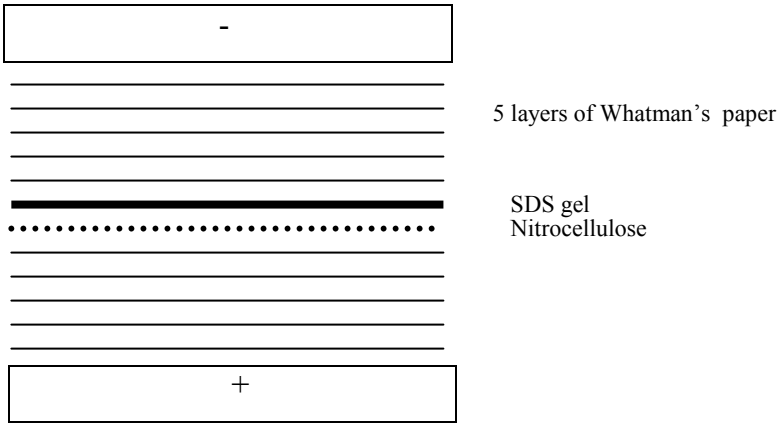

Figure 2.2 The setup for semi-dry protein transfer.

The surface area of the gel was measured and multiplied by a 1.54 to find out the required current in milli Amperes (mA) for protein transfer. For example, if the surface area was 8cm long and 6cm wide therefore, 8 x 6 x 1.54 = 73.92 mA current was applied for 90 minutes. Protein transfer was confirmed by staining the membranes in 0.1 % Ponceau Red for 10 minutes and then washed with dH_2O. Nitrocellulose membranes were scanned by using a lab scanner (Cannon).

2.8.8 Antibody labelling

Nitrocellulose membranes were blocked with 4% milk powder dissolved in 1 x TBS (10mM Tris and 150mM NaCl (pH 7.5))-0.1% Tween (1x TBS-T) for 30 minutes at room temperature. Membranes were washed with 1x TBS-T for 2 x 5 minutes and then incubated with primary antibody for 1 hour at room temperature or 4ºC for overnight with shaking. Membranes were washed in 1 x TBS-T for 3 x 10 minutes and then incubated with suitable fluorescent or horseradish peroxidase (HRP) secondary antibody for 1 hour at room temperature or overnight at 4ºC with shaking (see Table 2.9 for a list of antibodies used). The membranes were then washed in TBS-T for 3 x 10 minutes at room temperature with constant shaking. Fluorescent secondary antibody labelled membranes were scanned with a Li-COR scanner at 700 or 800nm (depending on antibody) and quantified by using Odyssey v1.2 whereas HRP labelled membranes were analysed by using the Enhanced Chemiluminescence (ECL) Method as described in the manufactures handbook. Image J was used to quantify ECL blots.

Table 2.9 List of antibodies used for Western blot analysis.

Antibody	Supplier	Dilution	species
Primary antibody			
S830	G. Bates (King's College, London, UK)	1:5000	Sheep
Anti-α-tubulin	Sigma, UK	1:5000	Mouse
Pan actin	Cell Signaling, USA	1:1000	Rabbit
EM48	Chemicon, UK	1:1000	Mouse
Anti-DJ-1	Cell Signaling, USA	1:1000	Rabbit
Anti-DJ-1	Neuromics, USA	1:2500	Mouse
Anti-Ox DJ-1	Serotec, UK	1:50	Human
Anti-ß-actin	Abcam, UK	1:500	Rabbit
Anti-Catalase	Sigma, UK	1:5000	Mouse
Secondary antibody			
Anti-rabbit 680	Rockland, USA	1:2500	Goat
Anti sheep 680	Invitrogen, UK	1:10,000	Donkey
Anti-rabbit 800	Rocklands, USA	1:10,000	Sheep
Anti-sheep 800	Invitrogen, UK	1:10,000	Donkey
Anti-mouse 800	Rocklands, USA	1:10,000	Goat
Anti-mouse HRP	Vector, UK	1:10,000	Horse
Human $F(ab')_2$ HRP	Jackson Immunoresearch, USA	1:5000	Goat
Anti-rabbit HRP	Vector, UK	1:10,000	Goat
Anti-sheep HRP	Jackson Immunoresearch, USA	1:10,000	Donkey

2.9 Dot blot analysis

HeLa cells were transfected with httEx1Q25/Q97-EGFP and mRFP and cell lysates were collected at 24, 48 and 72 hours by using the following protocol. Cells were washed with 2ml of PBS, trypsinised, collected in a 15ml centrifuge tube and centrifuged at 1500 rpm for 5 minutes. Supernatant was removed and the cell pellet was resuspended in 1ml 1x PBS and 1% FBS and transferred to 1.5ml eppendorf. Cells were centrifuged again at 2500rpm for 5 minutes and supernatant was removed. Cells were then lysed in 100µl of dot blot lysis buffer, (50mM Tris-HCL (pH 8.8), 100mM NaCl, 5mM $MgCl_2$, 0.5% w/v NP-40, 1mM EDTA and 1 tablet of complete protease inhibitor (Roche, UK) per 10ml) and incubated on ice for 20 minutes. Cell lysate was stored at -20ºC. Cells lysates were then thawed and spun at 13000 rpm and 4ºC for 8 minutes. Supernatant (soluble protein fraction) was transferred to another tube and used to determine the soluble protein concentration by using the Bio-Rad protein assay

(section 2.8.4). Cell pellets were washed in 1x PBS and incubated with 100µl of DNase I (0.5 mg/ml DNase I in 20mM Tris-HCl, pH 8.0 and 15mM $MgCl_2$) for one hour at 37ºC and after 1 hour pellets were triturated using p200 and further incubated at 37ºC for 30 minutes. Cell pellets were quenched by adjusting the mixture to 20mM EDTA, 2% (w/v) SDS and 50mM DTT solution and boiled at 95ºC for 5 minutes. Then 25µg of each sample was diluted into 300µl of 2% SDS. In the co-transfection experiments, 50µg of sample was diluted in the same SDS buffer. 100µl of the diluted samples were then further diluted into 100µl of 2% SDS in order to blot the samples at two fold dilutions. Samples were then loaded onto a Bio-Rad 96 well dot blot apparatus containing nitrocellulose acetate membrane (membrane was soaked with 2% SDS prior to use, pore size 200nm). Samples were passed through the membrane by suction and washed twice with 0.1% SDS followed by incubation with 3% skimmed milk in 1x TBS as blocking buffer for non-specific antibody binding. The membranes were then incubated with S830 primary antibody (for 1 hour at room temperature) and then the appropriate secondary antibody was applied for 1 hour at room temperature (Table 2.9). The dot blot membrane was finally developed using ECL. For co-transfection experiments the methods were the same as those described above for HeLa cells with the following exceptions. Astrocytes were co-transfected with DJ-1 or empty vector and httEx1Q25/Q97-mRFP with or without 5µM Antimycin A or 100µM H_2O_2 and 50µg of total insoluble material was used.

2.10 Measurement of ROS using live cell analysis

2.10.1 ROS analysis using confocal microscopy

Two dyes (Dihydroethidium/DHE and 5-(-6)-chloromethyl-2', 7'-dichlorodihydrofluorescein diacetate acetyl ester/CM-H_2DCFDA) were used to measure ROS in living cells.

HeLa and PC12 cells were both seeded and transfected in 35mm dishes (200,000 cells/35mm dish for HeLa cells and 700,000 cells/35mm dish for PC12 cells) with the httEx1-EGFP plasmids. After 24, 48 or 72 hours of transfection, supplemented media was replaced with 1ml of fresh DMEM containing 5µM DHE and incubated for 20 minutes at 37ºC with 95% humidity and 10% CO_2. Cells were subsequently washed three times with DMEM (without serum, L-glutamine and penicillin/streptomycin) and 2ml of DMEM was added. Cells were then analysed under the confocal microscope by

taking 6-8 images from randomly chosen fields and pixel intensities of the oxidised dye in cells expressing transgenes were quantified by using Metamorph software. Quantified pixel intensity measurements of each cell were normalised by area and this was performed by above mention software (see Figure 2.4). DHE is a non- fluorescent compound. Once it diffuses into the cell through cell membranes, it reacts relatively specifically with the superoxides to form a fluorescent end product called ethidium (Figure 2.3B) (Wilhelm et al., 2009). For experiments using the stable PC12 line (see result section 4.3.4), httEx1Q25/Q103-EGFP expressing cells were induced with 1µM of tebufenozide (Sigma) and at the appropriate time washed as described above and incubated with 5µM of DHE for 20 minutes. Cells were imaged and analysed as described above.

CM-H_2DCFDA is a derivate of fluorescein that diffuses into cell cytoplasm where esterases deacetylate CM-H_2DCFDA, which is further oxidised by many different ROS species (hydrogen peroxide, hydroxyl radicals and peroxynitrite) and forms a deacetylated oxidised product, DCF (Figure 2.3A) (Wyttenbach et al., 2002). 8µM of CM-H_2DCFDA was used for all experiments and cells were incubated for 20 minutes to image ROS in HeLa and PC12 cells after transient transfection of httEx1Q25/Q97-mRFP as mentioned above. Both DCF and DHE conditions used in ROS assays were initially optimised by Drs Hands in the Wyttenbach lab. A schematic for measuring ROS after transfection or induction of httEx1 is outlined in Figure 2.4.

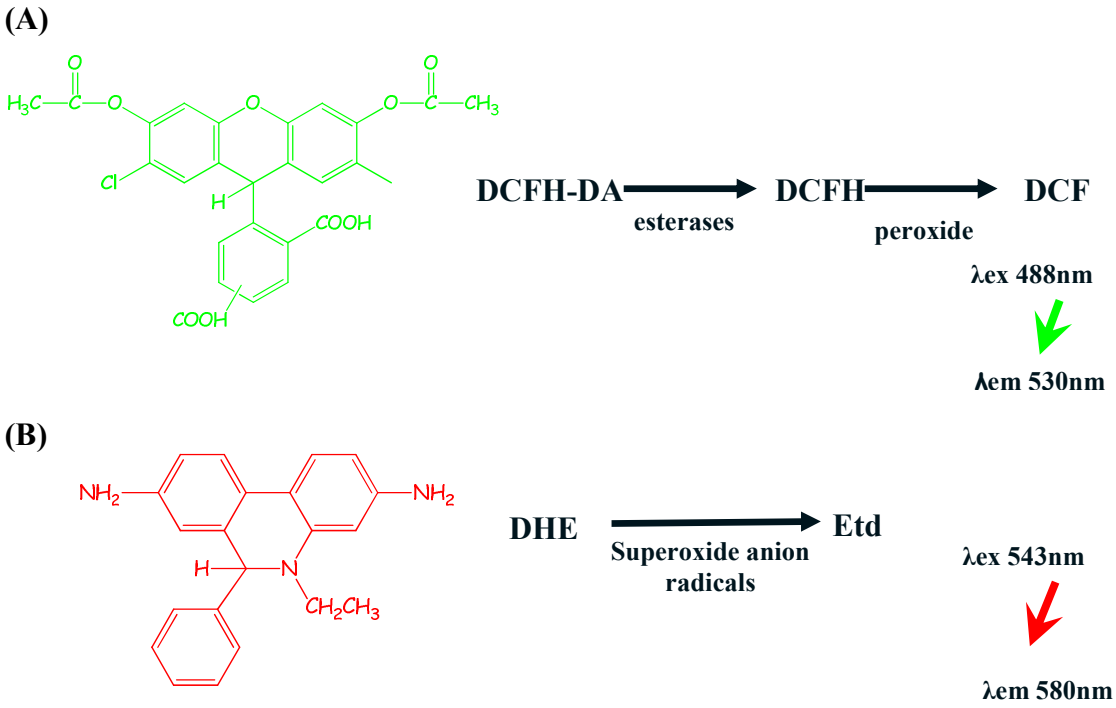

Figure 2.3 The mechanism of action of the redox sensitive dyes.
(A) DCFH-DA diffuses into the cytoplasm where cellular estrases deacetylate DCFH-DA into DCFH which can then further oxidised by peroxide and forms the green fluorescent end product, DCF (excitation/emission range: 488/530nm). **(B)** Similarly, DHE is specifically oxidised by superoxide anion radicals to form the bright red fluorescent end product, Etd (excitiation/emission range: 543/580nm).

In order to identify the origin of ROS, cells were treated with MitoQ (20nM) and, in parallel, with the triphenylphosphonium cation (TPP^+) (20nM) for seven days. Supplemented media (without MitoQ) was then added one day prior to transfection with httEx1Q25/Q97-mRFP and a ROS assay was performed 24 hours after transfection as mentioned above. MitoQ is a ubiquinone and accumulates within mitochondria driven by a conjugated TPP^+ (Figure 2.5). Once it is recruited into mitochondria it is reduced to its active form (ubiquinol) and is known to prevent mitochondrial induced oxidative stress (Kelso et al., 2001).

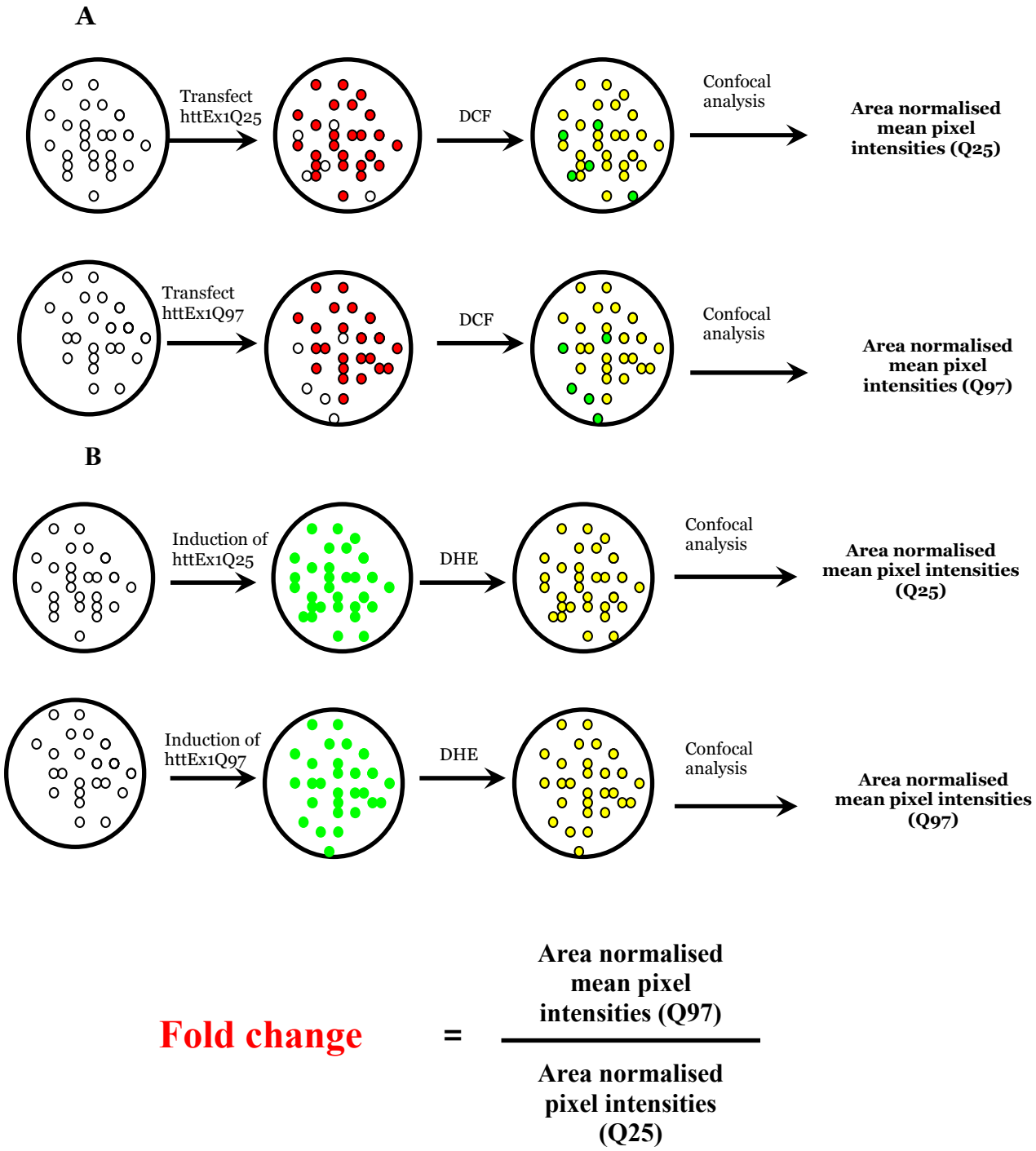

Figure 2.4 The approach to measure free radicals by using oxidative sensitive dyes in transient and stable cell systems. **(A)** HeLa and PC12 cells were transiently transfected with httEx1-mRFP constructs (red circles) and incubated with DCF (yellow circles, green circles: untransfected cell). **(B)** PC12 inducible cells expressing httEx1-EGFP (green dots) were incubated with DHE (yellow circles). Live cells were imaged with confocal microscope and area normalised pixel intensity values were calculated. Fold change in the oxidation of dye was calculated by dividing area normalised pixel intensities of cells expressing httEx1Q97 over cells expressing httEx1Q25.

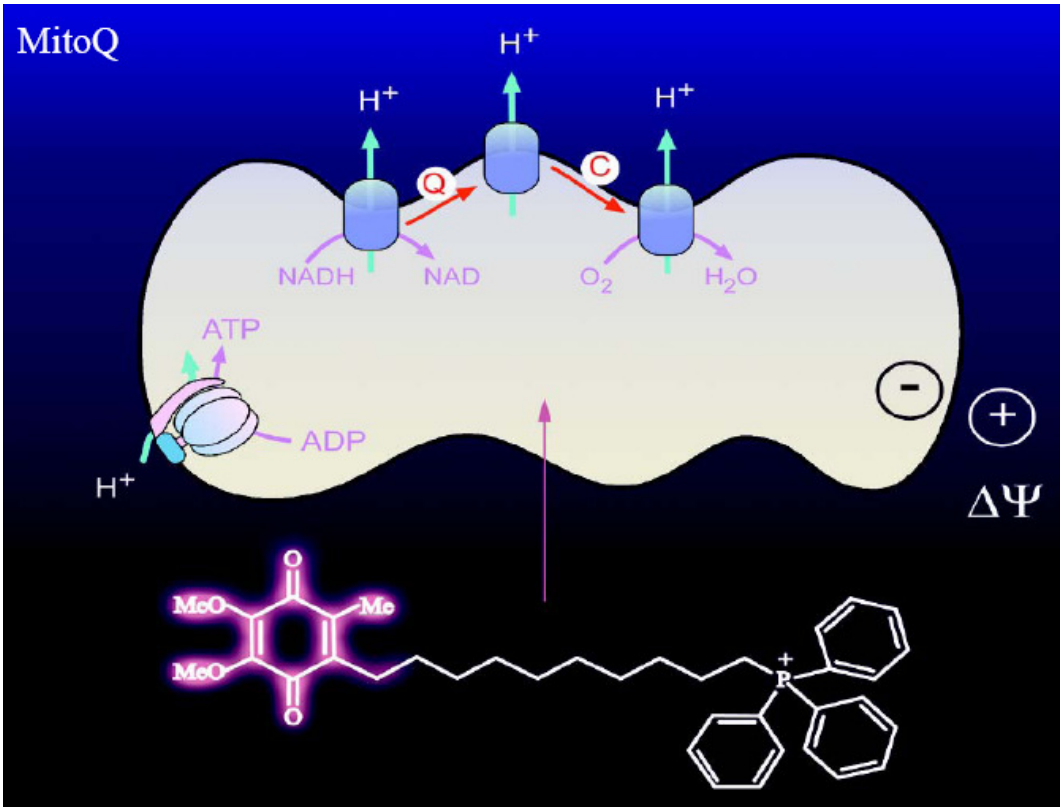

Figure 2.5 The mechanism of action of MitoQ. MitoQ covalently attached with a lipophilic triphenylphosphonium cation. The cation accumulates within cellular mitochondria due to high mitochondrial membrane potential and provides protective effect (adapted from Kelso et al., 2001)

2.10.2 Development of a ROS assay using a plate reader

A plate reader ROS assay was developed and optimised under different conditions using HeLa cells and the DCF dye. HeLa cells were seeded with three different cell densities (10,000, 20,000 and 30,000 cells per well in quadruplicate). For each cell density four different concentration of DCF (1, 10, 20 and 30μM) were used to determine the best concentration at which a relatively high DCF signal was produced with the least background. The incubation time was also optimised by incubating HeLa cells for different lengths of time. From these experiments it was found that a 30 minutes incubation was optimal. In addition to this, HeLa cells incubated at the above-mentioned concentrations and were then treated with H_2O_2 to optimise and test the correct concentration at which sufficient DCF is recruited by cells and oxidized upon further oxidative stress. Moreover, the number of cell washes, after DCF incubation, were also thought to be a factor that could alter the signal to noise ratio therefore cells

were washed 1-4 times and results revealed no major difference in DCF signal associated with the number of washes. Thus it was decided to wash twice after incubation with DCF. The conditions established via this optimisation protocol (and optimization assays previously performed by Dr. S. Hands) were then used for all other cell lines and dyes. For all PC12 inducible cell line experiments 100,000 cells per well in a 96 well plate were used.

Different cell models were used to study ROS using a BMG plate reader with fluorescent detection capability. As only results of the cell line 14A2.5 are relevant to the present study these conditions are given as follows: 100,000 cells/well of 14A2.5 cells were seeded in quadruplicate for each time point in black 96 Wells plate (Greiner Bio-One, UK). 24 hours after seeding, cells were induced with 5µM of ponasterone A. After 6, 12, 24 and 48 hours of induction, cells were incubated with 5 µM of DHE (using Hank's Buffer Salt solution, HBSS (Sigma, UK)) for 30 minutes followed by 2 washes with 100µl of HBSS per well and pixel intensities were read using the plate reader. For this particular experiment, uninduced cells were used as a control. Mean fold change in ROS was calculated as mentioned previously.

2.11 DJ-1 protein biochemistry

2.11.1 Mass spectrometry

Mass spectra were recorded on an LCT^{TM} (Waters, UK) orthogonal acceleration time-of-flight mass spectrometer fitted with a nanoelectrospray source. 4µl of 50pmol/µl, desalted (see section 2.11.2 for protein desalting) DJ-1 eluted in methanol/distilled water/formic acid ($CH_3OH/dH_2O/HCOOH$ (10:9:1)) mixture, was loaded into borosilicate capillaries (1.2mm o.d. x 0.69mm i.d.) (Clark Electromedical Instruments, UK) that had been drawn to a fine tip using a microelectrode puller (Narishige, Japan) and sputter coated with gold/palladium. Spectra were recorded in the positive ion mode between 500-1500 m/z using the following instrument settings: capillary 1318V, sample cone 36V, extraction cone 8V, source temperature 50ºC. Typically, 100 spectra were combined and deconvoluted using the maximum entropy algorithm MaxEntTM (Micromass, Altrincham, UK) to give relative molecular mass spectra over the range 5000 - 45000 daltons (Da) at 1 Da resolution. Spectra were externally calibrated using NaI/CsI spectra recorded under identical conditions immediately after each sample.

2.11.2 Protein desalting

DJ-1 (Abcam, UK) desalting was done on a micro-column made from Poros R2 resin (Perceptive Bioscience) packed in the tip of a pulled borosilicate glass capillary (1.2mM o.d. x 0.69mM i.d.) (Clark Electromedical Instruments, UK). 4µl of DJ-1 (stock solution, 1 mg/ml) was diluted with 4µl of 50mM Tris buffer (pH 8.0) and applied to the column by pipetting into the capillary with a fine gel-loading tip followed centrifuging for 20s in a microcentrifuge equipped with a home manufactured capillary holder. Using the above centrifuging method, the resin was washed with ddH2O (3 x 5µl) and the protein was eluted with CH3OH/dH2O/HCOOH (10:9:1) mixture directly into the nanospray capillary. Both mass spectrometry and protein desalting procedures were performed with the help of Neville Wright at the School of Biological Sciences, University of Southampton.

3 Characterisation of HD cell models to study protein aggregation, free radicals and toxicity

3.1 Introduction

Many cellular and animal models (e.g. *Caenorhabditis elegans*, *Drosophila melanogaster*, mice, sheep and rats) of HD have been developed to date (Faber et al., 1999; Jacobsen et al., 2010; Mangiarini et al., 1996; Marsh et al., 2003; von et al., 2003; Wyttenbach et al., 2000) and each system has its own advantages and disadvantages to model a particular aspect of HD.

As mentioned in the previous chapter, my overall aims are to study and elucidate the mechanisms involved in impaired redox homeostasis associated with intracellular aggregation and also to identify potential modulators of ROS and aggregation in HD. In order to perform these studies, cell models of HD were a preferred choice. Cells are easy to handle, cost- and time efficient and ideal for mechanistic studies that may be more complex to perform in *in vivo* models. Furthermore, cells expressing mutant htt or fragments of htt present with a robust aggregation and toxicity phenotype and can readily be applied to compound testing.

Various studies *in vitro* (Scherzinger et al., 1997), in cell models (Martindale et al., 1998) and in the HD brain (DiFiglia et al., 1997) support the hypothesis that full length htt is cleaved at it's N-terminus and that the various fragments produced from such cleavage events, including Exon 1, are toxic and tend to produce intracellular aggregates. This hypothesis was further supported by studies which showed that human htt has active cleavage sites for caspase-3 and -6 as well as calpain *in vitro* (Lunkes and Mandel, 1998; Sawa et al., 2005; Wellington et al., 1998) and in the post-mortem brain tissue (Kim et al., 2001). Recently, Landles et al., (2010) performed a proteolytic cleavage map analysis on mhtt in the Hdh Q150 knock-in mouse model of HD and reported that the smallest cleavage unit is Exon 1.

So far, various httEx1 cell models have been established that seem to recapitulate the major pathological features of HD (Aiken et al., 2004; Apostol et al., 2006; Lunkes and Mandel, 1998; Wyttenbach et al., 2000). Hence, it was decided to establish and

characterise several cell models expressing an N-terminal fragment of htt (Exon1), httEx1, with or without expanded polyQ stretches using cell lines of neuronal and non neuronal origin that were either transiently transfected with different lengths of glutamine repeats within httEx1, or that could be induced with steroid compounds or antibiotics in stable cells systems. Additionally, adenovirus mediated expression of httEx1 was used for some studies.

In this chapter cell models expressing httEx1Q25/Q97 constructs fused with two different fluorescent proteins (EGFP or mRFP) have been characterised. The reason of using two constructs tagged with different fluorescent proteins was that in the later described ROS studies (see Chapter 4) redox sensitive dyes were used that are oxidised in the presence of ROS and visualised under different excitation/emission spectra's. For example, for 5-(and-6)-chloromethyl-2',7'-dichlorodihydrofluorescein diacetate-acetyl ester (CM-H2DCFDA) the excitation/emission range is 488/530nm (blue light range), whereas the excitation/emission range of dihydroethidium (DHE) is 543/580nm. Therefore httEx1-transgenes fused to different fluorescent proteins could be matched with redox dyes absorbing/emitting in non-overlapping light ranges.

3.2 Aim

The aim of this chapter was to establish different cell systems in order to model polyQ aggregation and toxicity in time-course experiments that could then be used, in a second step, to measure changes in redox homeostasis in order to understand the relationship between these processes.

3.3 Results

3.3.1 Comparable transgene expression of httEx1Q25/Q72/Q97 fused with EGFP and mRFP

In order to perform toxicity, aggregation and ROS analysis it was first necessary to compare the expression levels of the various httEx1 constructs fused to two different fluorescent proteins (EGFP and mRFP). To obtain comparable results for each construct it was important to carefully control the amounts of DNA used for transfection. Thus a Nano drop ND-1000 UV-Vis Spectrophotometer was used to calculate the DNA concentrations and DNA gels were run to confirm equal concentration of each httEx1 construct prior to transfection (data not shown).

To test the transgene integrity of the various EGFP and mRFP plasmids and whether comparable expression levels could be obtained, HeLa cells were transiently transfected with httEx1Q25/Q72/Q97-mRFP and EGFP constructs and cell lysates were collected at 24, 48 and 72 hours after transfection. A Bio-Rad protein assay was performed to measure the total soluble protein fraction and 15 µg of protein was loaded into each well of SDS-PAGE gels. Western blots immunoprobed with S830 antibody raised against exon-1 show polyQ length dependent band sizes for httEx1Q25/Q72/Q97-EGFP/mRFP (Figure 3.1A and 3.2A). Coomassie gels run in parallel confirmed equal protein loading (Figure 3.1B and 3.2B). Figure 3.1A shows a polyQ length dependent cleavage product in cells expressing httEx1Q72 and Q97-mRFP whereas no such cleavage products were observed in cells expressing httEx1Q72 and Q97-EGFP (Figure 3.2A). As re-probing of the membranes with pan actin and α- tubulin did not show consistent results (data not shown), an antibody against catalase was used to additionally control for loading. Catalase immunoreactivity appeared to not be affected by expression of the various polyQ constructs in HeLa cells (data not shown).

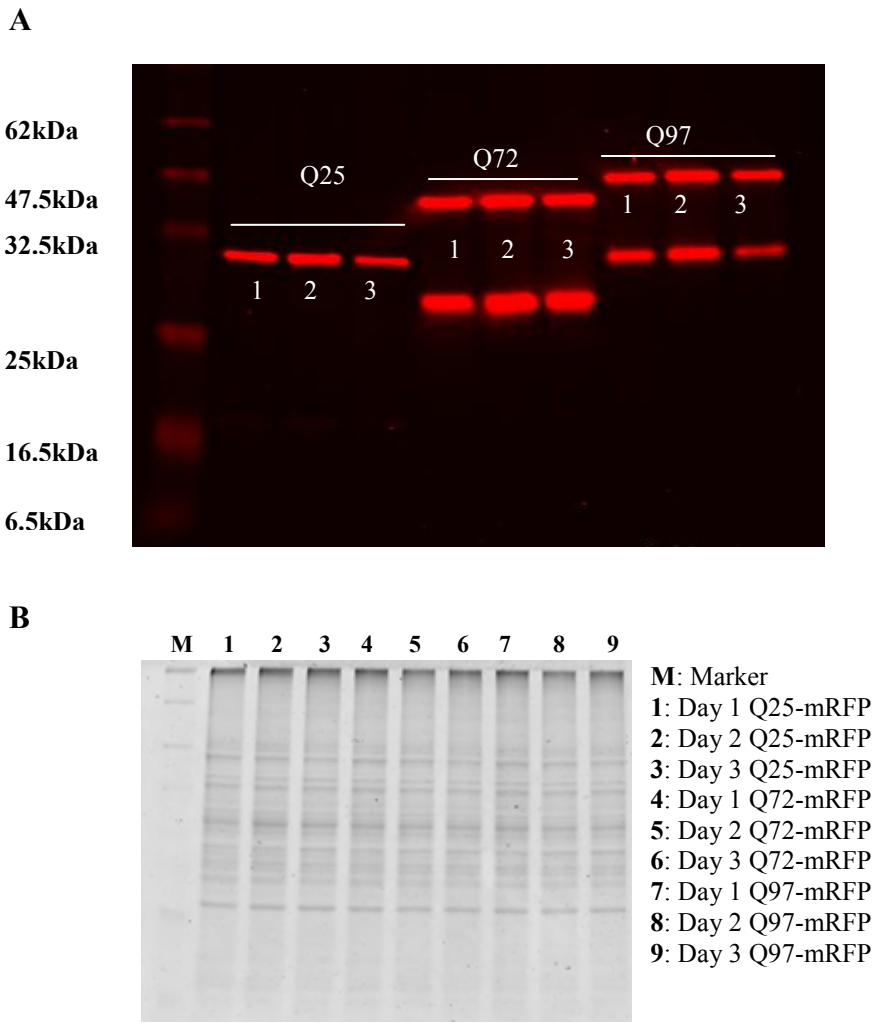

Figure 3.1 Transgene expression and integrity analysis of httEx1Q25/Q72/Q97-mRFP. (A) Integrity of httEx1Q25, Q72 and Q97- mRFP transgene expression of a three day time course in HeLa cells (1= day 1, 2= day 2, 3= day 3 and M = protein marker). Nitrocellulose membranes were probed with an anti- httEx1 antibody (S830, provided by Gilian Bates) followed by a fluorescently labelled secondary antibody which was detected by infrared fluorescence scanner. **(B)** A coomassie gel run in parallel shows equal protein loading of httEx1Q25/Q72/Q97-mRFP.

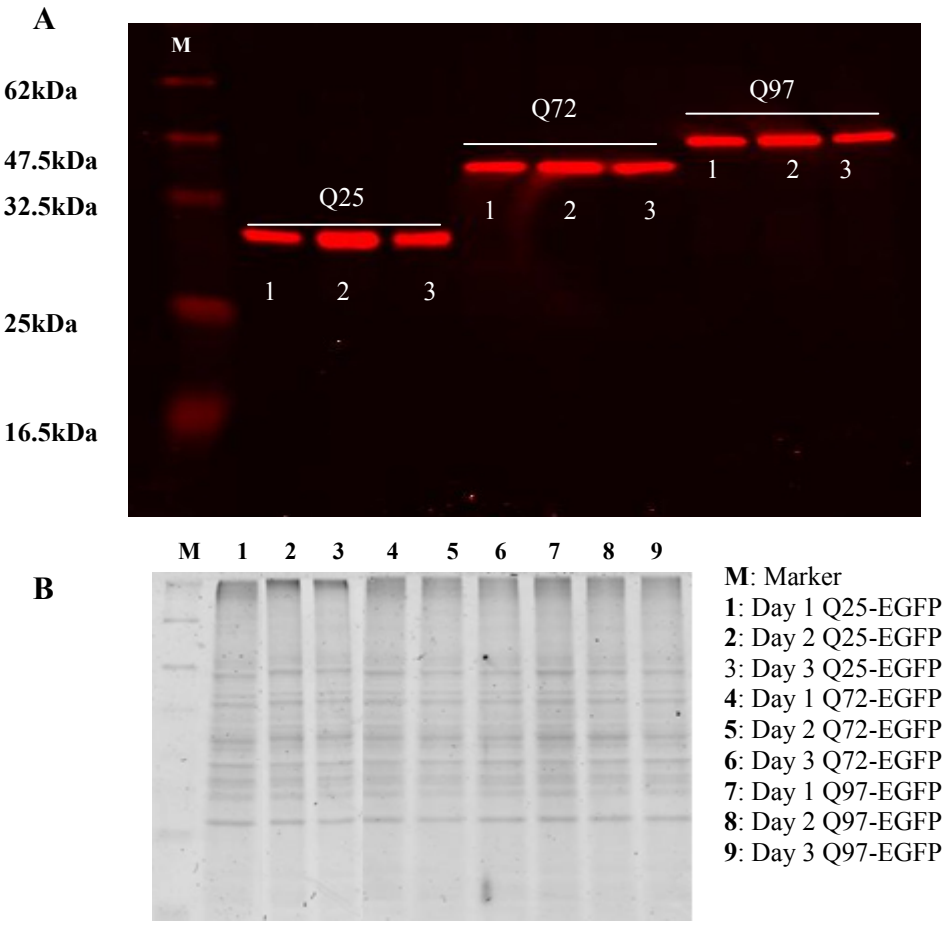

Figure 3.2 Transgene expression and integrity analysis of httEx1Q25/Q72/Q97-EGFP. (A) Integrity of httEx1Q25/72/97- EGFP transgene expression of a three day time course in HeLa cells (1= day 1, 2= day 2, 3= day 3). Nitrocellulose membranes were probed with an anti httEx1 antibody (S830, provided by Gilian Bates) followed by a fluorescently labelled secondary antibody which was detected by infrared fluorescence scanner. **(B)** A coomassie gel shows equal protein loading of httEx1Q25/Q72/Q97-EGFP.

Transgene expression levels of httEx1Q25/Q72/Q97 EGFP versus mRFP were quantified by using a computer programme (Odyssey). Pixel intensity data from cells expressing httEx1Q25/Q72/Q97-mRFP versus EGFP were not statistically different from each other (expression analysis from several experiments was adjusted with values obtained from coomassie gel lanes, Figure 3.3). Given that a cleavage fragment was observed in cells expressing httEx1Q72/Q97- mRFP at day 1-3, the transgene expression analysis was performed without considering the cleavage product (red hatched bars) and with including the extra band (red filled bars) (Fig.3.3). Although a clear trend toward higher expression of httEx1Q72/97 compared to EGFP transgene expression is seen when both bands are considered, due

to high variability between experiments the mRFP pixel intensity values were still not significantly different form EGFP values.

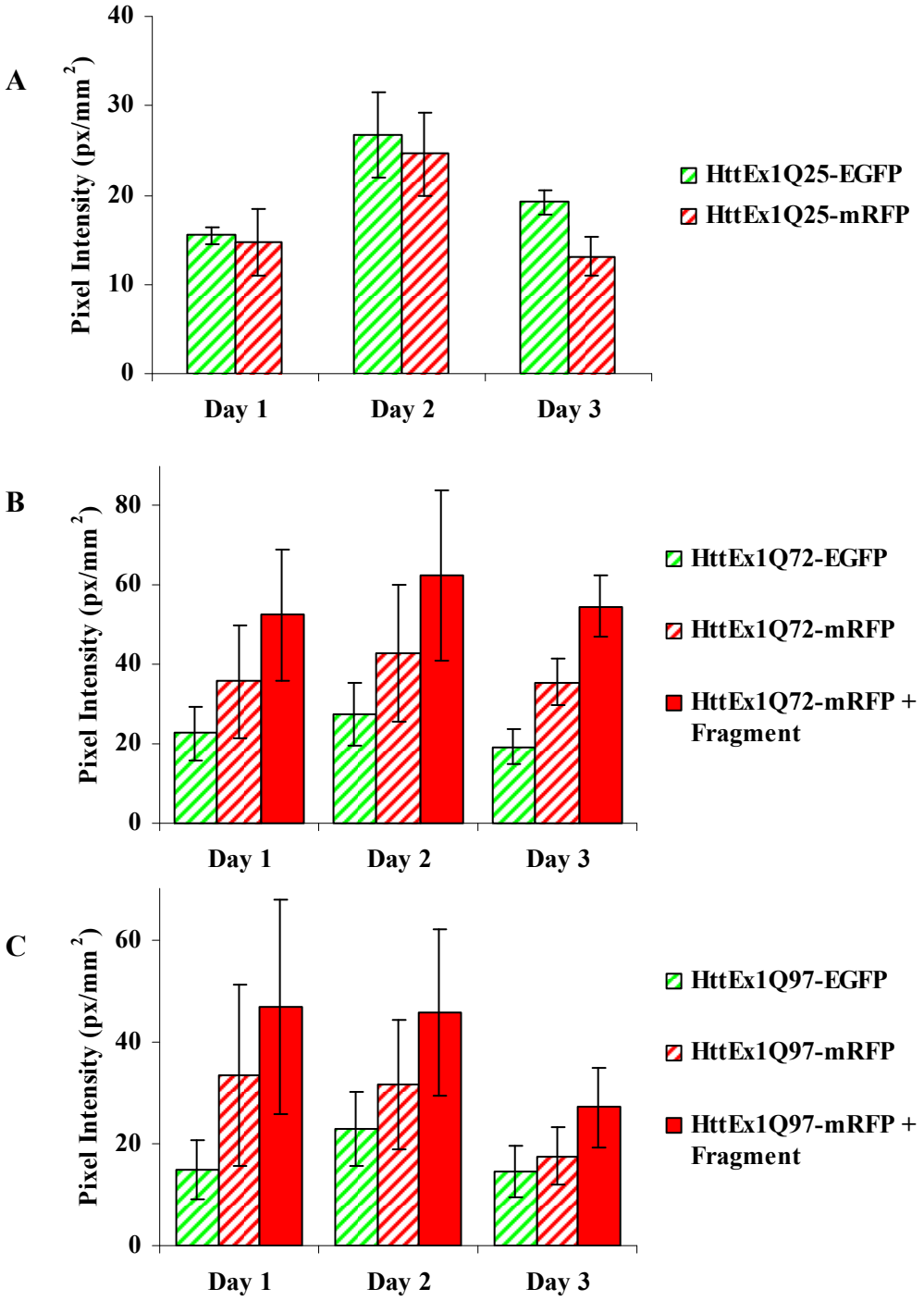

Figure 3.3 Quantification of transgene expression levels of httEx1Q25/72/97-EGFP versus mRFP. (A) Comparison of expression levels of httEx1Q25-EGFP and mRFP, **(B)** httEx1Q72-EGFP and mRFP with/without cleavage fragment and **(C)** httEx1Q97-EGFP and mRFP with/without cleavage fragment. Intensity values were measured by using odyssey infrared scanner software. Two way repeat measure ANOVA and Bonferroni posttests suggests no significant difference in the expression levels of EGFP and mRFP (with/without cleavage fragment) constructs at any time (n =3, P >0.05). Error bars represent standard errors of the means.

3.3.2 EM48 and 1C2 antibody do not detect httEx1Q25/Q97/-mRFP negative aggregates or cleavage products

Western blot analysis of httEx1Q72/Q97-mRFP constructs showed potential polyQ length dependent cleavage products (Figure 3.1A). Possibly, these cleavage products could participate in the polyQ aggregation process and lead to cellular toxicity and hence mRFP constructs would then not be comparable with EGFP constructs. For example, cleavage products could form mRFP negative aggregates. In order to find possible cleavage sites, our constructs were sequenced and uploaded into different databases (ExPASy Tools). As no caspase and calpain cleavage site/s were found, immunocytochemical analysis against the expanded polyQ-tract was performed in order to examine possible mRFP negative cleavage products and/or aggregates. The EM48 and 1C2 antibodies were employed for this analysis. EM48 antibody is expected to react with mhttEx1 of different repeat length (raised against first 256 amino acid of htt), whereas the 1C2 antibody (raised against TATA Box binding protein containing 38 glutamines) should react with any protein that contains polyQ expansions of 37 or more glutamines (Gutekunst et al., 1999; Trottier et al., 1995). Both antibodies detected httEx1Q25/Q97 when overexpressed, but no mRFP negative cleavage products or aggregates were found despite careful analysis of more than 50 cells in each of several experiments using confocal microscopy. However, using the 1C2 antibody speckle-like structures in some cells expressing both httEx1Q97-EGFP or mRFP constructs were occasionally detected (<1% of cells) (Figure 3.4B and 3.5B, white arrows). Whilst the EM48 antibody is able to detect IBs (white arrow head), the 1C2 antibody did not react with IBs (Figure 3.5B and D). In addition, Western blot analysis of httEx1Q72/Q97-mRFP probed with EM48 antibody did show the additional bands of lower molecular weight, as observed with S830 antibody (see appendix 5).

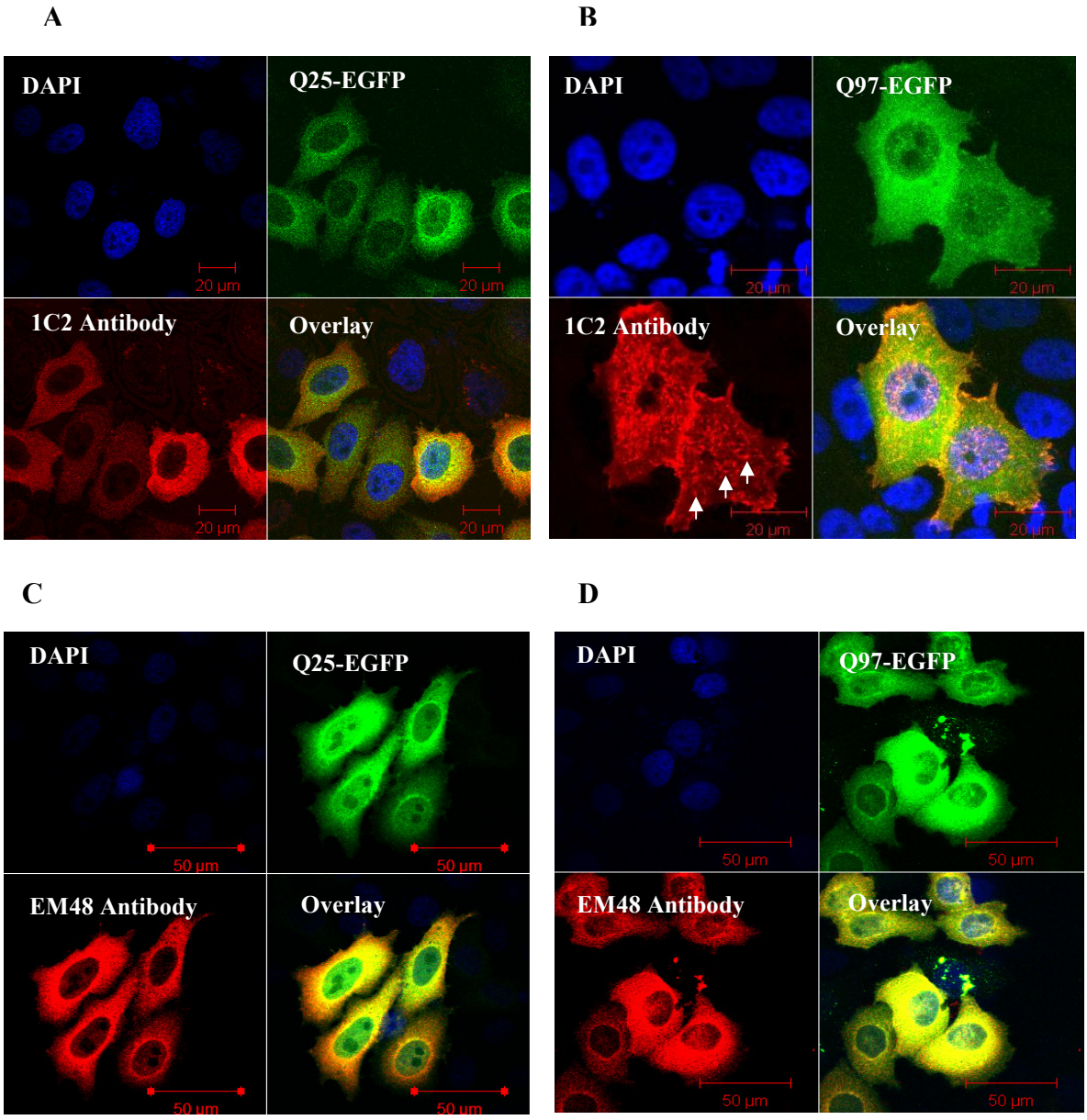

Figure 3.4 Immunocytochemical analysis of HeLa cells expressing httEx1Q25/Q97-EGFP. (A-B) Cells transiently transfected with httEx1Q25/Q97-EGFP were immunolabelled with 1C2 antibody and **(C-D)** EM48 antibody. IC2 antibody detected speckles-like structures in cells expressing httEx1Q97-EGFP (white arrow) whereas EGFP negative cleavage products or aggregates were not detected with both antibodies. Scale bar 20µm for A-B and 50µm for B-C.

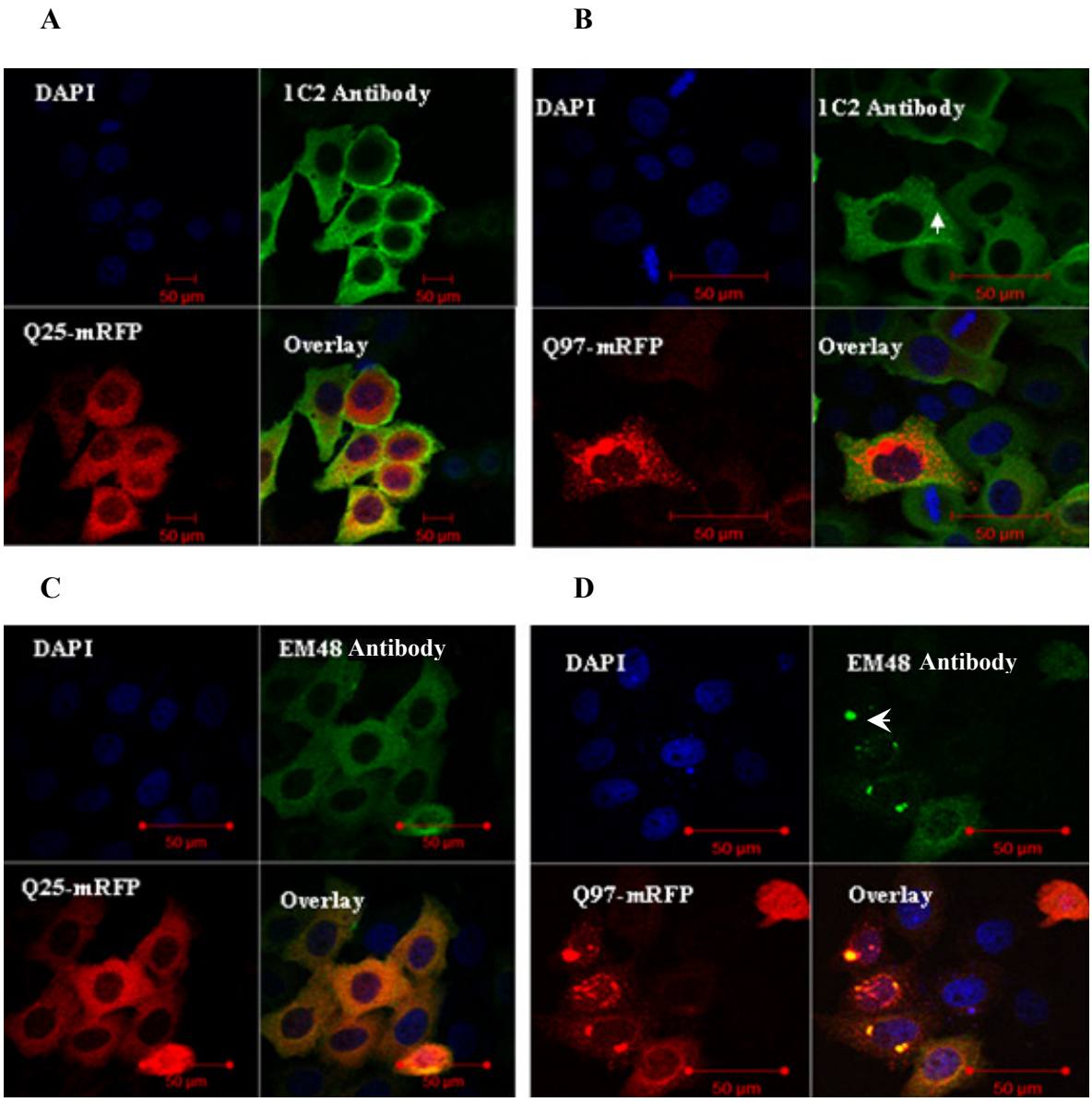

Figure 3.5 Immunocytochemical analysis of HeLa cells expressing httEx1Q25/Q97-mRFP. (A-B) Cells transiently transfected with httEx1Q25/Q97-mRFP were immunolabelled against 1C2 antibody and **(C-D)** EM48 antibody. IC2 antibody detects speckle-like structures in cells expressing httEx1Q97-mRFP (white arrow) whereas potentially aggregating mRFP negative aggregates were not detected with both antibodies. EM48 antibody colocalised with httEx1Q97 aggregates whereas 1C2 didn't detect mhttEx1 aggregates (white arrow heads). Scale bar 50µm.

3.3.3 HttEx1-mRFP/EGFP polyQ length dependant aggregation in HeLa cells

Figure 3.6A shows a time course of IB formation in cells expressing httEx1Q72/Q97-EGFP/mRFP. Cells expressing httEx1Q72/Q97-EGFP/mRFP showed an increase in IB formation over a three-day time course. There was no significant difference in cells expressing httEx1Q72/Q97-EGFP versus mRFP containing IBs. In Figure 3.6B and C examples of cells are shown that express each transgene with/out IBs (IBs are indicated by white arrows). Cells expressing both httEx1Q97-EGFP/mRFP constructs contained IBs mainly in the cytoplasmic compartment (>95%) (Figure 3.6B and C).

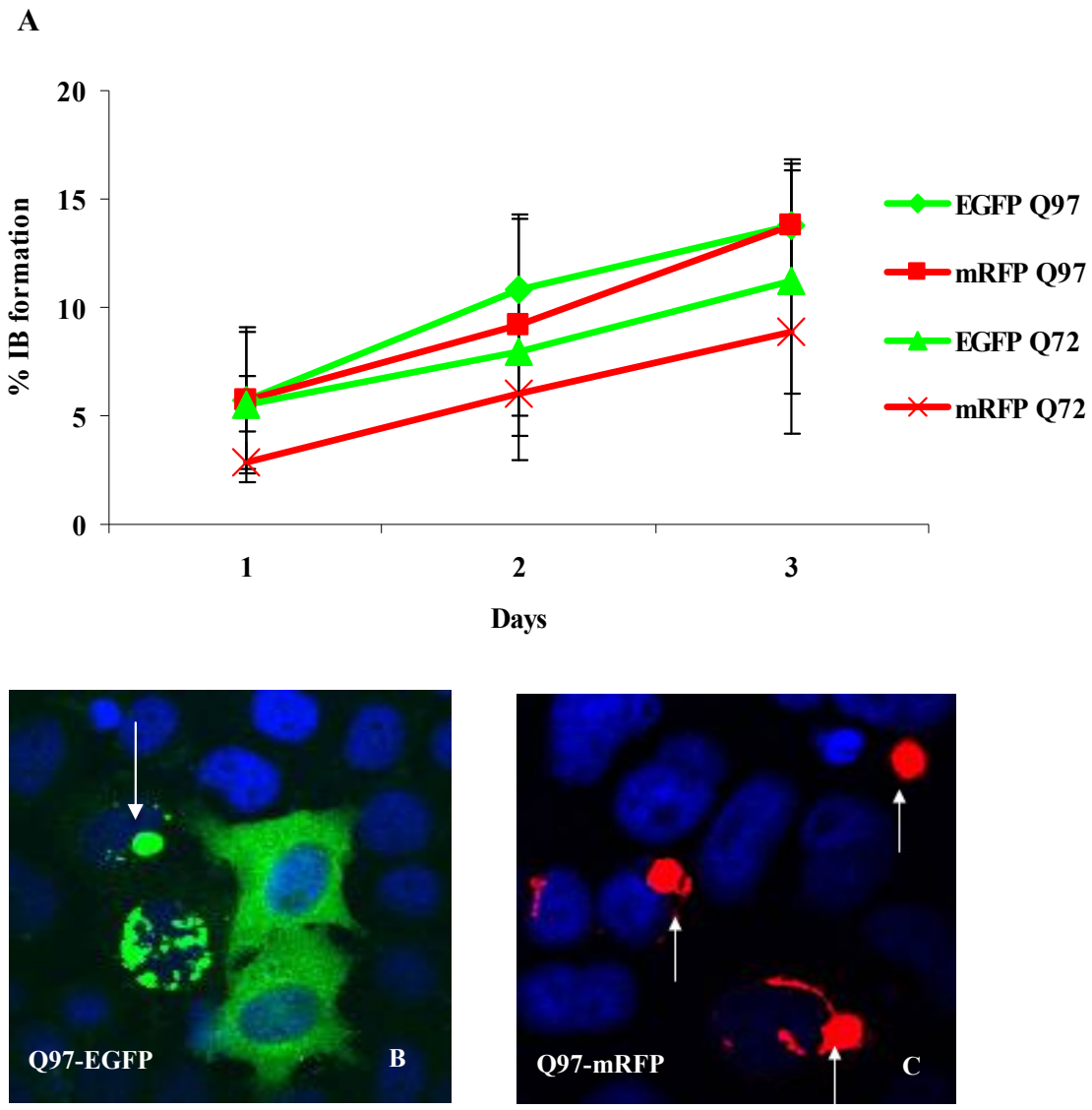

Figure 3.6 IB formation comparisons between cells expressing httEx1Q72/Q97-EGFP and mRFP. (A) No significant difference in IB formation observed between cells expressing httEx1Q72/Q97-mRFP and httEx1Q72/Q97-EGFP. **(B)** and **(C)** Examples of cells expressing httEx1Q97-EGFP and mRFP with IBs. White arrows show IBs. Error bars represent standard deviations. Two way repeat measure ANOVA and Bonferroni posttests were performed and no significant difference was observed with any of the construct at any time ($P > 0.05$, $n=3$).

3.3.3.1 Biochemical analysis of httEx1Q72/Q97-EGFP and mRFP aggregation in HeLa cells

In order to confirm IB aggregation data biochemically, as shown in Figure 3.6, dot blot assays were performed. In these assays, HeLa cells were transiently transfected with httEx1Q25/Q72/Q97-EGFP/mRFP and cell lysates were collected at different time points after transfection. Cell lysates were spun down and soluble and insoluble material was separated. Figure 3.7A is an illustration of a dot blot showing 2% SDS insoluble material of cells expressing httEx1Q25/Q97-EGFP/mRFP in a three-day time course. No signal was detected for httEx1Q25, as expected. Dot blot quantification from several experiments showed an increase of SDS-insoluble material from day 1 to day 2 in cells expressing httEx1Q72-EGFP and mRFP ($P > 0.05$) whereas there was a decrease in insoluble material at day 3 (Figure 3.7B). Similarly, httEx1Q97-EGFP/mRFP showed an increase in SDS-insoluble material at day 2 compared to day 1. At day 3 both httEx1Q97-EGFP and mRFP did not show any increase compared to day 1 and day 2 (Figure 3.7C). The reduction in insoluble material at day 3 could be explained by toxicity, whereby cells with IB's detach from the dish before lysates were collected, or a modest reduction in expression of the constructs (see Figure 3.3) or both. In general, two way repeat measure ANOVA and Bonferroni posttests suggest that the above mentioned changes were not significantly different in httEx1Q72 and/or Q97-mRFP versus EGFP SDS-insoluble material at any time point.

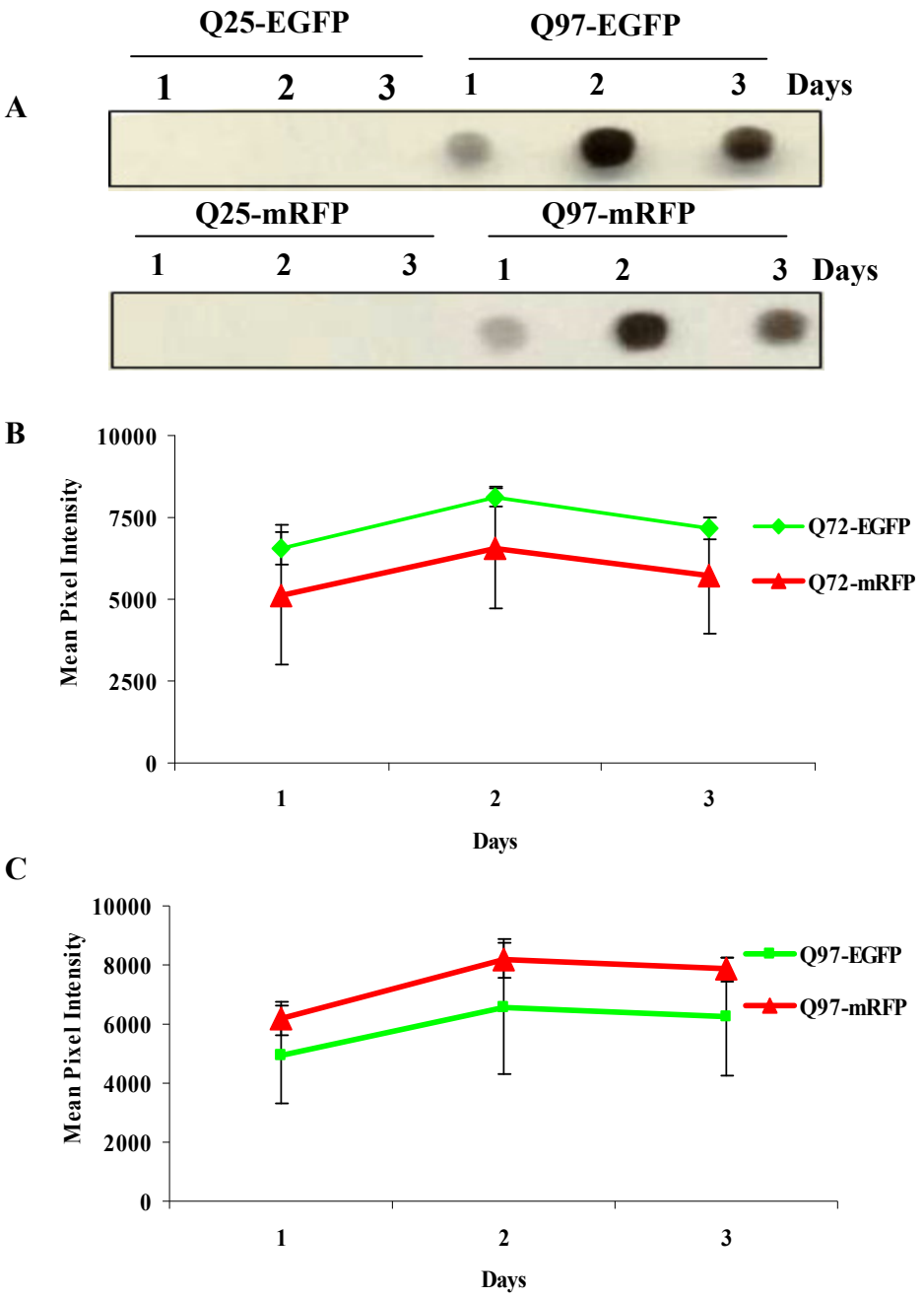

Figure 3.7 Filter trap assays demonstrate no difference in levels of SDS–insoluble httEx1Q72/Q97-EGFP versus mRFP aggregates. (A) SDS-insoluble httEx1Q72/Q97 increased at day 1 to day 2 whereas no change or a decrease in aggregation is observed at day 3. There was no significant difference in httEx1Q72/Q97-EGFP versus mRFP SDS insoluble material ($P > 0.05$) at any time point. SDS insoluble material was immunolabelled with the S830 antibody. **(B)** Quantification of httEx1Q72-EGFP versus mRFP and **(C)** Quantification of httEx1Q97-EGFP versus mRFP. Error bars represent standard errors of the means. Two way repeat measure ANOVA and Bonferroni posttests were performed for statistical analysis ($P < 0.05$, n=3).

3.3.4 PolyQ expansion causes toxicity in HeLa cells

As part of the characterisation of this HD cell system, HeLa cells were transiently transfected with httEx1Q25/72/Q97 EGFP and mRFP and cellular toxicity was quantified by scoring abnormal nuclei within cells expressing the respective transgenes (see Figure 3.8F for an example of a fragmented nucleus, white arrow). Hoechst was used as a nuclear stain and cells with either a fragmented or highly condensed nucleus (white arrow, Figure 3.8F) were counted as "dead". There was a significant increase in death in cells expressing httEx1Q72-EGFP/mRFP compared to cells expressing httEx1Q25-EGFP/mRFP at day 3 only (Figure 3.8A and B) whereas cells expressing httEx1Q97-EGFP/mRFP show a significant increase in toxicity at day 2 and 3 compared to cells expressing httEx1Q25-EGFP/mRFP (Figure 3.8A and B). No significant difference in toxicity was detected between cells expressing httEx1Q97-EGFP and httEx1Q97-mRFP at any time point except day 3 ($P < 0.05$). Figure 3.8C and D shows examples of transgene expression of httEx1Q25-EGFP and mRFP whereas Figure 3.8E and F shows transgene expression of httEx1Q97-EGFP and mRFP in HeLa cells.

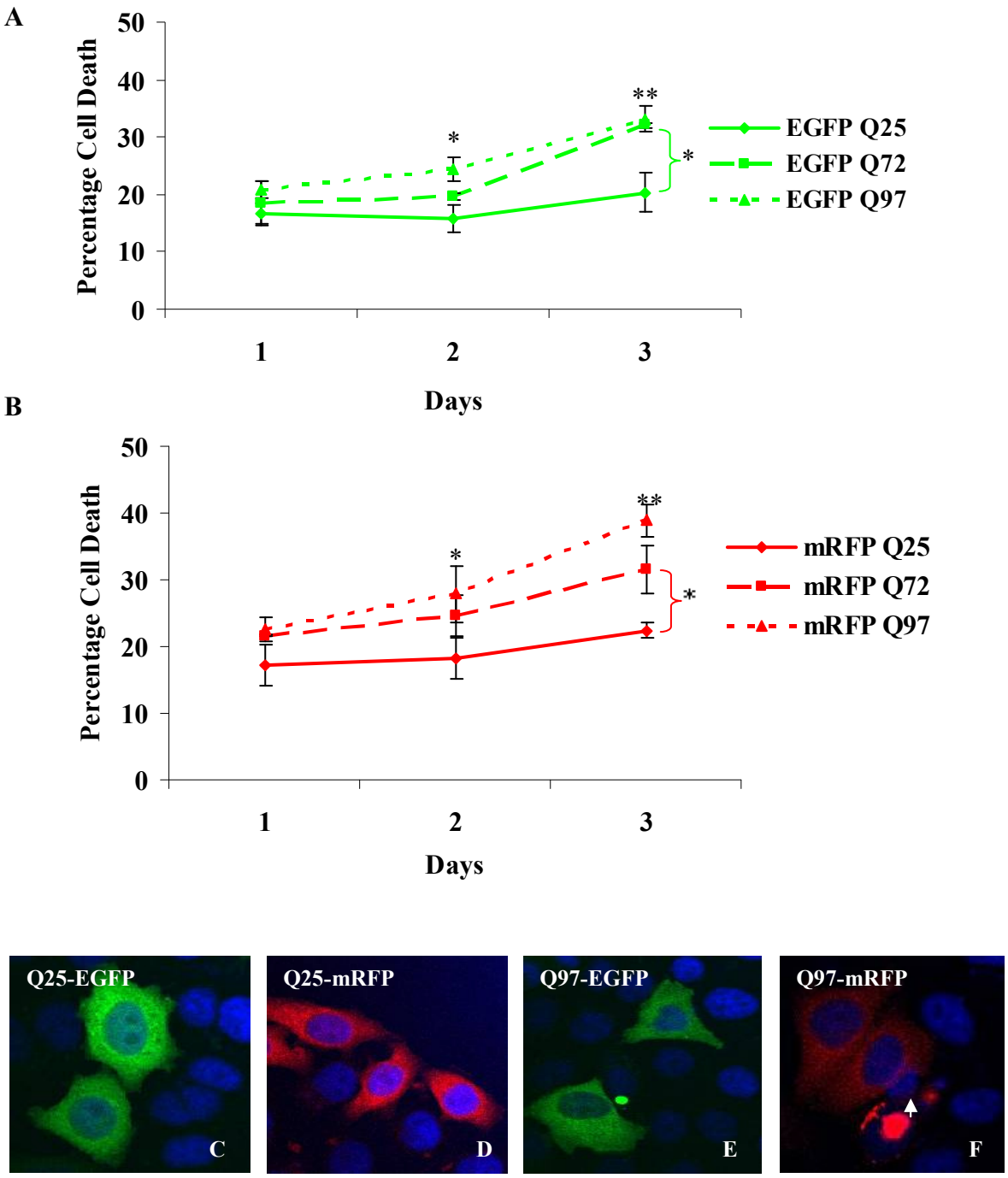

Figure 3.8 Cell death comparisons between cells expressing httEx1Q25/Q72/Q97-EGFP and mRFP. **(A)** Quantification of cellular toxicity of cells expressing httEx1Q25/72/97-EGFP. **(B)** Quantification of cellular toxicity of cells expressing httEx1Q25/72/97-mRFP. **(C-F)** Examples of cells expressing httEx1Q25/97-EGFP and mRFP. White arrow points to a cell with a nuclear abnormality. Error bars represent standard deviations. Two way repeat measure ANOVA and Bonferroni posttests were performed (* = $P < 0.05$, ** = $P < 0.01$, n=3 except httEx1Q72 EGFP/mRFP which is n=2).

3.3.4.1 Cytochrome *c* release and Caspase-3 activation

To further investigate htt toxicity it was decided to determine the effect of httEx1Q97 versus httEx1Q25 expression on cell death pathways using cell death markers such as an antibody against cytochrome *c* (cyt *c*) and active caspase-3 (an antibody directed against the p18 fragment of the active caspase 3). Cells were transiently transfected with either httEx1Q25/Q97-mRFP or EGFP and then immunostained for cyt *c* and activated caspase-3. Cells expressing httEx1Q97-mRFP showed a significant increase in cyt *c* release compared to cells expressing httEx1Q25-mRFP at day 3 (Figure 3.9A). Cyt *c* is normally localised to mitochondria and hence a punctate staining is observed. Cells with cyt *c* release from mitochondria can be detected as a diffuse staining or if cyt *c* is degraded no staining is detectable (Figure 3.9B, white arrow).

Cells expressing httEx1Q97 also showed a higher likelihood of exhibiting a signal for activated caspase-3 immunoreactivity over time, and this increase was only significant at day 3 (Figure 3.10A). Figure 3.10B shows HeLa cells transiently transfected with httEx1Q25/Q97-EGFP and immunostained against activated caspase-3 (indicated by white arrow).

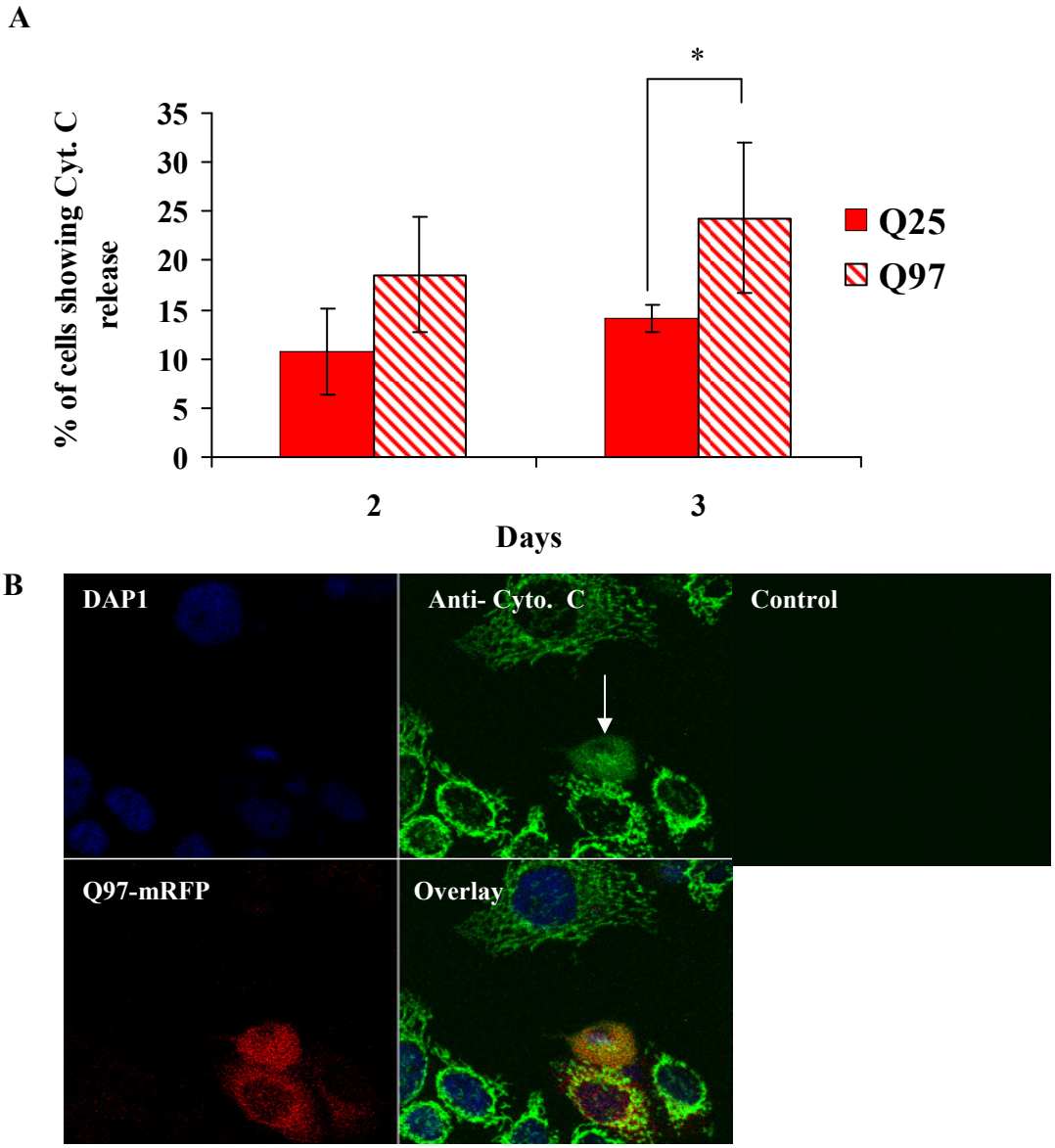

Figure 3.9 Cell death analysis of HeLa cells expressing httEx1Q25/Q97-mRFP by using an antibody detecting cyt *c* release. HeLa cells were transiently transfected with httEx1Q25/Q97-mRFP and analysed at day 2 and 3 for cyt *c* release after immunostaining with anti-cyt *c* antibody. **(A)** A significant increase in cells showing cyt *c* release is observed in cells expressing httEx1Q97-mRFP versus Q25-mRFP at day 3. **(B)** Example of a cell with cyt *c* release (white arrow). Here cyt *c* is homogenously distributed rather than localised to mitochondria. Error bars represent standard deviations. Unpaired t-test was performed for statistical analysis, * = $P < 0.05$ (n =3).

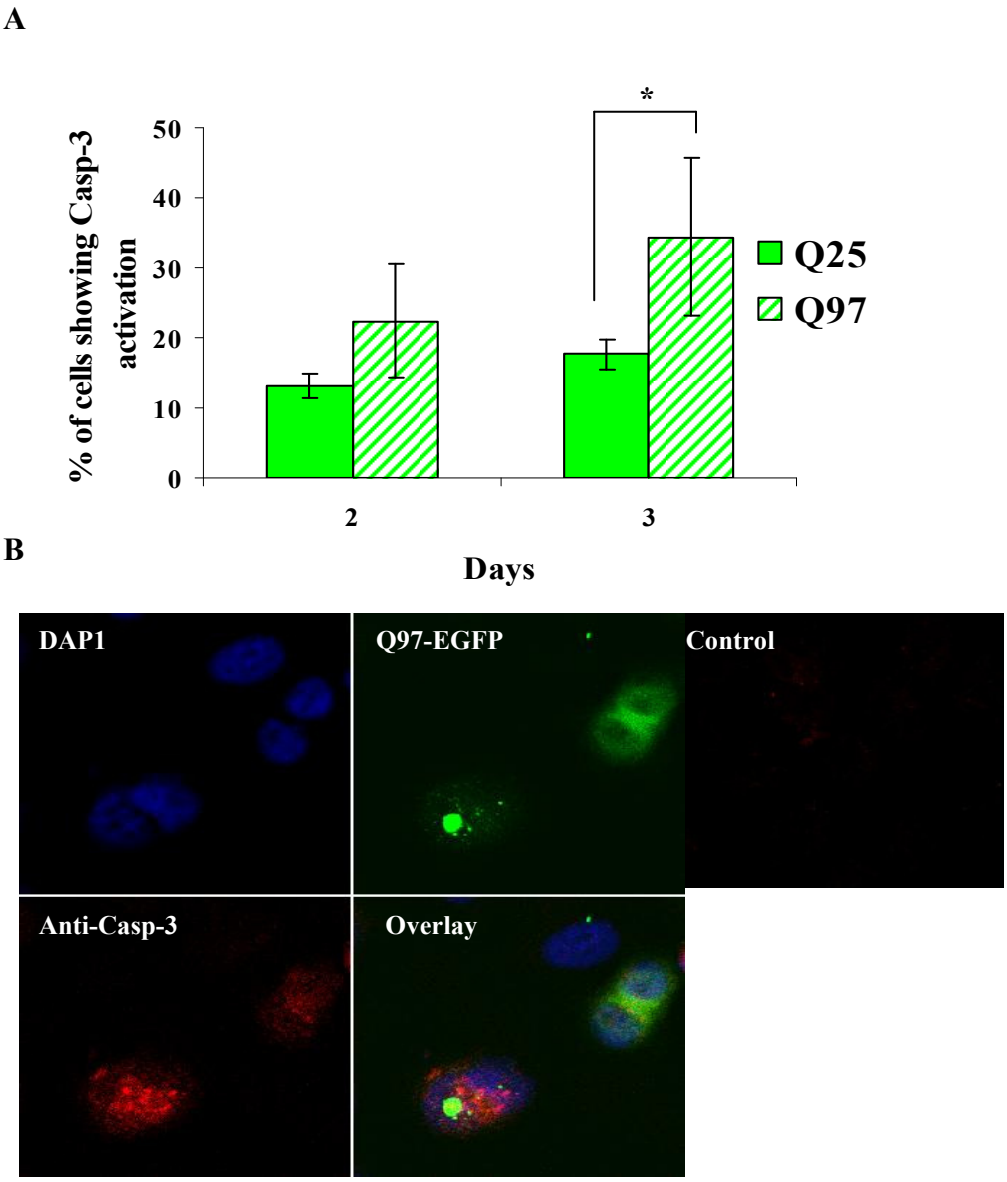

Figure 3.10 Cell death analysis of HeLa cells expressing httEx1Q25/Q97-EGFP by using an antibody against activated caspase-3. HeLa cells were transiently transfected with httEx1Q25/Q97-EGFP, fixed and immunostained against activated caspase-3 by using an anti-Active caspase-3 antibody. **(A)** A significant increase in caspase-3 activation was observed in cells expressing httEx1Q97 at day 3 compared to cells expressing httEx1Q25. **(B)** Example of a caspase-3 positive cell (indicated by white arrow). Error bars represent standard deviations. Unpaired t-test was used, * = $P < 0.05$ (n=3).

As shown in Figure 3.8, 3.9 and 3.10 the expression of the various mhttEx1 transgenes caused a significant increase in abnormal nuclear morphology of cells, a measure of cellular toxicity, and an increase in the cell death markers such as cyt *c* and caspase-3. Increased cyt *c* release and caspase-3 activation is consistent with an

activation of the mitochondrial cell death pathway and possible mitochondrial dysfunction. Therefore, it was decided to investigate whether the mitochondrial membrane potential in mhttEx1 expressing cells was intact by using a dye called MitoTracker. MitoTracker is retained in actively respiring mitochondria and washes out as soon as mitochondria lose their potential. HeLa cells transiently transfected with httEx1Q25/Q97-EGFP and mRFP and after 24, 48 and 72 hours of transfection cells were incubated with 200nM of MitoTracker orange for 30 minutes at 37ºC with subsequent fixation and imaging by using confocal microscopy. All Q25 and Q97 expressing cells loaded MitoTracker Orange indicating that the Δpsi was retained (Figure 3.11A and B). Untransfected cells were incubated with 2μM of carbonyl cyanide 4-(trifluoromethoxy) phenylhydrazone (FCCP) for 20 minutes followed by MitoTracker incubation as a positive control for loss of the mitochondrial membrane potential. FCCP is a protonphore and uncoupler of oxidative phosporylation in mitochondria. It depolarises the mitochondrial membrane hence MitoTracker cannot be retained in mitochondria as shown in Figure 3.11C compared to cells without FCCP treatment (Figure 3.11D). MitoTracker is a dye that measures an “all or nothing response” (membrane potential lost or not). To measure a partial change in Δpsi one would need to employ dyes that report on potential changes ratiometrically, such as TMRE or JC-1.

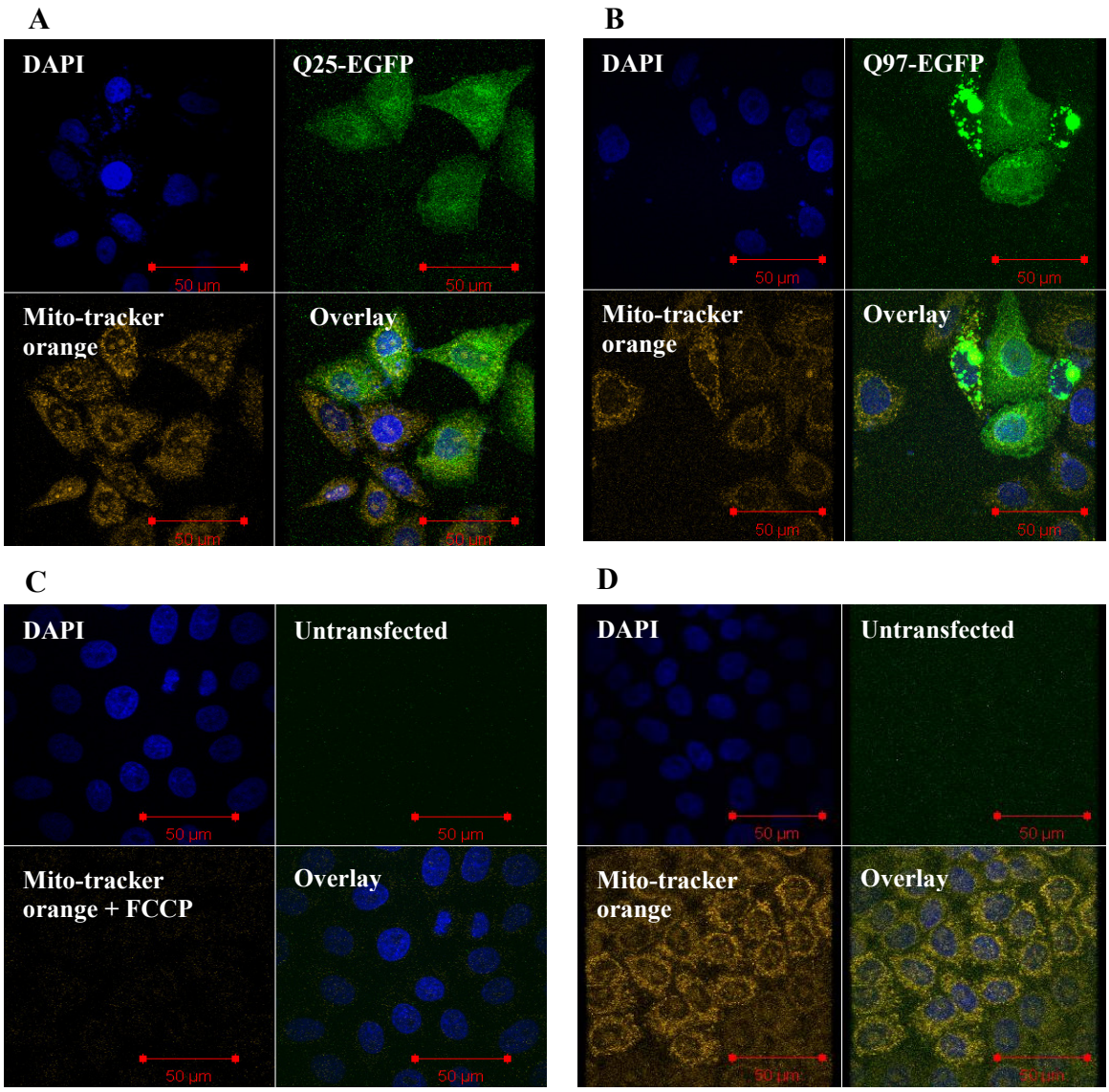

Figure 3.11 Effects of httEx1Q25/Q97-EGFP on the mitochondrial membrane potential of HeLa cells. **(A)** and **(B)** Cells were transiently transfected with httEx1Q25/Q97-EGFP and loaded with 200nM of MitoTracker orange. Nuclei were stained with DAPI. **(C)** FCCP treatment depolarised mitochondria hence the dye was not retained, **(D)** Untransfected cells without FCCP treatment also retain MitoTracker. This assay was performed at 24, 48 and 72 hours post-transfection (n=2). Scale bar 50µm.

3.3.5 PolyQ aggregation and toxicity analysis in PC12 cells

To expand and confirm the previous findings in HeLa cells, rat pheochromocytoma (PC12) cells were chosen as a neuronal cell line and similar experiments were performed as described above using the mRFP-tagged polyQ plasmids. The nuclear morphology and rate of aggregation, after transient transfection of PC12 cells with httEx1Q25/Q97-mRFP, was monitored for three days. Figure 3.12A shows an increase in toxicity (significant only at day 2 and 3) and aggregation in PC12 cells over time. Figure 3.12B and C show examples of cells expressing httEx1Q25-mRFP and httEx1Q97-mRFP (white arrow indicates IB formation). Compared to HeLa cells, transient transfection of httExQ97-mRFP into PC12 cells resulted in a faster rate of IB formation that occurred mainly in the cytoplasm (data not shown).

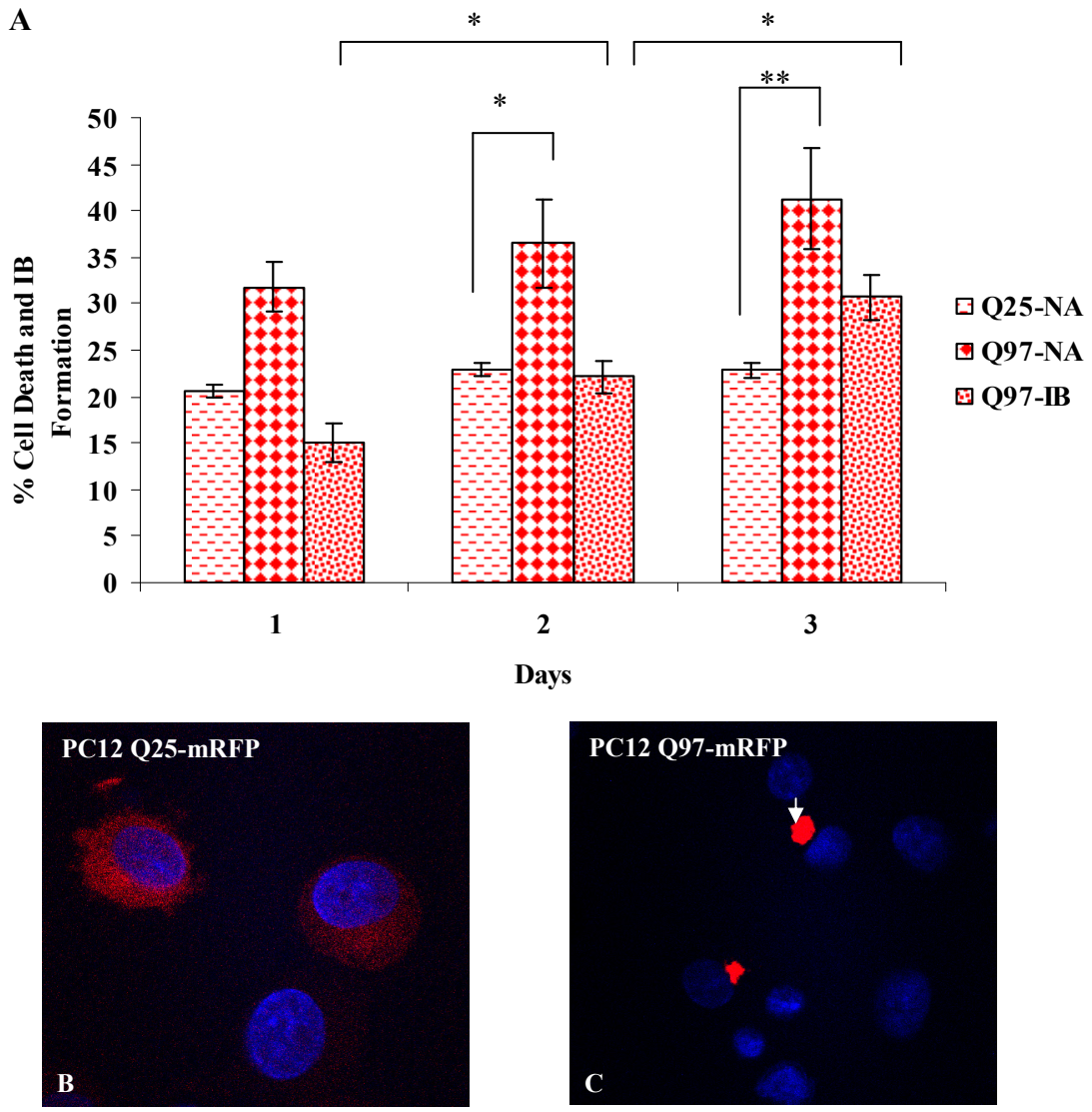

Figure 3.12 PolyQ toxicity and aggregation analysis in PC12 cells. (A) PC12 cells expressing httEx1Q97-mRFP showed a significant increase in toxicity and aggregation compared to cells expressing httEx1Q25-mRFP at day 1-3 (n=4). **(B)** and **(C)** Examples of PC12 cells expressing httEx1Q25 and Q97-mRFP. White arrow indicates inclusion body. Error bars represent standard errors of the means. Two way repeat measure ANOVA and Bonferroni posttests were performed for toxicity data. Unpaired t-test was used for IB data. * = P< 0.05, ** = P<0.01 (NAs, Nuclear Abnormalities and IBs, Inclusion Bodies).

3.3.6 PolyQ aggregation and toxicity analysis in httEx1 inducible PC12 cells

Transient transfection systems can be highly variable due to the transient expression of transgenes and, hence, it was decided to study a more stable system of neuronal origin in parallel to the aforementioned transient expression systems.

Therefore, PC12 cells inducibly expressing httEx1Q25/Q103 fused to EGFP at the C-terminal were used (provided by Dr F. Giorgini, University of Leicester, UK). These cell lines have been originally developed by Dr E. Schweitzer who showed that maximum transgene expression is obtained at 1µM of tebufenozide treatment (Aiken et al., 2004). Both, PC12-httEx1Q25 and PC12-httEx1Q103-EGFP cells were induced at this concentration and toxicity and IB formation were analysed. HttEx1Q103-EGFP-expressing cells showed an increase in cell death over time compared to httEx1Q25-EGFP expressing cells, but only reached statistical significance at day 2 and 3 (Figure 3.13A). Aggregation significantly increased over time (Figure 3.13A). Figure 3.13B and C show examples of PC12 cells expressing httEx1Q25 and httEx1Q103-EGFP. PC12-HttEx1Q103-EGFP expressing cells under the control of tebufenozide formed mostly cytoplasmic inclusions (white arrow, Figure 3.13C) but occasionally nuclear inclusion were also observed.

Additionally a second stable PC12 cell polyQ expression system was used expressing truncated exon 1 (first 17aa with 103 glutamines) under the control of ponasterone A (provided by Dr. F. Giorgini, University of Leicester, UK). This cell model is known to rapidly induce IBs with transcriptional dysregulation recapitulating early events in HD and has also been used for drug screens (Apostol et al., 2003). A significant increase in aggregation was observed over time (Figure 3.14A) whereas no significant change in toxicity was observed after induction with 5µM of ponasterone A over a 2 day time course (Figure 3.14B). An MTS assay was employed as a toxicity readout. Inspection of nuclear morphology did also not show any nuclear abnormalities (data not shown). Due to the availability of a mutant cell line only, both toxicity and aggregation analysis was performed on one cell line (tHttEx1Q103-EGFP). It is important to point out that toxicity and IB formation at day 3 was not studied due to an already high level of IBs at day 2 (Figure 3.14A). Data obtained from the ponasterone A inducible cell system are consistent with other cell models,

both transient and inducible, where an early increase in aggregation in cells expressing mhttEx1 (day 1) was not associated with immediate cellular toxicity at this time point. Thus these models are all suitable to study potentially early occurring polyQ aggregation and ROS production preceding cell death.

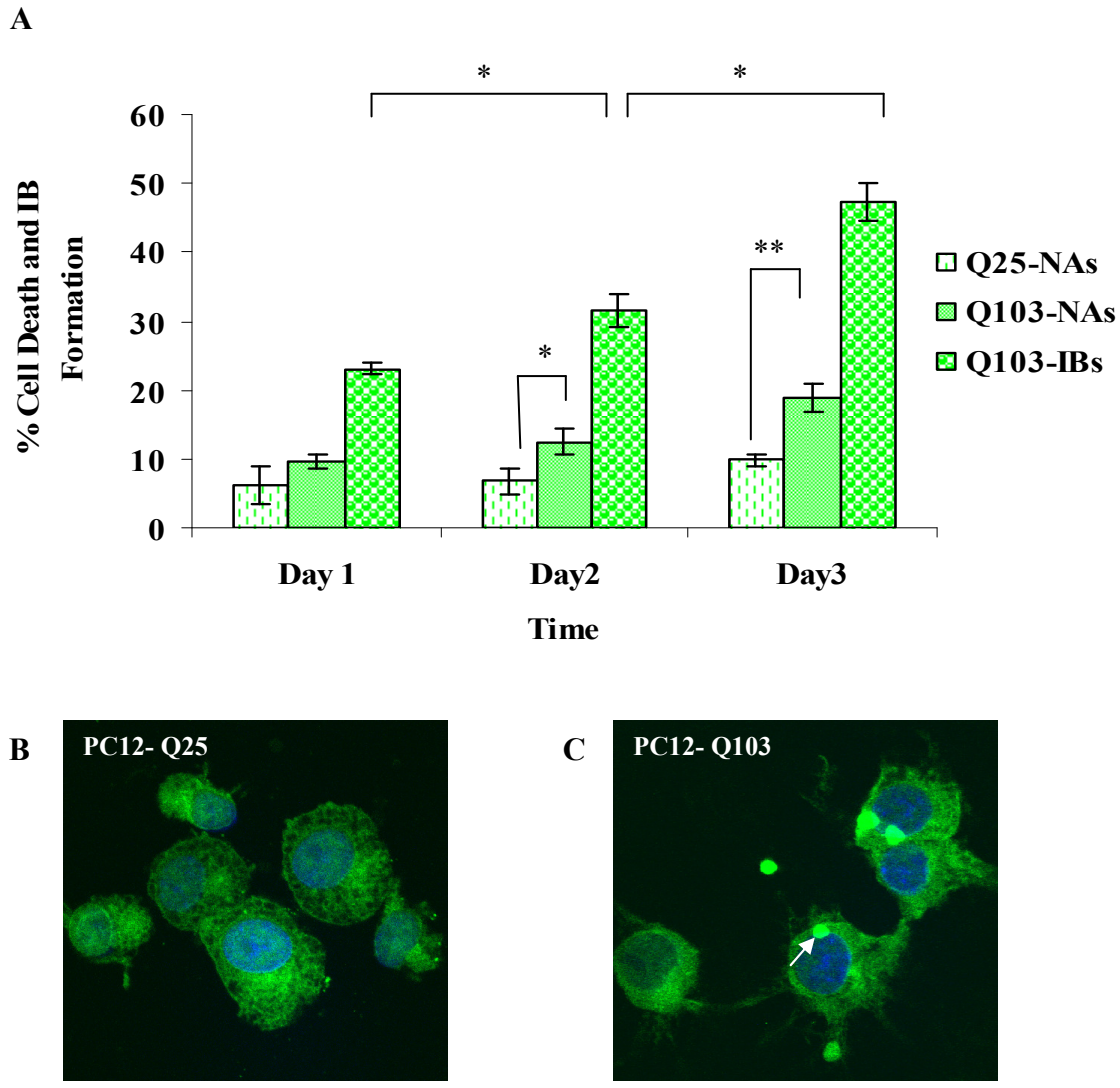

Figure 3.13 PolyQ toxicity and aggregation analysis in PC12 httEx1 inducible cells. **(A)** Cells expressing httEx1Q103 showed significant increase in aggregate formation over time. HttEx1Q103 also showed a significant increase in toxicity at day 2 and 3 due to the polyQ expansion (n=2; * = $P < 0.05$, ** = $P < 0.01$), (NAs, Nuclear abnormalities and IBs, Inclusion Bodies). **(B)** and **(C)** show transgene expression after induction of httEx1Q25/Q103 in PC12 cells with 1µM of tebufenozide after 48 hours. White arrow indicates an inclusion body. Error bars represent standard deviations. Two way repeat measure ANOVA and Bonferroni posttests were used for statistical analysis for toxicity whereas unpaired t-test was used for IB analysis.

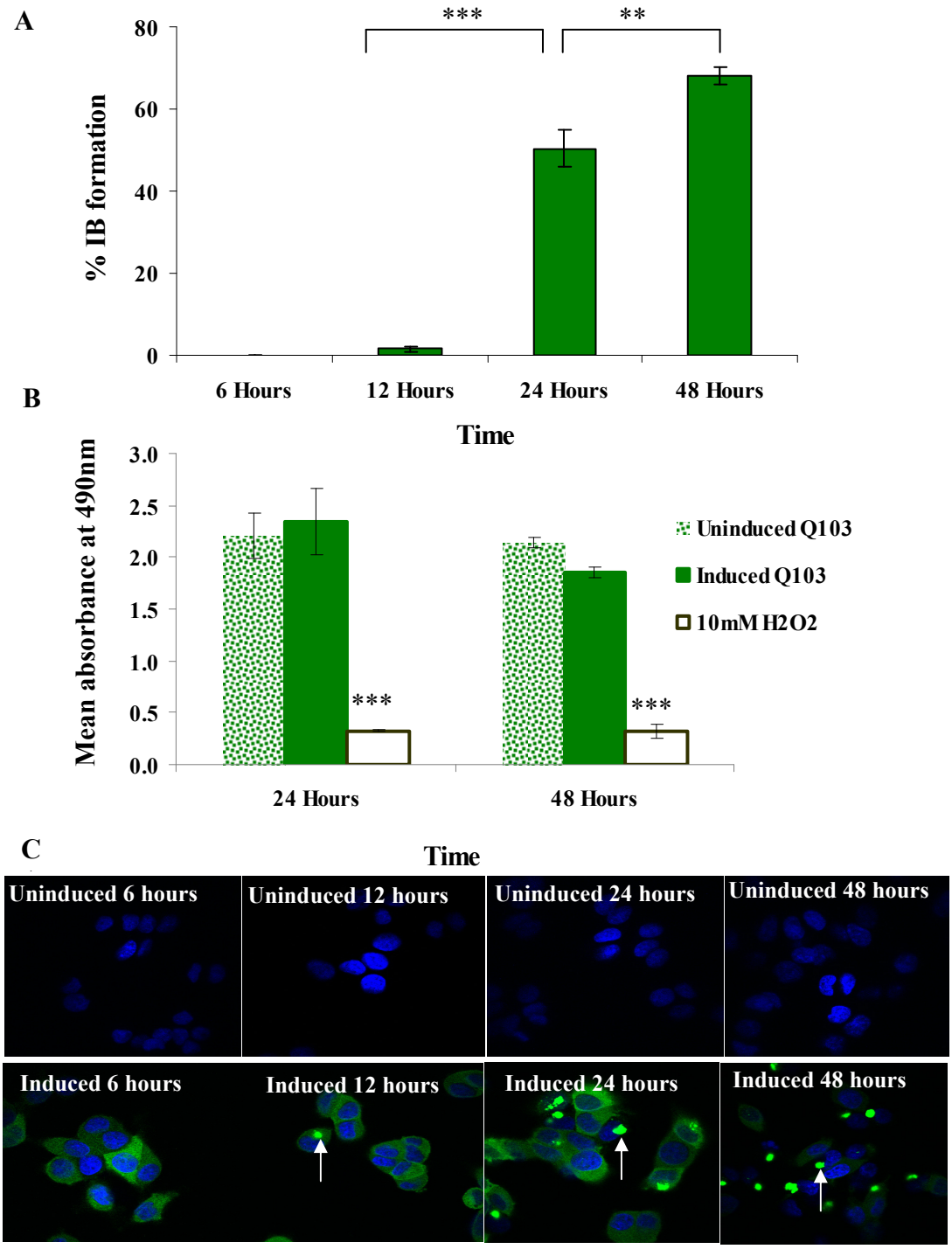

Figure 3.14 PolyQ aggregation and toxicity analysis in a PC12 ponasterone A inducible stable expression system. (A) tHttEx1Q103 aggregation analysis over time. **(B)** Comparative toxicity analysis using MTS assay of cells with or without tHttQ103 induction. 10mM H_2O_2 treatment was used as a positive control inducing significant cellular toxicity at 24 and 48 hours time points compared to uninduced cells. Error bars represent standard deviations. **(C)** Examples of uninduced (upper panel) and induced cells (lower panel) with 5µM of ponasterone A over time. Induced cells show cytoplasmic IBs (white arrows) whereas no transgenes expression is observed in uninduced cells. Unpaired T test was used for IB data analysis whereas two way repeat measure ANOVA and Bonferroni posttests were used for toxicity analysis. (n=3, ** = $P < 0.01$, *** = $P < 0.001$).

3.3.7 Adenovirus mediated mhttEx1 aggregation and toxicity analysis in HeLa cells

In addition to the transient and inducible cell systems, it was decided to characterise a third system to compare cellular toxicity and aggregation. For this purpose, httEx1Q25/Q97-mRFP expressing adenoviruses on cultured HeLa cells were used. HeLa cells were infected with httEx1Q25/Q97-mRFP in suspension and 96 wells plates were used for IB analysis and for the MTS assay to measure cellular toxicity caused by httEx1Q97. There were several potential advantages to using adenovirus: 1) a stable population of cells expressing httEx1Q25/Q97-mRFP can be produced, 2) infection is less time consuming and is highly reproducible in different cell types and 3) no transfection artefacts/toxicity were observed (in comparison to transient transfection systems). Figure 3.15A shows a significant increase in IB formation over time in cells expressing httEx1Q97-mRFP. The MTS assays suggest an increase in cellular toxicity of cells expressing httEx1Q97-mRFP compared to cells expressing httEx1Q25-mRFP and uninfected cells and this increase was significant at day 2 and 3 (Figure 3.16). The amount of viruses used in these assays was based on initial viral titration done by Dr S. Hands. Western blot analysis of cells expressing httEx1Q25/Q97-mRFP transgenes show correct band sizes over time (see appendix 6).

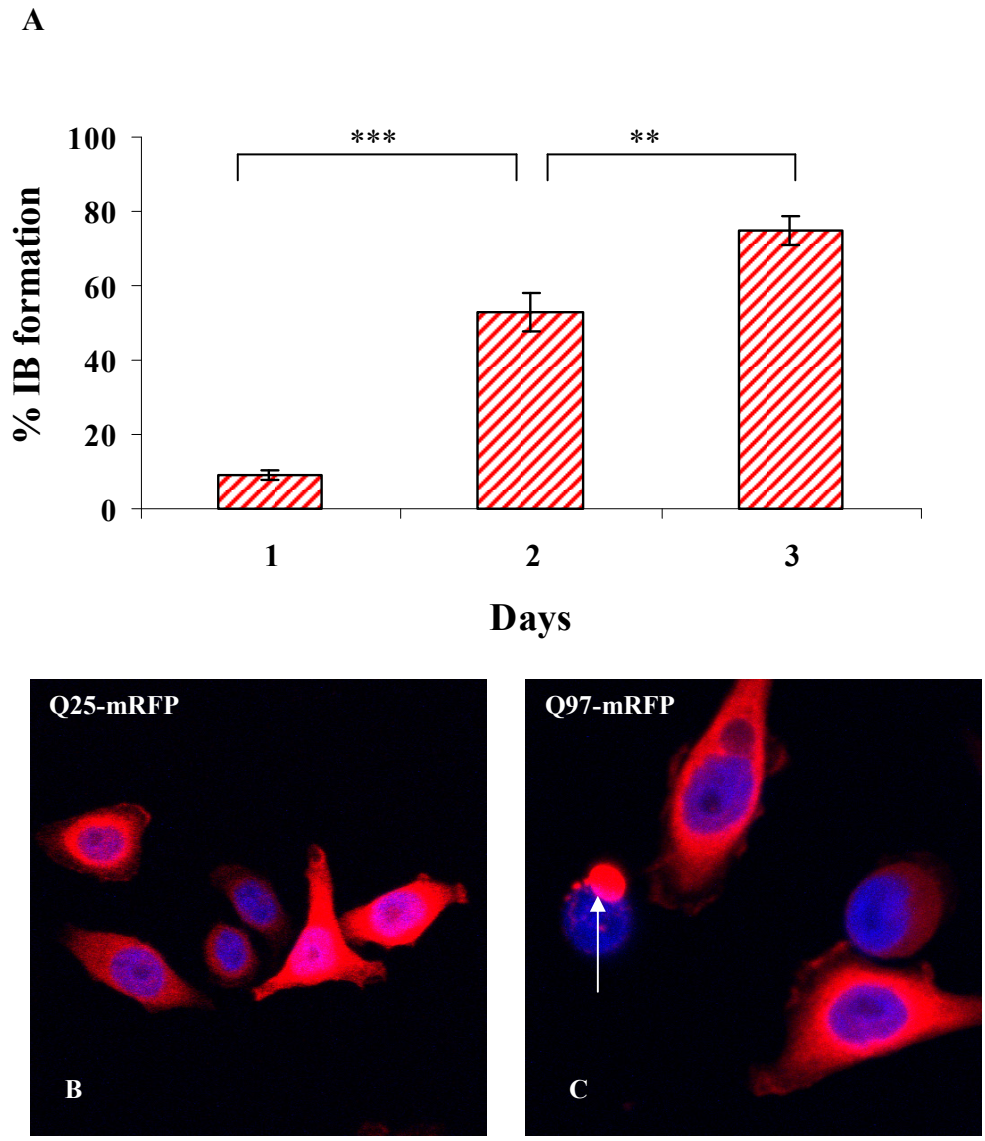

Figure 3.15 PolyQ aggregation analysis of HeLa cells infected with adenovirus carrying httEx1Q25/Q97-mRFP. (A) IB formation significantly increased over a 3-day time course (red hatched bars). **(B)** Example of cells expressing httEx1Q25-mRFP that does not produce aggregates. **(C)** Cells expressing httEx1Q97-mRFP form aggregates as shown by white arrow. Error bars represent standard error of the mean. ** = $P < 0.01$, *** = $P < 0.0001$ (n=3).

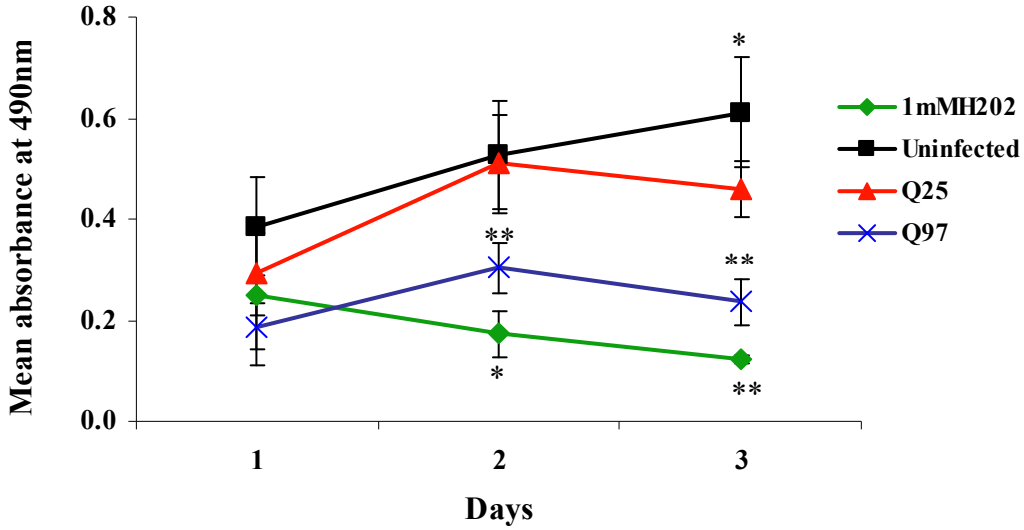

Figure 3.16 Cellular toxicity analysis of HeLa cells infected with adenovirus carrying httEx1Q25 or Q97-mRFP. HeLa cells were infected with adenovirus carrying httEx1Q25/Q97-mRFP. The MTS assay was used to measure dehydrogenase enzyme activity in metabolically active cells. The absorbance values are proportional to the cell viability at the given time points during analysis. Cells infected with httEx1Q97 showed higher cellular toxicity compared to cells expressing httEx1Q25 at day 2 and day 3 (** = $P < 0.01$) whereas httEx1Q97-mRFP induced toxicity was also significant at day 3 compared to uninfected cells ($P < 0.05$). 1mM H_2O_2 was used as a positive control and toxicity was significantly higher at day 2 ($P < 0.05$) and day 3 ($P < 0.01$) compared to uninfected cells. Error bars represent standard errors of the means and two way repeat measure ANOVA with Bonferroni posttests were used for statistical analysis (n=3).

3.3.8 Antioxidants rescue polyQ toxicity

Before embarking on analysing changes in ROS production in these cell systems the next aim was to show that antioxidant compounds were indeed able to significantly reduce polyQ induced toxicity suggesting ROS involvement in polyQ toxicity. Therefore, two ROS scavengers were used with the transient HeLa cell system, N-acetyl-L-cysteine (L-NAC), Trolox, and one Reactive Nitrogen Species (RNS) inhibitor, L-Nitro-Arginine Methyl Ester (L-NAME). This system was used because of its relatively slow induction of IB formation and also because it has been used in the lab previously for antioxidant studies (Unpublished data). HeLa cells were seeded in a 24 well plate and treated with 10mM L-NAC, 5mM L-NAME or 100µM of Trolox 12 hours before transfection. Relevant L-NAC and L-NAME concentrations were determined by Dr S. Hands previously. In these experiments a Trolox concentration of 100µM was found to be most protective against mhttEx1 induced

cell death. Antioxidants were replaced every 12 hours post-transfection for 3 days and cells were fixed with parafomaldehyde. Nuclear abnormalities were quantified as a measure of toxicity. Figure 3.17 shows that cells treated with L-NAC and Trolox significantly reduced cell death. In contrast, 3 day treatment of 1mM and 5 mM L-NAME showed baseline toxicity to both httEx1Q25/Q97 expressing cells (data not shown).

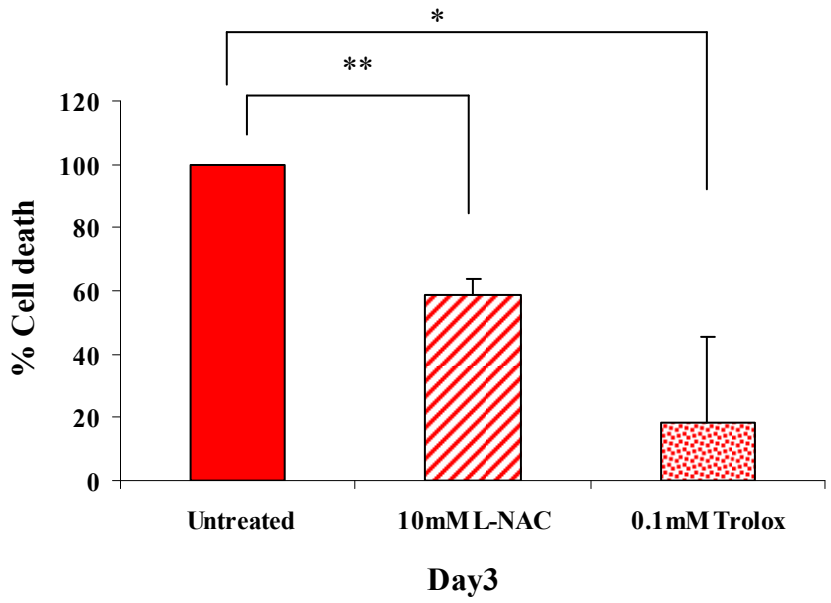

Figure 3.17 Toxicity analysis of HeLa cells expressing httEx1Q25/Q97-mRFP after treatment with antioxidants. Cells were pre-treated with 10mM NAC or 0.1mM Trolox for 12 hours before transfection and 72 hours after transfection, cellular toxicity was quantified. % cell death of cells expressing httEx1Q25-mRFP was subtracted from % cell death of httEx1Q97-mRFP to get a net toxicity caused by httEx1Q97-mRFP for all the samples (untreated and treated). The net toxicity of untreated httEx1Q97-mRFP was then considered as 100%. The relative change in % cell death of antioxidant treated cells compared to untreated cells was calculated (antioxidant treated httEx1Q97-mRFP/untreated httEx1Q97-mRFP x 100). Error bars represent standard errors of the means. Unpaired t-test was performed * = $P < 0.05$, (n=3).

3.4 Discussion

In this chapter polyQ aggregation- and toxicity in four different cell systems were studied. The characterisation for httEx1 aggregation and toxicity was performed with the view to later explore ROS production, in relation to polyQ aggregation and toxicity, in these cells. HeLa cells, a cervical cancer cell line, were the first to be examined because these cells are particularly easy to manipulate. Next, transiently transfected PC12 and inducible PC12 cell systems were analyzed. PC12 cells are derived from a rat neuroendocrine tumor and are a standard cell-line model for neurons (Samiathan et al. 2008). After that, adenovirus mediated httEx1Q25/Q97 gene expression in HeLa cells was studied. Adenovirus mediated httEx1 expression is a useful approach as it has a high transduction efficiency capacity and can infect both replicating and differentiated cells without integrating into the host genome. Lastly, the ability of antioxidants to suppress poly-Q toxicity was studied in order to justify later studies into the relevance of ROS in these cell models.

N-terminal Exon 1 fragments were chosen and these were transiently or stably expressed within cells. N-terminal Exon-1 fragments are known to provide a relatively quick and robust aggregation and toxicity phenotype in different cells types (Aiken et al., 2004; Apostol et al., 2003; Lunkes and Mandel, 1998; Wyttenbach et al., 2000) and in mouse models (Mangiarini et al., 1996). Numerous studies have shown that small htt fragments are more toxic than large fragments or full length htt (Lunkes et al., 2002; Ratovitski et al., 2007; Schilling et al., 2007; Weiss et al., 2009; Wyttenbach et al., 2002). Indeed some of the most commonly used mouse models of HD are those modified with an N-terminal Exon-1 transgene. The R6/2 line is the best studied. R6/2 mice expressing httEx1 with expanded polyQ repeats, httEx1Q145, under the human htt promoter and present with formation of IBs followed by a progressive neurological phenotype including motor abnormalities and weight loss as observed in HD patients (Mangiarini et al., 1996). Similarly HD post-mortem brain studies showed the presence of IBs (Becher et al., 1998; DiFiglia et al., 1997; Gourfinkel-An et al., 1998) before onset of symptoms that contain N-terminal htt cleavage products. Hence httEx1 cell models have some relevance to HD (Aiken et al., 2004; Apostol et al., 2003; Wyttenbach et al., 2001).

In the first series of experiments the expression, aggregation behaviour and toxicity of httEx1Q25/72/97-mRFP versus EGFP in HeLa cells was evaluated. The httEx1Q72/Q97-mRFP Western blot analysis showed additional, unexpected, bands (Figure 3.1A) using the S830 antibody that detects httEx1. These extra bands could be cleavage fragments produced by caspases and recognised by the S830 antibody (the EM48 antibody also detects these cleavage products on a Western blot (see appendix 5). Western blot analysis demonstrated that there was no statistically significant difference in expression levels between mRFP versus EGFP constructs at any time point (with/without including the mRFP cleavage fragment in the analysis) (Figure 3.3). Including the cleavage fragment in the transgene analysis and assuming that this fragment contains an expanded polyQ stretch, expression of httEx1Q97-mRFP seems to be higher (approximately 2-3 times) compared to httEx1Q97-EGFP predicting that polyQ aggregation and IB formation and subsequent cell death should also be increased in comparison to httEx1Q97-EGFP. However polyQ aggregation and cell death comparisons between httEx1Q97-mRFP versus EGFP were remarkably similar (Figure 3.6 and 3.8). Hence it is unlikely that the additional, lower molecular weight band detected by the S830 antibody contained a continuous expanded polyQ stretch.

A thorough search of various online databases was performed to look for possible caspase cleavage sites within the httEx1Q72 and Q97-mRFP sequences, but none were found. Immunocytochemical analysis was then performed on HeLa cells by using EM48 antibody and 1C2 antibody in order to detect possible mRFP negative cleavage products/aggregates that could potentially confound the analysis. EM48 antibody did not detect any mRFP negative microscopically visible aggregates expected to aggregate if the cleavage product contained the expanded polyQ stretch. Hence, it seems likely that aggregating structures (IBs) specific to httEx1Q97-mRFP cleavage were absent. It remains unclear however why additional bands are detected upon expression of httEx1Q72/Q97-mRFP, but not for the EGFP constructs. To further investigate this, HeLa cells expressing httEx1Q97-mRFP could be treated with caspase inhibiting compounds and then run on SDS-PAGE gels to see whether these additional bands disappeared. Previous *in vivo* and *in vitro* studies implied that caspases are activated by abnormal polyQ expansions and as a result, cleavage

products are formed (Kim et al., 2001; Mende-Mueller et al., 2001; Wellington et al., 1998; Wellington et al., 2000; Wellington et al., 2002).

The second set of experiments was to compare EGFP versus mRFP experiments over a set time course. A significant increase in IB formation (Figure 3.6) and cell death (Figure 3.8) of cells expressing mutant httEx1-EGFP/mRFP versus cell expressing wild-type httEx1-EGFP/mRFP constructs was observed. PolyQ-length dependant IB formation and toxicity is one of the features of HD and could hence be modelled in this system. IB formation and toxicity was not statistically significant between cells expressing httEx1Q97-EGFP versus mRFP (Figure 3.6 and 3.8). This finding is important as the constructs with the different fluorescent proteins can now be used for comparative ROS analysis (see Chapter 4). In addition to this, biochemical assays (dot blot) did also not show significant differences in SDS insoluble material in cells expressing httEx1Q97-EGFP versus mRFP at any time point (Figure 3.7). Similar to IB formation, an increase in SDS insoluble material from day 1 to day 2 was observed, whereas a reduction in SDS insoluble material was observed at day 3, likely due to cell death. Hence the dot blot assay, as a semi quantitative method, did exactly reflect IB counting data.

Following the HeLa cell experiments the response of PC12 cells to transient transfection with httEx1Q25/Q97-mRFP constructs was characterized. The PC12 cells showed faster IB formation and toxicity progression than HeLa cells did (Figure 3.12A). A PC12 inducible cell system that expresses httEx1Q25/Q103-EGFP transgenes under the control of a tebufenozide inducible promoter was then employed. In this system, cells again showed a significant increase in IBs and toxicity over time with significant toxicity only at day 2 and 3 (Figure 3.13A). Another PC12 inducible cell line (14A2.5) that expresses tHttEx1Q103 glutamines showed a progressive increase in IB formation (Figure 3.14A), but no significant toxicity was observed at any time as compared to uninduced cells (Figure 3.14B). Finally, adenovirus mediated expression of mhttEx1 produced a robust and a time dependant increase in polyQ aggregation and toxicity (Figure 3.15 and 3.16).

Although, a similar time dependant IB formation and toxicity was observed in all the systems the number of IBs at each time point varied from one system to the other. For

example using transient transfection, HeLa cells showed less IB formation compared to PC12 cells over time. In stable cell systems and adenovirus mediated httEx1 expression in HeLa cells, the rate of IB formation was higher compared to transient httEx1 expression in HeLa and PC12 cells. The tHttEx1 model showed the highest percentage of aggregates at 48 hours post-induction as compared to all other systems (Figure 3.14A). As mentioned earlier in this chapter, smaller fragments are more likely to aggregate and form IBs than bigger fragments. The fact that this tHttEx1 fragment model has the highest IB formation supports this notion.

PC12 cells showed a higher rate of IB formation in transient transfection experiments compared to HeLa cells and this difference seems likely a cell line effect as there was no difference observed in transfection efficiency. Wyttenbach et al., (2000) also reported that PC12 cells form more mhttEx1 aggregates than COS-7 and SH-SY5Y and there was no direct correlation observed between expression levels and IBs in these cell lines. These effects may be due to differences in the chaperone levels of each line. PC12 stable cell systems formed more mhttEx1 aggregates in comparison to the transient systems. This could be explained by integration of transgenes within the host DNA so that daughter cells express the transgene/s, whereas, in the case of transient transfection, DNA plasmids are lost and expression decreases over cell generations. On the other hand, Adenovirus mediated gene expression has been shown to be a more efficient and controllable means of gene delivery compared to other conventional transfection procedures (Kass-Eisler et al., 1993; Kirshenbaum et al., 1993). Various MOIs can be used in such experiments to control gene expression. For example, an MOI of 10 would mean there are 10 virus particles carrying mhttEx1 available to infect each cell, and indeed a more robust mhttEx1 aggregation can be observed with adenovirus as compared to transiently transfected HeLa cells.

Having compared the levels of IBs and toxicity seen in both HeLa and PC12 cells due to the presence of mhttEx1 the next step was to examine the possible mechanisms of cell death in these models, providing additional insight into a possible impaired redox homeostasis due to mhttEx1, as described in the next chapter. Mitochondria play a critical role in cell death by releasing apoptogenic factors, for example, cyt *c*, apoptosis inducing factor (AIF), Smac/Diablo, Omi/HtrA2 and endonuclease G from the intermediate space into the cytoplasm (Li et al., 1997). Cyt *c* is known to be

released from the mitochondria and binds to apoptosis inducing factor-1 activating caspase-9 that subsequently results in caspase-3 activation. Caspase-3 triggers many of the terminal cell death events. Caspase-1, -3 and -9 activation has been previously reported to be activated in end stage HD patients' brain specimens (Kiechle et al., 2002; Kim et al., 2001), mouse models (Ona et al., 1999; Sanchez Mejia and Friedlander, 2001) and cell models (Apostol et al., 2006; Sawa et al., 2005; Wellington et al., 1998; Wellington et al., 2000). Chang et al., (2002) described two mechanisms of cell death in post-mitotic cells such as neurons: 1) The classic pathways of cell death where e.g. NGF deprivation in the absence of caspase inhibitors causes Cyt *c* release which then leads to activation of caspases followed by cell death, 2) Slower forms of cell death due to the loss of the mitochondrial membrane potential in the presence of caspase inhibitors. Cyt *c* release and caspase-3 activation both occurred in HeLa cells expressing httEx1Q97-EGFP/mRFP on day 3 (Figure 3.9 and 3.10). Despite many differences compared to neurons, this observation suggests that mhttEx1 induced cell death occurs via the classical apoptotic pathways in our httEx1 HeLa cell model.

Mitochondrial membrane potential reflects the pumping ability of hydrogen ions across the inner mitochondrial membrane during the ETC and oxidative phosphorylation. Thus complete loss of mitochondrial membrane potential triggers apoptosis and is therefore also used as a death marker. Cells expressing httEx1Q97-EGFP did not show a loss in mitochondrial membrane potential, as determined by using MitoTracker Orange (Figure 3.11). MitoTracker was the only dye employed as the aim at this point was to obtain another marker for cell death and not to examine more modest mitochondrial dysfunction or mitochondrial potential changes. One potentially illuminating further experiment would be to carefully quantify the effect of polyQ expansions on mitochondrial membrane potential. Membrane potential can be monitored by using additional membrane-potential sensitive dyes such as TMRE or JC-1. For example, JC-1 is a cationic carbocyanine ratiometric dye that accumulates in mitochondria. The dye yields green fluorescent at low concentration and exists as a monomer whereas at higher concentrations, the dye forms J-aggregates that demonstrate a broad excitation spectrum with maximum emission at 595nm. These properties make this dye a much more sensitive and more quantitative membrane potential marker than MitoTracker.

Having established that cells expressing mhttEx1 died via a classical apoptotic route the next step was to begin to examine some of the causes of this cell death, one of which could be the induction of oxidative stress. L-NAC has previously been shown to significantly reduce polyQ induced cellular toxicity in COS-7 and SK-N-SH cells (Wyttenbach et al., 2002). Furthermore, Charvin et al., (2005) reported that dopamine aggravates mhttEx1 toxicity in striatal neurons through ROS production that ultimately leads to the activation of pro-apoptotic the c-Jun/JNK pathway and this effect was also rescued by an antioxidant called ascorbate. L-NAC and Trolox were indeed shown to rescue polyQ toxicity in HeLa cells (Figure 3.17). L-NAC is known to provide protection against oxidative stress by inducing endogenous cellular glutathione and is also known to have anti-apoptotic activity (Ceconi et al., 1988). Trolox, a water-soluble derivative of vitamin E, has been shown to be protective against ischemia and reperfusion induced oxidative stress (Sagach et al., 2002). Similarly, a human microglial cell line (HM06) was shown to increase intracellular Ca^{2+} level, ROS production and cell death when treated with 3-NP (Ryu et al., 2003) that was rescued with Trolox treatment. Furthermore, Trolox has been shown to provide protection in hippocampal neuronal slice cultures against pro-inflammatory cytokine (IL-1β) ROS induction associated with neuronal degeneration (see next chapter for mechanism of action of Trolox) (Radesater et al., 2003). Hence the use of Trolox (and L-NAC) warrants further investigation in *in vivo* models of HD. L-NAME, is an RNS inhibitor, and was also used in our studies as elevated levels of 3-nitrotyrosine, a marker for RNS damage to proteins, was previously observed to occur in chemical (3-NP) and genetic (R6/2) mouse models of HD (Matthews et al., 1998; Tabrizi et al., 2000) and in HD patient brains (Browne et al., 1999). However, L-NAME in the HeLa cell model did not provide protection and therefore future experiments focused only on ROS.

Due to the fact that the cell models used here established a clear temporal separation between onset of aggregation at day 1 and cell death at day 2-3, and antioxidants provided protection against cell death supporting a functionally relevant role for ROS, it provided a platform to study the role of ROS production in relation to polyQ aggregation and toxicity.

4 The production of ROS in neuronal and non-neuronal httEx1 cell models

4.1 Introduction

As shown in the previous chapter, polyQ expansions in Exon1 causes significant intracellular aggregation that correlates with toxicity in several HD cell models and these two phenomena are polyQ length dependent. PolyQ aggregation is a key feature of HD, but there are other factors, perhaps linked to aggregation, that are believed to contribute to the pathogenesis of HD (reviewed in Browne and Beal, 2006a; Ho et al., 2001; Landles and Bates, 2004). One such factor is oxidative stress and one aim of this thesis is to model oxidative stress in HD cell models.

As outlined in the general introduction, ROS likely contributes to neurodegeneration by causing damage to macromolecules such as proteins, lipids and DNA. Studies in rodent HD models and human HD patient post-mortem brain indeed showed the presence of oxidative damage (Browne et al., 1997; Perluigi et al., 2005; Tabrizi et al., 1999; Tabrizi et al., 2000). Antioxidant enzymes provide a major defence against ROS (reviewed in Mates et al., 1999) and some of these are also altered in rodent models of polyQ disease (Choo et al., 2005; Cui et al., 2006; St-Pierre et al., 2006; Tunez et al., 2006). Furthermore, HD transgenic mouse studies suggested that CoQ10 enzyme administration exerts a neuroprotective effect and slows down disease progression (Schilling et al., 2001). In HD cell models antioxidants are known to protect against mhttEx1 induced toxicity (Wyttenbach et al., 2002, also see previous chapter) and cells appear to react to polyQ expansions by up regulating ROS responsive genes (van Roon-Mom et al., 2008; Wyttenbach et al., 2001).

In the aforementioned cell studies, increased ROS was associated with expression of mhttEx1, but it remained unclear whether the increase in ROS was simply due to on-going cell death processes that are known to be associated with increased ROS (Greenlund et al., 1995; Manev et al., 1995; Valencia and Moran, 2004) or whether earlier events caused by the presence of mhttEx1 impacted on redox homeostasis. Furthermore, it is known that ROS are involved in the regulation of cell signalling and, therefore, are not solely detrimental (D'Autreaux and Toledano, 2007). Hence,

small alterations in ROS production occurring in HD could be involved in its pathogenesis due to abnormal ROS signalling.

There is sufficient evidence in the literature to suggest that an increase in ROS production could occur due to the presence of mhttEx1 (general introduction), therefore, it was important to discover the cellular origin of ROS production in this context. As outlined in the general introduction, intracellular ROS can be produced in the cytoplasm by various enzyme systems, the Fenton reaction and also by the leakage of electrons from the ETC of mitochondria (see section 1.6.5.4 for more detail). HD mouse models and patient studies reveal that ROS are likely to cause damage to mitochondria and hence are detrimental (cevedo-Torres et al., 2009; Polidori et al., 1999). The disruption of mitochondria by ROS can activate various signalling pathways that lead to cell death (Kirkland et al., 2002; Kirkland and Franklin, 2007). Interestingly, it has been shown that both wild-type and mhtt and some of its cleavage fragments are associated with the mitochondrial membrane and hence could directly contribute to mitochondrial dysfunctions (reviewed in Quintanilla and Johnson, 2009). Thus impaired mitochondrial functions could contribute to ROS production in HD.

Hence, this chapter outlines an analysis of ROS production in living cells expressing wild-type or mhttEx1 using oxidation sensitive dyes in time course experiments. Once the cellular origin of ROS is identified it might be possible to target it with specific inhibitors and ameliorate ROS-induced toxicity. Towards this end, mitochondrial targeted antioxidant (MitoQ) and Trolox were employed.

4.2 Aims

The first aim of this chapter was to study ROS kinetics in neuronal and non-neuronal cell systems by using transient- and stable httEx1 expression. The second aim was to determine the cellular origins of ROS, caused by the presence of mhttEx1, using a relatively specific inhibitor of the cellular ROS generating systems within mitochondria and to manipulate ROS production by using antioxidants.

4.3 Results

4.3.1 Live cell analysis of ROS in HeLa cells using 5-(and-6)-chloromethyl-2',7'-dichlorodihydrofluorescein diacetate, acetyl ester (CM-H_2DCFDA)

The concentration and incubation time of 5-(and-6)-chloromethyl-2',7'-dichlorodihydrofluorescein diacetate, acetyl ester (CM-H_2DCFDA, short: DCF) was previously optimized for HeLa cells (Dr. S. Hands, see methods). In order to ensure that cells have taken-up sufficient DCF and the availability of this compound was not limiting, HeLa cells were either untransfected or transiently transfected with httEx1Q25/Q97-mRFP and incubated with 8µM of DCF for 20 minutes and imaged on the confocal microscope before and after treatment with H_2O_2. Under these conditions, H_2O_2 was able to significantly and equally increase the signal obtained by DCF oxidation (data not shown). Hence, this showed that DCF was taken up similarly in either untransfected or httEx1Q25/Q97 expressing cells and there was enough DCF available inside cells to measure ROS (DCF oxidation was not saturated).

Time course experiments were then performed over 3 days and the fold difference in the oxidation of DCF was calculated by dividing the area controlled mean pixel intensity of Q97-mRFP expressing cells over the mean pixel intensity of Q25-mRFP expressing cells (as described in the Materials and Methods section 2.10.1). Pixel intensity analysis was only performed in cells expressing mRFP transgenes and these were selected by using computer software (Metamorph). Figure 4.1A shows a ca. 2-fold increase in DCF fluorescence intensity (ROS production) at 24 hours after transfection, whereas no change was observed at 48 and 72 hours. An analysis by using cumulative frequency distributions of DCF oxidation in HeLa cells expressing httEx1Q25/Q97-mRFP was additionally performed using two computer languages (‘R’ and ‘Python’, kindly provided and done in collaboration with Dr. R. Edwards). Cells expressing httEx1Q97-mRFP showed a clear shift in their distribution towards higher pixel intensity values compared to cells expressing httEx1Q25-mRFP at day 1, whereas no change was observed at later time points (see appendix 7).

Mean pixel intensity analysis of mRFP fluorescence only in cells expressing httEx1Q25-mRFP versus httEx1Q97-mRFP was also performed in addition to Western blot analysis (as shown in the previous chapter) to compare the expression

level of the two transgenes. Figure 4.1B shows no significant difference in the expression levels of cells expressing httEx1Q25-mRFP and httEx1Q97-mRFP at any time point. Figure 4.1 C and D are examples of cells expressing httEx1Q25/Q97-mRFP after incubation with DCF for 20 minutes under the above-described imaging conditions.

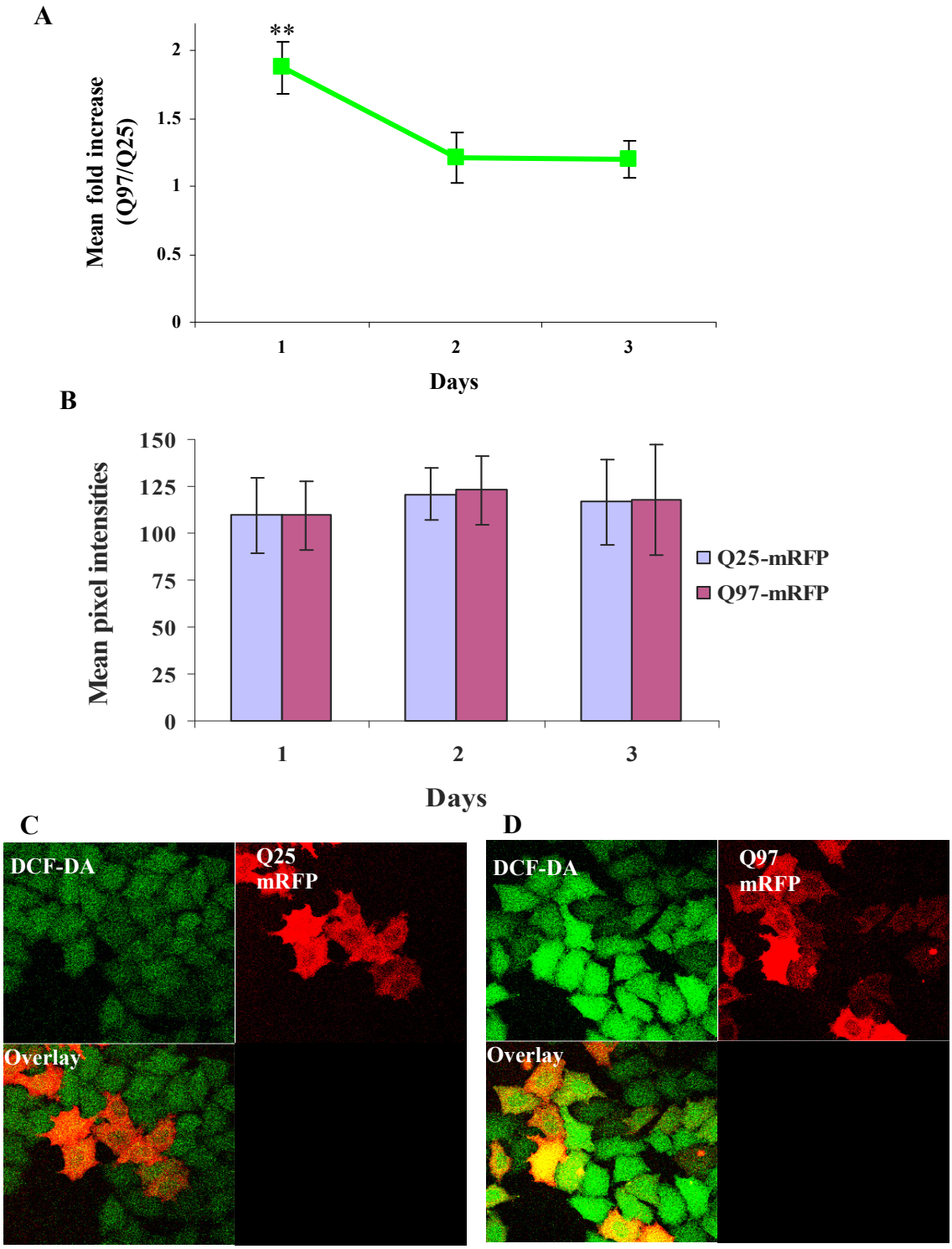

Figure 4.1 ROS analysis of cells expressing httEx1Q25-mRFP versus httEx1Q97-mRFP using DCF. (A) Fold increase in the oxidation of DCF in cells expressing httEx1Q97-mRFP versus httEx1Q25-mRFP at day 1-3. **(B)** Transgene expression analysis of cells expressing httEx1Q25-mRFP versus httEx1Q97-mRFP over time. **(C)** and **(D)** are examples of cells expressing httEx1Q25/Q97-mRFP imaged with the confocal microscope after incubation with DCF. Error bars represent standard deviations. Unpaired t-test was performed for statistical analysis. ** = $P<0.01$ (n=6 at day 1 and n=3 at day 2-3).

4.3.2 Measurement of ROS in living HeLa cells using Dihydroethidium (DHE)

In addition to the DCF analysis shown above, DHE was used as another ROS sensor to measure ROS in HeLa cells expressing EGFP tagged-httEx1 constructs with identical polyQ stretches. DHE is specifically oxidised by the superoxide anion radical, whereas DCF is not radical-specific and can be oxidised by hydrogen peroxide, hydroxyl radicals and peroxynitrite (Halliwell and Whiteman, 2004). As mentioned above, the use of oxidative sensitive dyes is problematic, therefore it was important to optimise the concentration and incubation time of DHE for HeLa cells. The optimal conditions for the experiments were 5µM of DHE applied for 20 minutes (data not shown). Antimycin A was used as a positive control to show that there was sufficient dye available inside cells at the various time points after transfection. Antimycin A is a mitochondrial complex III inhibitor and cells, upon Antimycin A treatment, produce superoxide anion radicals. Addition of Antimycin A (100µM) to HeLa cells transfected with either httEx1Q25 or httEx1Q97-mRFP transgenes caused a similar significant increase in mean fluorescence within cells after DHE incubation (6-7-fold compared to untreated cells, data not shown). Hence the above mentioned experiment suggests that oxidation of DHE (Figure 4.2) was below the saturation point and the availability of DHE at 5µM concentration was not limited.

ROS production was then measured in time course experiments of cells expressing httEx1Q25/Q97- EGFP with incubation of 5µM DHE and subsequent confocal imaging. The analysis was performed as explained in the Materials and Methods section 2.10.1. Figure 4.2A shows pooled data from three independent experiments. A ca. 2-fold increase in oxidation of DHE at day 1 was found, whereas no significant change in ROS was observed at day 2 and day 3. This result was similar to what was observed using DCF and mRFP constructs. There was no significant difference observed between either EGFP-tagged transgenes (EGFP fluorescence) at any time point for these experiments (Figure 4.2B). Figure 4.2C and D show cells expressing httEx1Q25/Q97-EGFP after incubation with DHE. Cumulative frequency distribution analysis of DHE oxidation was also performed over time (as outlined above). This analysis showed again that the DHE oxidation values shifted their distribution towards a higher intensity in cells expressing httEx1Q97-EGFP as compared to cells expressing httEx1Q25-EGFP at day 1, but not at day 2 and day 3 (data not shown).

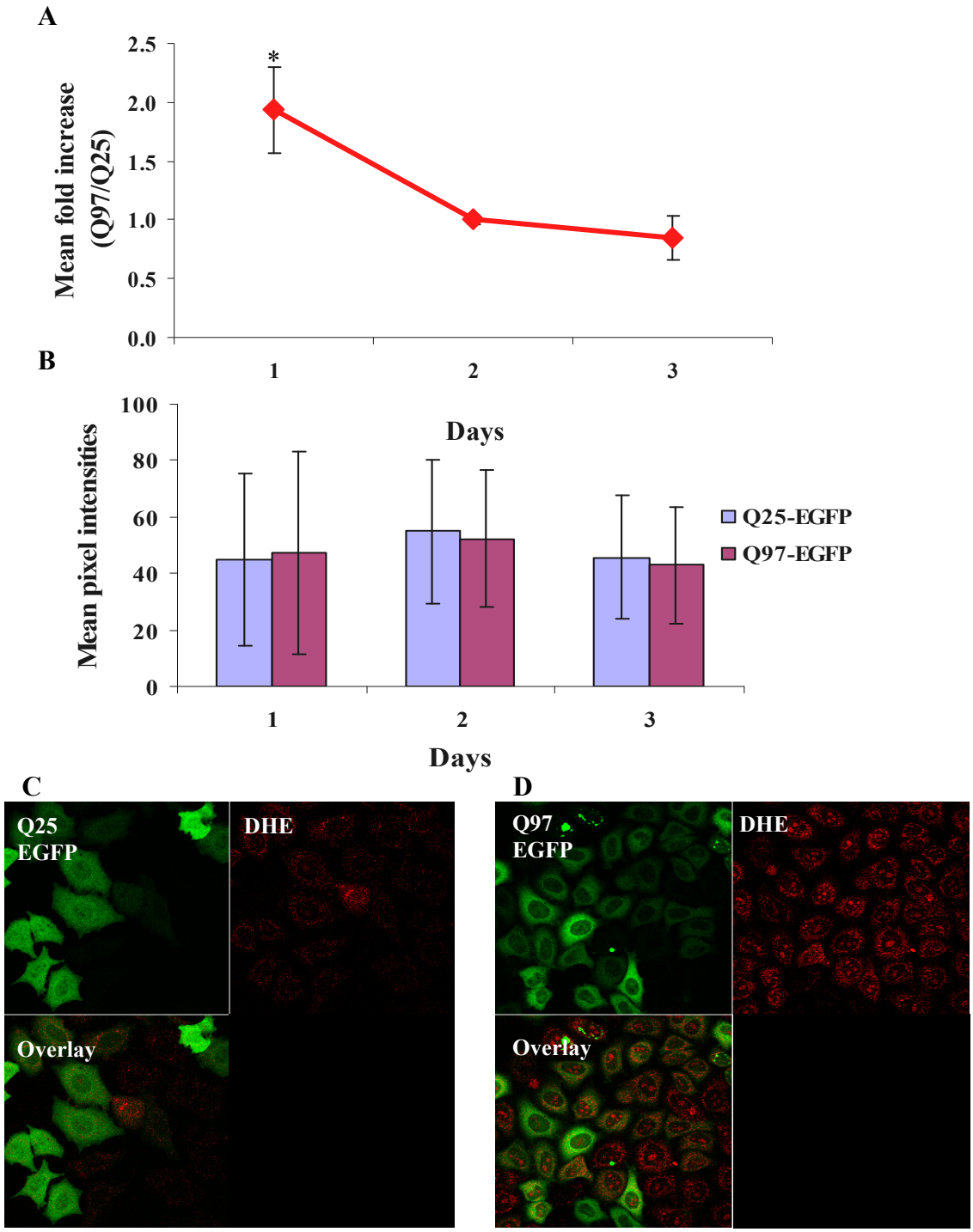

Figure 4.2 ROS analysis in cells expressing httEx1Q25/Q97-EGFP using DHE. **(A)** Fold increase in the oxidation of DHE in cells expressing httEx1Q97-EGFP versus httEx1Q25-EGFP at day 1-3. **(B)** Transgenes expression levels in HeLa cells over time. **(C)** and **(D)** are examples of cells expressing httEx1Q25/Q97-EGFP imaged with the confocal microscope after incubation with DHE. Error bars represent standard deviations and unpaired t-test was used for statistical analysis. * = $P < 0.05$ (n=3).

4.3.3 Measurement of ROS in living PC12 cells using DCF

HeLa cells (non-neuronal line) expressing httEx1Q97-EGFP or mRFP showed a significant increase in ROS at day 1. In order to confirm this finding in a neuronal cell line, the DCF- ROS analysis was repeated in rat pheochromocytoma (PC12) cells at day 1 only. PC12 cells were transiently transfected with httEx1Q25/Q97-mRFP using a different protocol (see the Materials and Methods section 2.2.3). PC12 cells expressing httEx1Q97-mRFP showed a statistically significant 1.7-fold increase in the oxidation of DCF at day 1 (Figure 4.3A). Cells expressing httEx1Q25 or Q97-mRFP showed equal levels of transgenes as measured by the red pixel intensity (Figure 4.3B). Figure 4.3C and D show examples of PC12 cells expressing httEx1Q25 or Q97-mRFP after incubation with 8μM of DCF. ROS data was also analysed as a cumulative frequency distribution, confirming an increase in ROS production in cells expressing httEx1Q97-mRFP at day 1 (see appendix 8). Additionally, cumulative frequency distribution analysis of DCF oxidation in PC12 cells expressing httEx1Q97-mRFP with or without IBs was performed. This analysis showed no difference in the oxidation of DCF at day 1 in cells with mhttEx1 IBs as compared to cells without mhttEx1 IBs (see appendix 9).

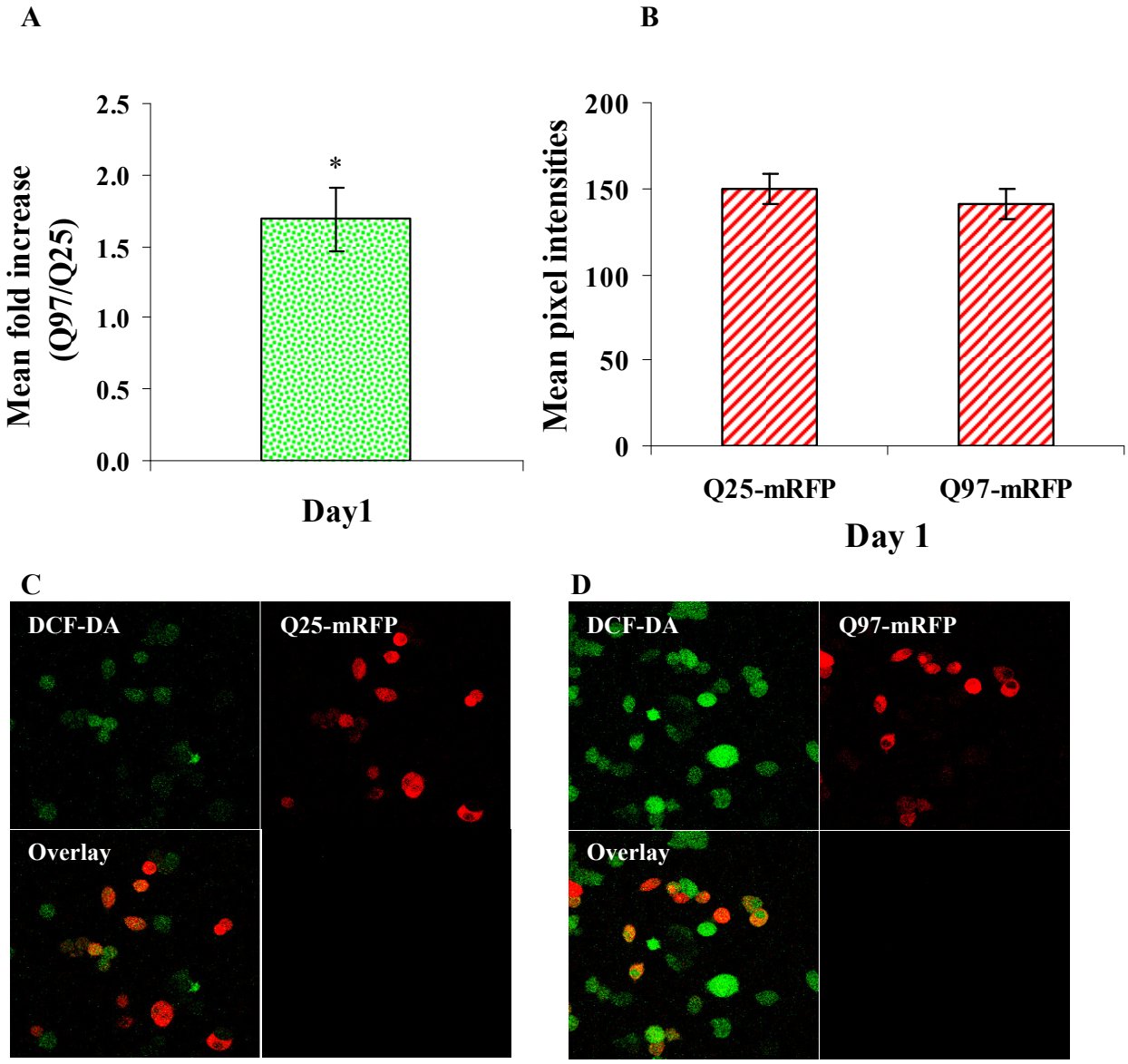

Figure 4.3 ROS analysis in PC12 cells transiently transfected httEx1Q25/Q97-mRFP at day 1 using DCF. (A) Fold increase in the oxidation of DCF in PC12 cells expressing httEx1Q97-mRFP versus httEx1Q25-mRFP. This increase was statistically significant. **(B)** Mean pixel intensity analysis of transgenes expression level in transiently transfected cells. **(C)** and **(D)** are examples of cells transfected with httEx1Q25/Q97-mRFP after incubation with DCF. Error bars represent standard deviations. T-test was used for statistical analysis * = $P<0.05$ (n=4).

4.3.4 ROS analysis in polyQ inducible PC12 cells using DHE

In order to gain further insight into the relationship between mhttEx1 and ROS production, an inducible cell system was used to exclude the possibility of any artificial change in ROS due to the use of transient transfection systems. Transient systems are relatively variable compared to inducible systems and hence inducible PC12 cells were used as another httEx1 model to re-confirm an increase in ROS observed in PC12 cells using transient transfection, as shown in Figure 4.3.

Tebufenozide- inducible PC12 cells were induced and incubated with 5μM of DHE and, after 10, 24 and 48 hours of induction, were imaged by using a confocal microscope. Because this cell system showed an earlier increase in polyQ aggregation as compared to the transient transfection systems (see Chapter 3), an earlier first time point (10 hours) was chosen. Figure 4.4A shows an increase in the oxidation of DHE at 10 and 24 hours, whereas no change in ROS production was observed at 48 hours after induction. These results are consistent with the findings in the transient cell systems and confirmed that the increase in ROS production was due to the presence of polyQ expanded httEx1 protein before any significant toxicity was detectable. There was no significant difference in the expression levels of httEx1Q25/Q103-EGFP at any time point (Figure 4.4B). Western blot analysis also showed correct band sizes of cells expressing httEx1Q25/Q103-EGFP (appendix 10). Once again, cumulative frequency distribution analysis of DHE oxidation was performed and confirmed that cells expressing httEx1Q103-EGFP shifted DHE oxidation frequency distribution to the right compared to cells expressing httEx1Q25-EGFP at 10 and 24 hours after induction. No change in distribution was observed at the later time point (see appendix 11).

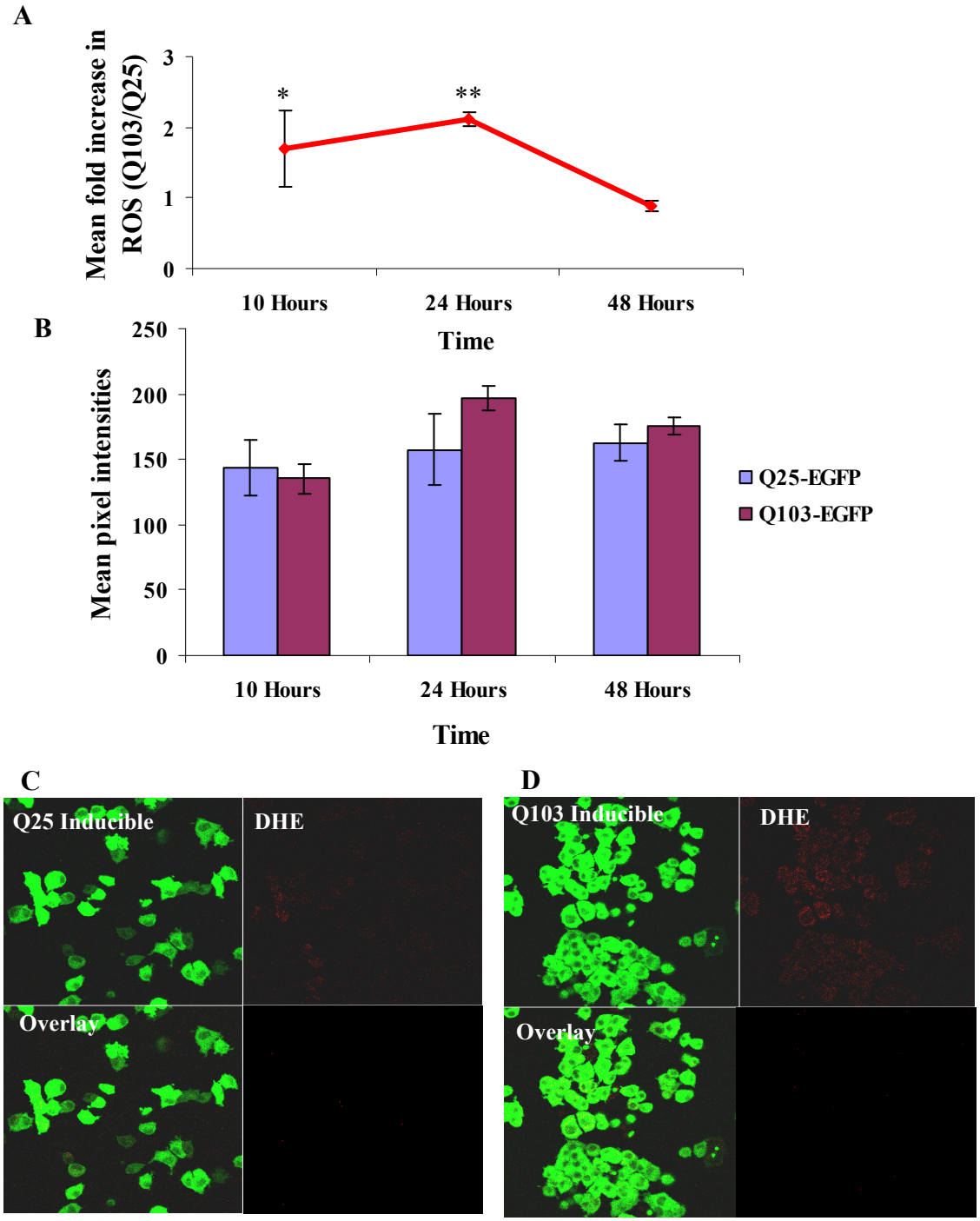

Figure 4.4 ROS analysis in PC12 inducible cells after transgene induction with 1µM tebufenozide at 10, 24 and 48 hours. **(A)** Fold increase in the oxidation of DHE in cells expressing httEx1Q103-EGFP versus httEx1Q25-EGFP **(B)** Transgene expression analysis of PC12 cells expressing httEx1Q25/Q103-EGFP at 10, 24 and 48 hours of induction. **(C)** and **(D)** are examples of PC12 cells after tebufenozide induced transgene expression of httEx1Q25/Q103-EGFP incubated with DHE. Error bars represent standard deviations and unpaired t-test was used for statistical analysis. * = $P < 0.05$ (n =3).

4.3.5 Cell population ROS assay confirms an early increase in ROS

The early increase in ROS in the transient- and PC12 inducible cell systems as measured by using confocal microscopy were confirmed using an entirely different approach. A fluorescent plate reader was applied to determine ROS changes in a population of cells. For this purpose, PC12 cells (14A2.5) containing an inducible mhtt Q103-EGFP transgene (a truncated htt exon 1 encoding only the first 17 aa of htt with 103 glutamine repeats and EGFP fused at its C-terminal, tHttEx1Q103-EGFP) were used, as described in Figure 3.14 (Chapter 3). 100,000 cells per well were seeded in a 96 well plate and tHttEx1Q103-EGFP expression was induced with 5μM of ponasterone A after 24 hours of seeding. Cells expressing tHttEx1Q103-EGFP showed a significant increase in ROS at 6-12 hours compared to un-induced cells, whereas no significant change in ROS was observed at later time points (Figure 4.5). These cells mostly form cytoplasmic IBs, with a significant increase in IB formation only after 12 hours (Figure 3.14C, Chapter 3). A control line expressing wild type tHttEx1 transgene was not used in this assay as it was not available, hence un-induced cells were used as a control. Transiently transfected cells were not appropriate for plate reader assays, as they were not transfected at a high enough efficiency (>90%) to detect differences in ROS.

PC12 tebufenozide inducible cells were not used for our plate reader analysis, as they presented with an early increase in IB formation during further passaging of cells compared to initial cell stocks (up to 50% of IBs at 10-12 hours, data no shown) due to unknown reasons.

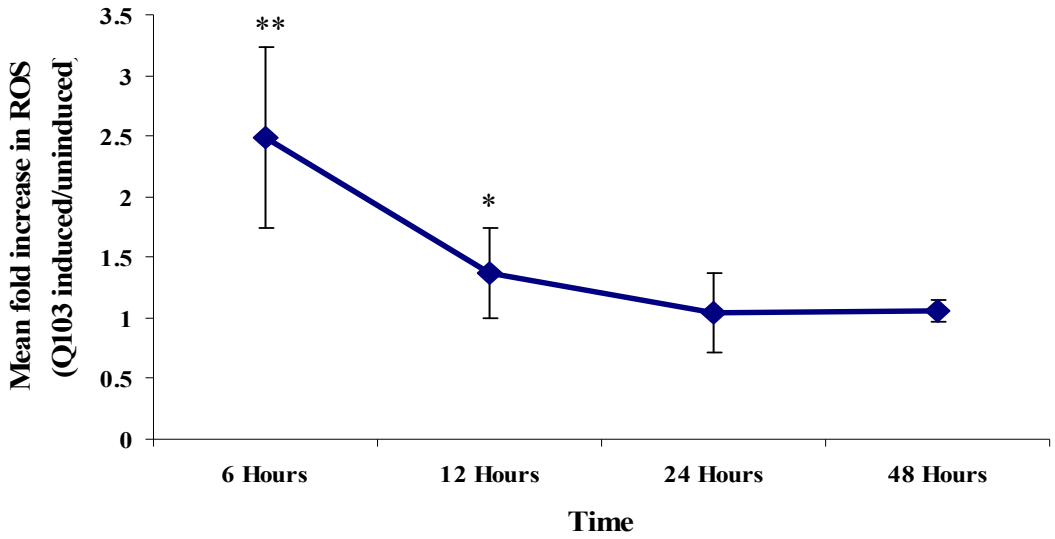

Figure 4.5 ROS analysis of PC12 inducible cell line expressing tHttEx1Q103-EGFP (14A2.5) by fluorescent plate reader. Cells were induced with 5µM of ponasterone A and analysed at 6, 12, 24 and 48 hours of induction. ROS was quantified in both induced and uninduced cells by incubating cells with 5µM of DHE at different time point. Unpaired t-test was performed for statistical analysis (n=3, * = $P<0.05$).

4.3.6 Inhibition of ROS by antioxidants and the cellular origin of ROS induced by mhttEx1

So far it has been demonstrated that aggregation-prone mhttEx1 causes a significant increase in early ROS. This increase in ROS seemed to occur before a significant amount of IBs were formed (Chapter 3, Figure 3.6 and 3.12-3.14). Although antioxidants such as L-NAC and Trolox inhibited polyQ toxicity in our cell models (Chapter 3, Figure 3.17), it is still unclear whether the early increase in ROS contributed to toxicity in the above-described cell systems, and where this ROS originates. Previous experiments have also shown that both glutathione and L-NAC inhibit cellular mhttEx1 toxicity in cells similar to the ones used in this study after transient transfection of httEx1Q103 (Wyttenbach et al., 2002) and a study by Ranganathan et al., (2009) showed elevated levels of ROS and toxicity in cellular models of SBMA, and this increased ROS and toxicity was inhibited by using the antioxidants Coenzyme Q10 and idebenone. The cellular origin of ROS in these studies remained unexplored.

In this section, experiments were performed using an antioxidant compound called MitoQ that specifically inhibits mitochondrial ROS. MitoQ is a mitochondrial-

targeted antioxidant consisting of a lipophilic triphenylphosphonium (TPP) cation that is covalently attached to an ubiquinol antioxidant (see Materials and Methods for details). A study by James et al., (2007) showed that the ubiquinone moiety of MitoQ quenches fluorophores deep within the membrane core of cells and this reflects a high concentration of the ubiquinone moiety within the membrane. In our initial experiments, cells were transiently transfected with httEx1Q25/Q97-mRFP constructs followed by treatment with 100nM of MitoQ for 1 hour prior to incubation of cells with 8μM of DCF. MitoQ quenched mRFP expression in cells transfected with httEx1Q25/Q97-mRFP and, as a result, the effects of MitoQ under these conditions could not be quantified (data not shown). Hence a different protocol had to be adapted to investigate the effects of MitoQ.

Pletjushkina et al., (2006) showed that HeLa cells pre-treated with MitoQ for 7 days significantly inhibited H_2O_2 (50μM for 4 hours) induced mitochondrial fission leading to cellular toxicity due to oxidative stress. Therefore a similar approach was examined and adopted. First, HeLa cells were pretreated with 20nM of MitoQ or TPP^+ for 7 days in order to verify MitoQ effects on mitochondrial network morphology, as described by Pletjushkina et al., (2006). MitoQ or TPP^+ pre-treated and untreated HeLa cells were then incubated with 100μM of H_2O_2 for 4 hours followed by MitoTracker deep red incubation. Figure 4.6 shows that both untreated and TPP^+ treated cells have fragmented mitochondrial morphology when incubated with H_2O_2, whereas cells treated with MitoQ retain mitochondrial morphology in a more fused state under H_2O_2 stress, confirming previous studies.

To investigate whether MitoQ had any effects on the increased ROS production after httEx1Q97-mRFP expression, HeLa cells were treated with 20nM of MitoQ for 7 days, then washed with PBS before replacing the media. Cells were then grown without MitoQ for two days, transfected with httEx1Q25/Q97-mRFP constructs for 24 hours followed by incubation with 8μM of DCF (see Figure 4.7 for comparisons of confocal pictures). There was a >2- fold increase in the oxidation of DCF in untreated cells expressing httEx1Q97-mRFP compared to httEx1Q25-mRFP whereas cells pre-treated with 20nM of MitoQ expressing httEx1Q97-mRFP showed a significant decrease in the oxidation of DCF compared to untreated cells (Figure 4.8A). As mentioned earlier, MitoQ consists of Coenzyme Q10 covalently attached to

TPP^+. In order to confirm that the effect of MitoQ was due to the ubiquinol, cells were treated with TPP^+ in parallel experiments with MitoQ. Cells treated with TPP^+ still showed a ca. 2-fold increase in the oxidation of DCF. Transgene expression data did not show any significant difference in expression levels of transgenes at 24 hours (Figure 4.8B). These findings suggest that mitochondria could be the origin of ROS production due to httEx1Q97-mRFP expression.

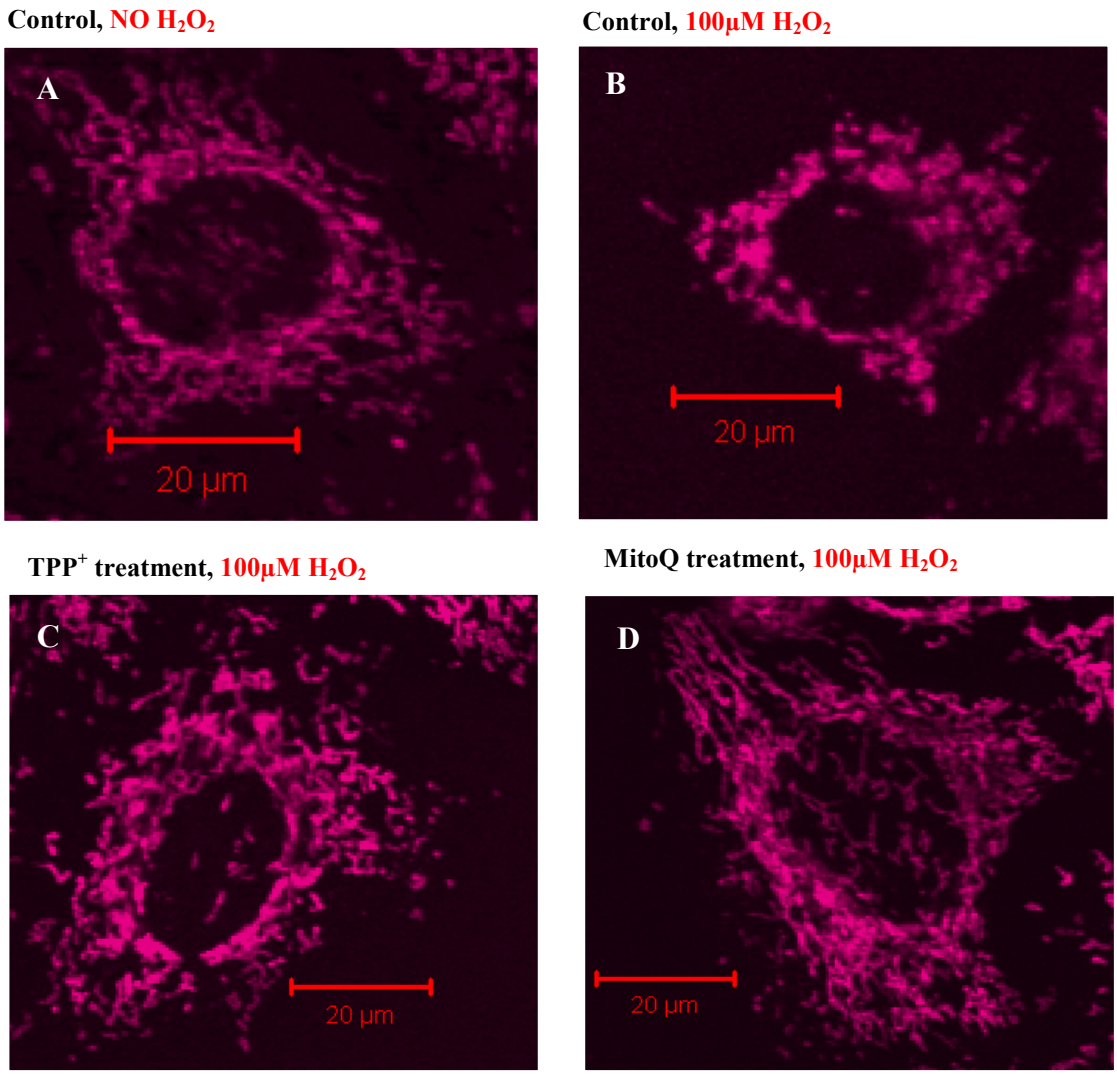

Figure 4.6 Mitochondrial morphological analysis of HeLa cells treated with MitoQ and TPP+ under normal and oxidative stress conditions. HeLa cells were treated with 20nM of MitoQ and TPP^+ for 7 days followed by incubation with MitoTracker deep red and live cells were imaged using a confocal microscope. **(A)** Tubular mitochondrial morphology under normal conditions. **(B)** 100µM H_2O_2 treatment for 4 hours causes mitochondrial fragmentation. **(C)** TPP^+ pre-treatment does not provide a protection against H_2O_2 induced fragmentation. **(D)** MitoQ pre-treatment prevents mitochondrial fragmentation under oxidative stress condition. Scale bar is 20 µm.

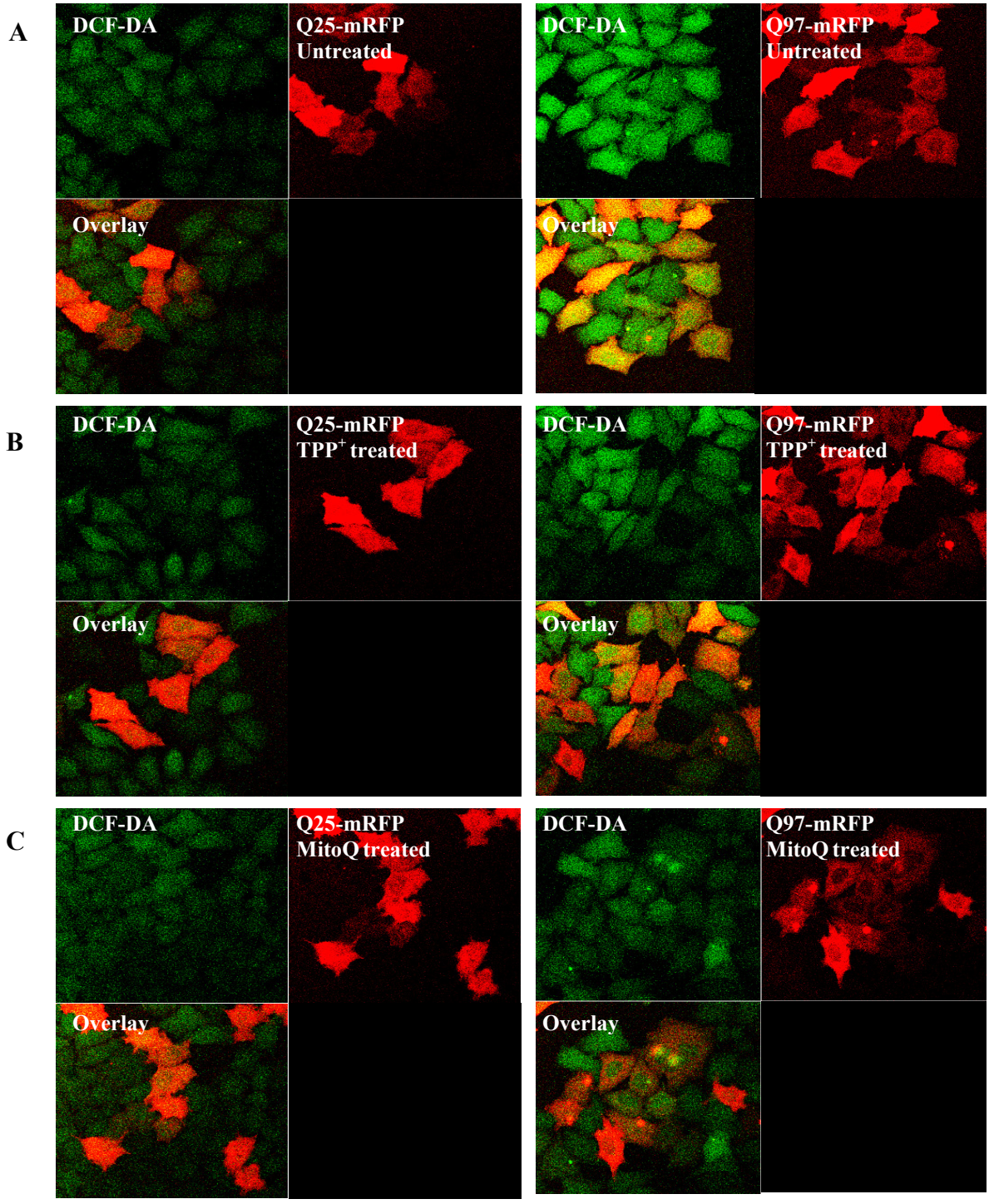

Figure 4.7 ROS analysis of HeLa cells expressing httEx1Q25/Q97-mRFP without treatment or with MitoQ or TPP^+ treatment. (A) HeLa cells expressing httEx1-Q25/Q97-mRFP in the presence of DCF-DA after 24 hours of transfection without any treatment, **(B)** with TPP^+ treatment and **(C)** with MitoQ treated.

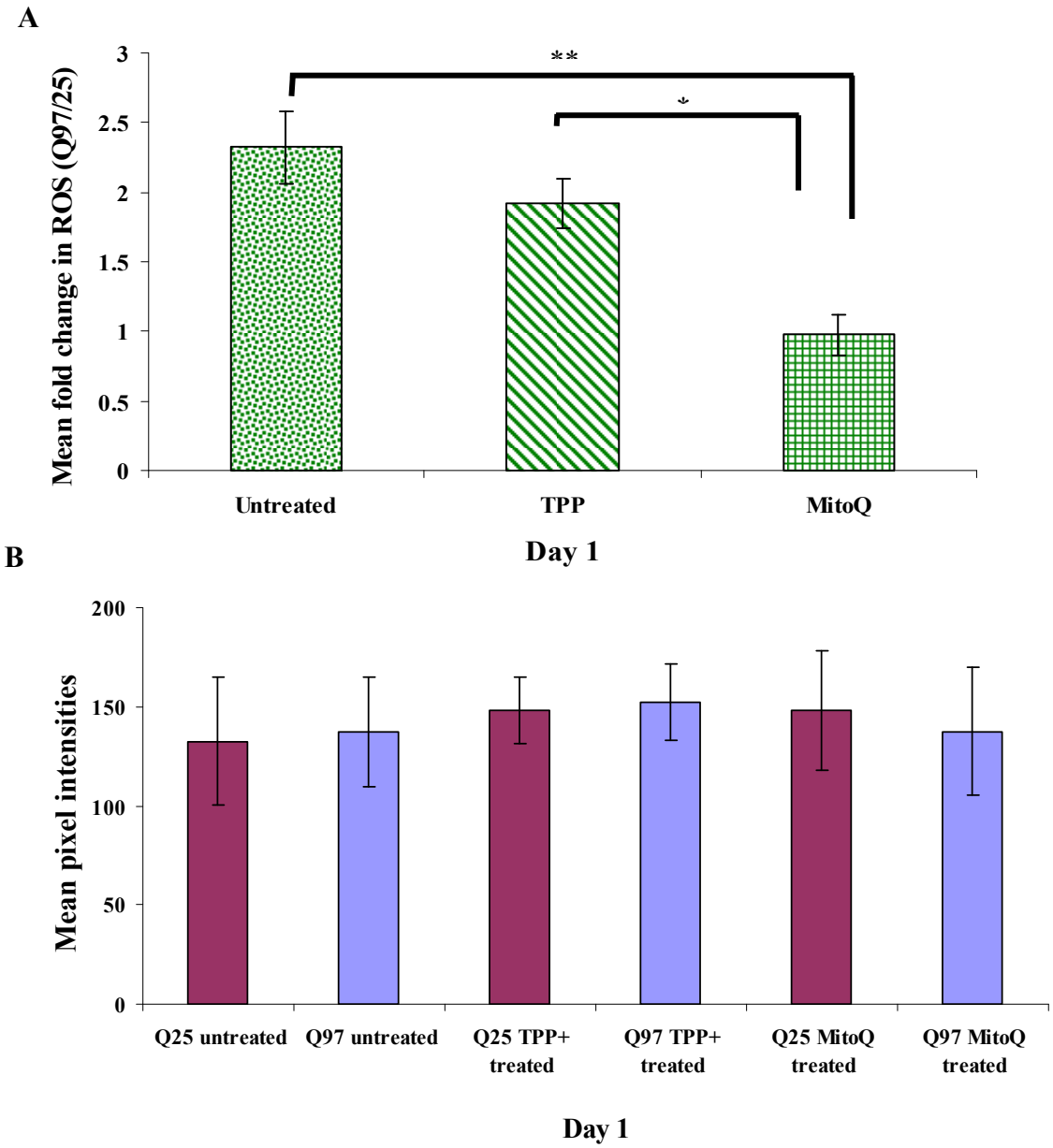

Figure 4.8 Effect of TPP^+ or MitoQ treatment on httEx1Q25/Q97-mRFP induced ROS in HeLa cells. (A) Fold difference in the oxidation of DCF in untreated cells expressing httEx1Q97 versus httEx1Q25, cells treated with TPP^+, and cells treated with MitoQ. **(B)** Pixel intensity analysis of transgenes in cells expressing httEx1Q25/Q97-mRFP untreated or treated with TPP^+ or MitoQ. Error bars represent standard deviations. 50-100 cells expressing httEx1Q25 or Q97-mRFP were quantified for each experiment (n=3, * = $P<0.05$, ** = $P<0.01$).

To demonstrate that other antioxidants were able to suppress httEx1Q97 induced ROS, cells were exposed to Trolox with subsequent ROS analysis. Trolox is a water-soluble derivate of vitamin E which integrates into cell- and mitochondrial membranes where it provides protection against oxidative stress (see discussion for details). 100μM of Trolox treatment 12 hours prior to transfection significantly decreased mhttEx1-mRFP induced ROS as compared to untreated cells (Figure 4.9A). Figure 4.9B shows that there is no significant difference in pixel intensities between cells expressing httEx1-Q25/Q97-mRFP with or without Trolox treatment. L-NAC also reduced the early ROS peak (Dr. S. Hands, personal communication). Together, these results suggest that two antioxidants other than MitoQ that were shown to reduce httEx1Q97-mRFP toxicity (Figure 3.17, Chapter 3) also suppressed the early ROS peak.

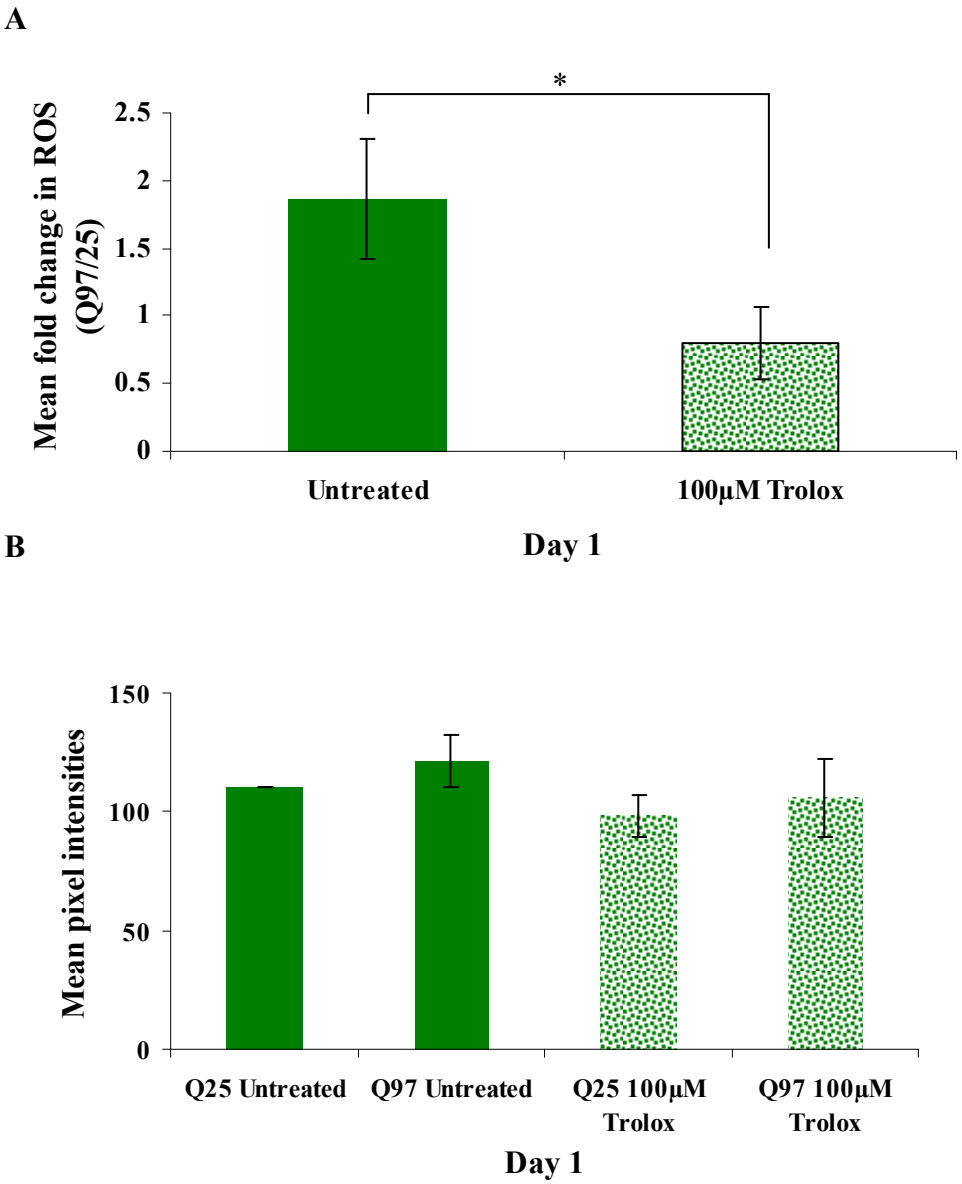

Figure 4.9 Antioxidant effect of Trolox on HeLa cells expressing httEx1 Q25/Q97-mRFP. (A) Effect of 100µM Trolox in the oxidation of DCF-DA in HeLa cells expressing wild-type (httEx1Q25) and mhtt (httEx1Q97). (**B)** Pixel intensity analysis of HeLa cells expressing httEx1Q25/Q97-mRFP with and without Trolox treatment. Error bars represent standard deviations. Unpaired t-test was used for statistical analysis. (n=3; * = $P<0.05$).

4.4 Discussion

Increased oxidative stress has been documented to occur in the HD brain (Browne et al., 1997; Klepac et al., 2007; Polidori et al., 1999), in several mouse models of HD (Bogdanov et al., 2001; cevedo-Torres et al., 2009; Perez-Severiano et al., 2000; Perez-Severiano et al., 2004; Tabrizi et al., 2000) and in cell models after expression of expanded polyQ stretches (Li et al., 2010; van Roon-Mom et al., 2008; Wyttenbach et al., 2002). However, in all these studies it was unclear if increased ROS was due to on-going cell death processes (e.g. apoptosis) or occurred before cell death. Hence the aim of this chapter was to carefully monitor ROS for comparison to polyQ aggregation and cell death in the HD cell models characterised in the previous chapter.

An increase in ROS production in living HeLa cells transiently transfected with httEx1Q97-mRFP or EGFP was observed by using DCF and DHE (respectively). These experiments were performed over a three-day time course and a significant ROS increase was observed only at 24 hours after transfection (Figure 4.1A and 4.2A). PC12 cells were then used to confirm this early increased ROS due to httEx1Q97 expression (Figure 4.3A). Furthermore, an inducible PC12 cell system was employed in which expression of httEx1Q25 or Q103-EGFP could be obtained after addition of tebufenozide. Again, an early increase in ROS was found during mhttEx1 expression (Figure 4.4A). This early increase in ROS was also observed in a population of cells (PC12 ponasterone A inducible cell system) using a plate reader assay (Figure 4.5).

The expression levels of the different transgenes used are important in the interpretation of these results, as, for example, a higher expression level of mhttEx1 may cause higher ROS production. The transgene expression data using Western blot analysis (Figure 3.3, Chapter 3) and a comparative analysis of pixel intensities of EGFP- and mRFP tagged transgenes suggested that there was no significant difference between transgene expression levels in all of our experiments. Hence, it is unlikely that a difference in expression levels is a confounding factor. It is important to notice however that pixel intensity analysis of transgenes tagged with fluorescent proteins may not truly reflect transgene expression levels. This may be due to a difference of the expanded polyQ region in mhttEx1 compared to wild-type httEx1 showing a different protein folding capacity and potentially resulting in different fluorescence properties. Furthermore, cells expressing mhtt (httEx1Q97-EGFP or mRFP) form fluorescent bright IBs that

may well contribute to a false measurement of high transgene expression levels as compared to wild-type htt (httEx1Q25-EGFP or mRFP) expressing cells. This is however an unlikely confounding factor as the proportion of cells with IBs at early time points was minimal (when ROS was highest).

The ROS kinetics in all of the cell models and cell types (transient and inducible) using two different analysis of ROS measurements suggested that an early increase in ROS occurred due to mhttEx1 expression (Figure 4.1- 4.5) and not due to ongoing cell death, as this occurred only at later time points (day 2-3) (Figure 3.8-3.10, 3.12 and 3.13, Chapter 3). Also a significant amount of IB formation in these cell systems was only observed after the early ROS peak and hence a significant presence of IBs was not associated with increased cellular ROS. These results imply that increased early ROS could be due to the formation of toxic intermediate species such as oligomers and precursors of fibrils that lead to aggregate/IB formation. This hypothesis is supported by unpublished findings showing that inhibition of polyQ aggregation using intrabodies or chemical compounds (e.g. Pgl-135) indeed abolish ROS in the cell systems described here (Dr. S. Hands, unpublished data).This idea is contradictory to the recent suggestion that IBs themselves could be the origin of ROS (Firdaus et al., 2006b).

In the study of Firdaus and colleagues cells expressing httEx1Q103-EGFP were exposed to DHE and increased oxidation was observed by using confocal microscopy (Firdaus et al., 2006a). Furthermore, partial purification of IBs from PC12 cells expressing mhttEx1 were also shown to be enriched in oxidised proteins (Firdaus et al., 2006b). These results lead the authors to conclude that IBs are centers of oxidation within cells. In an attempt to replicate the results obtained by Firdaus and colleagues, IB forming constructs used in this study (and identical to the ones used by Firdaus et al., 2006a) were transfected into HeLa cells to examine whether exposure to oxidative sensitive dyes resulted in an increased oxidation at IBs (A. Wyttenbach and S. Hands, personal communication). Although co-localisation of increased fluorescence using DCF or DHE with IB could occasionally be detected (<1% of cells containing an IB), in the majority of cases the co-localisation was due to bleach-through effects given the extraordinary accumulation and hence fluorescence intensity of httEx1Q97-EGFP/mRFP IBs (S. Hands, unpublished data). These findings contradict the results by Firdaus et al., 2006b. It is interesting to note however that if polyQ aggregation

intermediates (precursors of IBs) indeed produce free radicals (likely with the help of transition metals, Allsop et al., 2008), it is possible that increased activity in oxidation processes occur at IBs because oligomeric species have been shown to localise at the outside of IBs *in vitro* and *in vivo* by EM analysis (Legleiter et al., 2010).

Further evidence arguing against IB being a key producer of intracellular ROS stems from a comparative analysis of dye oxidation in PC12 cells between IB containing cells and cells without IBs showing no difference (appendix 9). This result has also been confirmed in HeLa cells by Dr. S. Hands (personal communication). Hence although IBs could contribute to ROS generation locally and hence may be a source of ROS, the results presented in this chapter support the hypothesis that the majority of ROS produced due to expression of httEx1 with a polyQ expansion occurs when cells do not contain microscopically visible IBs.

Further attempts were made to use other cell systems to measure free radicals due to polyQ expression. Adenovirus mediated expression of httEx1Q25/97-mRFP in HeLa cells using the plate reader was used, but failed to detect differences in DCF fluorescence (data not shown). It is currently unclear why no difference could be detected. Furthermore, increased ROS could not be detected in a Tet-inducible cell system (Wyttenbach et al., 2001) expressing httEx1Q74-EGFP (72.10) versus a clonal line expressing httEx1Q23-EGFP (21.20) (data not shown). However, basal ROS levels of uninduced httEx1Q74-EGFP cells presented with higher ROS levels compared to uninduced httEx1Q23 EGFP. As the promoter of both Tet- inducible cell lines is leaky, a chronic, low expression of mhttEx1 could have contributed to this difference supporting the idea that httEx1 with a polyQ expansion induces ROS. Chronic leakage of httEx1Q74-EGFP may have introduced a compensatory mechanism whereby these cells maintained their redox homeostasis at higher ROS levels compared to the wild-type clone and upon induction showed better protection against ROS, and hence no difference could be detected. Another difference is that httEx1Q74-EGFP cells show polyQ aggregation in the nucleus and not within the cytoplasm, as shown for HeLa and PC12 cells where increased ROS levels were observed. If an early polyQ aggregation process contributes to ROS production (see above), compartment-specific effects are likely to occur. For example, cytoplasmic ROS produced by polyQ aggregation could impact on mitochondria that are not located inside the nucleus.

Another key question was to elucidate whether enzymes or particular organelles constituted a source of ROS. This question was approached by using antioxidants such as MitoQ and Trolox. The MitoQ experiments demonstrated that the origin of ROS could be mitochondrial. The data presented in Figure 4.7 and 4.8 support the idea that MitoQ exposure leads to mitochondrial specific superoxide anion radical reduction in cells expressing httEx1Q97-mRFP. Jauslin et al., (2003) showed that the lipophilic cations of MitoQ allow it to permeate into the lipid bilayer and accumulate within mitochondria due to the large, negative membrane potential. Ubiquinol moieties of MitoQ are then reduced by the respiratory chain and provide an effective antioxidant effect against lipid peroxidation and protect mitochondria against oxidative stress. MitoQ is known to recycle its ubiquinol moiety via the mitochondrial respiration chain after the detoxification of ROS (Kelso et al., 2001). Therefore, it is very effective as an antioxidant at low concentration. In the experiments presented herein the compound appeared efficient at a concentration of 20nM indeed supporting the above findings. Hence MitoQ effects within mitochondria may contribute to the prevention of httEx1Q97 induced ROS.

However, MitoQ is known to inhibit mitochondrial fission due to oxidative stress (Pletjushkina et al., 2006). Changes in mitochondrial functional states, such as the fusion and fission machinery, also lead to oxidative stress (Barsoum et al., 2006). H_2O_2 insults of untreated or TPP^+ treated HeLa cells caused mitochondria to fragment and MitoQ treatment inhibited this effect (Figure 4.6) suggesting that promoting mitochondrial fusion inhibits H_2O_2 induced fission and ROS (acting upstream to mitochondrial fragmentation). Barsoum and colleagues (2006) showed that mitochondrial fission is accompanied by mitochondrial damage, low ATP levels and high levels of ROS. In addition to this, a study by Wang et al., (2009) reported that HeLa cells expressing mhttEx1 were prone to oxidative stress induced mitochondrial fragmentation and reduced ATP levels as compared to cells expressing wild-type httEx1. They showed that this effect was due to reduced mitochondrial movement and fusion. They overexpressed either a dominant negative mitochondrial fission mutant (Drp-1^{K38A}) or mitofusin 2 (mfn2, a mitochondrial membrane protein that actively participates in mitochondrial fusion) in HeLa cells and this promoted mitochondrial fusion, a reduction in cellular toxicity and improved ATP levels. Similarly, knock down

of Drp-1 in a *C. elegans* model of HD (Wang et al., 2009) blocked mitochondrial fission and ameliorated a motility defect caused by mhttEx1. Wang el al., (2009) also suggested that mhttEx1 preferentially binds to Mfn-2 and this binding compromised the normal function of Mfn-2, hence causing mitochondrial fragmentation. Given these studies, it is possible that polyQ aggregation in the model systems examined in our studies leads to mitochondrial fission which subsequently leads to an early increase in ROS (see Figure 4.10, Model A). This model would predict that aggregation inhibitors would inhibit ROS via their downstream effects on mitochondrial fusion/fission. This hypothesis could be tested by investigating whether polyQ aggregation inhibitors reduce mhttEx1 induced mitochondrial fission. Alternatively, free radicals produced by the polyQ process could lead to mitochondrial fission which in turn could increase ROS even more (see Figure 4.10 Model B) This model would predict that aggregation inhibitors and MitoQ have an additive effect in reducing mhttEx1 induced ROS.

It is likely that the processes described above are not the only ones involved in contributing to the redox homeostasis that occurs in HD, and other ROS producing enzymes and mitochondrial regulating proteins are involved in modulating ROS. An interesting candidate protein involved in mitochondrial network dynamics, ROS and cell death is BAX. Karbowski et al., (2004) reported that mitochondrial fragmentation is associated with the activation of a pro-apoptotic protein, BAX and Kirkland et al., (2002) showed that NGF deprived sympathetic neurons produced a BAX dependant increase in ROS that was shown to trigger an apoptotic cascade in these cells. This increase in ROS was inhibited by BAX deletion which suggests that ROS production is upstream to mitochondrial fragmentation. In addition to this, both the presence of ROS and BAX activation are required for cyt *c* redistribution which is needed for the activation of caspases that are known to attack mitochondrial respiratory complexes leading to further ROS production associated with apoptosis (Ricci et al., 2004). Later on, Kirkland and Franklin, (2007) also reported that BAX induction alters mitochondrial membrane potential which then leads to ROS production in non-apoptotic sympathetic neurons. Hence proteins such as BAX would be an interesting avenue for further studies on ROS and mitochondrial events in HD cell models. These above studies also found that several antioxidants inhibit ROS production and ensuing apoptotic downstream events, and therefore the use of other antioxidants and their precise actions than MitoQ (see above) would be a useful problem to address.

In the present study Trolox (which is a derivative of vitamin E) also showed a significant ROS reducing effect due to httEx1Q97 expression (see Figure 4.9). Trushina and McMurray, (2007) suggested that ROS scavengers such as vitamin E incorporate into the mitochondrial membrane and inhibit ROS production. Hence it is possible that the effects of Trolox are also mediated via mitochondrial actions. Mitochondrial actions mediated via Trolox are supported by several other studies. Chronic treatment of Trolox to complex I deficient patient fibroblasts provided protection against elevated ROS levels, normalised impaired mitochondrial membrane potential and improved ATP levels (Distelmaier et al., 2009). In addition to this, impaired membrane potential causes increased mitochondrial membrane transition permeability accompanied by leakage of protons. Trolox has been shown to act as an inhibitor against proton leakage and normalises membrane potential (Brookes et al., 1998) leading to a normalisation of mitochondrial ATP levels. However, Jin et al., (2010) reported that Trolox provided protection against exogenous stimulus of ROS by maintaining glutathione levels in various cell lines. Hence Trolox works as a potent antioxidant against exogenous or endogenous elevated ROS likely in various cellular compartments.

The present investigations and findings on polyQ induced ROS production and the effects of antioxidants need now further confirmation in primary cells because such cells are known to have a different ROS signalling homeostasis compared to cell lines (Santamaria et al., 2006). For example, primary neurons are less glycolytic than cell lines and, therefore, ROS signalling homeostasis would be different in neurons (see general discussion for more detail). Enhanced ROS levels were recently reported in neurons from a *knock-in* full length htt mouse model (Li et al., 2010). This study suggested that a reduced uptake of the glutathione (GSH) precursor cysteine, due to reduced trafficking of its transporter to the cell surface (EAAC1), leads to an early loss of GSH with subsequent elevation of ROS. Hence this study provided a mechanism on how, in a htt full-length context, oxidative stress could occur in an apparently mitochondrial-independent fashion, and it is possible that oxidative damage is mediated via full-length and httEx1 mediated events in an additive way.

Further studies are clearly needed, especially the confirmation of mitochondrial generated ROS in HD cell models given that mitochondria are a key target to ameliorate chronic neurodegeneration. There are several other ways than changing

mitochondrial network dynamics in which mhtt could impact on mitochondria to increase ROS. For example, impaired mitochondrial respiration complexes (particularly complex II and III and IV) are impaired in HD patient brains. Similarly, Tabrizi et al., (2000) reported a reduction in the activity of complex IV of mitochondrial ETC in the striatum and the cortex at 12 weeks of age of R6/2 mouse model. Seo et al., (2008) also reported that YAC72 mouse model present altered mitochondrial complex II and III activity at 16 months of age. Hence, impaired mitochondrial ETC components activity is thought to impair mitochondrial redox homeostasis. Parone et al., (2008) reported the role of fission in mitochondrial homeostasis and they showed that down-regulation of Drp-1, regulates mitochondrial fission, causes mitochondrial dysfunctions such as decrease in mitochondrial respiration coupled with an increase in cellular ROS levels and loss of mtDNA associated with decrease in cellular ATP levels. Another important factor contributing to oxidative stress is likely to occur via transcriptional abnormalities in HD. PGC-1α, a potent ROS suppressor and regulator of mitochondrial biogenesis and respiration, has been shown to be down-regulated in a HD *knock-in* mouse model and in HD patient brains (Cui et al., 2006; Weydt et al., 2006). These studies not only support the hypothesis that the increased ROS could be driven via transcription events, but also primarily originates in the mitochondria possibly through more than one mechanism. Thus the use of antioxidants, particularly MitoQ, are hence likely to be an attractive therapeutic option to selectively targeting ROS at various intracellular locations. Although several studies with a negative- and positive outcome on antioxidants have been performed or are under way (http://www.huntington-study-group.org/ClinicalResearch/CompletedClinicalTrials/tabid/65/Default.aspx), the major challenge for the future will be the appropriate delivery and targeting of ROS producing systems inside CNS cells. Further work must show whether mitochondria are indeed the source of redox-dysregulation in HD.

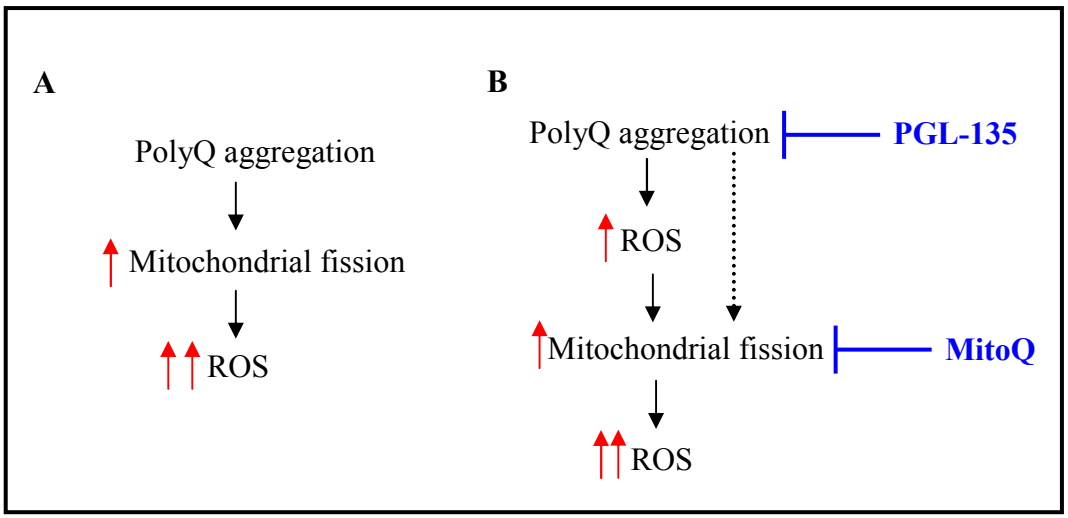

Figure 4.10 Proposed models of impaired redox homeostasis in HD cell models. **(A)** This model suggests that polyQ aggregation may enhance mitochondrial fission that leads to elevated ROS levels. **(B)** PolyQ aggregation may directly produce ROS that leads to an increase in mitochondrial fission and as a consequence even further ROS is generated. On the other hand, polyQ aggregation may directly increase mitochondrial fission (dotted arrow) that leads to enhanced ROS production. Therefore, the use of aggregation inhibitor (e.g. PGL-135) and mitochondrial ROS scavenger (MitoQ) is expected to inhibit ROS. Red arrows indicate the magnitude of ROS change.

5 Redox dependant inhibition of polyQ aggregation and toxicity by DJ-1 and its upregulation in HD

5.1 Introduction

The previous chapter demonstrated that expression of httEx1 protein containing an expanded polyQ stretch causes an early and significant increase in free radical production. Cells appeared to counteract this increased ROS, but oxidative toxicity likely resulted in cell death. Among many proteins counteracting increased ROS due to polyQ expansions are not only antioxidant enzymes, but also redox-chaperones, a group of proteins that have the capacity of counteracting protein misfolding and oxidative stress, as outlined in the general introduction. Previous studies indeed showed that an increased expression of stress- inducible sHSPs protect against polyQ toxicity likely via their antioxidant activity (Perrin et al., 2007; Wyttenbach et al., 2002). Given the emerging role of the redox-activatable chaperone protein DJ-1 in AD and PD (see general introduction), the next aim of this thesis was to examine the potential role of DJ-1 during polyQ aggregation and toxicity. Due to the abnormal redox homeostasis in HD and the finding in Chapter 4 that polyQ expression leads to ROS production, it was possible that redox-chaperones such as DJ-1 were induced and activated to counteract ROS, and perhaps polyQ aggregation causing ROS.

Shendelman *et al.* already demonstrated that DJ-1 can reduce α-synuclein aggregation and toxicity (Shendelman et al., 2004) and several studies have provided strong evidence that DJ-1 induction provides protection from oxidative stress (Kinumi et al., 2004; Taira et al., 2004; Yokota et al., 2003). DJ-1 deficient embryonic stem cells differentiated into dopaminergic neurons also show decreased survival and increased sensitivity to oxidative stress (Martinat et al., 2004). Similarly, Meulener et al., (2005a) reported that DJ-1 double knockout (DJ-1α and β) *Drosophila* flies were viable and had a normal life span, but exhibited a selective sensitivity to environmental oxidative insults associated with PD, such as paraquat and rotenone. Similar results have been presented in several mutant mouse studies (Chen et al., 2005; Goldberg et al., 2005; Kim et al., 2005). The consequence of structural and functional disruptions of the DJ-1 protein is well illustrated by the number of genetic

variants of DJ-1 that are associated with PD (see Table 5.1). DJ-1 has also been shown to inhibit various apoptotic pathways known to be activated in HD (Junn et al., 2005; Sekito et al., 2006; Xu et al., 2005)(see discussion for more detail).

Table 5.1 Genetic sequence variants of DJ-1 and their proposed associations with changes in structural and functional aspects in PD (Anderson and Daggett, 2008; Kahle et al., 2009; Logan et al., 2010; Ramsey and Giasson, 2008).

Mutation	Inheritance	Structural effects	Functional effects
L166P	Homozygous	Destablises the dimeric structure	Loss of function
14-kb deletion	Homozygous	Loss of protein	Loss of function
M26I	Homozygous	Destablises the dimeric structure	Loss of function
D149A	Heterozygous	Unknown	Unknown
A104T	Heterozygous	Destablises the dimeric structure	Loss of function
R98Q (polymorphism)	Heterozygous	Unknowm	Unknown
E64D	Homozygous	Unknown	Unknown
E163K	Compound	No structural effect	Altered antioxidant activity
IVS6-1 G-C	Heterozygous	Unknown	Altered transcription
c.56delC c.57G→A	Heterozygous	Unknown	Loss of function
g.168_185del (polymorphism)	Both	Unknown	Unknown
Ex 5-7del	Heterozygous	Unknown	Altered transcription
IVS5+2-12del	Heterozygous	Unknown	Altered transcription
g.168_185dup	Homozygous	Unknown	Unknown
P158del	Homozygous	Unknown	Unknown
A179T	Heterozygous	Unknown	Unknown
Ex1-5dup	Heterozygous	Unknown	Unknown

It is known that the chaperone activity of DJ-1 is regulated by the partial oxidation of its cysteines, particularly Cys106 (Shendelman et al., 2004) (general introduction), whereas complete oxidation of Cys106 is associated with loss of secondary structures that leads to impairment of its chaperone activity (Zhou et al., 2006). Thus the focus of this chapter was to understand the role of DJ-1 upon overexpression in the presence and absence of Cys106 in the HD cell models described in the previous chapters. In order to clarify the potential involvement of DJ-1 in HD, the expression levels of DJ-1 in cell-and animal models and also in human HD brain samples were examined too.

Under physiological conditions in the human brain DJ-1 is mainly expressed in astrocytes (Bandopadhyay et al., 2004). Astrocytes are supportive brain cells that

have been shown to provide protection against oxidative insults (reviewed in Belanger and Magistretti, 2009; Vargas and Johnson, 2009). Yanagida et al., (2009) reported that astrocytes express six fold more endogenous DJ-1 levels compared to SH-SY5Y cells under oxidative stress and this difference correlated with levels of cellular protection. Therefore, in this chapter, astrocytes were employed as a relevant cell type to study the role of DJ-1 in polyQ induced aggregation and toxicity, in addition to HeLa cells.

5.2 Aims

The aims of this chapter were 1) to study the effect of DJ-1 overexpression in cellular models of HD (both cell lines and primary astrocytes) under basal and oxidative stress conditions; 2) to establish the role of Cys106 as an essential residue for DJ-1 chaperone activity; 3) to quantify DJ-1 expression levels in cell models, animal model (R6/2, transgenic mice) and brain samples from HD patients (un-oxidised and oxidised DJ-1).

5.3 Results

5.3.1 Exogenous DJ-1 overexpression analysis in HD cell models

DJ-1 overexpression analysis under normal and mild oxidative stress was performed in two cell models (HeLa and primary astrocytes). Cells were stimulated with exogenous oxidative stress for two reasons, 1) to further induce the expression levels of DJ-1, and 2) to oxidise DJ-1 at Cys106 to potentially achieve its protective chaperone functions.

5.3.1.1 Western blot and immunocytochemical analysis of DJ-1 overexpression in HeLa cells

In order to determine the effect of DJ-1 overexpression on mhttEx1 induced aggregation and toxicity it was important to first confirm its overexpression upon transfection. Therefore, a Western blot analysis was performed in HeLa cells. DJ-1 or empty vector (EV) was co-transfected with httEx1Q25/Q97-mRFP in a 3:1 DNA ratio. Cell lysates were collected at day 2 and day 3 after transfection and, after SDS-PAGE electrophoresis, nitrocellulose membranes were immunolabelled with a polyclonal DJ-1 antibody (from Cell Signaling). Figure 5.1A shows overexpression of DJ-1 at day 2 and 3 in cells expressing DJ-1 and httEx1Q25/Q97-mRFP. No endogenous DJ-1 was detected in HeLa cells expressing empty vector (EV) and httEx1Q25/Q97-mRFP with this antibody, while a band of the predicted size was visible in cells transfected with a DJ-1 expressing plasmid. A coomassie gel was run in parallel as a loading control (Figure 5.1B). DJ-1 overexpression analysis was also performed by using another polyclonal DJ-1 antibody with similar results (antibody from Neuromics, see appendix 12).

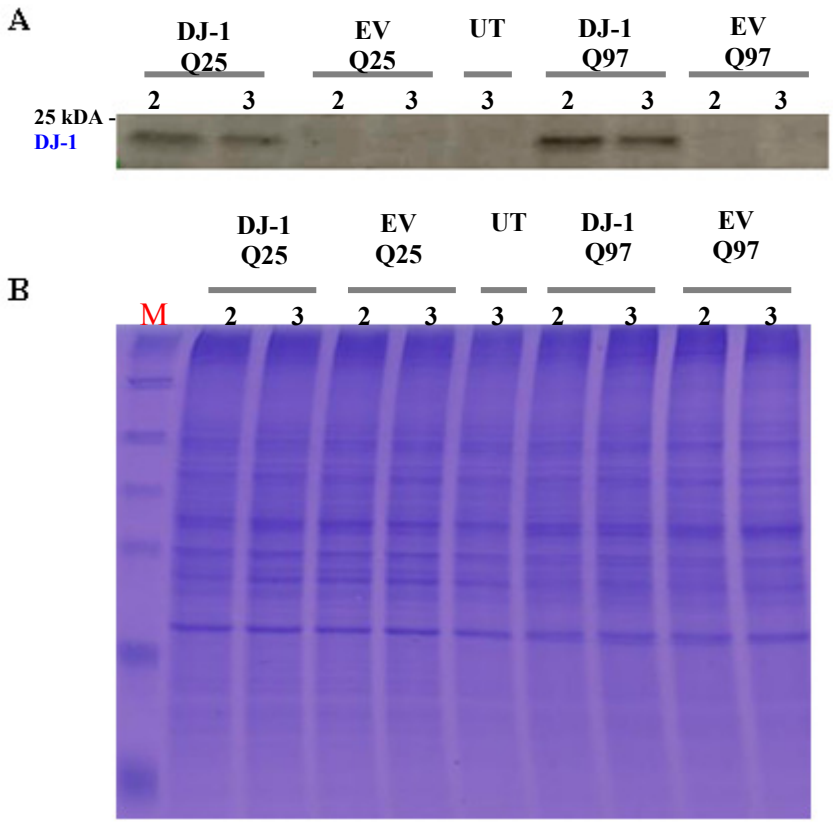

Figure 5.1 Western blot analysis of overexpression of DJ-1 at day 2 and day 3 after co-transfection of DJ-1 or EV with httEx1Q25/Q97-mRFP. 20µg of total protein from cells co-transfected with DJ-1 or EV and httEx1Q25/Q97-mRFP were resolved by SDS-PAGE and the expression level of DJ-1 was quantified by incubating membranes with antibody raised against human DJ-1 **(A)** DJ-1 overexpression in HeLa cells after co-transfection with httEx1Q25/Q97-mRFP. **(B)** Coomassie gel was run as a loading control. (n=2, UT = untransfected, EV = empty vector and M = marker).

Immunocytochemical analysis was next performed on HeLa cells co-transfected with DJ-1 or EV with either httEx1Q25 or Q97-mRFP. Cells were fixed on the third day after transfection and then immunolabelled with polyclonal DJ-1 antibody (Cell Signaling). Cells co-transfected with DJ-1 and httEx1Q25/Q97-mRFP show much brighter DJ-1 staining compared to cells co-transfected with EV and httEx1Q25/Q97-mRFP, confirming overexpression of DJ-1 in HeLa cells (Figure 5.2). As a negative control, cells expressing httEx1Q25-mRFP were incubated with either primary or secondary antibody only (anti-rabbit 488) and no signal was detected when imaged at 488nm wavelength using confocal microscopy (Figure 5.2A and B). Hence, these findings confirmed that cells expressing the httEx1-mRFP constructs co-transfected with DJ-1, also showed an elevated expression of DJ-1.

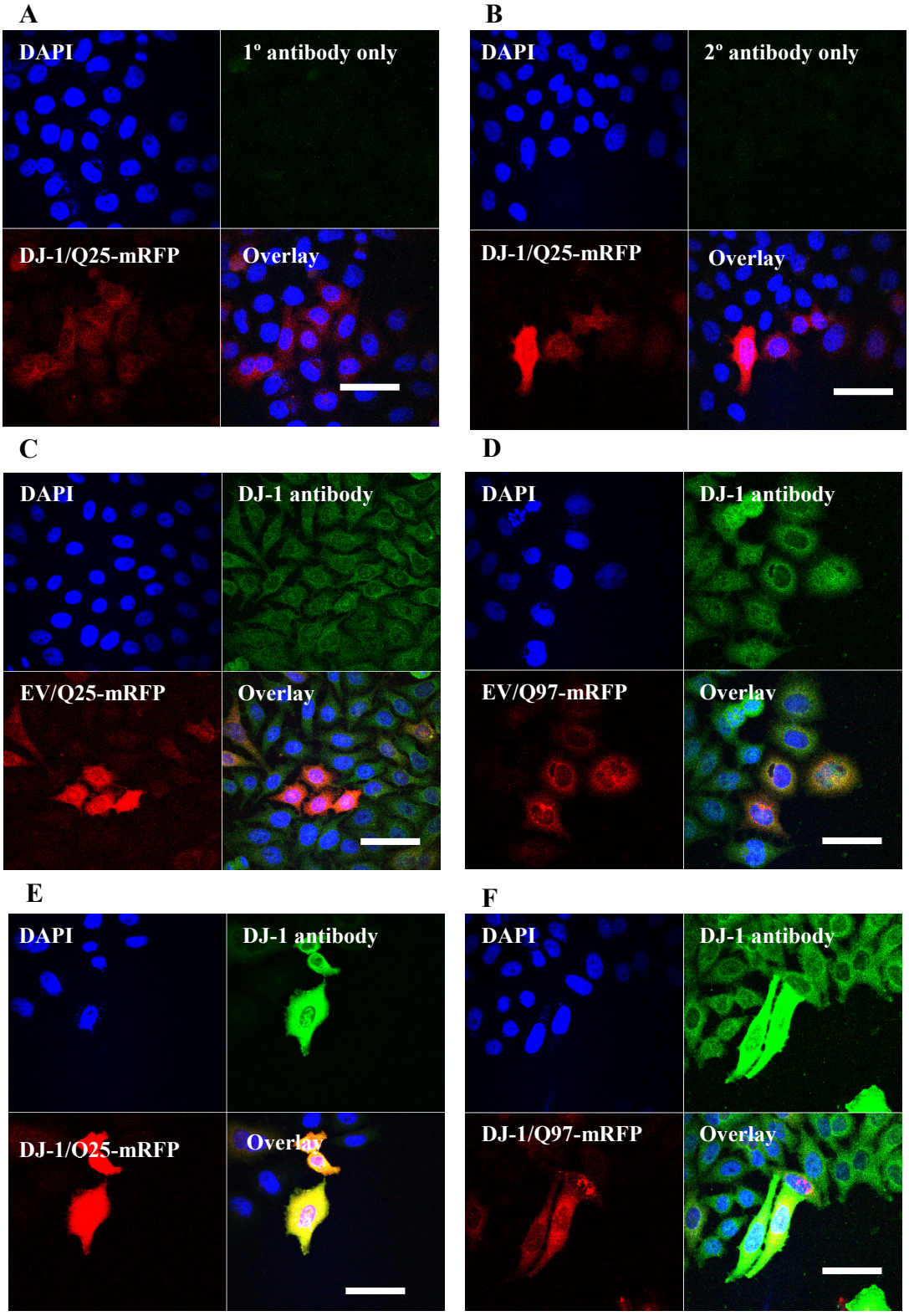

Figure 5.2 Immunocytochemical analysis of DJ-1 overexpression in HeLa cells. **(A)** and **(B)** Negative controls showing no staining with either primary or secondary antibody when imaged by confocal microscopy under identical settings, **(C)** and **(D)** EV construct co-transfected with httEx1Q25/Q97-mRFP and, **(E)** and **(F)** DJ-1 construct co-transfected with httEx1Q25/Q97-mRFP. Cells co-transfected with DJ-1 and httEx1Q25/Q97-mRFP show comparatively high levels of DJ-1 immunoreactivity compared to cells co-transfected with EV and httEx1Q25/Q97-mRFP. Scale bar is 50µm.

5.3.1.2 Effects of overexpression of DJ-1 on mhttEx1 induced IB formation and toxicity in HeLa cells

Overexpression of DJ-1 in cells expressing httEx1Q97-mRFP showed a significant increase in IB formation compared to cells expressing EV and httEx1Q97-mRFP (Figure 5.3).

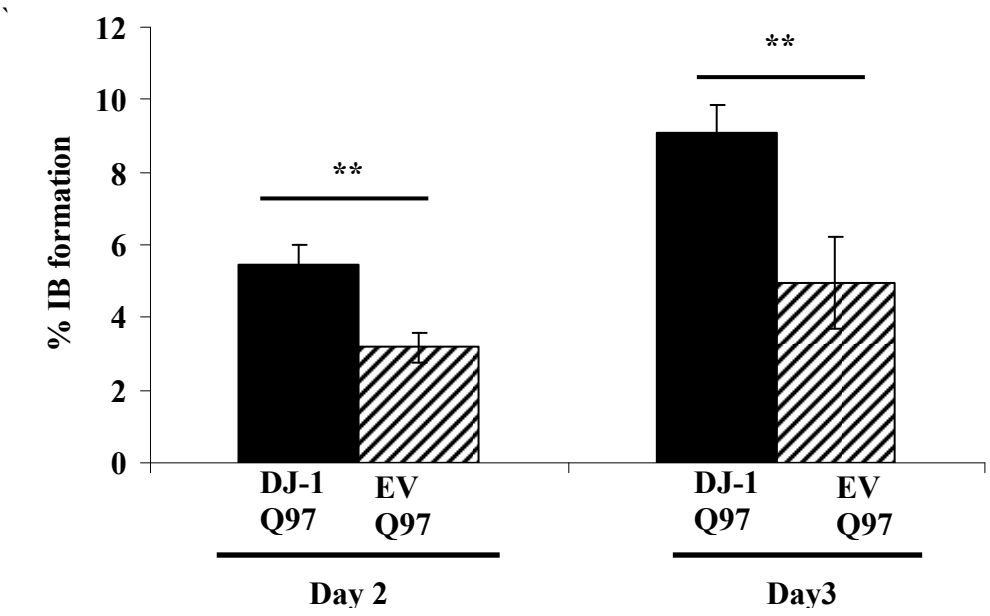

Figure 5.3 DJ-1 overexpression increases mhttEx1 IB formation. HeLa cells were transiently co-transfected with either DJ-1 or EV and httEx1Q97-mRFP (3:1 DNA ratio). Percentage IB formation was scored by counting mRFP positive cells with IBs of cells expressing httEx1Q97-mRFP co-transfected with DJ-1 or EV. Cells co-transfected with DJ-1 and httEx1Q97-mRFP showed a significant increase in IB formation over time. Error bars represent standard errors of the means. Paired t-test was performed for statistical analysis ** = $P < 0.01$ (n= 4).

HeLa cells expressing DJ-1 and httEx1Q97-mRFP also showed a significant increase in cell death at day 2 and day 3 compared to cells co-transfected with EV and httEx1Q97-mRFP (Figure 5.4). Hence, the increase in toxicity due to DJ-1 overexpression could be due to an increase in polyQ IBs. Overexpression of DJ-1 on the other hand, reduced basal death in cells expressing httEx1Q25-mRFP compared to EV and this decrease in cell death was only significant at day 3 (Figure 5.5).

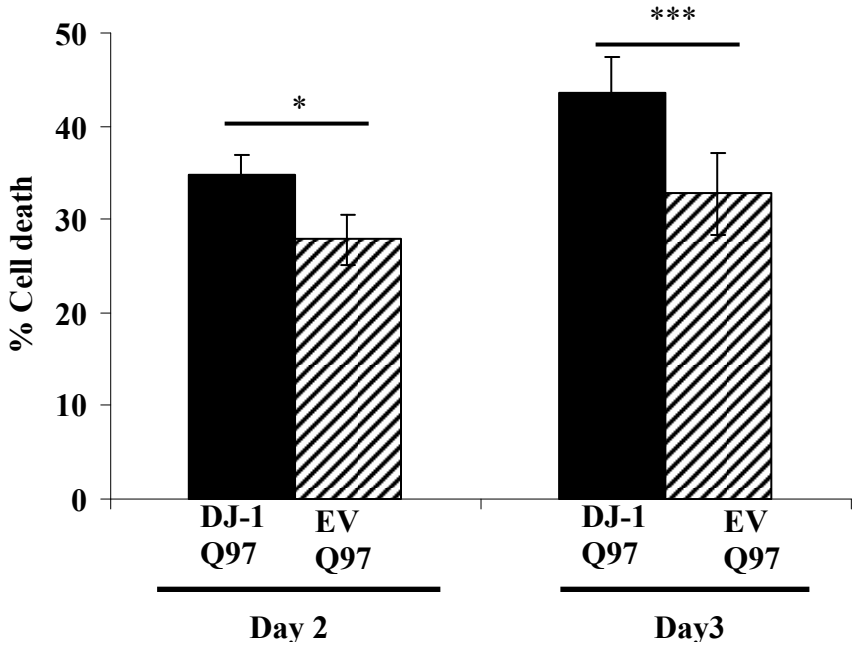

Figure 5.4 Overexpression of DJ-1 increases mhttEx1 induced toxicity. HeLa cells were transiently co-transfected with either DJ-1 or EV and httEx1Q97-mRFP (3:1 DNA ratio). Percentage cell death was scored by counting abnormal nuclear morphology of cells expressing httEx1Q97-mRFP co-transfected with either DJ-1 or EV. Cells co-transfected with DJ-1 and httEx1Q97-mRFP showed a significant increase in cell death at 48 and 72 hours after transfection. Error bars represent standard errors of the means. Paired t-test was performed for statistical analysis * = P <0.05 and *** = P <0.001, (n=4).

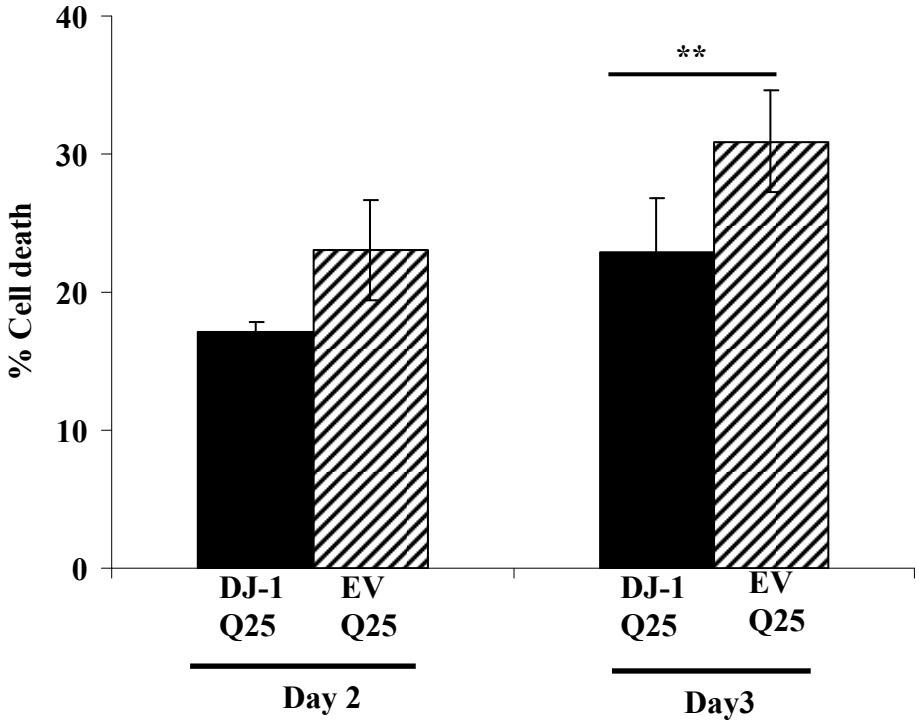

Figure 5.5 Overexpression of DJ-1 reduces basal cell death in cells expressing httEx1Q25-mRFP. HeLa cells were transiently co-transfected with either EV or DJ-1 and httEx1Q25-mRFP (3:1 DNA plasmid ratio), fixed and analysed after 2 and 3 days. Percentage cell death was scored by counting the proportion of cells with abnormal nuclear morphology expressing httEx1Q25-mRFP co-transfected with DJ-1 or EV. Error bars represent standard errors of the means. Paired t-test was performed for statistical analysis ** = $P < 0.01$ (n=4).

5.3.1.3 Antimycin A or H_2O_2 treatment of cells expressing mhttEx1 and DJ-1 reduces polyQ induced aggregation and toxicity

Given that DJ-1 can act as a chaperone under increased ROS and increased ROS was indeed present in cells expressing httEx1Q97-mRFP (see Chapter 4), it was unexpected that overexpression of DJ-1 leads to increased IB formation (Figure 5.3). The level of endogenous ROS may have been insufficient to activate DJ-1 via its redox reactive cysteines (Cys46, Cys53 and Cys106). Therefore, an attempt was made to activate DJ-1 through the addition of 100μM of exogenous hydrogen peroxide or via treatment with 5μM of Antimycin A. Antimycin A functions by blocking complex III of the ETC which then causes the production of endogenous superoxide anion radicals (Spitkovsky et al., 2004).

HeLa cells were co-transfected with either DJ-1 or EV and httEx1Q25/97mRFP and after 5 hours of transfection treated with either 5μM of Antimycin A or 100μM of H_2O_2 for 19 hours. Cells were then washed after 24 hours and fresh media was added without Antimycin A or H_2O_2. Cells were then fixed after a total of 48 and 72 hours of transfection and IB's and toxicity were analysed as described in Materials and Methods. Figure 5.6B shows a significant decrease in IB formation in cells expressing httEx1Q97-mRFP and DJ-1 treated with Antimycin A or H_2O_2 at day 3 compared to untreated cells. Similarly, a reduction in cellular toxicity was observed in cells expressing DJ-1 with httEx1Q97-mRFP when DJ-1 was "activated" (using Antimycin A or H_2O_2) (Figure 5.7B) compared to untreated cells expressing DJ-1 and httEx1Q97-mRFP at day 3.

Under these transfection conditions there were no significant toxicity differences observed between cells co-transfected with EV and either httEx1Q25-mRFP or httEx1Q97-mRFP. This lack of httEx1Q97 toxicity may well be because three times less httEx1Q25/Q97-mRFP constructs were used as compared to routine transfection procedures used as outlined in Chapter 2. Hence when referring to modulation of mhttEx1 aggregation or toxicity (also see below), we refer to the effects obtained via DJ-1 overexpression. As fairly high variability was observed between each experiment, therefore data were presented as % change in IB formation or toxicity due to overexpression of DJ-1or EV with httEx1Q97-mRFP.

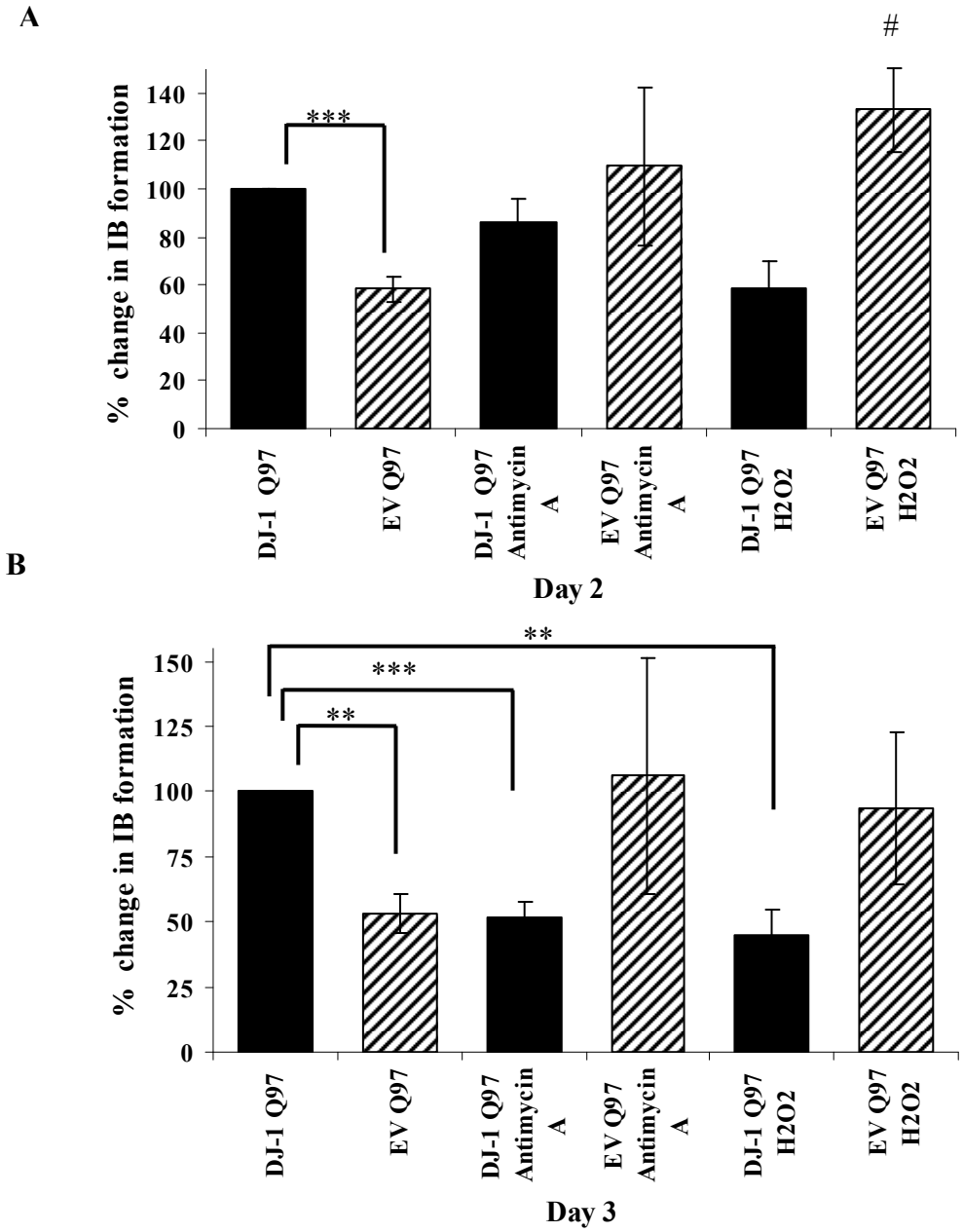

Figure 5.6 DJ-1 suppresses mhttEx1 IB's under oxidising conditions. HeLa cells were transiently co-transfected with either EV or DJ-1 and httEx1Q97-mRFP (3:1 DNA ratio). Cells were treated with either 5μM of Antimycin A or 100μM of H_2O_2 after 5 hours of transfection for 19 hours in parallel to untreated cells. Percentage IB formation was scored at day 2 **(A)** and day 3 **(B)** by counting mRFP positive cells with IBs co-transfected with either DJ-1 or EV and httEx1Q97-mRFP. Data is presented as % change in IB formation. Error bars represent standard errors of the means. # represents a statistical difference between untreated cells expressing EV-httEx1Q97-mRFP and EV-httEx1Q97-mRFP treated with H_2O_2. One sample t-test was performed for statistical analysis (n = 3-6, # = $P<0.05$, ** = $P < 0.01$, *** = $P <0.001$).

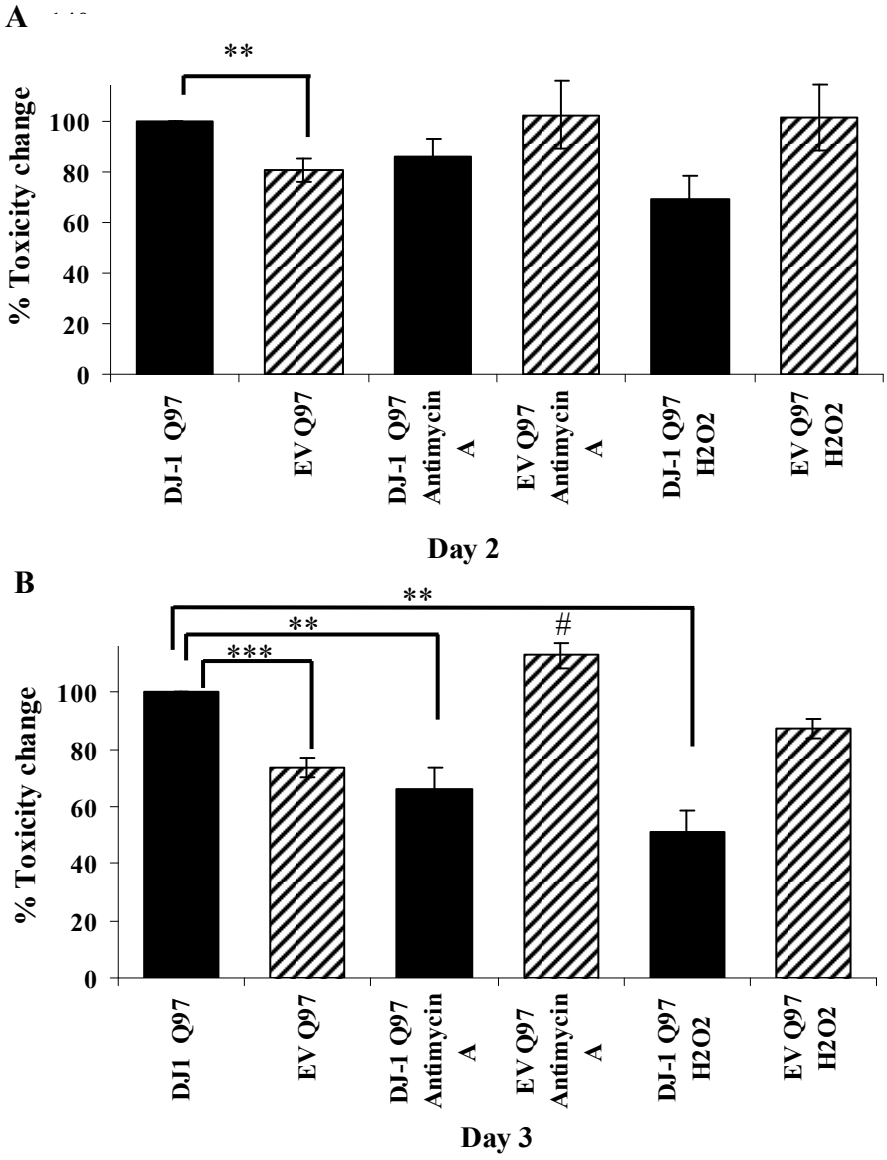

Figure 5.7 DJ-1 suppresses mhttEx1 toxicity under oxidising conditions in HeLa cells. HeLa cells were transiently co-transfected with either EV or DJ-1 and httEx1Q97-mRFP (3:1 DNA ratio). Cells were treated with 5µM of Antimycin A or 100µM of H_2O_2 after 5 hours of transfection for 19 hours in parallel to untreated cells. Cell death was measured by scoring abnormal nuclear morphology of cells co-transfected with either DJ-1 or EV and httEx1Q97-mRFP at day 2-3. Data is presented as % change in toxicity. **(A)** Antimycin A or H_2O_2 treatment did not significantly reduce cellular toxicity in cells co-transfected with DJ-1 and httEx1Q97-mRFP at day 2. **(B)** There was a significant reduction in cell death in cells co-transfected with DJ-1 and httEx1Q97-mRFP when treated with Antimycin A or H_2O_2 compared to untreated cells at day 3. HeLa cells co-transfected with EV and httEx1Q97-mRFP treated with Antimycin A show significant more toxicity compared to untreated cell at day 3. # represents a statistical difference between untreated cells expressing EV-httEx1Q97-mRFP and EV-httEx1Q97-mRFP treated with Antimycin A. Error bars represent standard errors of the means. One sample t-test was performed for statistical analysis (# = $P < 0.05$, ** = $P < 0.01$ and *** = $P < 0.001$, n = 3-6).

5.3.1.4 Antimycin A or H_2O_2 treatment reduces mhttEx1 induced SDS insoluble proteins

As illustrated in Figure 5.6, when DJ-1 was co-transfected with httEx1Q97-mRFP, it significantly increased IBs compared to cells co-transfected with EV and httEx1Q97-mRFP. This increase was reduced when cells were treated with either H_2O_2 or Antimycin A. In order to confirm the effect on aggregation as measured by estimating cellular IBs, dot blot experiments were performed. Cells after 3 days of transfection were lysed and treated with 2% SDS. SDS insoluble material was then blotted onto a cellulose acetate membrane. Analysis of several dot blot experiments showed that cells co-transfected with DJ-1 and httEx1Q97-mRFP produced more SDS insoluble material compared to cells co-transfected with EV and httEx1Q97-mRFP, but this increase was not statistically significant ($p>0.05$). Furthermore, Antimycin A or H_2O_2 treatment significantly decreases SDS insoluble material of cells expressing DJ-1 and httEx1Q97-mRFP compared to untreated cells (see Figure 5.8). Thus, these dot blot experiments confirmed the IB counting data.

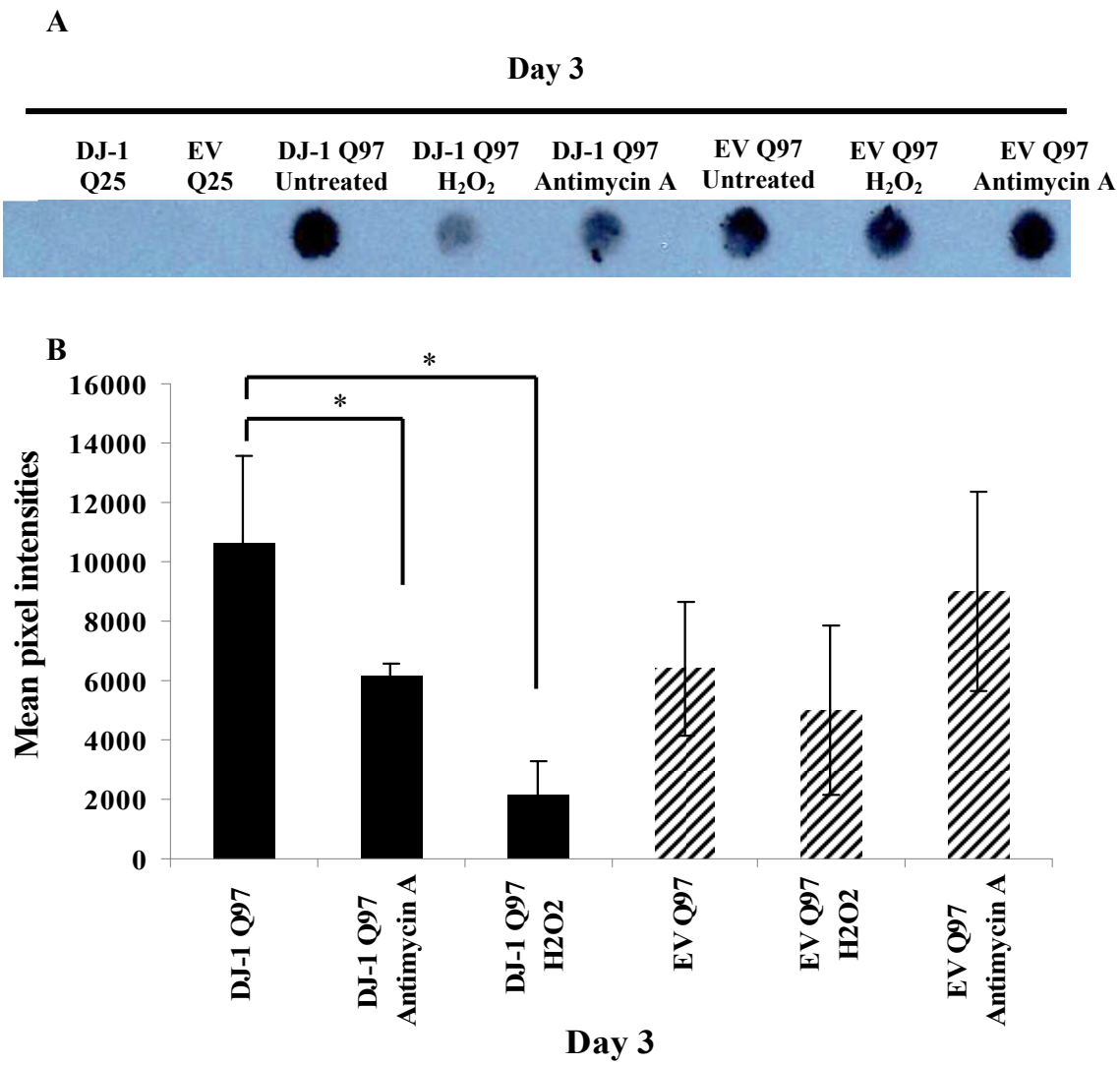

Figure 5.8 DJ-1 reduces mhttEx1 SDS insoluble aggregates under oxidising conditions. 50µg of homogenates from cells expressing either DJ-1 or EV with httEx1Q97-mRFP treated with/out Antimycin A or H_2O_2 were passed through nitrocellulose acetate membranes. Immunoreactivity against httEx1Q97-mRFP SDS insoluble material was detected by incubating with S830 primary antibody and HRP labelled secondary antibody which was detected by ECL. Intensity values were quantified by using Image J software. **(A)** A representation of a single dot blot experiment and **(B)** quantification of dot blot images. HeLa cells co-transfected with DJ-1 and httEx1Q97-mRFP show an increase in SDS insoluble aggregates compared to cells co-transfected with EV and httEx1Q97-mRFP. This increase was inhibited when DJ-1 and httEx1Q97-mRFP expressing cells were treated with either 100µM of H_2O_2 or 5 µM of Antimycin A for 19 hours after 5 hours of transfection. Cells expressing EV and httEx1Q97-mRFP did not reduce SDS insoluble aggregates upon treatment with mild oxidants. Error bars represent standard errors of the means. One sample t-test was performed for statistical analysis (n=3 except DJ-1/EV and httEx1Q97-mRFP treated with Antimycin A, n=2; * = $P < 0.05$).

5.3.1.5 DJ-1-Cys106 regulates its redox sensitive molecular chaperone function in HeLa cells

As mentioned in the introduction, DJ-1 has three reactive cysteines (Cys46, Cys53 and Cys106) that can be post-translationaly modified. A few studies have stated that Cys106 is fundamental to DJ-1 function and that it is the most oxidative stress susceptible DJ-1 cysteine residue (Canet-Aviles et al., 2004; Kinumi et al., 2004; Lee et al., 2003; Wilson et al., 2003). Therefore, an experiment was performed in which Cys106 of DJ-1 was replaced with serine (C106S-DJ-1) (this construct was kindly provided by Prof. Hiroyoshi Ariga, Hokkaido University, Japan) and co-transfected with httEx1Q97-mRFP in HeLa cells under the assumption that C106S-DJ-1 would not be oxidatively modified and that this would abolish its chaperone activity when treated with H_2O_2 or Antimycin A. Surprisingly, HeLa cells co-transfected with C106S-DJ-1 and httEx1Q97-mRFP showed a significant increase in IB formation compared to cells co-transfected with wild-type DJ-1 and httEx1Q97-mRFP (Figure 5.9A). As expected, treatment with either H_2O_2 or Antimycin A did not modulate IB levels (Figure 5.9A). Thus, C106S-DJ-1 did not show any potential chaperone function but, curiously, C106S-DJ-1 co-transfected with httEx1Q97-mRFP showed an unexpected increase in the number of IBs in most of the cells (arrow heads, Figure 5.9D) compared to cells expressing wt DJ-1 and httEx1Q97-mRFP (showing intracellular IBs, white arrows, Figure 5.9C). Moreover, increased mhttEx1 IBs due to C106S-DJ-1 overexpression also increased cellular toxicity (Figure 5.9B). Importantly, toxicity due to C106S-DJ-1/httEx1-mRFP was not inhibited when cells were treated with either H_2O_2 or Antimycin A (Figure 5.9B). In addition to this, Western blot analysis confirmed that DJ-1-C106S was expressed in these cells (see appendix 12).

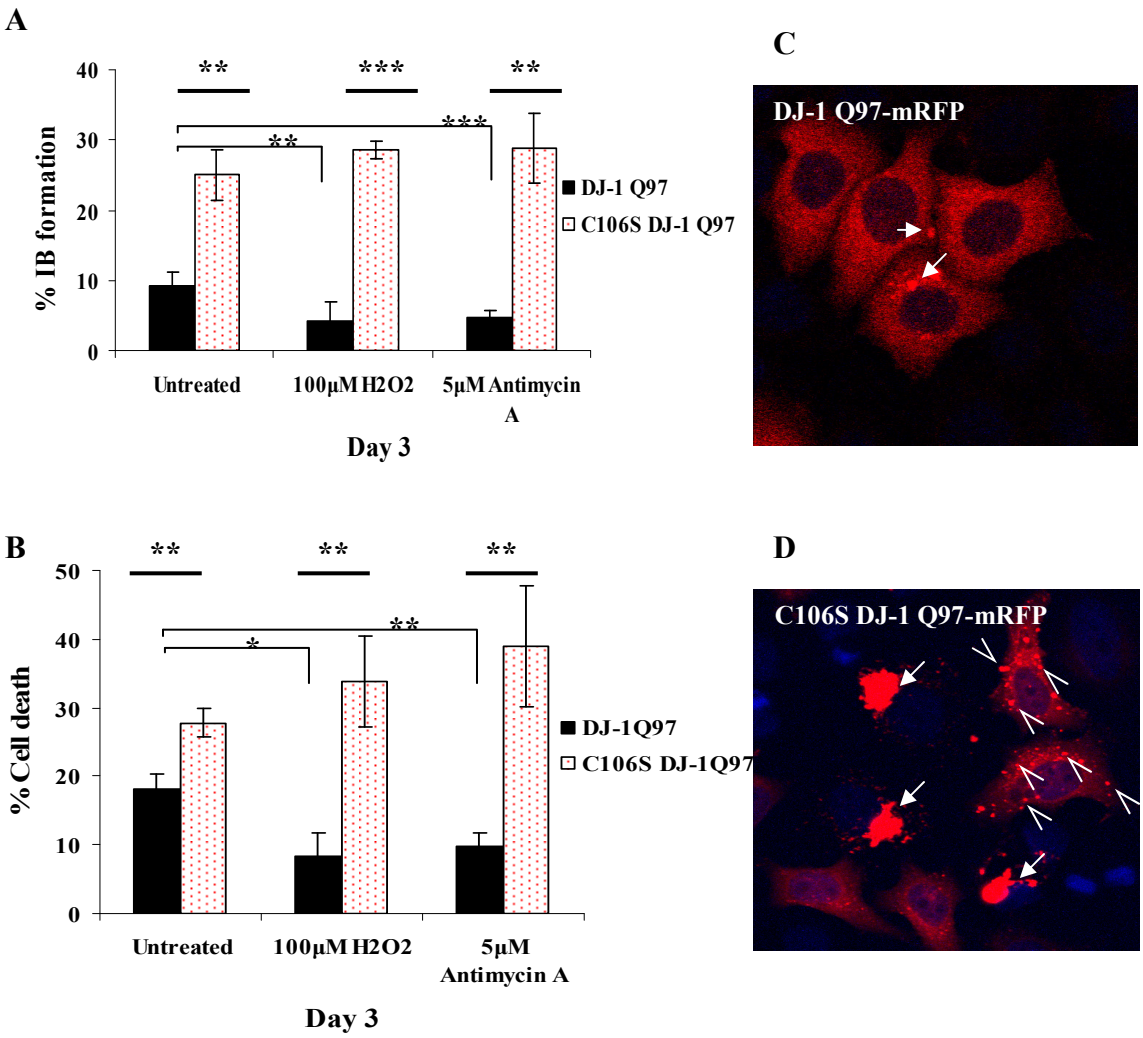

Figure 5.9 C106S-DJ-1 mutant is unable to decrease IBs under oxidising conditions and causes an increase in IB formation associated with cellular toxicity. HeLa cells co-transfected with DJ-1and httEx1Q97-mRFP (3:1) form less IBs **(A)** and exhibit less toxicity **(B)** as compared to cells expressing C106S-DJ-1 with httEx1Q97-mRFP. 100µM H_2O_2 and 5µM Antimycin A treatment reduces IBs **(A)** and toxicity **(B)** whereas C106S-DJ-1 co-transfected with httEx1Q97-mRFP does not suppress aggregation and toxicity. Percentage IBs were measured by counting mRFP positive cells with IBs. **(C)** Example of cells expressing DJ-1 and httEx1Q97-mRFP typically showing one or two IBs (white arrows) whereas cells expressing C106S-DJ-1 with httExQ97-mRFP **(D)** show multiple IB foci throughout the cells (white arrow heads). Error bars represent standard deviations. Unpaired t-test was performed for statistical analysis (* = $P < 0.05$, ** = $P < 0.01$ and *** = $P < 0.001$, n = 3-6).

5.3.1.6 Overexpression of DJ-1 under oxidising conditions reduces mhttEx1 induced IBs and toxicity in primary astrocytes

To confirm the results obtained in HeLa cell line, DJ-1 was overexpressed in relatively mature mouse cortical astrocytes (primary cells) cultured for 15-20 days. The astrocyte cell system was extensively characterised by Ben Samson and it was shown that >80 % of these cells were GFAP positive astrocytes and 99% were connexin 43 positive (both astrocytes specific markers) suggesting a highly pure astrocyte culture (unpublished results). In addition to this, these cultures did not present with microglial, oligodendroglial or fibroblast contamination. Astrocytes were isolated and cultured as described in the Materials and Methods section 2.2.2.

Figure 5.10A shows overexpression of DJ-1 in astrocytes significantly increased mhttEx1 IBs whereas upon Antimycin A or H_2O_2 treatment, mhttEx1 IBs were significantly decreased as compared to untreated astrocytes expressing DJ-1 and httEx1Q97-mRFP. Astrocytes IB data recapitulate HeLa cells data as shown in Figure 5.6.

Cell death data suggested that the overexpression of DJ-1 reduced basal cell death in astrocytes expressing httEx1Q25-mRFP (this reduction was not statistically significant, P= 0.1) compared to EV control at day 3 (Figure 5.11A), whereas overexpression of DJ-1 significantly increased cellular toxicity in the cells expressing httEx1Q97-mRFP compared to EV at day 3 (Figure 5.11B), similar to what was found for HeLa cells (Figure 5.7).

In addition to this, astrocytes were also co-transfected with either C106S-DJ-1 or wild-type DJ-1 with httEx1Q97-mRFP to examine whether the rate of aggregation and toxicity increased, as observed in HeLa cells. Interestingly, similar aggregation (Figure 5.12A) and cellular toxicity (Figure 5.12B) results were observed in astrocytes as seen in HeLa cells, where C106S-DJ-1 enhanced mhttEx1 IBs and lost its potential chaperone ability when treated with 100µM H_2O_2 or 5µM of Antimycin A (Figure 5.12). Astrocytes co-transfected with C106S-DJ-1 and httEx1Q97-mRFP also showed a similar pattern of multiple aggregation foci (5-40 per cell) of that observed in HeLa cells (Figure 5.9D and 5.12D).

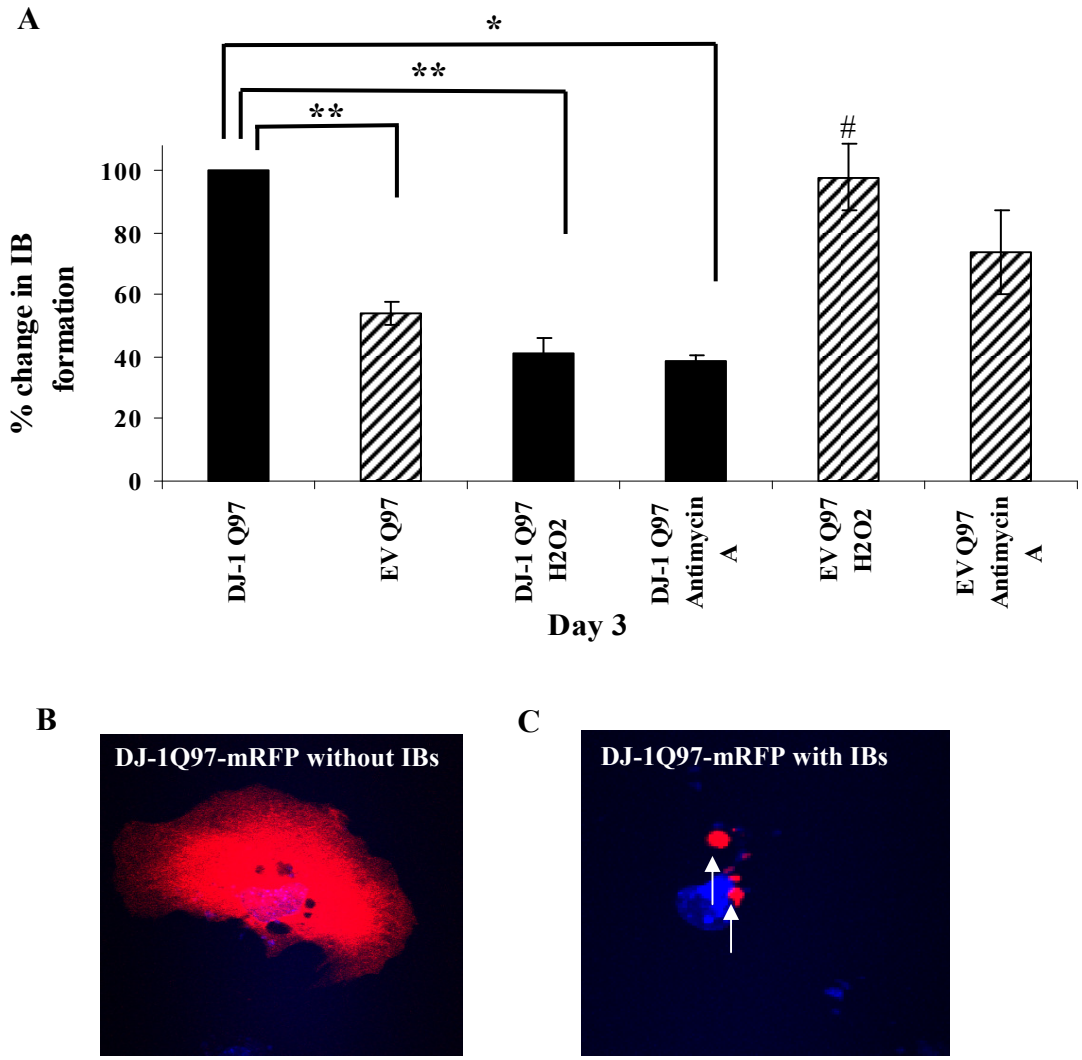

Figure 5.10 DJ-1 reduces mhttEx1 IB's under oxidising conditions in primary astrocytes. Astrocytes were cultured and transiently co-transfected with either EV or DJ-1 and httEx1Q25/Q97-mRFP (3:1 plasmid ratio) for 3 days. **(A)** DJ-1 overexpression with httEx1Q97-mRFP show enhanced IB formation at day 3 compared to cells expressing EV with httEx1Q97-mRFP. Astrocytes were co-transfected with DJ-1 and httEx1Q97-mRFP and when treated with either 100µM of H_2O_2 or 5µM of Antimycin A exhibit a significant reduction in IBs at day 3. A significant increase in IB formation was observed when cells expressing EV with httEx1Q97-mRFP were treated with H_2O_2 compared to untreated cells **(B)** and **(C)** Examples of primary astrocytes expressing DJ-1and httEx1Q97-mRFP without and with IBs (white arrows). Data presented as % change in IB formation. # represents a statistical difference between untreated cells expressing EV-httEx1Q97-mRFP and EV-httEx1Q97-mRFP treated with H_2O_2. Error bars represent standard errors of the means. One sample t-test was performed for statistical analysis. # = P <0.05, * = P < 0.05, ** = P < 0.01 (n=3).

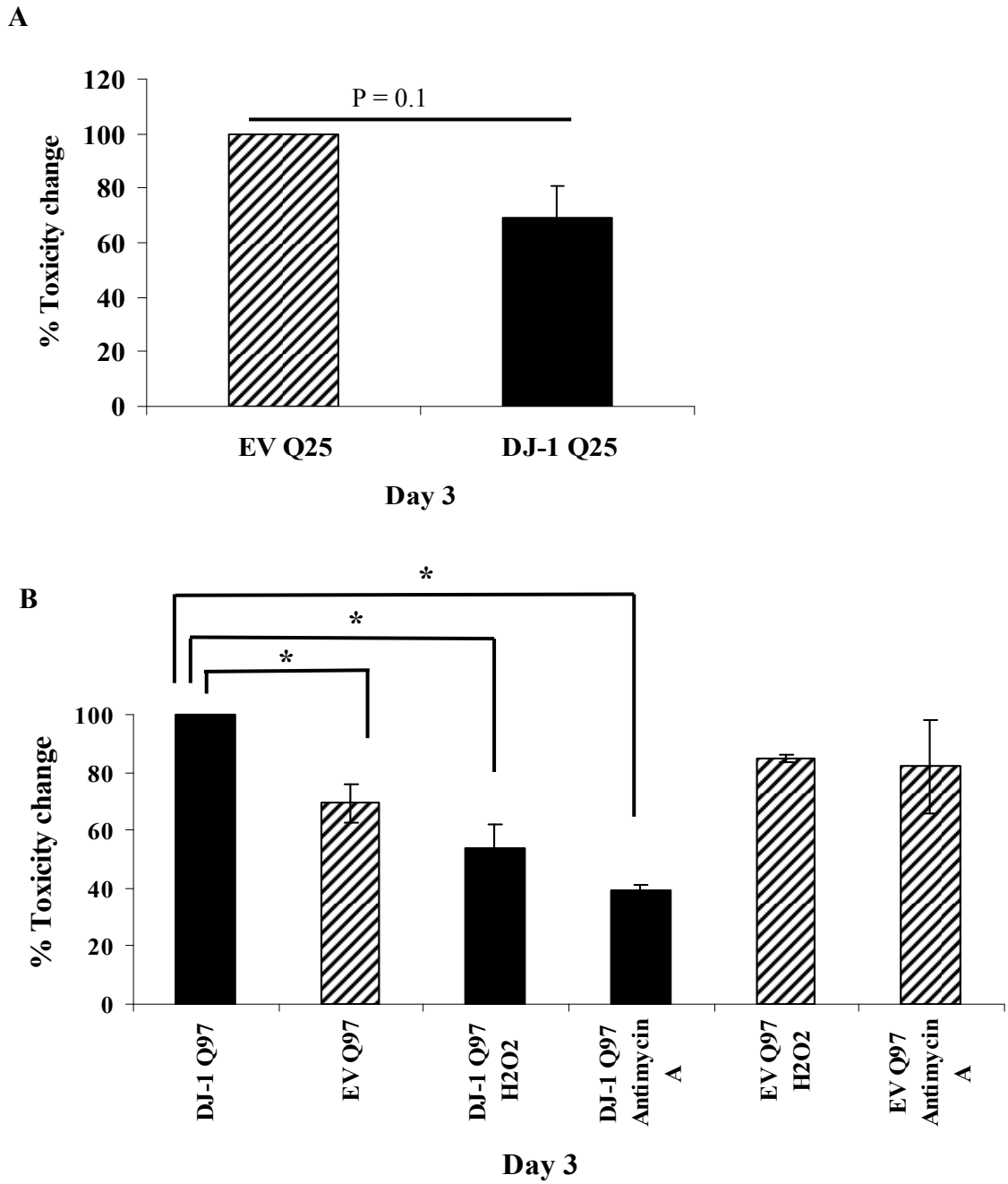

Figure 5.11 DJ-1 inhibits httEx1Q97-mRFP toxicity under oxidising conditions in primary astrocytes. Astrocytes were transiently co-transfected with either DJ-1 or EV and httEx1Q25/Q97-mRFP. Astrocytes cell death was measured by scoring the number of cells with abnormal nuclear morphology in cells co-transfected with either DJ-1 or EV and httEx1Q25/Q97-mRFP. **(A)** Astrocytes expressing DJ-1 with httEx1Q25-mRFP showed less cellular toxicity compared to cells expressing EV and httEx1Q25-mRFP. **(B)** Astrocytes co-transfected with DJ-1 and httEx1Q97-mRFP showed a significant increase in cell death compared to cells co-transfected with EV and httEx1Q97-mRFP. This increase in toxicity was inhibited when cells were treated with either 100μM of H_2O_2 or 5μM of Antimycin A. Error bars represent standard errors of the means. n=3 (except for cells co-transfected with DJ-1 or EV and httEx1Q97-mRFP treated with Antimycin A, n=2). One sample t-test was used for statistical analysis (* = $P < 0.05$).

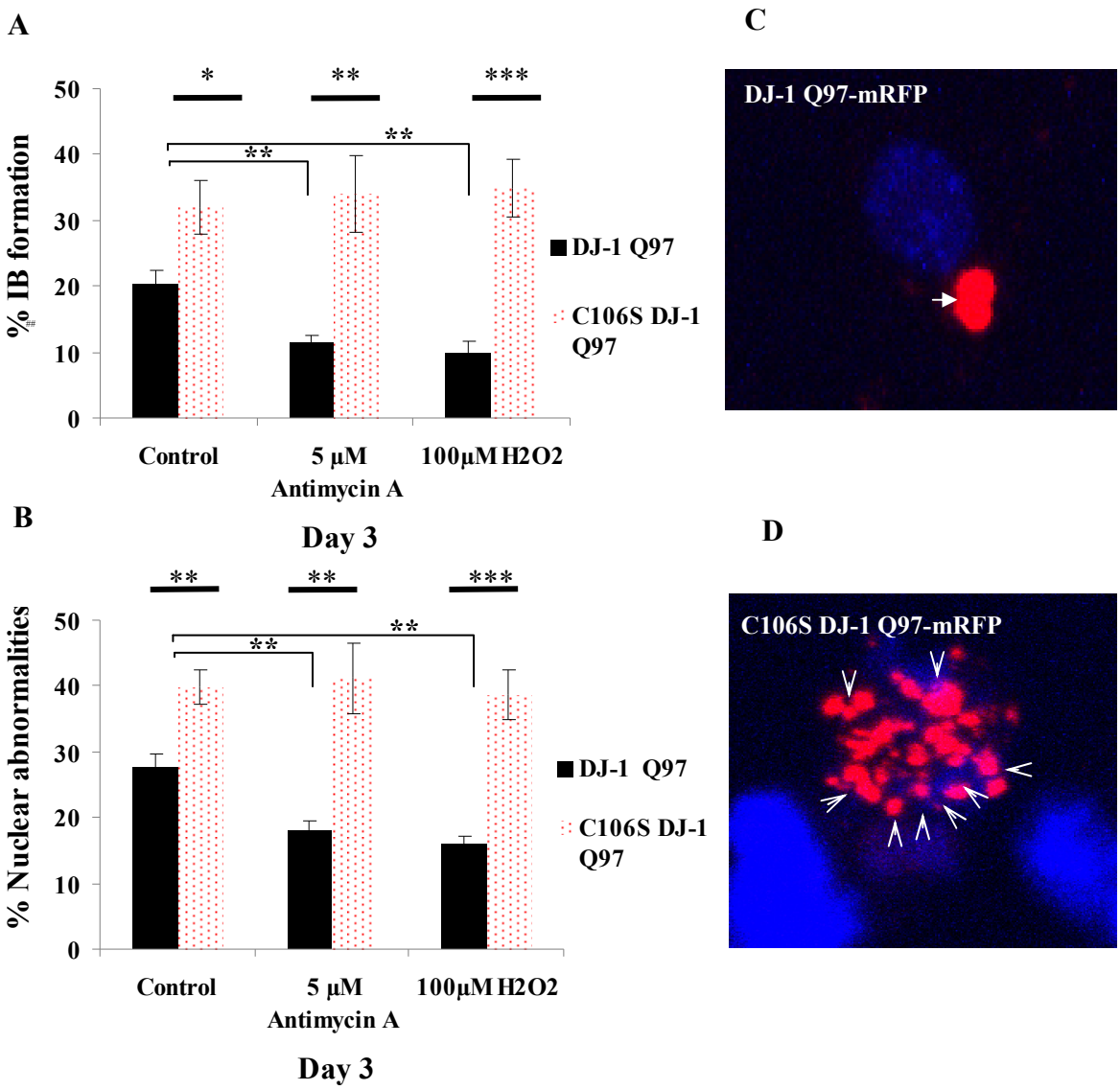

Figure 5.12 C106S-DJ-1 overexpression aggravates mhttEx1 induced IB formation and toxicity. Astrocytes co-transfected with DJ-1 and httEx1Q97-mRFP show significantly less IBs **(A)** and nuclear abnormalities **(B)** compared to astrocytes expressing C106S-DJ-1 and httEx1Q97-mRFP at day3 of transfection. % of IBs **(A)** and nuclear fragmentation **(B)** of astrocytes expressing DJ-1 and httEx1Q97-mRFP was reduced when astrocytes were treated with either 100µM of H_2O_2 or 5µM of Antimycin A, whereas this inhibition was not observed in astrocytes co-transfected with C106S-DJ-1 and httEx1Q97-mRFP. **(C)** Example of an astrocyte co-transfected with DJ-1 and httEx1Q97-mRFP showing an IB (white arrow) whereas **(D)** a cell expressing C106S-DJ-1 and httEx1Q97-mRFP shows multiple IB foci (arrow heads). Error bars represent standard deviation. Unpaired t-test was performed for statistical analysis * = $P < 0.05$, ** = $P < 0.01$ and *** = $P < 0.001$ (n=3).

5.3.1.7 Oxidative stress induces DJ-1 expression and translocation to the cytoplasm in astrocytes

The data presented in this chapter so far demonstrated that DJ-1 overexpression caused cellular toxicity dependent on mhttEx1, whereas when cells were treated with mild oxidative stress mhttEx1 mediated toxicity was abrogated. The latter protective effect was lost when the cysteine at position 106 of DJ-1 was replaced with a serine. However, it was unclear as to whether the distribution of endogenous or exogenously overexpressed DJ-1 changed due to polyQ expression or the addition of mild oxidising compounds. Mitsumoto and colleagues reported that DJ-1 responds to oxidative stress by changing its isoelectric point to a more acidic form (6.2 to 5.8) (Mitsumoto et al., 2001; Mitsumoto and Nakagawa, 2001). Canet-Aviles et al., (2004) suggested that this acidic form of DJ-1 is redistributed to mitochondria and provides protection against oxidative stress induced cell death. Therefore, the below described experiments were designed to examine whether DJ-1 changed its distribution in the presence of oxidative stress and/or polyQ proteins.

Astrocytes were treated with 100μM of H_2O_2 for 19 hours after 5 hours of transfection and then fixed with 4% paraformaldehyde after 3 days of transfection followed by immunolabelling with a polyclonal anti-rabbit DJ-1 antibody (Neuromics). As expected and seen in Figure 5.13Ai astrocytes that were untransfected and not treated with H_2O_2 exhibited a strong nuclear localisation of DJ-1, whereas cells that were H_2O_2 treated showed some translocation of DJ-1 to the cytoplasm and possibly mitochondria (arrow heads, Figure 5.13Aii). Astrocytes transfected with httEx1Q25-mRFP showed a nuclear and some cytoplasmic localisation of DJ-1 (Figure 5.13Bi). Interestingly, httEx1Q97-mRFP expressing cells mostly showed nuclear localisation of DJ-1 (Figure 5.13Bii). On the other hand, when httEx1Q25/Q97-mRFP expressing astrocytes were treated with 100μM of H_2O_2 both showed some translocation of DJ-1 from nucleus to cytoplasm (Figure 5.13C). Furthermore, cells treated with 100μM of H_2O_2 tended to show increased immunoreactivity compared to untreated cells (data not shown) suggesting an up-regulation of endogenous DJ-1 upon oxidant addition. This observation was confirmed by a Western blot analysis of astrocytes treated with H_2O_2 for different lengths of time which showed that oxidative stress induced DJ-1 expression levels in astrocytes increased by 1.5 fold at 12 hours and 3 fold at 24 hours of treatment whereas

48 hours after treatment its likely that there was a compensatory effect as no change was detected at this time point (see appendix 13).

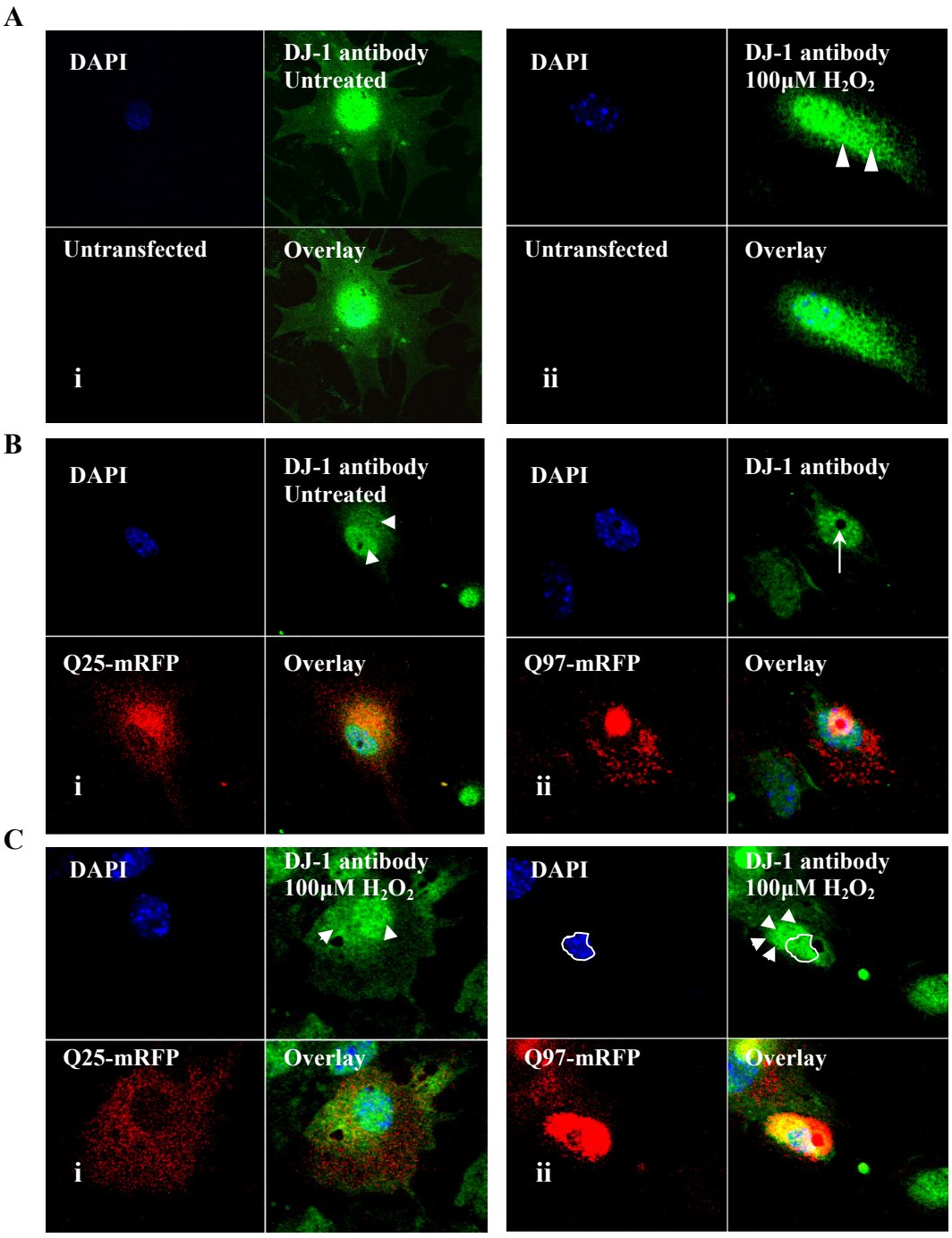

Figure 5.13 Endogenous levels and localisation of DJ-1 in astrocytes under different conditions. (A) Endogenous levels and localisation of DJ-1 in untreated astrocytes (i) and 100µM H_2O_2 treated astrocytes (ii). **(B)** HttEx1Q25-mRFP (i) or Q97-mRFP (ii) transfected astrocytes showing DJ-1 levels and localisation. **(C)** DJ-1 immunoreactivity of astrocytes expressing httEx1Q25 (i) or Q97-mRFP (ii) when treated with 100µM of H_2O_2. Arrow heads indicate localisation of cytoplasmic and nuclear DJ-1 and white circle indicates nucleus. DJ-1 did not colocalise with mhttEx1 IBs (white arrow, polyclonal DJ-1 antibody from Neuromics).

DJ-1 in HeLa cells also translocated to and from the nucleus in the presence and absence of H_2O_2 in a similar fashion to astrocytes. HeLa cells under normal culture conditions displayed a nuclear localisation of DJ-1 (Figure 5.14A) whereas when treated with 100μM of H_2O_2 (in this case for 6 hours), DJ-1 appeared to translocate to the cytoplasm (Figure 5.14B). DJ-1 in cells overexpressing httEx1Q25-mRFP with or without H_2O_2 treatment was present in both the cytoplasm and the nucleus (Figure 5.14C and E). This distribution pattern was not observed when cells were transfected with httEx1Q97-mRFP (Figure 5.14D) and upon H_2O_2 treatment DJ-1 seems to translocate to the cytoplasm, although a strong DJ-1 signal was still observed in the nucleus (Figure 5.14F). A stronger DJ-1 signal was observed when cells expressing httEx1Q25/Q97-mRFP were treated with 100μM of H_2O_2 suggesting again that DJ-1 is upregulated under oxidative stress conditions (Figure 5.14E and F).

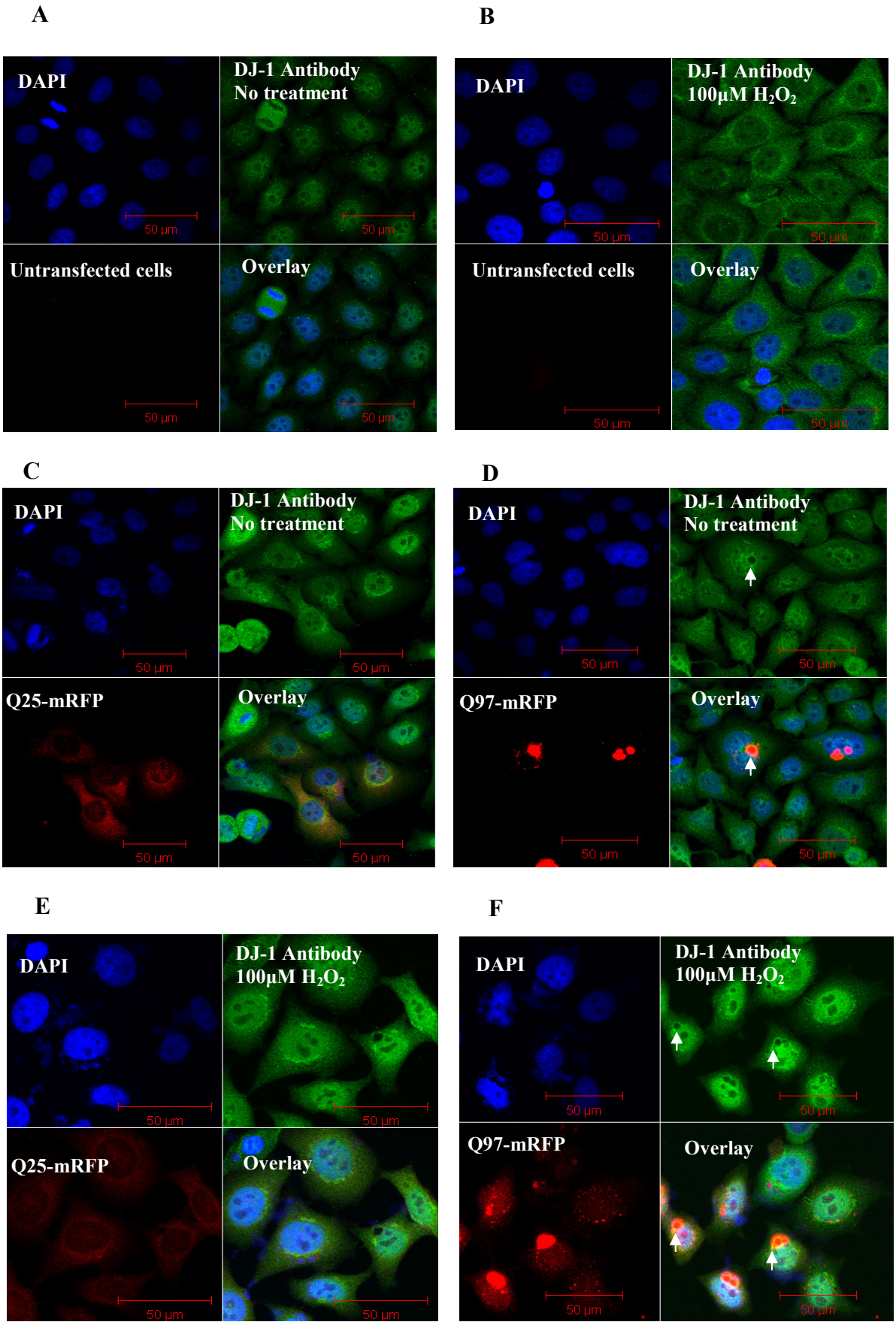
A
DAPI
DJ-1 Antibody
No treatment
Untransfected cells
Overlay
B
DAPI
DJ-1 Antibody
100μM H_2O_2
Untransfected cells
Overlay
C
DAPI
DJ-1 Antibody
No treatment
Q25-mRFP
Overlay
D
DAPI
DJ-1 Antibody
No treatment
Q97-mRFP
Overlay
E
DAPI
DJ-1 Antibody
100μM H_2O_2
Q25-mRFP
Overlay
F
DAPI
DJ-1 Antibody
100μM H_2O_2
Q97-mRFP
Overlay
50 μm

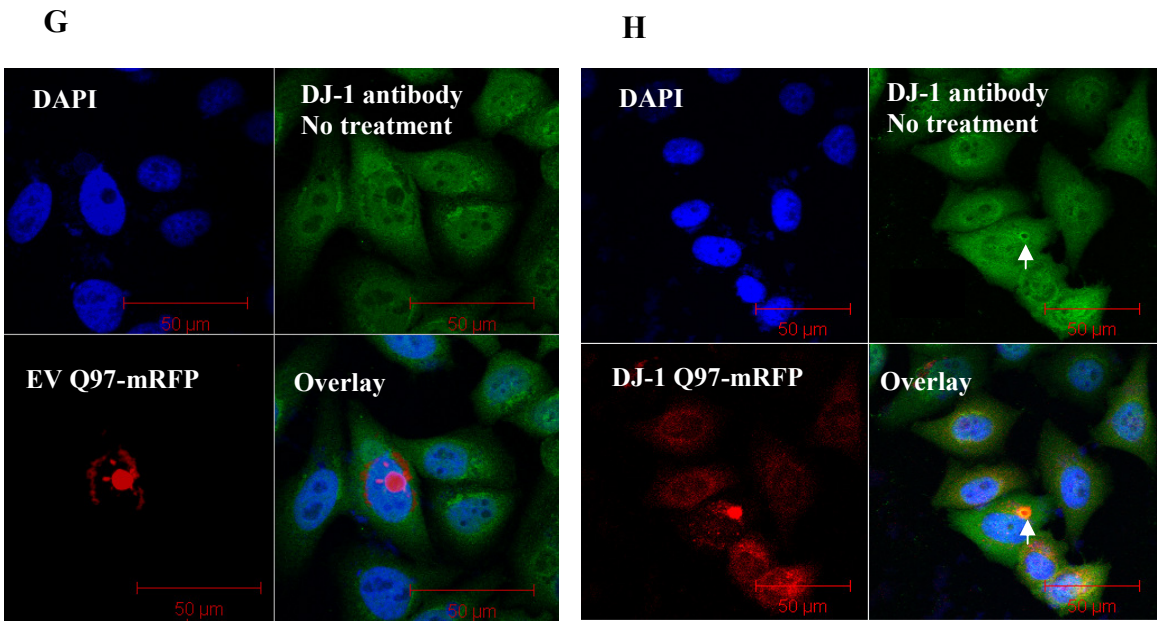

Figure 5.14 Localisation of DJ-1 after treatment of H_2O_2 and transfection with httEx1Q25/Q97-mRFP. Cells were fixed with 4% paraformaldehyde 3 days post-transfection and immunolabelled with polyclonal DJ-1 antibody followed by a fluorescently labelled secondary antibody and imaged on confocal microscope under the same settings. In some conditions HeLa cells were treated with 100µM of H_2O_2 for 6 hours prior to fixation at day 3. **(A)** Untreated and untransfected cells show nuclear DJ-1 localisation whereas **(B)** Untransfected HeLa cells treated with 100µM of H_2O_2 for 6 hours show both cytoplasmic and nuclear localisation. **(C)** HeLa cells transfected with httEx1Q25-mRFP exhibit both nuclear and cytoplasmic staining whereas **(D)** cells expressing httEx1Q97-mRFP mostly show nuclear localisation with some weak cytoplasmic staining. In these cells DJ-1 colocalises with mhttEx1-IB by forming a ring structure around it (see white arrow). **(E-F)** 100µM H_2O_2 treated HeLa cells expressing httEx1Q25/Q97-mRFP increases DJ-1 expression levels compared to untreated cells. **(E)** HttEx1Q25-mRFP show mostly cytoplasmic and nuclear staining whereas **(F)** httEx1Q97-mRFP show predominantly higher expression levels of DJ-1 in the nucleus compared to cytoplasm and more prominently colocalised with mhttEx1 IBs (ring structure (arrow head) when treated with H_2O_2. **(G-H)** HeLa cells co-transfected with either DJ-1 or EV and httEx1Q97-mRFP (3:1) show cytoplasmic and nuclear DJ-1 staining. DJ-1 overexpression seems to increase the colocalisation signal with mhttEx1 IB. Scale bars 50µm.

5.3.1.8 Co-localisation analysis of DJ-1 and mhttEx1 aggregates

Several studies have shown that DJ-1 is colocalised with neurofibrillary tangles (NFTs), neuropil threads (NTs) in AD extracellular plaques and also distributes to the pathological tau inclusions of PD and FTDP-17 (Bandopadhyay et al., 2004; Meulener et al., 2005b; Rizzu et al., 2004). As a molecular chaperone, DJ-1 could potentially interact with mhtt and colocalise with mhttEx1 IBs. To examine this idea further astrocytes were infected with adenovirus carrying httEx1Q25/Q97-mRFP and were subsequently immunolabelled with a polyclonal DJ-1 antibody (Cell Signaling). Adenoviruses were used in order to achieve a high level of IB formation. Analysis was performed using a confocal microscope under conditions that allowed httEx1Q97-mRFP IBs to be detected under high and low confocal laser gains and ensuring that mRFP IBs did not "spill through" into the channel settings used for detection of the secondary antibody used against DJ-1 (Alexa 488). Figure 5.15 is an illustration of an immunocytochemical analysis of httEx1Q97-mRFP infected astrocytes that produced several mhttEx1 IBs. Identical conditions were used for all of these analyses in httEx1Q25/Q97-mRFP expressing cells. Under such conditions no mhttEx1-mRFP IBs did "spill through" to the 488/512nm detection channels (Figure 5.15). Cells expressing httEx1Q25-mRFP do not produce IBs and DJ-1 protein seemed to homogenously localise within the cytoplasm (Figure 5.16A), but some cells showed a nuclear localization of DJ-1 (white arrow head) and also seemed to have mitochondrial localisation (punctate distribution, white arrow). Figure 5.16A illustrates that httEx1Q25-mRFP-expressing cells exhibit a different distribution of DJ-1 staining compared to uninfected cells (white arrow, Figure 5.16A) where a more nuclear/mitochondrial localisation can be seen. It is unclear why this difference occurs. On the other hand DJ-1 occasionally colocalised with IBs in cells expressing httEx1Q97-mRFP immunolabelled with polyclonal (Cell Signaling) DJ-1 antibody (Figure 5.16B, arrow heads).

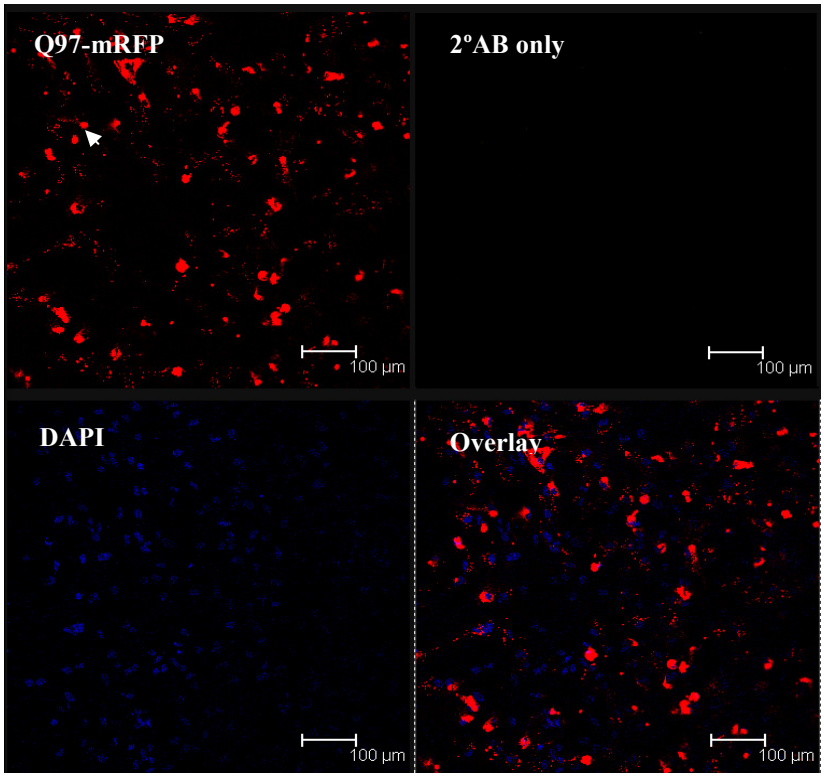

Figure 5.15 Negative control for DJ-1 immunolabelled astrocytes expressing httEx1Q97-mRFP. Astrocytes were infected with httEx1Q97-mRFP adenovirus and fixed with 4 % paraformaldehyde at day 3 after infection. Adenovirus carrying httEx1Q97-mRFP makes cytoplasmic IBs (white arrow). Cells were labelled with secondary antibody only as a control (top right). DAPI was used as a nuclear stain. Scale bar 100µm.

A

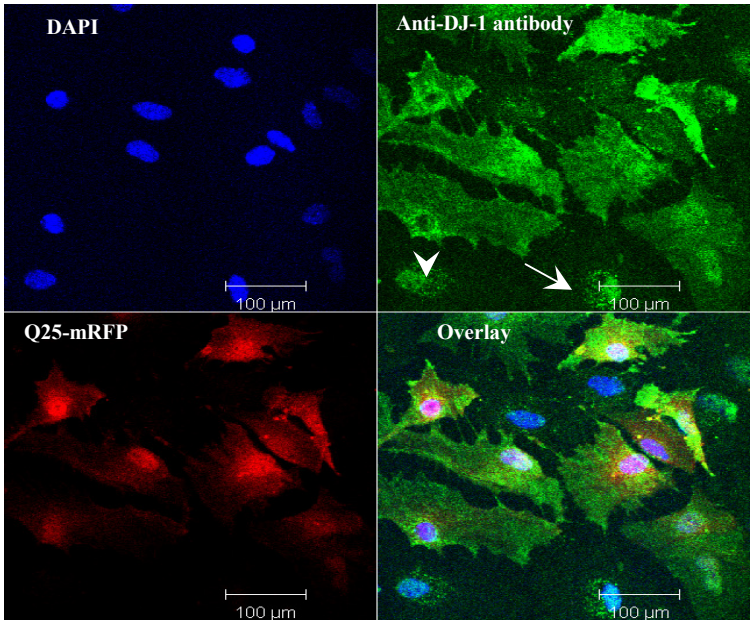

B

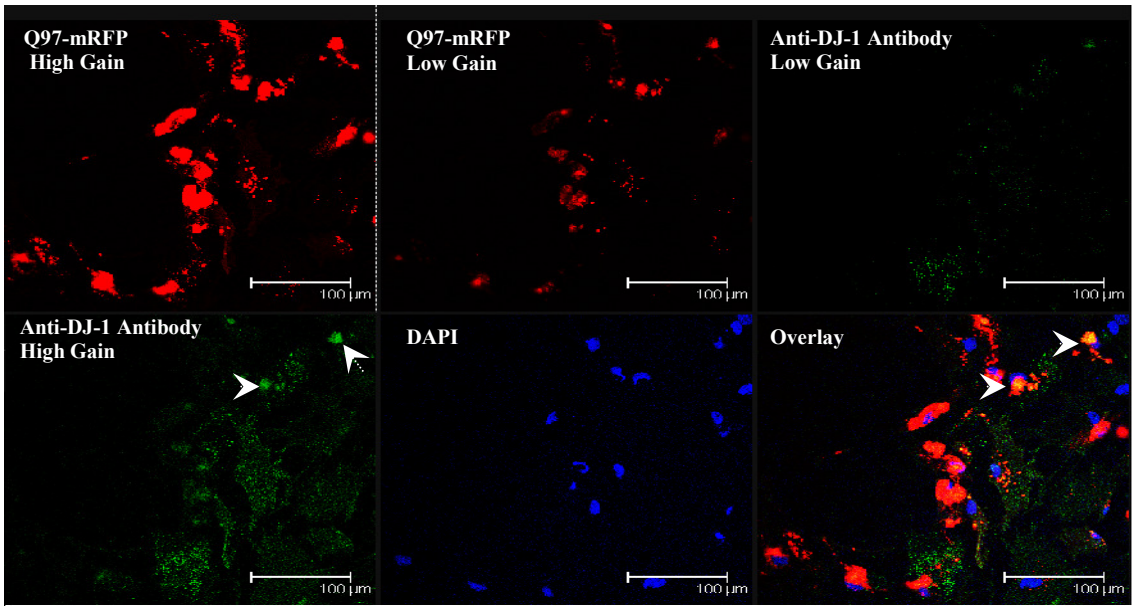

Figure 5.16 Localisation of DJ-1 in astrocytes expressing httEx1Q25/Q97-mRFP. Astrocytes infected with adenovirus carrying httEx1Q25/Q97-mRFP were fixed with 4% paraformaldehyde at day 3 and immunolabelled with polyclonal (Cell Signaling) DJ-1 antibody. **(A)** Astrocytes infected with httEx1Q25-mRFP. DJ-1 also seemed to localise inside the nucleus (arrow head) whereas it may also have mitochondrial localisation (white arrow, punctate staining). **(B)** Astrocytes infected with httEx1Q97-mRFP and DJ-1 occasionally co-localised with httEx1Q97-mRFP IBs (arrow heads). DAPI was used as nuclear stain. Scale bar 100µm.

Different antibodies provided opposite results. The polyclonal Cell Signaling DJ-1 antibody showed occasional colocalisation of endogenous DJ-1 with mhttEx1 IBs (Figure 5.16B) within astrocytes, whereas the polyclonal antibody from Neuromics did not show any colocalisation when astrocytes were transfected with httEx1Q97-mRFP (Figure 5.13Bii). Hence, it was decided to perform this analysis also in HeLa cells with or without overexpression of DJ-1 or EV and httEx1Q97-mRFP. Figure 5.14D shows that endogenous DJ-1 colocalised with mhttEx1 IB and formed a ring-like structure around it (white arrow) whereas endogenous or exogenously overexpressed DJ-1 with mhttEx1 showed frequent and prominent colocalisation with IBs (ring like structure around IBs, white arrows) (Figure 5.14F and H). This experiment was performed by using the polyclonal Neuromics antibody in HeLa cells (Figure 5.14).

5.3.2 DJ-1 expression analysis in HD cell-and animal models and HD patients brain

Recently, Baulac et al., (2009) reported that DJ-1 expression levels were induced in zebrafish brain under oxidative stress conditions suggesting that DJ-1 is a component of the stress response machinery. There are a few other studies that suggest that DJ-1 levels are upregulated in the brain (Choi et al., 2006) and plasma of AD and PD patients (Waragai et al., 2007). In addition to this, a study by Saito et al., (2009) reported that early stage PD patients erythrocytes show higher levels of DJ-1 compared to a control group. As shown in Chapter 4, mhttEx1 causes an impaired redox homeostais in HD cell models and this could potentially alter the levels of DJ-1 in HD which in turn may play a key role in IB formation and toxicity, as shown in the overexpression experiments. Hence DJ-1 expression analysis was performed using various cell models, an animal model of HD and CNS tissue samples from HD patients (Vonsattel grade 2) and control brains by using a Western blot approach.

5.3.2.1 Mhtt upregulates DJ-1 expression levels in several httEx1 cell models

Westen blot analysis was performed on both Tet-inducible and tebufenozide inducible cell systems (Figure 5.17A and B). Total soluble protein was extracted in 2% SDS sample buffer and 20µg of protein was loaded. Coomassie gels run in parallel were used as a loading control (Figure 5.17C and D). Western blot analysis showed that the DJ-1 expression level is significantly increased (1.6 fold) at day 1 after induction of

httEx1-EGFP with 1μM of doxycycline in mutant Tet 72.10 cells compared to wild-type 21.20 cells (Figure 5.17E). Tebufenozide inducible mhttEx1 expressing cells showed a 1.8-fold increase in DJ-1 expression levels after 6 hours of induction compared to wild-type cells, whereas no change was observed at later time points (Figure 5.17F). Although this change was not significant due to the high variation in the two experiments these results confirm a similar trend as found in the Tet-inducible cell system. As mentioned previously, the tebufenozide-inducible cell system presented an increased rate of IB formation during passaging which may partly explain the high variability. It may be that the early increase in IB formation is associated with an early increase in DJ-1 levels in the tebufenozide-inducible cell system, whereas the increase in DJ-1 expression levels observed at a later time point in the Tet-inducible cell system may be because the system presents with a delayed aggregation phenotype (Wyttenbach et al., 2001).

After showing an induction of DJ-1 due to the expression of httEx1 with a polyQ expansion in two PC12 cell models, DJ-1 expression during polyQ misfolding stress was examined in astrocytes. Given that transient transfection did not result in the transduction of the majority of astrocytes and caused a relatively high baseline toxicity (% nuclear fragmentation), primary astrocytes were infected with an adenovirus expressing httEx1Q25 and/or Q97–mRFP at multiplicity of infection (MOI) of 10-20 (see appendix 14 for aggregation and toxicity data). Cell lysates were obtained at 12, 24 and 48 hours after infection. Under these conditions >95% of astrocytes expressed the respective transgenes (see appendix 14). Western blot analysis showed that astrocytes infected with httEx1Q97-mRFP contained higer levels of DJ-1 after 24 hours of infection as compared to cells infected with an adenovirus expressing httEx1Q25-mRFP (Figure 5.18). However, this increase did not reach statistical significance.

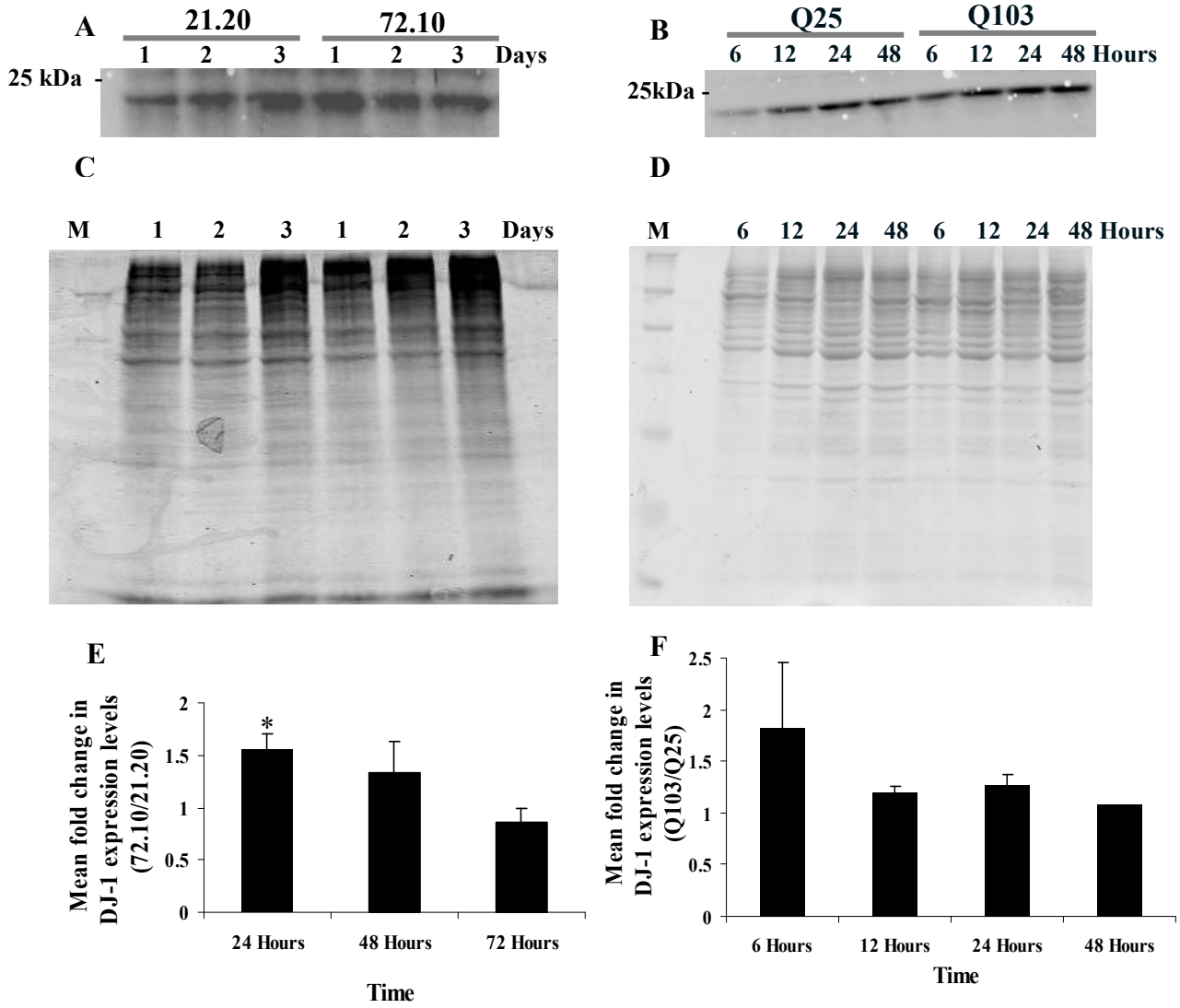

Figure 5.17 Western blot analysis showing DJ-1 expression levels in httEx1 inducible cell systems during a time course regime. 20µg of 2% SDS solubilised protein from Tet-on and tebufenozide inducible cells expressing wild-type httEx1 and mhttEx1 were resolved by SDS-PAGE and the expression level of DJ-1 was quantified by incubating membranes with antibody raised against DJ-1 (Neuromics) followed by a fluorescently labelled secondary antibody which was detected by an infrared fluorescence scanner. Pixel intensity values were quantified by using Odyssey Infrared Scanner software and presented as fold change (mhttEx1/httEx1) for both inducible cell systems after normalising for protein loading. **(A)** and **(B)** Western blot analysis showing levels of DJ-1 in Tet-inducible and tebufenozide inducible cell system. (**C)** and **(D)** Coomassie gels were used as a loading control for both the Tet- and the tebufenozide inducible cell system **(E)** Quantification of a Western blot showing that DJ-1 was significantly upregulated in mhttEx1 (72.10) inducing cells as compared to wild-type httEx1 (21.20) inducing cells after 24 hours of induction with 1µM of doxycycline. **(F)** DJ-1 expression level analysis in a tebufenozide inducible cell system showing that mutant httEx1Q103-EGFP seems to have high levels of DJ-1 in the first 6 hours of induction as compared to cells expressing httEx1Q25-EGFP. (n=3 for the tetracycline inducible system and n=2 for the tebufenozide inducible cells. One sample t-test was used for statistical analysis (*= $p<0.05$).

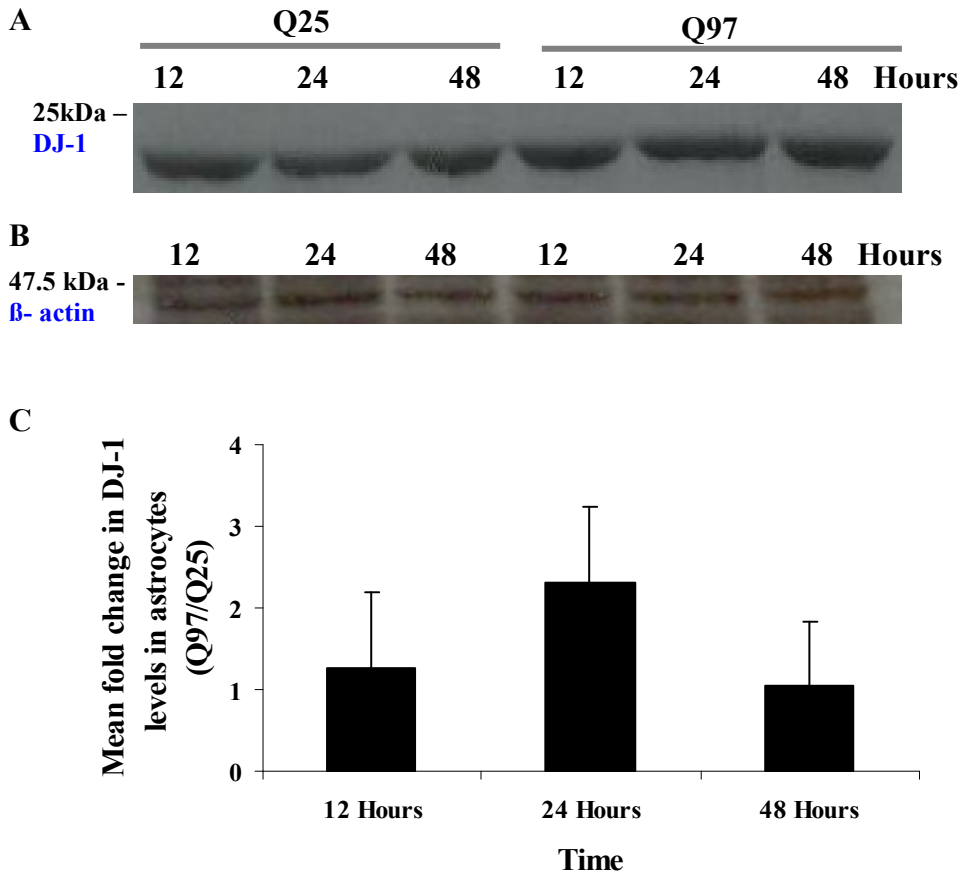

Figure 5.18 Mean fold increase in the expression levels of DJ-1 in astrocytes expressing httEx1Q25 or Q97-mRFP. 20µg of 2% SDS solubilised protein from primary astrocytes expressing httEx1Q25/Q97-mRFP were resolved by SDS-PAGE and the expression level of DJ-1 was quantified. Astrocytes were infected with adenovirus carrying httEx1Q25 or Q97-mRFP at MOI of 10-20. Pixel intensity values were quantified by using Odyssey Infrared Scanner software and presented as fold change (Q97/25) after normalising for protein loading **(A)** Western blot shows expression levels of DJ-1 at different time points when infected with adenovirus carrying wild-type httEx1 or mhttEx1, **(B)** ß- actin was used as a loading control and **(C)** Quantification shows a trend toward an increase in DJ-1 levels in cells expressing mhttEx1. N=2 at 12 and 48 hours whereas n=3 at 24 hours. Error bars represent standard errors of the means. One sample t-test was performed for statistical analysis ($P > 0.05$).

5.3.2.2 DJ-1 is up-regulated in the R6/2 mouse model of HD

A set of experiments was next performed to confirm the results obtained in HD cell models in an HD animal model. There are several widely used animal models of HD. R6/1 and R6/2 were the first HD transgenic mice produced that express exon-1 of the human *HD* gene with around 115 and 150 CAG repeats, respectively (Mangiarini et al., 1996). R6/1 has disease onset at 5 months and they die at aproximately one year of age, whereas R6/2 shows a more robust phenotype (both for behaviour and pathology) and an age of onset at around 8 weeks of age and they then live only 16-17 weeks (Li et al., 2005). Hence the analysis was performed on 17 week old R6/2 mouse frontal cortex, striatum and cerebellum samples that were kindly provided by Prof. Jenny Morton (University of Cambridge, UK). All brain samples were homogenised and extracted by Shmma Quraishe (University of Southampton). Total soluble protein fractions of these samples were extracted by using 2% SDS. Samples were then seperated by gel electrophoresis followed by immunolabelling with a polyclonal DJ-1 antibody (Neuromics). Western blot quantification shows that DJ-1 is significantly upregulated in the frontal cortex of R6/2 animals compared to age matched wild-type control animals (Figure 5.19A and B). In contrast, no change in DJ-1 expression levels were observed in the cerebllum (Figure 5.19C and D) and striatum (Figure 5.20) of R6/2 compared to their age matched wild-type control animals. Coomasie gels were run in parallel for all samples to control for total protein loading (see appendix 17 for coomassie gels) whereas α-tubulin was used as a loading control for striatum samples due to limited sample quantity.

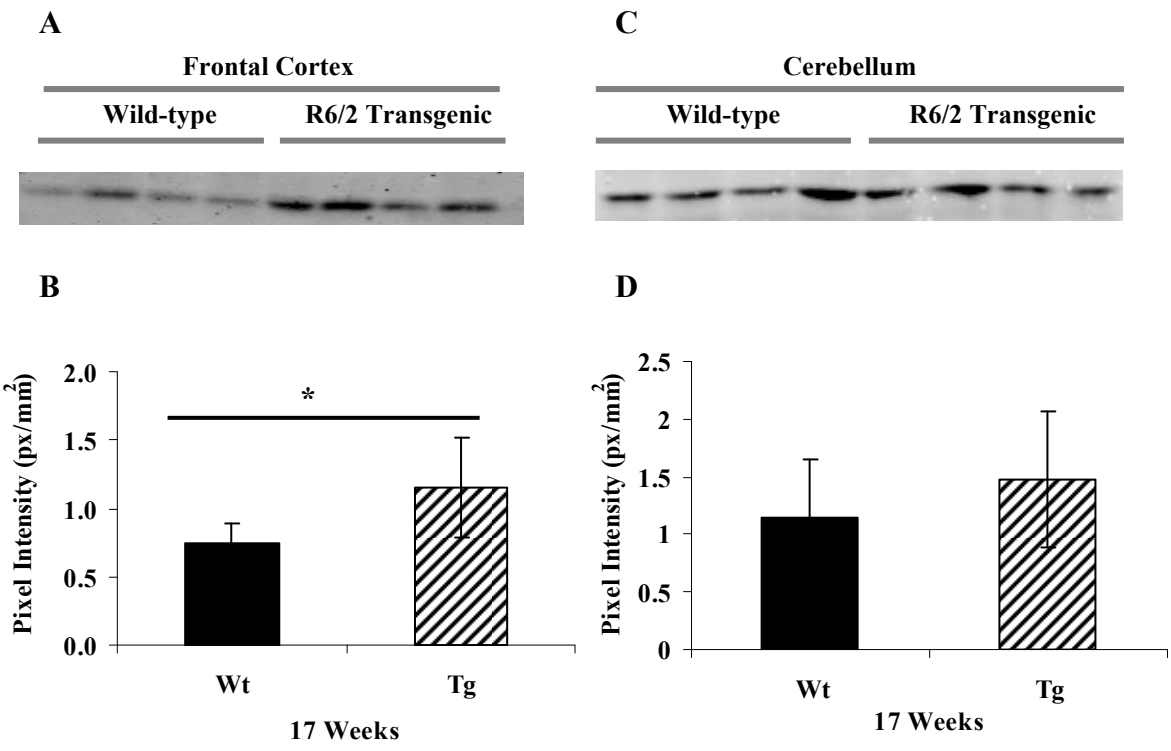

Figure 5.19 Western blot analysis showing DJ-1 expression levels in different brain regions of R6/2 mouse model at 17 weeks of age. 40µg of 2% SDS solubilised protein samples from the frontal cortex and the cerebellum of R6/2 and control animals were resolved by SDS-PAGE and the expression level of DJ-1 was quantified. Pixel intensity values were quantified by using Odyssey Infrared Scanner software and presented as pixel intensities per mm^2 after normalising for protein loading **(A)** Western blots showing levels of DJ-1 in R6/2 frontal cortex quantified in **(B). (C)** Western blot showing DJ-1 expression in cerebellum and **(D)** quantification showing no change in expression levels. Coomassie gels were used as loading control. n=4 for frontal cortex and n=5 for cerebellum. Error bars represent standard deviations. Unpaired t-test was used for statistical analysis. * = $P < 0.05$.

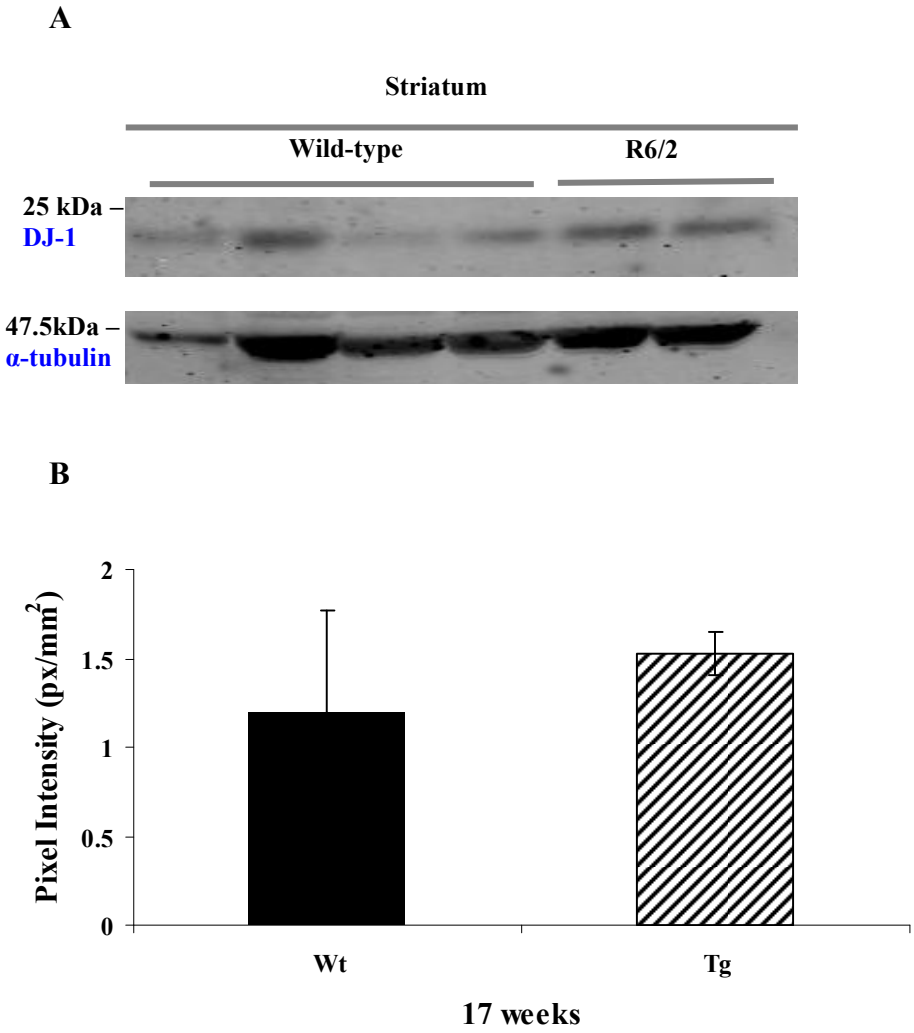

Figure 5.20 DJ-1 expression levels in the striatum of 17 week old HD animals compared to age matched controls. 40µg of 2% SDS solubilised protein from the striatum were resolved by SDS-PAGE and the expression level of DJ-1 was quantified. Pixel intensity values were quantified by using Odyssey Infrared Scanner software and presented as pixel intensities per mm^2 after normalising for protein loading. **(A)** Western blot probed with anti-DJ-1 antibody followed by a re-probing with α-tubulin antibody, used as loading control. **(B)** Western blot quantification showed no significant difference in DJ-1 levels between R6/2 and age control animals striatum. Error bars represents standard deviations. Unpaired t-test was performed for statistical analysis ($P > 0.05$, n=4 wild-type animals, n=2 transgenic animals).

5.3.2.3 DJ-1 is up-regulated in the frontal cortex of HD human brain

In order to follow up the results from R6/2 brains, a biochemical analysis of HD Vonsattel grade 2 human brain samples from frontal cortex and cerebellum was performed and compared to age matched control brains (Figure 5.21). Western blot analysis was performed on 5 HD samples and 5 control samples. Total soluble protein fractions of these samples were extracted by using again 2% SDS in a buffer describe in section 2.8.3. 40µg protein of each sample was resolved with SDS page and Western blot analysis revealed that DJ-1 is significantly up-regulated in the frontal cortex of HD brain as compared to control brains (Figure 5.21A and E). On the other hand, there was no significant change in DJ-1 levels observed in the cerebellum of HD brain versus control brain (Figure 5.21B and F). Coomassie gels ran in parallel were used as loading controls, as described above.

As mentioned in the general introduction, Choi et al., (2006) observed an upregulation of DJ-1 levels in both the AD and the PD patient brains. Their results also suggested that DJ-1 protein is irreversibly oxidised by carbonylation as well as methionine oxidation. More recently, Saito et al., (2009) showed that there is significantly more oxidised DJ-1 (at the Cys106 position) in the blood of unmedicated PD patients as compared to medicated PD patients or a control group. Based on these observations, a Western blot analysis was carried out on HD brain samples to test whether there are changes in DJ-1 oxidation at Cys106 position. Oxidised DJ-1 at Cys106 in the frontal cortex of HD brain was significantly increased in comparison to the control group (Figure 5.22A and E). On the other hand, samples from HD cerebellum did exhibit a trend towards increased oxidised DJ-1 (Figure 5.22B and F).

In order to confirm the oxidation of DJ-1 at C106 position, 2µg of commercially purified recombinant DJ-1 protein (Abcam, UK) was treated with 2, 20 or 60mM H_2O_2 for 1 hour at room temperature and resolved on SDS-PAGE followed by incubation with the anti Cys106 oxidised DJ-1 antibody. As a positive control 2 samples from HD and control group cerebellum were used. This antibody did not detect oxidised DJ-1 at the above mentioned concentrations of H_2O_2 whereas samples from the cerebellum of HD and control brains detected oxidised DJ-1 at the correct molecular weight (appendix 15, Figure A13A). Reprobing of the membrane with

polyclonal DJ-1 antibody detected recombinant DJ-1 protein treated with/without H_2O_2 (see appendix 15, Figure A13B). Mass spectrometry analysis (MS) has then used to confirm that this recombinant protein was indeed DJ-1 (appendix 16). MS analysis showed that this untreated protein was already oxidise (2 oxygens) and treatment of 2mM H_2O_2 for 1 hour at room temperature did not further oxidised this protein (see appendix 16). However, using this MS approach it cannot be described in which residues the oxygen molecules are located. Therefore it appears that the DJ-1 antibody supposedly detecting oxidised DJ-1 does perhaps not necessarily detect specific oxidation of DJ-1 at the Cys106 position, but it may have detected oxidatively damaged DJ-1. It is also possible that the incubation experiments with H_2O_2 did not succeed for unknown reasons.

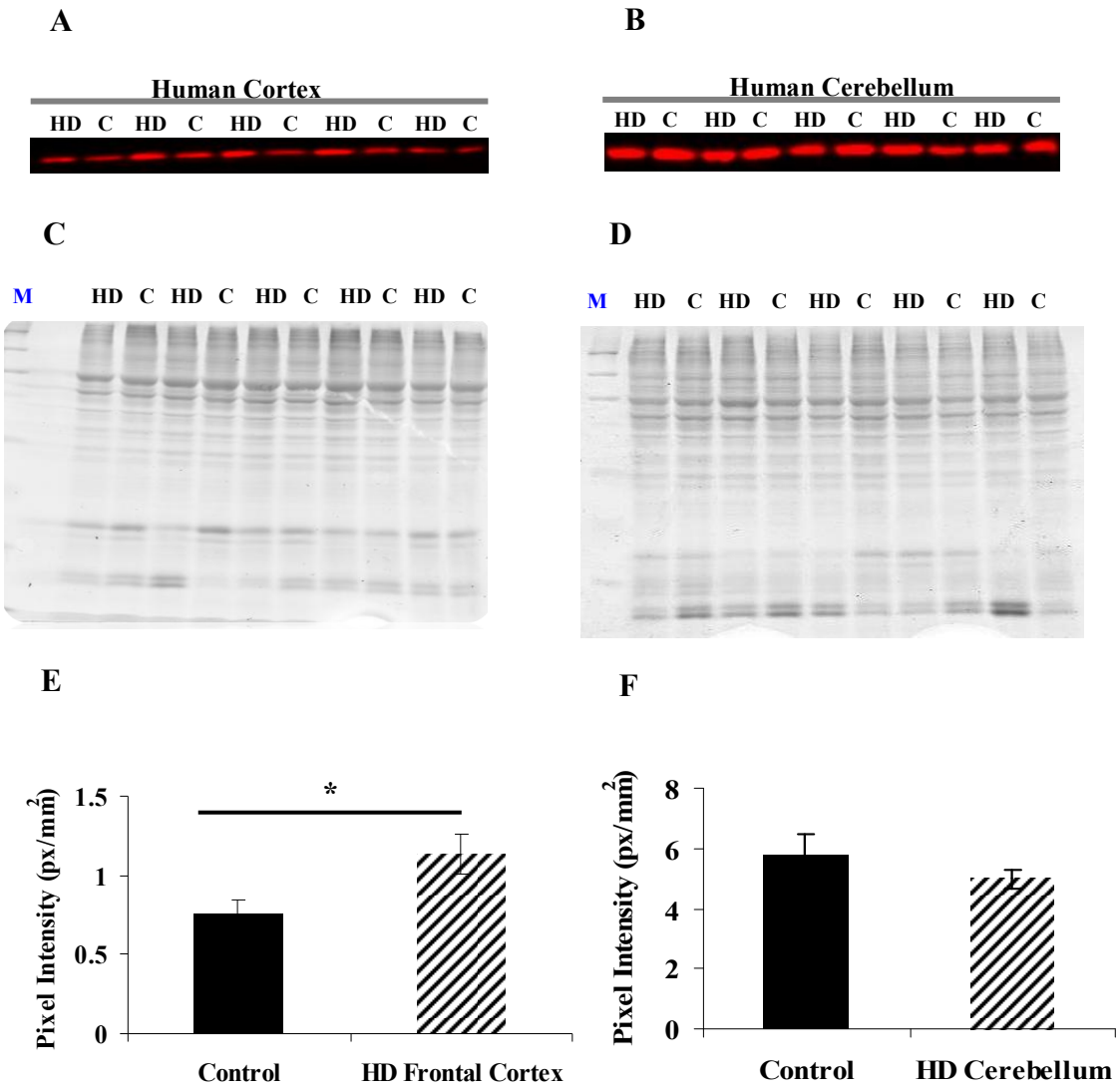

Figure 5.21 DJ-1 expression levels in HD and age matched control human frontal cortex and cerebellum. 40µg of 2% SDS solubilised protein samples from the frontal cortex and cerebellum were resolved by SDS-PAGE and the expression level of DJ-1 was quantified. Intensity values were measured by using Odyssey Infrared Scanner software. **(A)** and **(B**) Western blot analysis showed expression levels of DJ-1 in the frontal cortex and cerebellum. (**C)** and (**D**) Coomassie gels were used as a loading control for samples from frontal cortex and cerebellum. (**E)** and **(F**) Quantification of DJ-1 expression levels as pixel intensity corrected for protein loading presented as pixel per mm^2. Frontal cortices of HD patients show higher levels of DJ-1 as compared to control brains whereas no change was observed in the cerebellum of HD patient brains. Error bars represents standard errors of the means. Unpaired t-test was performed for statistical analysis (* = $P < 0.05$, n = 5, frontal cortex and cerebellum, M = Marker, HD = Huntington's disease patient and C = control group).

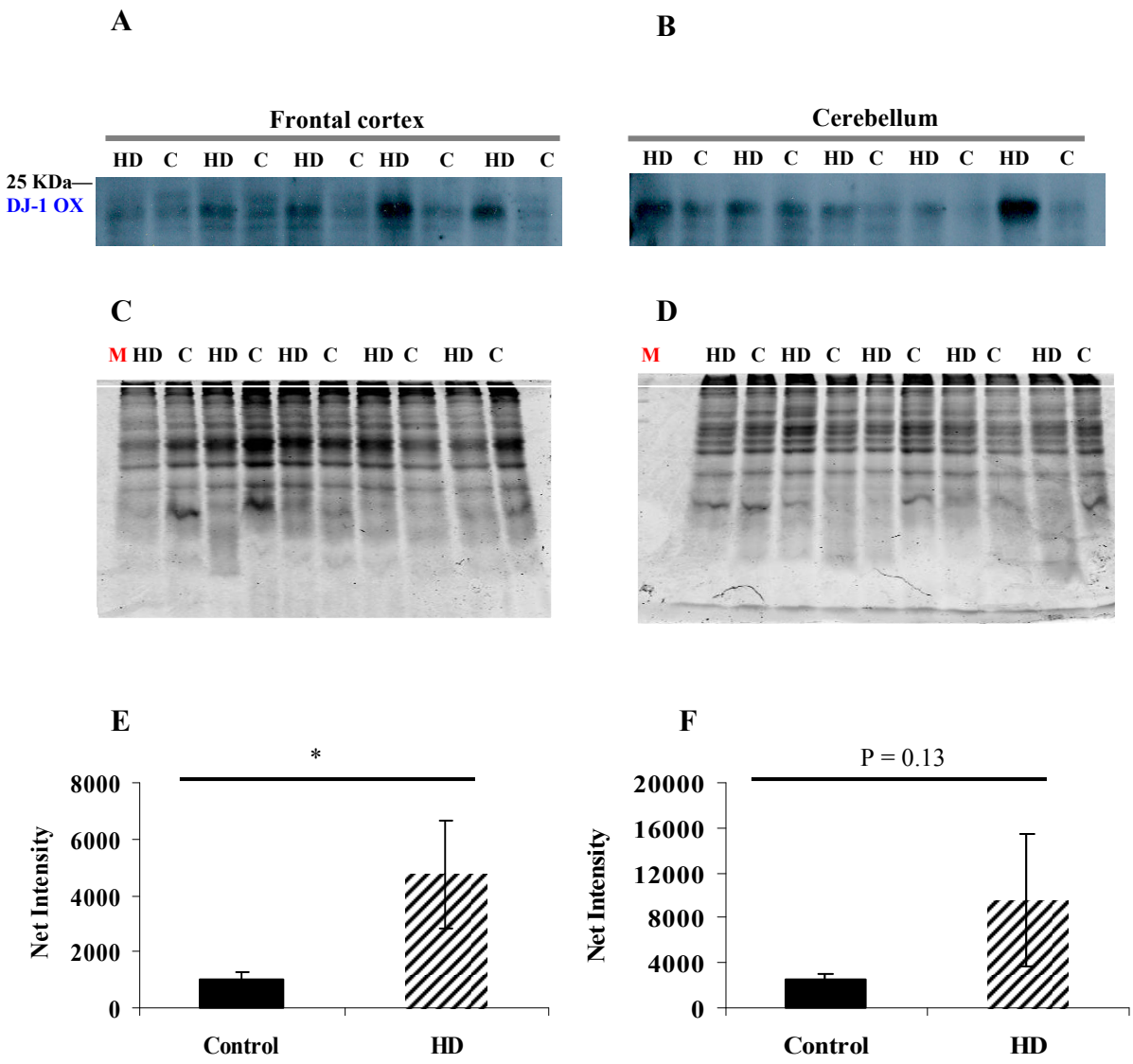

Figure 5.22 Western blot analysis detects more oxidised DJ-1 in HD brains compared to control brains. 40µg of 2% SDS solubilised protein from the frontal cortex and cerebellum were resolved by SDS-PAGE and the expression of oxidised DJ-1 was measured by incubating membranes with antibody against oxidised DJ-1 followed by incubation with an enzyme (HRP) linked secondary antibody which was detected by using ECL method. Intensity values were calculated by using Image J software. **(A)** and **(B**) Oxidised Cys106-DJ-1 specific antibody labelled human frontal cortex and cerebellum samples. **(C)** and **(D)** Coomassie gels were used as a loading control for both frontal cortex and cerebellum and intensity values were measured by using Infrared Scanner software. **(E)** and **(F**) Quantification of oxidised Cys106-DJ-1 isoform in human frontal cortex and cerebellum. Cys106-DJ-1 immunolabelling was significantly increased in patients' frontal cortex compared to the control group. Error bars represent standard errors of the means. Unpaired t-test for performed for statistical analysis (n=5 patients and control samples, * = $P< 0.05$ for frontal cortex and $P= 0.13$ for cerebellum).

5.4 Discussion

Redox-regulated/regulating chaperones such as HSP27, ABC, HSP33 and DJ-1 have been shown to affect both protein aggregation and the cellular redox state in models of neurodegenerative diseases and other human diseases (Graumann et al., 2001; Shendelman et al., 2004; Rajasekaran et al., 2007; Wyttenbach et al., 2002). Shendelman et al., (2004) suggested that DJ-1 is a redox-dependant chaperone that inhibits aggregation formation of α- synuclein in PD *in vivo* and *in vitro* models. Therefore, the effect of DJ-1 overexpression in relation to polyQ IB formation and toxicity suppression was examined in this chapter. The expression of DJ-1 itself was increased in httEx1 cell-and animal models and in the human HD brain suggesting that DJ-1 is upregulated in HD. Overexpression of DJ-1 in cell models increased polyQ aggregation and toxicity, but under mild oxidative conditions this detrimental effect was reversed depending on the functionality of Cys106 implicating both altered expression and the redox-activation of DJ-1 in polyQ aggregation and toxicity.

5.4.1 DJ-1 overexpression reduces basal cell death in cells expressing httEx1Q25-mRFP

DJ-1 overexpression in cells expressing control httEx1Q25-mRFP (without exogenous ROS) significantly reduced basal toxicity in HeLa cells (similarly a trend toward reduced basal toxicity was observed in astrocytes) compared to cells co-transfected with empty vector and httEx1Q25-mRFP. Hence, DJ-1 may have anti-apoptotic activity when overexpressed with httEx1Q25-mRFP. It has been demonstrated that the protective effect of DJ-1 against mutant α- synuclein (A53T)-induced toxicity involved the upregulation of HSP70 (Zhou et al., 2004). They later showed that DJ-1 increases cellular levels of glutathione under oxidative stress conditions and provide cellular protection against oxidative stress (Zhou and Freed, 2005). Batelli et al., (2008) indicated that DJ-1 inactivation (RNAi knockdown) may enhance α-synuclein aggregation and its related toxicity. They also suggested that HSP70 is a downstream mediator of the antioxidant properties of DJ-1 (Batelli et al., 2008). In addition to this, Fan et al., (2008) reported that DJ-1 overexpression exerts its cytoprotective effects by inhibiting BAX in a p53 dependant manner when Neuro2a cells were treated with H_2O_2 or exposed to UV to induce cell death. Hence, DJ-1 overexpression in cells expressing wild-type httEx1 may well reduce basal cell death by enhancing endogenous HSP70 levels or by inhibiting the p53-BAX-caspase

pathway or by interfering with cell death via other signalling pathways (see below). Hsp70 is well known for its anti-apoptotic activity (reviewed in Lu et al., 2010) and there is some evidence to suggest that it prevents polyQ-induced death in primary neurons in both cerebellar (Tagawa et al., 2007) and sympathetic neurons (King et al., 2008a). These various possibilities deserve further examination.

5.4.2 Oxidatively "activated" DJ-1 suppresses mhttEx1 mediated aggregation and cell death

Shendelman et al., (2004) reported that Cys 46, 53 and 106 stabilise the chaperone activity and protective functions of DJ-1 against ROS. Also, DJ-1 is known to enhance its chaperone activity in oxidising conditions (Zhou et al., 2006). Hence, it is conceivable that the increased ROS production in HeLa cells expressing httEx1Q97-mRFP, shown in Chapter 4, could lead to redox-activation of DJ-1 and suppress polyQ aggregation and toxicity. This was not the case. Instead DJ-1 overexpression increased IB formation (Figure 5.3) and cell death (Figure 5.4) whereas under oxidising conditions (endogenous generated or exogenously added ROS) polyQ aggregation and mhttEx1 toxicity was significantly suppressed both in HeLa (Figure 5.6 and 5.7) and astrocytes (Figure 5.10 and 5.11). This showed that DJ-1, when at high levels under non-oxidizing conditions, increased polyQ aggregation likely also leading to increased toxicity due to the acceleration of polyQ aggregation.

Muchowski et al., (2000) proposed that HSP70 binds to the polyQ-containing segment of mhttEx1 and represses its aggregation and toxicity. Indeed other studies showed that HSP chaperones normally suppress polyQ aggregation (Cummings et al., 1998; Cummings et al., 2001; Howarth et al., 2007; Jana et al., 2000; Wacker et al., 2004), but some reports showed that members of the HSP40 family are able to increase IB formation (Fayazi et al., 2006; Wyttenbach et al., 2000). Given that the overexpression of DJ-1 in the present study enhanced mhttEx1 induced aggregation, it is possible that DJ-1 interacted with mhttEx1 leading to an increase in nucleation events, or, later along the fibrillization pathway, promoted fibril formation. The above-mentioned potentially activated anti-apoptotic pathways due to DJ-1 overexpression leading to elevated HSP70 levels or inhibition of the p53-BAX-caspase pathway, are perhaps not anti-apoptotic enough or may not be activated at all

in this case. After addition of exogenous ROS, DJ-1 is then likely to function as a chaperone and lose its detrimental effects due to its overexpression.

It is important to mention here that expression of DJ-1 and httEx1Q97-mRFP may have selectively killed cells without IBs, a possibility that cannot be excluded without performing single-cell, longitudinal analysis. Aggregation precursors such as monomers or oligomers are thought to be the more toxic form of mhtt (reviewed in Hands and Wyttenbach, 2010). Such a scenario might therefore have resulted in the occurrence of a higher proportion of cells with IBs under DJ-1 and mhttEx1 overexpression conditions. In order to prove that DJ-1 directly enhanced polyQ aggregation, an aggregation inhibitor effective against aggregation intermediates, such as PGL-135, could be employed to show that the DJ-1 polyQ aggregation enhancing effect could be inhibited. Another possibility explaining an increase in aggregation due to DJ-1 overexpression is a reduced clearance of mhttEx1. DJ-1 may be a part of complex with httEx1 and IκB kinase (Ikk) complex (Ali Khoshnan, personal communication). It is known that Ikk modifies the N-terminus of mhtt and activates the Ikk complex that seems to phosphorylate mhttEx1 less efficiently than wild-type httEx1 and this phenomenon is also true for full length htt (Khoshnan et al., 2004; Thompson et al., 2009). This impaired posttranslational modification, in a full-length htt context however, has been suggested to lead to increased caspase cleavage and decreased clearance of mhtt due to impaired proteasomal and lysosomal protein degradation pathways that in turn lead to increased protein aggregation and toxicity in HD (Thompson et al., 2009). Hence an alteration of posttranslational modifications of mhttEx1 in the presence of increased expression of DJ-1 could result in its accumulation leading to increased aggregation.

In order to confirm that DJ-1 is redox-activated and acts as a chaperone in the experiments described above, the httEx1 aggregation modulating ability of DJ-1 was directly tested *in vitro* by using recombinant DJ-1 protein (Abcam) under normal and oxidising conditions in co-incubation experiments with httEx1Q20 or Q53 at 1:1 stoichiometry (Dr. S. Hands, personal communication). Atomic force microscopy (AFM) analysis showed that DJ-1 accelerated the aggregation of mhttEx1 whereas after pre-treatment of DJ-1 with 2mM H_2O_2 the aggregation enhancing effect was lost, or polyQ aggregation was even modestly inhibited (as measured by fibril lengths

and the number of fibrils formed after 24hours) (Dr S. Hands, unpublished data). DJ-1 protein mass- and integrity was confirmed by using mass spectrometry and Western blot analysis (see appendix 15 and 16). These observations indicate that the DJ-1 polyQ aggregation enhancing activity upon overexpression within cells could be mediated via direct interaction.

If this were true DJ-1 would be expected to co-localise with httEx1 aggregates within cells. Overexpression of DJ-1 in HeLa cells indeed showed frequent DJ-1 colocalisation with mhttEx1 IBs (using the polyclonal DJ-1 (Neuromics) antibody, see Figure 5.14). IB co-localisation analysis in astrocytes also showed that endogenous astrocytic DJ-1 does occasionally colocalise with mhttEx1 IBs (visualized with a polyclonal DJ-1 antibody from Cell Signaling). However, no DJ-1 colocalisation could be observed when astrocytes expressing httEx1Q97-mRFP were immunolabelled with the polyclonal DJ-1 antibody from Neuromics. Hence these investigations would need confirmation, including elucidation of such in studies using immunohistochemical analysis of mouse brain (e.g. the R6/2 mouse) before firm conclusions could be drawn. Furthermore, immunoprecipitation studies should be performed to further clarify whether DJ-1 associates with mhttEx1.

5.4.3 Cys106 residue of DJ-1 promotes the protective function against polyQ aggregation and toxicity under mild oxidizing conditions

Several studies have reported that Cys106 is the most sensitive cysteine of DJ-1 and is more prone to oxidation as compared to Cys46 and Cys53 (Canet-Aviles et al., 2004; Kinumi et al., 2004; Lee et al., 2003; Wilson et al., 2003). This notion is further supported by studies showing that oxidation of Cys106 forms Cys106- sulfinic acid (Canet-Aviles et al., 2004; Witt et al., 2008; Zhou et al., 2006). Cys106 is evolutionarily conserved and its posttranslational modification is known to regulate DJ-1's protective function against oxidative stress acting as a sensor for DJ-1's chaperone activity (Blackinton et al., 2009b; Canet-Aviles et al., 2004; Honbou et al., 2003; Logan et al., 2010; Shendelman et al., 2004; Witt et al., 2008).

In order to confirm that DJ-1 was activated via the oxidation of its cysteines, believed responsible for its chaperone activity, a cysteine mutant (C106S) of DJ-1 was co-

transfected into HeLa cells and astrocytes with httEx1Q97-mRFP and compared to cells transfected with wild-type DJ-1 and httEx1Q97-mRFP. Surprisingly, C106S-DJ-1 overexpression with mhttEx1 significantly increased IB formation and toxicity both in HeLa and astrocytes and no aggregation suppression was observed when treated with either 100μM of H_2O_2 or 5 μM of Antimycin A. In contrast, oxidant treatment of cells expressing wild-type DJ-1 suppressed IB formation and toxicity. C106S-DJ-1 overexpression with mhttEx1 showed a unique IB pattern (multiple IB foci) in both HeLa and astrocytes (see Figure 5.9D and 5.12D). It has been shown that Cys106 is surrounded by three charged amino acids (Glu18, His126 and Arg 28) from both subunits of DJ-1 which are likely to be involved in its functionally important quaternary structure (Wilson et al., 2003; Witt et al., 2008). Furthermore, it is also well established that point mutation at Cys106 of wild-type DJ-1 causes a loss of its antioxidant protective function (Canet-Aviles et al., 2004; Shendelman et al., 2004; Takahashi-Niki et al., 2004). Hence more recently, Logan et al, (2010) suggests that the chaperone activity of DJ-1 is dependant on protein stability and oxidation of Cys106. These studies and suggestions are consistent with Cys106 being required in HD cell models to allow DJ-1 to act as a redox sensitive chaperone after oxidant treatment reducing mhttEx1 aggregation and toxicity. However, the mechanism for increased polyQ aggregation due to the Cys106 mutation remains unclear.

5.4.4 Modulation of polyQ aggregation and toxicity by DJ-1 and stress signalling pathways

There are other possibilities by which DJ-1 could modulate polyQ aggregation and toxicity under oxidizing conditions. For example, Mo et al., (2008) reported that DJ-1 physically interacts with mitogen-activated protein kinase/extracellular signal-regulated kinase kinase kinase 1 (MEKK1) and inhibits its activation which then leads to the suppression of MEKK1 mediated cell death by acting as a negative regulator of the oxidative stress induced JNK1 signalling pathway. Interestingly, Meriin et al., (2001) showed that activated MEKK1 enhances polyQ IB formation and suggested that activated MEKK1 generally affects protein aggregation. Therefore, it could be argued that a C106S-DJ-1 loss-of function against oxidative stress or a dominant negative function towards endogenous DJ-1, unable to negatively regulate MEKK1 activity, leads to increased MEKK1 activity and hence to enhanced aggregation and toxicity perhaps by activating JNK.

Recently, a study performed by Im et al., (2010) claimed that DJ-1 provides its protective function against oxidative stress by regulating the thioredoxin1 (Trx1)/ MAP3 kinase apoptosis signal-regulating kinase 1 (ASK1) complex. It is also well established that oxidative stress dissociates the inhibitor of the ASK1 complex, Thioredoxin (Trx1), from the complex (Noguchi et al., 2005; Saitoh et al., 1998) which then activates other signalling pathways, such as the JNK and p38 MAP kinase pathways that induce apoptosis (Ichijo et al., 1997; Nishitoh et al., 1998). Overexpression of DJ-1 suppressed ASK1 under oxidative stress conditions (Im et al., 2010; Junn et al., 2005). Im et al., (2010) also investigated the role of Cys46, 53 and 106 in the inhibition of Trx1/ASK1 complex dissociation and found that Cys106 is essential for this but not Cys46 and Cys53. Therefore DJ-1 Cys106 is an important regulator of the Trx1/ASK1 complex and provides protection to cells under stress conditions. Consequently, the DJ-1Cys106 effects observed in our study could partially be mediated via a ASK1 dependent mechanism.

Finally, yet another mechanism relating to the intracellular localisation of DJ-1 was investigated by Canet-Aviles et al., (2004). These authors showed that oxidation of Cys106 relocates DJ-1 to the mitochondria and provides protection against cell death. In Figure 5.13 and 5.14 it appears that under basal conditions DJ-1 is primarily localised within the nucleus, whereas when cells were treated with H_2O_2, some DJ-1 appears to translocate to the cytoplasm. In addition to this, cells expressing httEx1Q25-mRFP showed both nuclear and cytoplasmic DJ-1 immunostaining, whereas cells expressing httEx1Q97-mRFP showed mainly nuclear staining and upon oxidant treatment DJ-1 seemed again to translocate to the cytoplasm. These results are supported by the above-mentioned study in which Im et al., (2010) suggests that cytoplasmic DJ-1 acts as a negative regulator of the Trx1/ASK1 complex by preventing the dissociation of Trx1 from ASK1 in response to exogenously or endogenously produced oxidative stress.

In addition to this, nuclear localised DJ-1 binds to a cell death protein, called Daxx and prevents Daxx translocation to the cytoplasm and from binding and activating its effector kinase ASK1 (Junn et al., 2005). Preventing Daxx translocation to the cytoplasm is known to prevent cell death (Junn et al., 2005). The protective effect of

untreated DJ-1 on httEx1Q25-mRFP overexpressing cells (see above) and oxidants treated cells expressing DJ-1 and httEx1Q97-mRFP may be due to inhibition of Daxx translocation from the nucleus. However, overexpressed DJ-1 tends to remain in the nucleus in cells expressing httEx1Q97-mRFP and does not exhibit a protective function in an httEx1 context. This supports the hypothesis that the protective effect of DJ-1 in cells expressing mhttEx1 was due to its chaperone activity when treated with oxidants, and not via Daxx/ASK1 effects.

5.4.5 DJ-1 is upregulated due to expanded polyQ expression

DJ-1 has been shown to be primarily expressed under oxidative stress conditions in astrocytes (Lev et al., 2006). In contrast, Olzmann et al., (2007) showed that DJ-1 is also expressed in neurons within the substantia nigra pars compacta and striatum of human and non human primate brain. Given the polyQ aggregation modulating role of DJ-1 it was important to investigate whether the expression levels of DJ-1 changed during HD. To test this idea immunoblot analysis was performed to analyse the expression levels of DJ-1 in cell models, mouse models (R6/2) and the HD brain.

DJ-1 expression was upregulated in cell models (Figure 5.17), R6/2 cortex (Figure 5.19A and B) and HD cortical samples (Figure 5.21A and E) compared to control samples. Thus increased DJ-1 expression levels in mouse and HD cortex was not simply due to ageing, but was a response likely due to the presence of misfolded mhtt. In contrast, no change in expression levels was observed in R6/2 striatum (Figure 5.20), the normally most affected part of the brain in HD. However, this result needs to be interpreted with caution because only two samples were available for analysis. The cerebellum, a part of the brain that is not usually affected in HD, from both R6/2 animals and HD brains didn't show any change in DJ-1 expression levels compared to their control groups.

Browne et al., (1999) reviewed various HD patients studies that show elevated levels of oxidative damage to lipids, DNA and proteins of striatum and cortex and these are the brain regions that degenerate in HD as mentioned in the general introduction. The reason that upregulation of DJ-1 was observed in the cortex and not in the cerebellum (Figure 5.21) could be due to the presence of elevated levels of mhtt induced oxidative stress in the cortex compared to the cerebellum (Browne et al., 1999). It

seems that human and mouse cerebellum present stronger DJ-1 expression levels compared to cortex (Figure 5.19 and 5.21) that may provide protection against oxidative damage and limits additional upregulation of DJ-1. In addition to this, Bonafati et al., (2003b) suggested that DJ-1 is directly involved in the oxidative stress redox buffering and/or its modulation via transcriptional or post-transcriptional mechanisms. So far, it is unknown how DJ-1 is upregulated in the HD patients cortex (e.g., transcriptionally) and performing further experiments using QPCR may answer this question. It would also be useful to know whether there is a particular cell type in the cortex in which DJ-1 expression is increased (glial or neuronal cells). Using immunohistochemical approaches this question could be easily resolved.

The next set of experiments was to examine oxidative modification of DJ-1 in the HD brain in comparison to control brain. HD cortex and cerebellum was run on an SDS-PAGE and immunolabelled with a DJ-1 antibody specific for when oxidised at Cys106 (Ooe et al., 2006). This experiment showed that DJ-1 is more oxidised in the HD cortex (Figure 5.22A and E) compared to the control group (although a strong trend for increased oxidation also occurred in the cerebellum). This increase in oxidised DJ-1 was significant whereas no difference was detected in the cerebellum (Figure 5.22B and F) of HD patients as compared to the control group. The increase in oxidised DJ-1 in the HD brain is an interesting result. It is well established that over oxidized DJ-1 leads to a loss of function and this could also participate in mhtt induced aggregation and toxicity. However, apparently the Cys106 oxidation-sensitive DJ-1 antibody only detected the oxidised Cys106 residue in the brain samples whereas no immunoreactivity was observed when recombinant DJ-1 was treated with 2mM H_2O_2 (appendix 15). It is unclear whether H_2O_2 treatment was insufficient in oxidizing Cys106. If repeated, this experiment could suggest that the apparently oxidation-sensitive Cys106 DJ-1 antibody detects general DJ-1 protein oxidation rather than specific oxidised DJ-1 residue Cys106.

DJ-1 is more oxidised in the brain of other neurodegenerative disorders such as AD and PD (Blackinton et al., 2009a; Choi et al., 2006). In addition to this, DJ-1 levels have been reported to be elevated in the CSF and plasma of PD and ALS patients (see introduction) and hence elevated DJ-1 levels in HD patients' brains suggest that DJ-1

may well also be elevated in the CSF or plasma of HD patients. DJ-1 could, therefore, be validated as a potential biomarker for HD.

Based on the experiments and findings discussed above, it would be crucial to next examine whether knocking down DJ-1 (that appears to be induced due to polyQ stress) results in protection per se. This could be achieved by using RNAi approaches in the HD cell models described in Chapter 3. Eventually this could also be tested in DJ-1 knockout *Drosophila* or mouse models in order to confirm the role of DJ-1 in protein aggregation and toxicity in HD. These experiments would clarify whether endogenously induced DJ-1 is detrimental or not.

Based on the overexpression data presented in this chapter it is assumed that increased expression of DJ-1 is detrimental in the presence of mhttEx1 and the following working model of DJ-1 in HD is proposed (see Figure 5.23). Mhtt/httEx1 may directly interact with DJ-1 or regulate its expression levels transcriptionally and/or via post-transcriptional modifications leading to increased aggregation and toxicity. Loss of DJ-1 function may occur due to the complete oxidation of DJ-1 (Cys106-SO_3H) in the mitochondria and/or the cytoplasm of CNS cells in the HD brain and this may enhance mhtt/mhttEx1 aggregation and toxicity whereas partially oxidised DJ-1 (Cys106-SO_2H) could provide beneficial chaperone functions that reduce aggregation and toxicity and perhaps also afford protection to oxidative stress due to mhttEx1, especially needed in the ageing brain when chaperones are in decline generally, and oxidative stress increases (see Figure 5.23 legend for more detail).

However, an alternative hypothesis is that DJ-1 exerts an unknown activity, that is unlikely related to a chaperone function, in cells expressing httEx1Q97 that leads to an increase in mhtt aggregation followed by cellular toxicity (see above). It is known that even chaperone proteins are able to increase amyloid fibril formation (Tam et al., 2009) and/or IB formation (Wyttenbach et al., 2000). Hence, for example, DJ-1 Cys106-SO_2H could increase httEx 1 aggregation and upon exposure to H_2O_2 or Antimycin A DJ-1 may overoxidise to form Cys106-SO_3H which is an irreversible posttranslational modification that leads to a loss of DJ-1 function. The role of DJ-1 in mhtt aggregation seems to be complicated hence further investigation is clearly needed to identify how DJ-1 modulates mhtt aggregation. Thus, DJ-1 can be

considered as a therapeutic target molecule for HD for further exploration, both in the CNS and in the periphery.

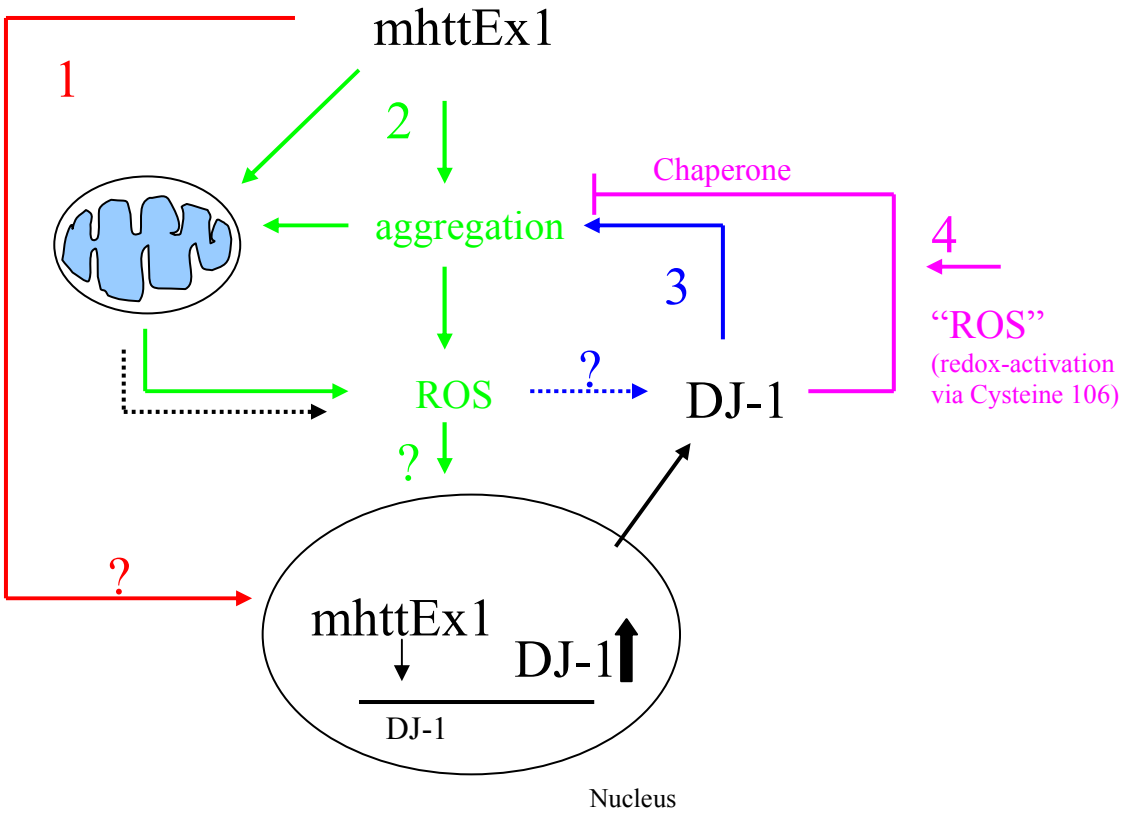

Figure 5.23 Proposed functional model of DJ-1 in HD.
(1) Red: mhttEx1 could induce DJ-1 transcriptionally. **(2)** Green: mhttEx1 acts directly on mitochondria leading to dysfunction (perhaps via an aggregation-mediated mechanism) resulting in ROS production. Chronically increased ROS production could then lead to DJ-1 induction and translocation to the cytoplasm and/or mitochondria where **(3)** (Blue) DJ-1 might suffer oxidative damage and lose its function (dotted blue arrow) which would then also contribute to ROS and cellular dysfunction and toxicity. DJ-1 is known to interact with mitochondrial complex I (Hayashi et al., 2009) and this complex is impaired in HD patients (Arenas et al., 1998) suggesting a potential role of DJ-1 in HD via this mechanism. **(4)** Pink: oxidative activation of DJ-1 at Cys106 (Cys106-SO_2H modification) activates DJ-1 as a redox chaperone, which reduces mhttEx1 aggregation and its associated toxicity. However, further oxidation of DJ-1 inactivates it (loss of function, Blue); perhaps this may be the case in the HD brain contributing to aggregation. DJ-1 could also contribute to aggregation as a non-oxidised protein in a complex with httEx1.

6 General Discussion

Abnormal redox homeostasis is thought to be a common pathology amongst most major neurodegenerative diseases such as AD, PD, ALS and HD, but the relationship between protein misfolding and ROS has yet to be elucidated. To this end, various cell systems such as HeLa, PC12 transient and inducible cell systems were used in this study to model intracellular protein aggregation associated with altered redox homeostasis by expressing httEx1 or a part of it with/out polyQ expansions and fused to fluorescent proteins. These HD cell systems showed polyQ length- and time dependant aggregation and toxicity over time (Chapter 3). In order to understand the role of polyQ expression/aggregation associated with impaired redox homeostasis and toxicity time-course experiments were performed. PolyQ aggregation was detectable well before toxicity occurred and this was observed in all cell systems (transient and inducible) (Chapter 3).

An early increase in ROS production was observed in HeLa and PC12 transient cell system as measured by two different oxidative sensitive probes (DHE, DCF). Inducible PC12 cell systems were also used to perform ROS assays. These cell systems also replicated early increases in ROS production due to polyQ expanded httEx1 as observed with transient cell systems (Chapter 4). Our study supports an existing hypothesis that early aggregation intermediates (monomers and oligomers) could be most toxic and are probably a source of ROS, something that remains to be tested. Our study needs to be repeated in primary cells, such as neurons, because their redox signalling regulation is different compared to immortalised cell lines. For instance, immortalised cell lines are known to be resistant against oxidative stress whereas primary cells undergo senescence when exposed to toxins that increase the production of ROS (Kondoh et al., 2005). Hence the ROS differences measured in cell lines could be an underestimation. Primary neurons have different redox signalling mechanisms compared to cell lines due to differences in their bioenergetics. For example, neurons are not very glycolytic because most of the brain glucose is taken up by the astrocytes and glycolytically metabolized into lactate or pyruvate and released into the extracellular space to be utilized by the neurons (Pellerin, 2005). On the other hand, immortalized cell lines are generally rather glycolytic. Wu et al., (2007) characterized the bioenergetic phenotype of two cancer cell lines and showed that their increased

glycolytic rate and capacity are linked to attenuated mitochondrial function. They suggested that metabolic alteration in tumour cells promotes their cell survival, growth, invasion and metastasis. In addition to this, Santamaria et al., (2006) showed that the H^+-ATP synthase inhibitor, staurosporine, enhances cell death by producing ROS in non-glycolytic cells that are dependant on oxidative phosphorylation for energy whereas no significant death was observed in glycolytic cells. The glycolytic cells responded to increased ROS by down-regulating H^+-ATP synthase which leads to oxidative phosphorylation and a blunted ROS production. Hence, clearly, the next logical step for examining the mechanistic relationship between intracellular aggregation and redox homeostasis is to use neurons followed by work *in vivo*. On the other hand, primary neurons freshly isolated from rodent brain are likely to undergo an oxidative stress response when exposed to 21% oxygen in an incubator (standard conditions) as opposed to the physiological partial pressure and oxygen concentration (ca. 3% oxygen) experienced *in vivo* (Guyton and Hall, 1996). Such a compensation could be a confounding factor for ROS analysis. However, primary neurons could be incubated under reduced oxygen conditions that may reflect more physiological levels of oxygen for analysis (Patel and Brewer, 2008).

PolyQ aggregation occurs mainly in postmitotic cells (e.g. neurons) in HD and in rodent models (reviewed in Perutz, 1999), but various other cell types in the CNS could also be dysfunctional, due to aggregation or not, and promote the production of ROS. It is unlikely that astrocytes are a primary source of ROS in HD as these glial cells are known to play major roles in the antioxidant defence in the CNS (Wilson, 1997) and are rather resistant to oxidative stress. Nevertheless, astrocytes have recently been shown to be defective in HD (Bradford et al., 2009; Faideau et al., 2010), and hence may contribute to redox-alterations in HD via impaired oxidative defence functions (e.g., through glutamate-related toxicity). Microglial cells are able to produce high levels of ROS (reviewed in Block et al., 2007) and in HD this could lead to damage of microglia itself or neurons. Indeed these cells have been proposed to play a role in ROS production due to polyQ toxicity via effects of an altered kynurenine pathway (Giorgini et al., 2005). Finally, oligodendrocytes have been shown to be highly sensitive to oxidative stress (Mronga et al., 2004), and perhaps to polyQ misfolding stress, but whether these cells could damage neurons directly or indirectly is unknown. Our study shows that cell-autonomous ROS production due to polyQ expanded httEx1 occurs and

therefore, in principle, any cells inside or even outside the CNS could be damaged or altered by such ROS. This does not exclude the possibility of non-cell autonomous free radical damage in HD.

A simple *in vivo* model to investigate the relationship between polyQ aggregation, ROS and toxicity would be to use either *Caenorhabditis elegans* or *Drosophila melanogaster* expressing httEx1, or only a fluorescent protein, with/out polyQ expansions. One possibility is to also use oxidation sensitive dyes in such animals, but another approach would be to produce transgenic animals expressing genetic ROS reporters (roGFP1, roGFP1-R12 and/or roGFP2) (Cannon and Remington, 2006; Hanson et al., 2004) and cross these with the polyQ animals. An elevated level of ROS due to the presence of an expanded polyQ stretch in progeny could then perhaps be quantified in real time by measuring the oxidation of these reporters. RoGFP1 and roGFP1-R12 are modified redox sensitive green fluorescent proteins, whereas roGFP2 is a redox sensitive and pH sensitive GFP. These genetic reporters could be further modified in such a manner as to target them to mitochondria or any other cellular compartment that would likely provide useful insight into the role of ROS during HD pathogenesis.

Having demonstrated the presence of an altered ROS homeostasis in cell models the next step was to start determining the origin of ROS (Chapter 4). Targeting of drugs directly to the site of ROS production might ameliorate their effects prior to the initiation of other cell death signalling pathways. The application of broad spectrum antioxidants can have side effects such as causing a reduction in the basal ROS required for various physiological processes as well as inhibiting autophagy, which is associated with increased protein aggregation and cell death (Underwood et al., 2010). In order to prove the principle of altered redox homeostasis, an experiment was performed that demonstrated that mhttEx1 induced ROS can be inhibited by antioxidants such as L-NAC and Trolox and that these compounds also reduce cell death (Chapter 3 and 4). In addition to this the mitochondrial specific ROS scavenger, MitoQ, suppressed the early increase in ROS seen in the studied httEx1 cell models. This makes it likely that mhttEx1 induced ROS originates in the mitochondria. This is consistent with animal models of HD and patient studies that show oxidative damage to the mitochondria (cevedo-Torres et al., 2009; Polidori et al., 1999).

Since MitoQ has been hypothesized to enter other cellular compartments (Michael Duchen, University College London, personal communication), it is important to test for other possible sources of ROS. This could also be further studied by the use of inhibitors of enzymes such as NADPH oxidase (inhibited by apocynin) and xanthine oxidase (inhibited by oxypurinol) which could be involved in the production of ROS. As discussed in Chapter 4, under normal circumstances mitochondria exist in a fused state and mitochondrial fission is one indication of oxidative stress. MhttEx1 has been shown to interfere with mitochondrial functional states and cause mitochondrial fragmentation which is thought to be associated with oxidative stress and reduced ATP levels (Lee et al., 2007; Pletjushkina et al., 2006; Wang et al., 2009) and hence exploration of ROS production and mitochondrial fusion/fission events is a further relevant avenue for investigation.

Another way of confirming the source or sources of ROS would be to use mitochondrial DNA depleted cells (Rho cells). These cells are unable to carry out normal mitochondrial ETC or ATP synthesis and their survival and growth is entirely dependant upon ATP generated by anaerobic glycolysis (King and Attardi, 1989; King and Attardi, 1996). Chandel and Schumacker (1999) stated that these cells are unable to produce mitochondrial superoxide and do not have the impaired signalling processes associated with mitochondrial ROS. Hence overexpression of mhttEx1 in these cells would be a promising approach of finding any other cellular sources of ROS, or confirm a mitochondrial origin of ROS due to mhttEx1 expression.

Impairment of intracellular redox homeostasis seems to be central to HD pathology. Hence various antioxidants, such as Coenzyme Q10 (CoQ10), vitamin E and creatine, have been considered as potential HD ameliorating drugs (reviewed in Mancuso et al., 2010). CoQ10 and vitamin E treatment in the 3-NP rat model of HD has been shown to reduce creatine kinase (CK), a marker for brain energy metabolism dysfunction, but it seems that the protective activity of both of these compounds was limited to the cytoplasm and hence they were perhaps unable to prevent the inhibition of ETC function (Kasparova et al., 2006). At the same time another study by Smith and colleagues showed that R6/2 mice treated with CoQ10 had significantly improved life span, motor function, and reduced weight loss, brain atrophy and IBs (Smith et al., 2006). Similar results were also reported when CoQ10 was used in combination with

minocycline (an antibiotic that possesses anti-apoptotic activity) in R6/2 mice (Stack et al., 2006). Although CoQ10 was successful in animal models of HD, only a modest total functional improvement was observed in HD patients (Huntington Study Group, 2001). More recently, Yang et al., (2009) reported that CoQ10 combined with creatine (1:2 ratios) provided additional neuroprotective effects against 3-NP induced impairment of glutathione reduction and oxidative damage to lipids, DNA and protein in the striatum of 3-NP treated rats. Furthermore, CoQ10 and creatine treatment was also more effective than the application of either alone in improving motor function and life span of R6/2 mice (Yang et al., 2009). The reason that the combination of CoQ10 and creatine has such potent neuroprotective effects may well be because they work in different ways, or perhaps act on multiple sources/mechanisms of redox-regulation. Creatine is known to play a role during energy buffering between mitochondria and the cytoplasm and CoQ10 allows efficient transfer of electrons from complex I to II of the ETC. This drug combination is currently in phase III HD clinical trials (Yang et al., 2009).

There are a number of stress proteins that are up-regulated under oxidative stress conditions providing protection against oxidative damage (see general introduction). DJ-1 is one of them and loss of its function has been shown to be associated with PD. The initial hypothesis of Chapter 5 was that the overexpression of DJ-1, given its role as a redox-induced chaperone, would reduce IB formation and toxicity. However, DJ-1 overexpression in HeLa cells and astrocytes enhanced mhttEx1 IBs and toxicity whereas exposure of cells to H_2O_2 or Antimycin A resulted in reduced IBs and toxicity in both HeLa and astrocytes. As mentioned in the general introduction, DJ-1 posses three reactive cysteines (Cys46, 53 and 106), but Cys106 appears to be the key residue regulating oxidative stress induced chaperone function (see Chapter 1 and 5). Although we did not show biochemically that cysteines in DJ-1 were oxidised after oxidant exposure within cells, we confirmed the redox activatable chaperone capacity of DJ-1 on polyQ aggregation and toxicity via the use of the cysteine mutant (C106S-DJ-1). When overexpressed in HD cell models C106S-DJ-1 appeared to have diminished chaperone activity and worsened the IB formation and toxicity (Chapter 5).

In addition to this, the endogenous cellular levels of DJ-1 were also studied in various cell models, the R6/2 mouse CNS and HD patients brains and all of these consistently

showed enhanced DJ-1 expression (Chapter 5). These results were not surprising as plenty of evidence exist that shows oxidative damage in HD animal models and patient brains (reviewed in Browne et al., 1999), and hence DJ-1 up-regulation as an anti-oxidant defence mechanism may be expected. Interestingly, Western blot analysis of HD patient brains showed significantly higher immunolabelling for oxidized DJ-1 compared to control brains. As mentioned in the discussion of Chapter 5 this antibody may well have detected oxidatively damaged DJ-1 protein. Zhou et al., (2006) reported that the complete oxidation of Cys106 inactivates DJ-1 by losing its secondary structures. Hence in the HD brain DJ-1 may not only be induced and have detrimental effects, but also inactivated to some extent and hence result in a loss of some of its functions with negative impact. For example, Krebiehl et al., (2010) showed that the loss of DJ-1 function is associated with various mitochondrial dysfunctions such as impaired mitochondrial membrane potential, respiration, increased mitochondrial ROS as well as impaired mitochondrial functional states (increased mitochondrial fission). These events have all been reported to be associated with HD (see general introduction). Furthermore, these authors also showed that cells lacking DJ-1 also presented with a decrease in the degradation of impaired or aged mitochondria which then lead to an increase in mitochondrial mass as well as reduced lysosomal activity and basal autophagy levels (Krebiehl et al., 2010), again factors that are implicated in HD. Finally, Hayashi and colleagues demonstrated that DJ-1 binds directly to the nuclear (NDUFA4) and mitochondrial (ND1) subunits of complex I especially under oxidative stress conditions (Hayashi et al., 2009). They suggested that DJ-1 binds to complex I, whereas mutant DJ-1 reduced this binding and may hence participate in PD disease pathogenesis.

Several studies have observed the impairment of mitochondrial complex I activity in the platelets, muscles tissues and brain tissues of HD patients (Arenas et al., 1998; Parker, Jr. et al., 1990). The above-mentioned role of DJ-1 in mitochondrial function and the results obtained from HD brain samples (Chapter 5) suggest that oxidative stress perhaps due to misfolded htt may lead to oxidatively damaged DJ-1. Over-oxidized DJ-1 loses its function and may cause it to lose its interaction with complex I leading to an impairment in complex I which could then result in further ROS production, impaired mitochondrial functional states and energy metabolism deficits. Mitochondrial complex I activity is also altered in AD (Manczak et al., 2004), ALS

(Rizzardini et al., 2006) and PD (reviewed in Dawson and Dawson, 2003). DJ-1 seems to have a common role in all of the above-mentioned diseases where it has been shown to be up-regulated in CSF and/or blood (Waragai et al., 2006; Waragai et al., 2007; Yamashita et al., 2010). DJ-1 actions on complex I function could prove a common mechanism that is altered during chronic neurodegeneration. It would also be useful to examine the levels of DJ-1 in HD patient blood or CSF because it could potentially be used as a biomarker for HD.

If DJ-1 oxidation is altered in HD, a promising avenue is to explore the role of DJ-1 modulating drugs. Miyazaki et al., (2008) performed an *in silico* virtual screen and identified compounds (UCP0045037 and UCP0054278) that bind to the Cys106 region of the reduced form (C106-SH) and partially oxidised (Cys106-SOH/SO_2H) forms of DJ-1, respectively. These compounds are well characterised and have been shown to prevent the complete oxidation of Cys106 (Cys106 SO_3H). These drugs prevent a functional loss of DJ-1 by stabilising the reduced form of DJ-1 or by mimicking partially oxidised (Cys106 SOH/SO_2H) DJ-1 (Miyazaki et al., 2008; Yamane et al., 2009). These compounds have been shown to inhibit ROS production and provide protection against oxidative stress induced cell death in SH-SY5Y cells, stem cell derived dopaminergic cells and also in primary neuronal culture (Miyazaki et al., 2008). These compounds were also reported to restore impaired mitochondrial complex I as well as tyrosine hydroxylase activities that were compromised due to oxidative stress (Miyazaki et al., 2008). Strikingly, these compounds have the capacity to pass through the blood brain barrier and have been demonstrated to protect against dopaminergic cell death in the substantia nigra of a 6-hydroxydopamine injected rat model of PD (Miyazaki et al., 2008). Considering the potential of these compounds against oxidative stress and their ability to restore mitochondrial complex I activity in cell models and a rat model of PD they are attractive potential HD drugs, and one such compound (UCP0045037) is currently under investigation in the Wyttenbach lab.

Ageing and many neurodegenerative diseases share some common mechanisms such as impaired mitochondrial function associated with elevated ROS levels and malfunctioning protein degradation pathways leading to the accumulation of oxidised protein under physiological conditions and enhanced cellular toxicity (reviewed in Hands et al., 2009; Lin and Beal, 2006). As mentioned in the general introduction, the

pharmacological induction of autophagy enhances mhtt degradation and provides neuroprotection in animal models of HD (Bauer et al., 2010; Ravikumar and Rubinsztein, 2006). In addition to this, Simonsen et al., (2008) reported that autophagy-related 8a (Atg-8a) gene overexpression in the aged *Drosophila* brain increased life span as well as resistance against oxidative stress and accumulation of ubiquitinated and oxidised proteins. Hands and colleagues (2009) also suggested that altered autophagy may be a source of ROS that could participate in cellular damage, due to its age dependant reduction in activity and accumulation of damaged cellular organelles particularly mitochondria. Thus, it could be suggested that the induction of autophagy provides protection against oxidative damage. Therefore, the use of mTOR (a negative regulator of autophagy) inhibitors could be another potential avenue for HD therapy impacting on the redox homeostasis.

Given the many possibilities of redox-alterations in HD it will not be straightforward to determine which mechanisms should be targeted for therapy. What is increasingly clear however, is that the misfolding and aggregation process in HD is toxic and could be directly involved in the production of free radicals, with the help of metal ions such as iron or copper, both elevated in the HD brain (Hands et al., 2010b). Therefore, targeting the aggregation process itself may be a valid approach to correct an abnormal redox homeostasis in HD. But indirect effects of htt/httEx1 on mitochondrial functions and autophagy to increase ROS are equally important mechanisms to evaluate. Finally, the use of antioxidants is being considered and tested for HD therapy to delay the disease onset. Here it is proposed that the chemical or genetic manipulation of redox sensitive chaperones such as DJ-1 can also be considered as an attractive therapeutic option due to the nature of this protein (chaperone and antioxidant) (Sajjad et al., 2010). Given that both in PD and HD intracellular aggregation is associated with an upregulation of DJ-1 levels and a possible eventual functional loss of DJ-1, it would also be interesting to explore whether there are common downstream targets regulated by DJ-1 that could impact on disease progression and hence constitute further therapeutic targets to combat these devastating diseases, especially HD for which there is no cure available.

Appendices

Appendix 1

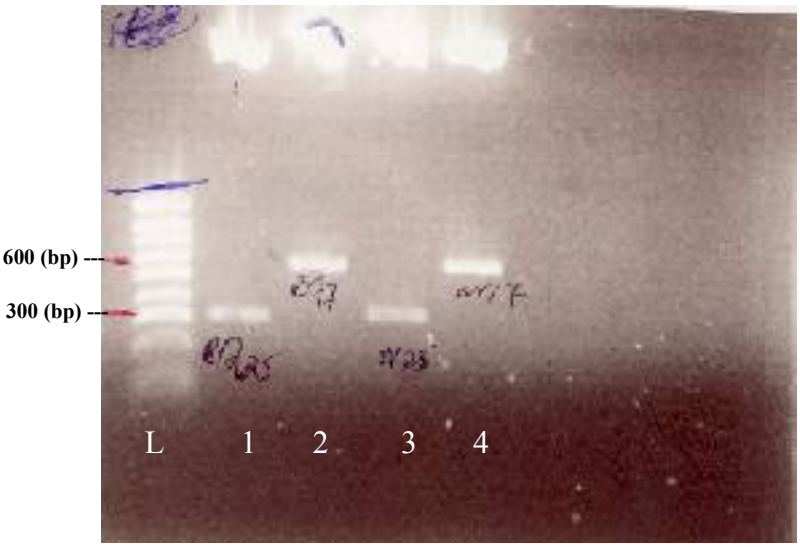

Figure A1. Restriction digest of httEx1Q25/Q97-EGFP/mRFP.

L: Hyper ladder IV
1: HttEx1Q25-EGFP
2: HttEx1Q97-EGFP
3: HttEx1Q25-mRFP
4: HttEx1Q97-mRFP

Appendix 2

Table A1. Sequences of various constructs used. Start codons are indicated as ATG* (red) and stop codon are shown as TGA* or TAG* (blue). DJ-1 Cys106 point mutation to Serine is higlighted as yellow. HttEx1 constructs with various CAA/CAG repeat lengths (Bold) show only start codon and Exon1 which is attached to EGFP/mRFP.

Constructs	Sequence
DJ-1	ATAGCAGAGCTCTCTGGCTAACTAGAGAACCCACTGCTTACTGGCTTATCGAAATTAATA CGACTCACTATAGGGAGACCCAAGCTGGCTAGTTAAGCTTGGTACCGAGCTCGGATCCAC TAGTCCAGTGTGGTGGAATTCACC**ATG***GCTTCCAAAAGAGCTCTGGTCATCCTGGCTAAA GGAGCAGAGGAAATGGAGACGGTCATCCCTGTAGATGTCATGAGGCGAGCTGGGATTAAG GTCACCGTTGCAGGCCTGGCTGGAAAAGACCCAGTACAGTGTAGCCGTGATGTGGTCATTT GTCCTGATGCCAGCCTTGAAGATGCAAAAAAAGAGGGACCATATGATGTGGTGGTTCTACC AGGAGGTAATCTGGGCGCACAGAATTTATCTGAGTCTGCTGCTGTGAAGGAGATACTGAAG GAGCAGGAAAACCGGAAGGGCCTGATAGCCGCCATCTGTGCAGGTCCTACTGCTCTGTTGG CTCATGAAATAGGTTTTGGAAGTAAAGTTACAACACACCCTCTTGCTAAAGACAAAATGATG AATGGAGGTCATTACACCTACTCTGAGAATCGTGTGGAAAAAGACGGCCTGATTCTTACAA GCCGGGGGCCTGGGACCAGCTTCGAGTTTGCGCTTGCAATTGTTGAAGCCCTGAATGGCAAG GAGGTGGCGGCTCAAGTGAAGGCTCCACTTGTTCTTAAAGACTCTAGAGGGCCCTTCGAACA AAAACTCATCTCAGAAGAGGATCTGAATATGCATACCGGTCATCATCACCATCACCAT**TGA***G TTTAAACCCGCTGATCAGCCTCGACTGTGCCTTCTAGTTGCCAGCCATCTGTTGTTTGCCCCTC CCCCGTGCCTTCCTTGACCCTGGAAGGTGCCACTCCCACTGTCCTTTCCTAATAAAA
C106S-DJ-1	ATAGCAGAGCTCTCTGGCTAACTAGAGAACCCACTGCTTACTGGCTTATCGAAATTAATA CGACTCACTATAGGGAGACCCAAGCTGGCTAGCACCATGGACTACAAAGACCATGACGGT GATTATAAAGATCATGACATCGATTACAAGGATGACGATGACAAGCTTGGATCCGAATTC **ATG***GCTTCCAAAAGAGCTCTGGTCATCCTGGCTAAAGGAGCAGAGGAAATGGAGACGGTC ATCCCTGTAGACGTCATGAGGCGAGCTGGGATTAAGGTCACCGTTGCAGGCCTGGCTGGA AAAGACCCAGTACAGTGTAGCCGTGATGTGGTCATTTGTCCTGATGCCAGCCTTGAAGAT GCAAAAAAAGAGGGACCATATGATGTGGTGGTTCTACCAGGAGGTAATCTGGGCGCACAG AATTTATCTGAGTCTGCTGCTGTGAAGGAGATACTGAAGGAGCAGGAAAACCGGAAGGGC CTGATAGCCGCCATCTCTGCAGGTCCTACTGCTCTGTTGGCTCATGAAATAGGTTTTGGA AGTAAAGTTACAACACACCCTCTTGCTAAAGACAAAATGATGAATGGAGGTCATTACACC TACTCTGAGAATCGTGTGGAAAAAGACGGCCTGATTCTTACAAGCCGGGGGCCTGGGACC AGCTTCGAGTTTGCGCTTGCAATTGTTGAAGCCCTGAATGGCAAGGAGGTGGCGGCTCAA GTGAAGGCTCCACTTGTTCTTAAAGAC**TAG***AGCAGCGAACTGCGACGATCACTTAGAGAA ACAGGCCGTTAGGAATCCATTCTCACTGTGTTCGCTCTAAACAAAACAGTGGTAGGTT
HttEx1Q25-mRFP	ATAGCAGAGCTCTCTGGCTAACTAGAGAACCCACTGCTTACTGGCTTATCGAAATTAATA CGACTCACTATAGGGAGACCCAAGCTGGCTAGTTAAGCTTGGTACCGGGCCCCCCCTCGA GGTCGACCGCC**ATG***GCGACCCTGGAAAAGCTGATGAAGGCCTTCGAGTCCCTCAAAAGCT TC**CAACAGCAGCAACAGCAACAACAGCAGCAACAGCAACAACAGCAGCAACAGCAACAA CAGCAGCAACAGCAACAA**CCGCCACCACCTCCCCCTCCACCCCCACCTCCTCAACTTCCTC AACCTCCTCCACAGGCACAGCCTCTGCTGCCTCAGCCACAACCTCCTCCACCTCCACCTC CACCTCCTCCAGGCCCAGCTGTGGCTGAGGAGCCTCTGCACCGACC…**mRFP**
HttEx1Q72-mRFP	ACTGCTTACTGGCTTATCGAAATTAATACGACTCACTATAGGGAGACCCAAGCTGGCTAG TTAAGCTTGGTACCGGGCCCCCCCTCGATCGAGGTCGACCGCC**ATG***GCGACCCTGGAAAA GCTGATGAAGGCCTTCGAGTCCCTCAAAAGCTTC**CAACAGCAGCAACAGCAACAACAGCA GCAACAGCAACAACAGCAGCAACAGCAACAACAGCAGCAACAACAGCAGCAACAGCAAC AACAGCAGCAACAGCAACAACAGCAGCAGCAGCAACAACAGCAGCAACAGCAACAACAAC AGCAGCAACAGCAACAACAGCAGCAACAGCAACAACAGCAGCAACAGCAACAACAGCAGC AACAGCAACAA**CCGCCACCACCTCCCCCTCCACCCCCACCTCCTCAACTTCCTCAACCTCCTC CACAGGCACAGCCTCTGCTGCCTCAGCCACAACCTCCTCCACCTCCACCTCCACCTCCTCCAG GCCCAGCTGTGGCTGAGGAGCCTCTGCACCGACC…**mRFP**
HttEx1Q97-mRFP	ATAGCAGAGCTCTCTGGCTACTAGAGAACCCACTGCTTACTGGCTTATCGAAATTAATAC GACTCACTATAGGGAGACCCAAGCTGGCTAGTTAAGCTTGGTACCGGGCCCCCCCTCGAG GTCGACCGCC**ATG***GCGACCCTGGAAAAGCTGATGAAGGCCTTCGAGTCCCTCAAAAGCTT C**CAACAGCAGCAACAGCAACAACAGCAGCAACAGCAACAACAGCAGCAACAGCAACAACA GCAGCAACAGCAACAACAGCAGCAACAGCAACAACAGCAGCAACAGCAACAACAGCAGCA ACAGCAACAACAGCAGCAACAGCAACAACAGCAGCAACAGCAACAACAGCAGCAACAGCA ACAACAGCAGCAACAGCAACAACAGCAGCAACAGCAACAACAGCAGCAACAGCAACAACA GCAGCAACAGCAACAACAGCAGCAACAGCAACAACAGCAGCAACAGCAACAA**CCGCCACC ACCTCCCCTCCACCCCACCTCCTCAACTTCCTCAACCTCCTCCACAGGCACAGCCTCTGCTGCCT CAGCCACAACCTCCTCCACCTCCACCTCCACCTCCTCCAGGCCCAGCTGTGGCTGAGGAGCCTCT GCACCGACC…**mRFP**

HttEx1Q25-EGFP	ATAGCAGAGCTCTCTGGCTAACTAGAGAACCCACTGCTTACTGGCTTATCGAAATTAATA CGACTCACTATAGGGAGACCCAAGCTGGCTAGTTAAGCTTGGTACCGGGCCCCCCCTCGA GGTCGACCGCC**ATG***GCGACCCTGGAAAAGCTGATGAAGGCCTTCGAGTCCCTCAAAAGCT TC**CAACAGCAGCAACAGCAACAACAGCAGCAACAGCAACAACAGCAGCAACAGCAACAA CAGCAGCAACAGCAACAA**CCGCCACCACCTCCCCCTCCACCCCCACCTCCTCAACTTCCTC AACCTCCTCCACAGGCACAGCCTCTGCTGCCTCAGCCACAACCTCCTCCACCTCCACCTC CACCTCCTCCAGGCCCAGCTGTGGCTGAGGAGCCTCTGCACCGACC…**EGFP**
HttEx1Q72-EGFP	ACTGCTTACTGGCTTATCGAAATTAATACGACTCACTATAGGGAGACCCAAGCTGGCTAG TTAAGCTTGGTACCGGGCCCCCCCTCGATCGAGGTCGACCGCC**ATG***GCGACCCTGGAAAA GCTGATGAAGGCCTTCGAGTCCCTCAAAAGCTTC**CAACAGCAGCAACAGCAACAACAGCA GCAACAGCAACAACAGCAGCAACAGCAACAACAGCAGCAACAACAGCAGCAACAGCAACA ACAGCAGCAACAGCAACAACAGCAGCAGCAGCAACAACAGCAGCAACAGCAACAACAACA GCAGCAACAGCAACAACAGCAGCAACAGCAACAACAGCAGCAACAGCAACAACAGCAGCA ACAGCAACAA**CCGCCACCACCTCCCCCTCCACCCCCACCTCCTCAACTTCCTCAACCTCCTCCAC AGGCACAGCCTCTGCTGCCTCAGCCACAACCTCCTCCACCTCCACCTCCACCTCCTCCAGGCCC AGCTGTGGCTGAGGAGCCTCTGCACCGACC…**EGFP**
HttEX1Q97-EGFP	ATAGCAGAGCTCTCTGGCTAACTAGAGAACCCACTGCTTACTGGCTTATCGAAATTAATA CGACTCACTATAGGGAGACCCAAGCTGGCTAGTTAAGCTTGGTACCGGGCCCCCCCTCGA GGTCGACCGCC**ATG***GCGACCCTGGAAAAGCTGATGAAGGCCTTCGAGTCCCTCAAAAGCT TC**CAACAGCAGCAACAGCAACAACAGCAGCAACAGCAACAACAGCAGCAACAGCAACAAC AGCAGCAACAGCAACAACAGCAGCAACAGCAACAACAGCAGCAACAGCAACAACAGCAGC AACAGCAACAACAGCAGCAACAGCAACAACAGCAGCAACAGCAACAACAGCAGCAACAGC AACAACAGCAGCAACAGCAACAACAGCAGCAACAGCAACAACAGCAGCAACAGCAACAAC AGCAGCAACAGCAACAACAGCAGCAACAGCAACAACAGCAGCAACAGCAACAA**CCGCCAC CACCTCCCCCTCCACCCCCACCTCCTCAACTTCCTCAACCTCCTCCACAGGCACAGCCTCTGCTG CCTCAGCCACAACCTCCTCCACCTCCACCTCCACCTCCTCCAGGCCCAGCTGTGGCTGAGGAGCC TCTGCACCGACC…**EGFP**

Appendix 3

Table A2. Computer Language "R" code used for cumulative frequency distribution analysis of oxidation of redox sensitive dyes.

```
### ~~~~~ GENERAL SETUP ~~~~~ ###
# rm(list=ls(all=TRUE))       # This removes ALL current objects
source("rje_col.r")    # This loads basic Southampton Colours
colTest()                     # This shows the colours of soton$col and their indices

## ~ Setup colours to be used in plots ~ ##
ucol = list(All=soton$col[21], Day1=soton$col[2], Day2=soton$col[3], Day3=soton$col[5],
Green=soton$col[18], Red=soton$col[15], Q25=soton$col[1], Q97=soton$col[5])
for(i in 1:6){ ucol[[paste("DCF",i,sep="")]] = soton$col[i*2] }
## Plot colours ##
plot(0:1,0:1,type="n",axes=FALSE,ann=FALSE,mar=c(0.1,0.5,0.5,0.1))
x = 1.0 / length(soton$col)
for (i in 1:length(soton$col)){
       rect((i-1)*x,0.5,i*x,1,col=soton$col[i])
      text((i-0.5)*x,0.75,i,adj=c(0.5,0.5),font=2)#,col=soton$col[17],cex=2)
}
x = 1.0 / length(ucol)
i = 1
for (u in names(ucol)){
       rect((i-1)*x,0,i*x,0.5,col=ucol[[u]])
       text((i-0.5)*x,0.25,u,adj=c(0.5,0.5),srt=-90)
       i = i + 1
}
rm(list=c("x","i"))


### ~~~~~ LOAD AND TIDY DATA ~~~~~ ###
umar = read.table("umar.tdt",sep="\t",header=TRUE)
summary(umar)  # Summarise Umar data
dim(umar)             # Returns the number of rows & cols as vector

## ~ Correct dodgy Day data ~ ##
for (i in 1:nrow(umar)){             # Each row in turn
       if (umar$Time[i] == " Day1"){ umar$Time[i] = "Day1" }
       if (umar$Time[i] == " Day2"){ umar$Time[i] = "Day2" }
}
umar$Time = factor(umar$Time,levels=c("Day1","Day2","Day3"))
summary(umar)

## ~ Create "wide" data table with "Red" and "Green" paired columns ~ #
wideumar = reshape(umar, direction="wide", idvar=c("Experiment","Time","CellType","ID"),
timevar="Colour")
summary(wideumar)


### ~~~~~ DEFINE FUNCTIONS ~~~~~ ###
reducedData = function(fulldata,experiment="All",celltype="All",time="All",colour="All"){
       if(experiment != "All"){ fulldata = fulldata[fulldata$Experiment == experiment,] }
       if(celltype != "All"){ fulldata = fulldata[fulldata$CellType == celltype,] }
       if(time != "All"){ fulldata = fulldata[fulldata$Time == time,] }
       if(colour != "All"){ fulldata = fulldata[fulldata$Colour == colour,] }
       return(fulldata)
}

timePlot = function(fulldata,experiment="All",celltype="All",colour="All"){
       ## Get Data ##
       breaks = c(0:51 * 5)
       xdata = c(1:51 *5) - 2.5
       xdata = c(0,xdata,255)
       pdata =
list(all=hist(reducedData(fulldata,experiment,celltype,colour=colour)$Intensity,breaks=break
s,plot=FALSE)$counts)
       for(time in c("Day1","Day2","Day3")){
              pdata[[time]] =
hist(reducedData(fulldata,experiment,celltype,time,colour)$Intensity,breaks=breaks,plot=FALS
E)$counts
       }
```

```
        ## Adjust data to Freqs ##
        ymax = 0.0
        for(i in 1:length(pdata)){
                if(sum(pdata[[i]]) > 0){
                        pdata[[i]] = c(0,pdata[[i]],0) / sum(pdata[[i]])
                        ymax = max(c(ymax,pdata[[i]]))
                }else{
                        pdata[[i]] = rep(NA,length(xdata))
                }
        }
        ## Setup Plot ##
        ltypes = c("dotted","solid","solid","solid")
        ltimes = c("All","Day1","Day2","Day3")
        ltitle = paste("Time Plot for ",experiment,"-",celltype," (",colour,")",sep="")
        plot(c(0,255),c(0,ymax),type="n",main=ltitle,xlab="Intensity",ylab="Frequency")
        for(i in 1:length(pdata)){
                time = ltimes[i]
                lines(xdata,pdata[[i]],col=ucol[[time]],lwd=2,lty=ltypes[i])
                ypos = ymax - ((ymax/15.0) * (i - 1))
                text(200,ypos,time,adj=c(1,0.5))
                lines(c(210,250),c(ypos,ypos),col=ucol[[time]],lwd=2,lty=ltypes[i])
        }
}
timePlot(umar)

timePlotCumFreq = function(fulldata,experiment="All",celltype="All",colour="All"){
        ## Get Data ##
        breaks = c(0:51 * 5)
        xdata = c(1:51 *5) - 2.5
        pdata =
list(all=sort(reducedData(fulldata,experiment,celltype,colour=colour)$Intensity))
        cdata = list(all=c(0:length(pdata$all))*100.0/length(pdata$all))
        for(time in c("Day1","Day2","Day3")){
                pdata[[time]] =
sort(reducedData(fulldata,experiment,celltype,time,colour)$Intensity)
                cdata[[time]] = c(0:length(pdata[[time]]))*100.0/length(pdata[[time]])
        }
        ## Adjust data to Freqs ##
        ymax = 100.0
        ## Setup Plot ##
        ltypes = c("dotted","solid","solid","solid")
        ltimes = c("All","Day1","Day2","Day3")
        ltitle = paste("Time Plot for ",experiment,"-",celltype," (",colour,")",sep="")
        plot(c(0,255),c(0,ymax),type="n",main=ltitle,xlab="Intensity",ylab="Cum. Freq.")
        for(i in 1:length(pdata)){
                time = ltimes[i]
                lines(c(0,pdata[[i]]),cdata[[i]],col=ucol[[time]],lwd=2,lty=ltypes[i])
                ypos = ymax/3.0 - ((ymax/15.0) * (i - 1))
                text(200,ypos,time,adj=c(1,0.5))
                lines(c(210,250),c(ypos,ypos),col=ucol[[time]],lwd=2,lty=ltypes[i])
        }
}
#timePlotCumFreq(umar)


cellComp = function(fulldata,experiment="All",time="All",colour="All"){
        ## Get Data ##
        breaks = c(0:51 * 5)
        xdata = c(1:51 *5) - 2.5
        xdata = c(0,xdata,255)
        pdata =
list(all=hist(reducedData(fulldata,experiment,time=time,colour=colour)$Intensity,breaks=brea
ks,plot=FALSE)$counts)
        for(celltype in c("Q25","Q97")){
                pdata[[celltype]] =
hist(reducedData(fulldata,experiment,celltype,time,colour)$Intensity,breaks=breaks,plot=FALS
E)$counts
        }
        ## Adjust data to Freqs ##
        ymax = 0.0
        for(i in 1:length(pdata)){
                if(sum(pdata[[i]]) > 0){
                        pdata[[i]] = c(0,pdata[[i]],0) / sum(pdata[[i]])
                        ymax = max(c(ymax,pdata[[i]]))
                }else{
                        pdata[[i]] = rep(NA,length(xdata))
```

```
                }
        }
        ## Setup Plot ##
        ltypes = c("dotted","solid","solid")
        lcells = c("All","Q25","Q97")
        ltitle = paste("Cell Plot for ",experiment,"-",time," (",colour,")",sep="")
        plot(c(0,255),c(0,ymax),type="n",main=ltitle,xlab="Intensity",ylab="Frequency")
        for(i in 1:length(pdata)){
                celltype = lcells[i]
                lines(xdata,pdata[[i]],col=ucol[[celltype]],lwd=2,lty=ltypes[i])
                ypos = ymax - ((ymax/15.0) * (i - 1))
                text(200,ypos,celltype,adj=c(1,0.5))
                lines(c(210,250),c(ypos,ypos),col=ucol[[celltype]],lwd=2,lty=ltypes[i])
        }
}
#cellComp(umar)

cellCompCumFreq = function(fulldata,experiment="All",time="All",colour="All"){
        ## Get Data ##
        breaks = c(0:51 * 5)
        xdata = c(1:51 *5) - 2.5
        pdata =
list(all=sort(reducedData(fulldata,experiment,time=time,colour=colour)$Intensity))
        cdata = list(all=c(0:length(pdata$all))*100.0/length(pdata$all))
        for(celltype in c("Q25","Q97")){
                pdata[[celltype]] =
sort(reducedData(fulldata,experiment,celltype,time,colour)$Intensity)
                cdata[[celltype]] =
c(0:length(pdata[[celltype]]))*100.0/length(pdata[[celltype]])
        }
        ## Adjust data to Freqs ##
        ymax = 100.0
        ## Setup Plot ##
        ltypes = c("dotted","solid","solid")
        lcells = c("All","Q25","Q97")
        ltitle = paste("Cell Plot for ",experiment,"-",time," (",colour,")",sep="")
        plot(c(0,255),c(0,ymax),type="n",main=ltitle,xlab="Intensity",ylab="Cum. Freq.")
        for(i in 1:length(pdata)){
                celltype = lcells[i]
                lines(c(0,pdata[[i]]),cdata[[i]],col=ucol[[celltype]],lwd=2,lty=ltypes[i])
                ypos = ymax/3.0 - ((ymax/15.0) * (i - 1))
                text(200,ypos,celltype,adj=c(1,0.5))
                lines(c(210,250),c(ypos,ypos),col=ucol[[celltype]],lwd=2,lty=ltypes[i])
        }
}
#cellCompCumFreq(umar)

singleExpt = function(experiment,celltype){
        layout(matrix(c(1,1,2,3,1,1,4,5),byrow=TRUE,nrow=2))
        ## Red/Green Correlation ##
        cdata = reducedData(wideumar,experiment,celltype)
        plot(c(0,255),c(0,max(cdata$Intensity.Green)),xlab="Red",ylab="Green",type="n",main=p
aste(experiment,celltype))
        for(time in c("Day1","Day2","Day3")){

        points(cdata$Intensity.Red[cdata$Time==time],cdata$Intensity.Green[cdata$Time==time],
col=ucol[[time]],pch=19)
                ulm = try(lm(Intensity.Green ~ Intensity.Red,cdata[cdata$Time==time,]),
silent=TRUE)
                try(abline(ulm,col=ucol[[time]]), silent=TRUE)
        }
        #!# Add linear correlation #!#
        ## Red/Green histogram plots ##
        breaks = c(0:51 * 5)
        xdata = c(1:51 *5) - 2.5
        gdata =
list(all=hist(reducedData(umar,experiment,celltype,colour="Green")$Intensity,breaks=breaks,p
lot=FALSE)$counts)
        rdata =
list(all=hist(reducedData(umar,experiment,celltype,colour="Red")$Intensity,breaks=breaks,plo
t=FALSE)$counts)
        for(time in c("Day1","Day2","Day3")){
                gdata[[time]] =
hist(reducedData(umar,experiment,celltype,time,colour="Green")$Intensity,breaks=breaks,plot=
FALSE)$counts
                rdata[[time]] =
```

```
hist(reducedData(umar,experiment,celltype,time,colour="Red")$Intensity,breaks=breaks,plot=FA
LSE)$counts
        }
        ## Adjust data to Freqs ##
        ymax = 0.0
        for(i in 1:length(gdata)){
                if(sum(gdata[[i]]) > 0){
                        gdata[[i]] = c(0,gdata[[i]],0) / sum(gdata[[i]])
                        ymax = max(c(ymax,gdata[[i]]))
                }else{ gdata[[i]] = rep(NA,length(xdata)) }
                if(sum(rdata[[i]]) > 0){
                        rdata[[i]] = c(0,rdata[[i]],0) / sum(rdata[[i]])
                        ymax = max(c(ymax,rdata[[i]]))
                }else{ rdata[[i]] = rep(NA,length(xdata)) }
        }
        ## Setup Plot ##
        ltimes = c("All","Day1","Day2","Day3")
        for(i in 1:length(gdata)){

        plot(c(0,255),c(0,ymax),type="n",main=ltimes[i],xlab="Intensity",ylab="Frequency")
                try(lines(c(0,xdata,255),c(gdata[[i]]),col=ucol$Green,lwd=2),silent=TRUE)
                try(lines(c(0,xdata,255),c(rdata[[i]]),col=ucol$Red,lwd=2),silent=TRUE)
        }
}
#singleExpt("DCF3","Q25")

fourWayTime = function(experiment="All"){
        ## ~ Time Plots for All experiments, Red and Green ~ ##
        layout(matrix(1:8,byrow=FALSE,nrow=2))
        for(colour in c("Green","Red")){
                for(celltype in c("Q25","Q97")){
                        timePlot(umar,experiment,celltype=celltype,colour=colour)
                        timePlotCumFreq(umar,experiment,celltype=celltype,colour=colour)
                }
        }
}
#fourWayTime("All")
#fourWayTime("DCF1")

fourTimeCell = function(experiment="All",colour="All"){
        layout(matrix(1:8,byrow=FALSE,nrow=2))
        for(time in c("All","Day1","Day2","Day3")){
                cellComp(umar,experiment,time,colour=colour)
                cellCompCumFreq(umar,experiment,time,colour=colour)
        }
}
#fourTimeCell("All","All")

### ~~~~~ GENERATE PNG FILES ~~~~~ ###
pngh = 1800
pngw = 2 * pngh
for(experiment in c("All","DCF1","DCF2","DCF3","DCF4","DCF5","DCF6")){
        ## Single Experiment Chart ##
        for(celltype in c("All","Q25","Q97")){
                pngfile = paste(experiment,celltype,"Expt","png",sep=".")
                png(pngfile,height=pngh,width=pngw,pointsize=24)
                singleExpt(experiment,celltype)
                dev.off()
        }

        ## Four-way Time Plots ##
        pngfile = paste(experiment,"TimeCourse","png",sep=".")
        png(pngfile,height=pngh,width=pngw,pointsize=24)
        fourWayTime(experiment)
        dev.off()

        ## Cell Comparisons by Time ##
        for (colour in c("Red","Green")){
                pngfile = paste(experiment,colour,"CellComp","png",sep=".")
                png(pngfile,height=pngh,width=pngw,pointsize=24)
                fourTimeCell(experiment,colour)
                dev.off()
        }
}

## ~ Time Plots for Green ~ ##
```

```
layout(matrix(1:12,byrow=TRUE,nrow=2))
for(celltype in c("Q25","Q97")){
        for(i in 1:6){
                expt = paste("DCF",as.character(i),sep="")
                timePlot(umar,experiment=expt,celltype=celltype,colour="Green")
        }
}
```

Appendix 4

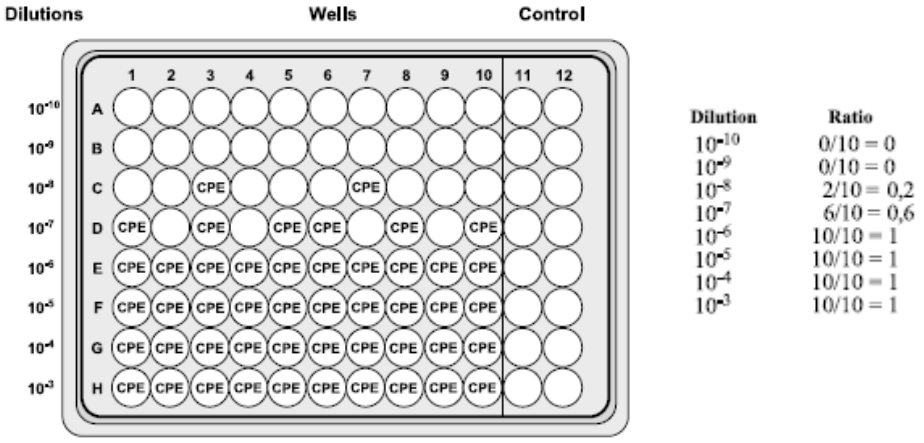

Figure A2. Example of adenovirus infection dose dilution series in a 96 well plate for TC1D50 calculations. 100 % of the wells at dilution 10-6 are positive, and 0 % of the wells at dilution 10-9 are positive (Obtained from, Quantum AdEasy adenovirus preparation protocol handbook).

Appendix 5

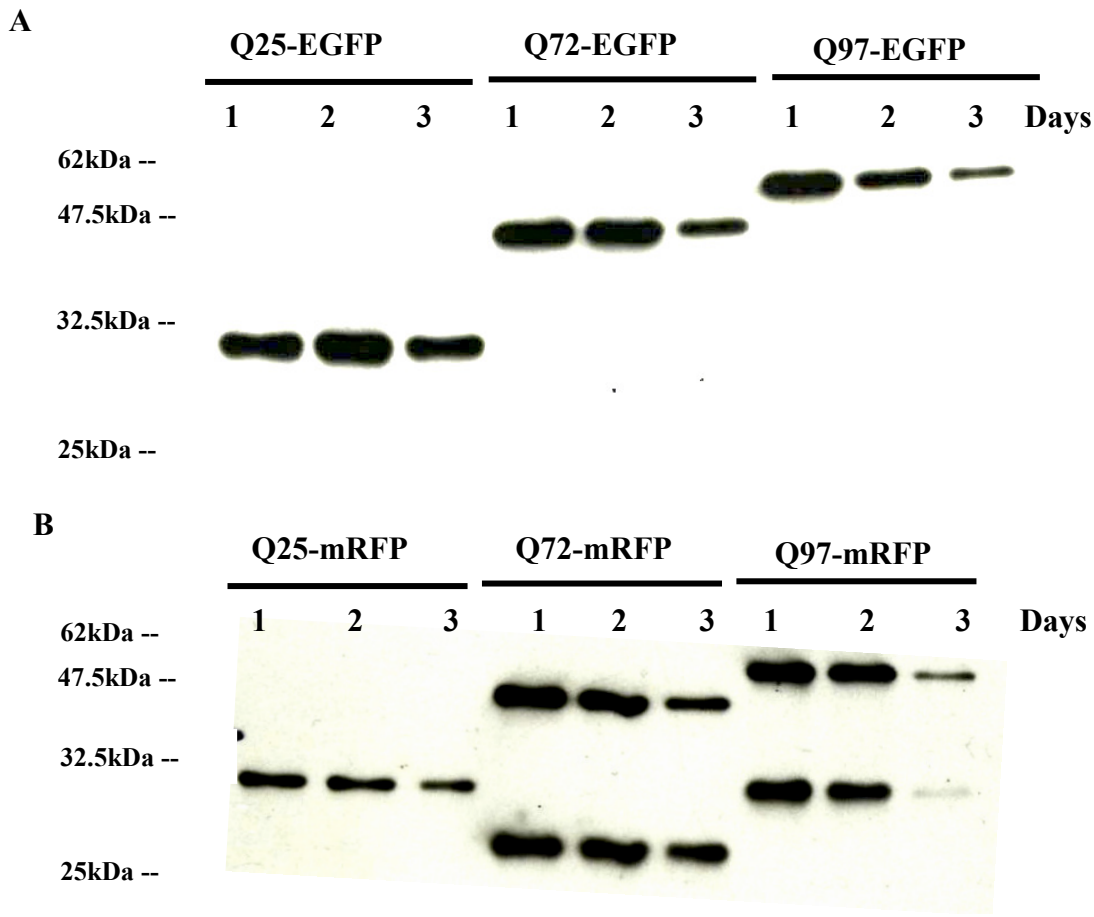

Figure A3. Transgene expression and integrity analysis of httEx1Q25/ Q72/Q97-EGFP/mRFP. (A) Integrity of httEx1Q25/Q72/Q97- EGFP and **(B)** - mRFP transgenes expression of a three day time course in HeLa cells (1= day 1, 2= day 2, 3= day 3). Nitrocellulose membranes were probed with EM48 primary antibody followed by HRP linked secondary antibody which was detected ECL method.

Appendix 6

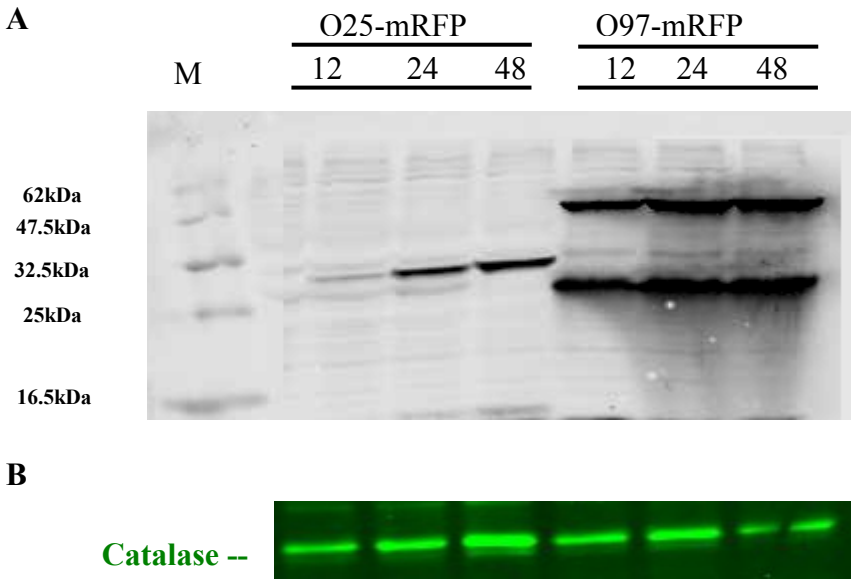

Figure A4. Western blot analysis shows transgene integrity of httEx1Q25/Q97-mRFP in astrocytes. 20µg of solubilised protein samples from astrocytes expressing httEx1Q25/Q97-mRFP were resolved on SDS-PAGE followed by incubation with primary anti-DJ-1 antibody and a secondary fluorescent antibody which was detected by using an infrared fluorescence scanner. **(A)** A representation of the Western blot showing astrocytes infected with httEx1Q25/Q97-mRFP at MOI 10 over time and **(B)** Catalase was used as a loading control.

Appendix 7

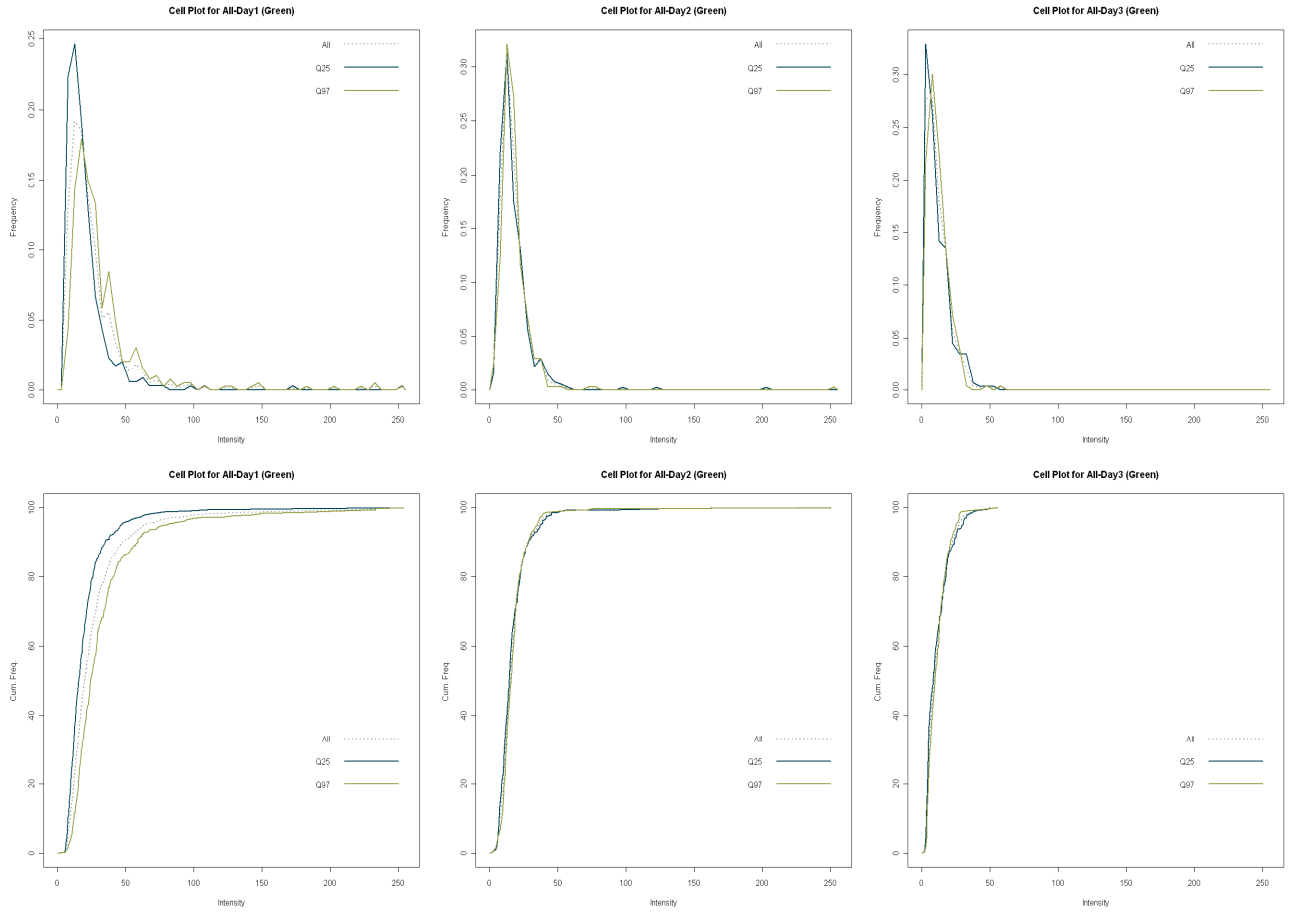

Figure A5. Distribution of pixel intensity analysis of oxidation of DCF in HeLa cells expressing httEx1Q25/Q97-mRFP. Cells expressing httEx1Q97-mRFP showed a shift in pixel intensity of DCF oxidation to the right at 24 hours whereas no change was observed at 48 and 72 hours after transfection. Graph 1, 2 and 3 (left to right) from top and bottom panels represent 24, 48 and 72 hours time points, respectively (n=6 at day 1 and n=3 at day 2-3).

Appendix 8

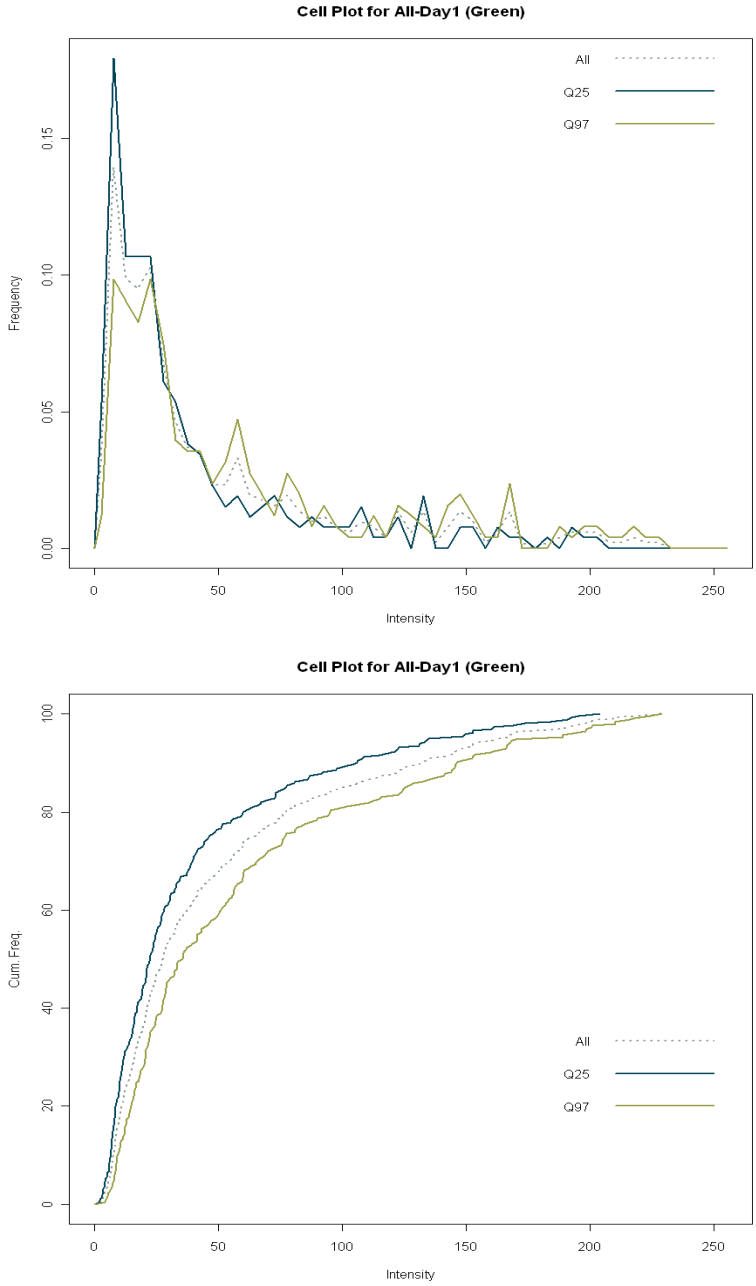

Figure A6. Cumulative pixel intensity distribution analysis of oxidation of DCF in PC12 cells expressing httEx1Q25/Q97-mRFP. Cells expressing httEx1Q97-mRFP showed a shift in pixel intensity of DCF oxidation to the right at 24 hours after transfection (n=4).

Appendix 9

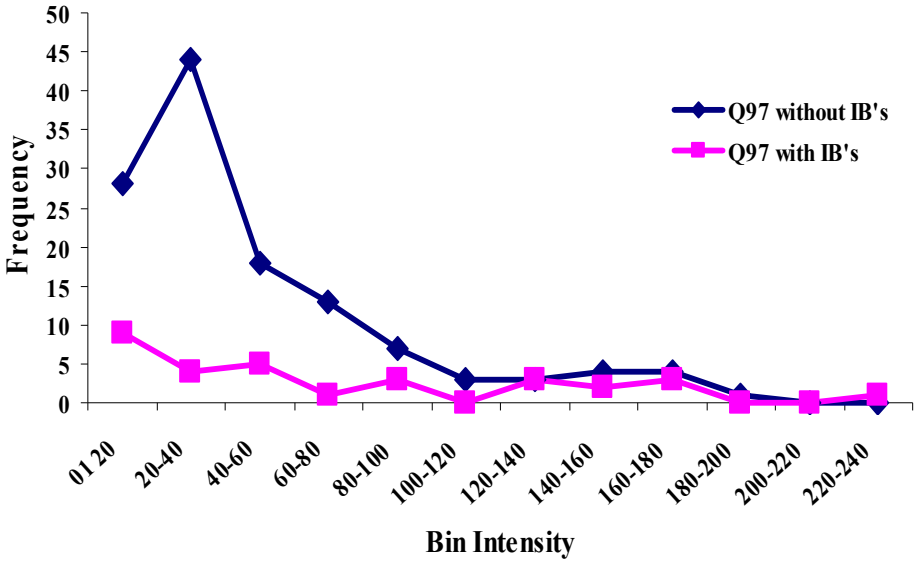

Figure A7, Frequency distribution analysis of DCF oxidation in PC12 cells expressing httEx1Q97-mRFP with IBs or without IBs. There was no significant difference observed between cell with mhttEx1 IBs or without. Unpaired t-test was performed for statistical analysis (P>0.05).

Appendix 10

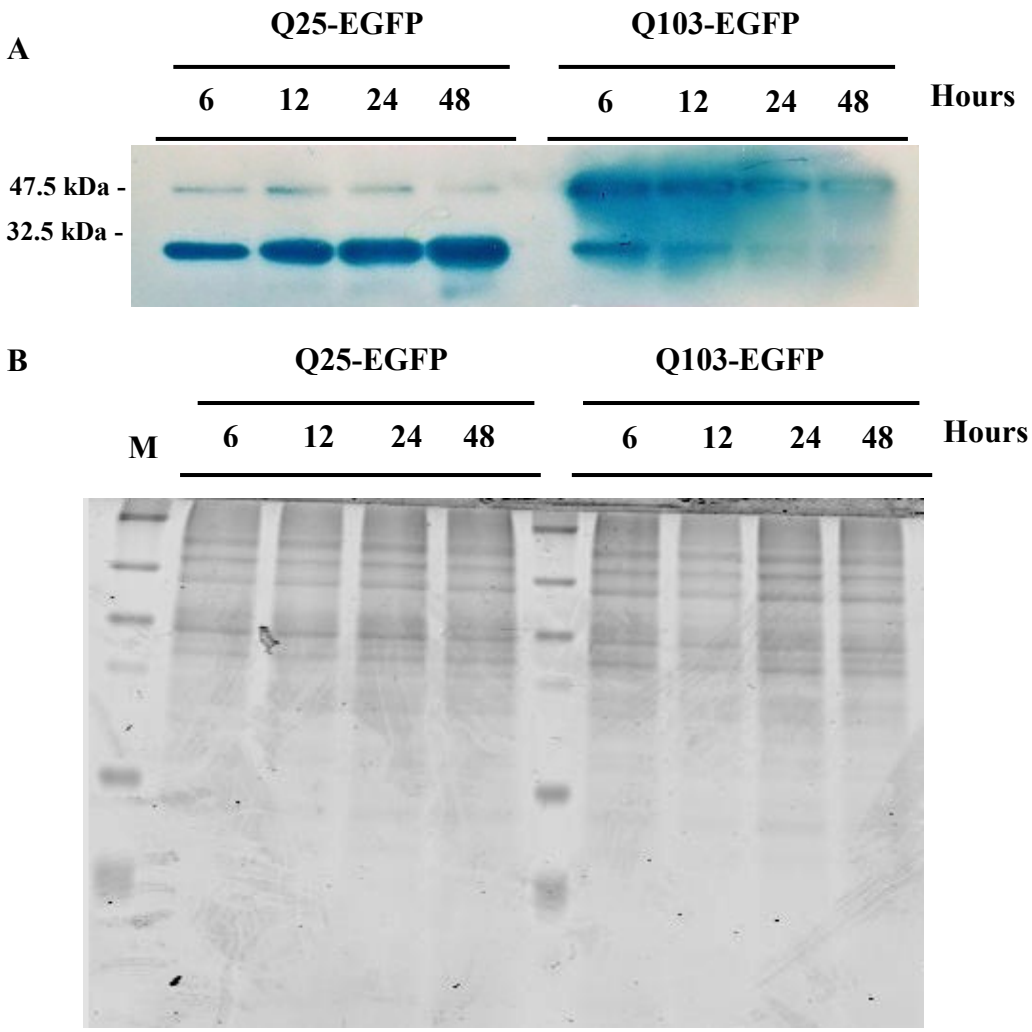

Figure A8. Transgene integrity analysis of tebufenozide inducible PC12 cells expressing httEx1Q25/Q103-EGFP. **(A)** PC12-cells expressing httEx1Q25/Q103-EGFP were lysed at 6, 12, 24 and 48 hours of induction and immunolabelled against S830 antibody. **(B)** Coomassie gel was run as a loading control.

Appendix 11

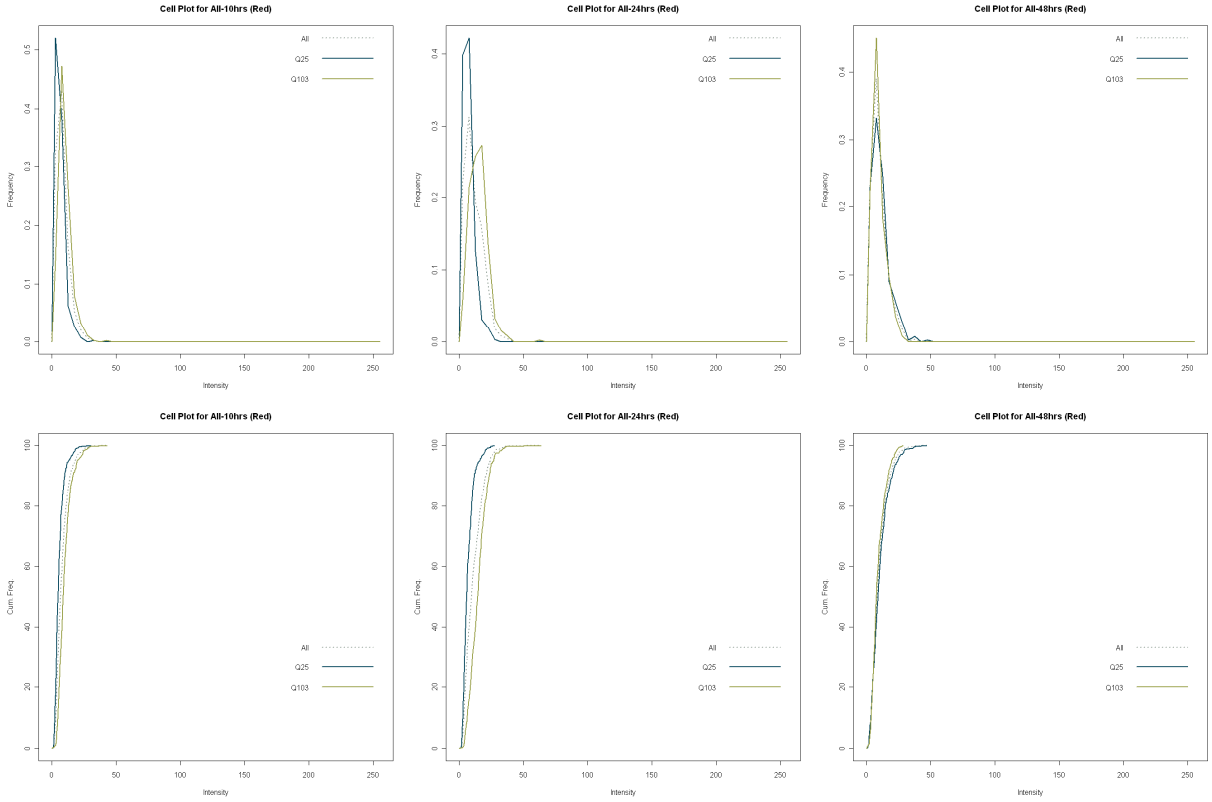

Figure A9. Distribution of pixel intensity analysis of the oxidation of DHE in PC12-Q25/Q103 cells induced with 1µM of tebufenozide. Cells expressing httEx1Q97-EGFP showed pixel intensity of oxidation of DHE shift to the right at 10 hours and 24 hours after induction whereas no changes in shift observed at 48 hours after induction. Graph 1, 2 and 3 from top and bottom panel represent 10, 24, and 48 hour time points.

Appendix 12

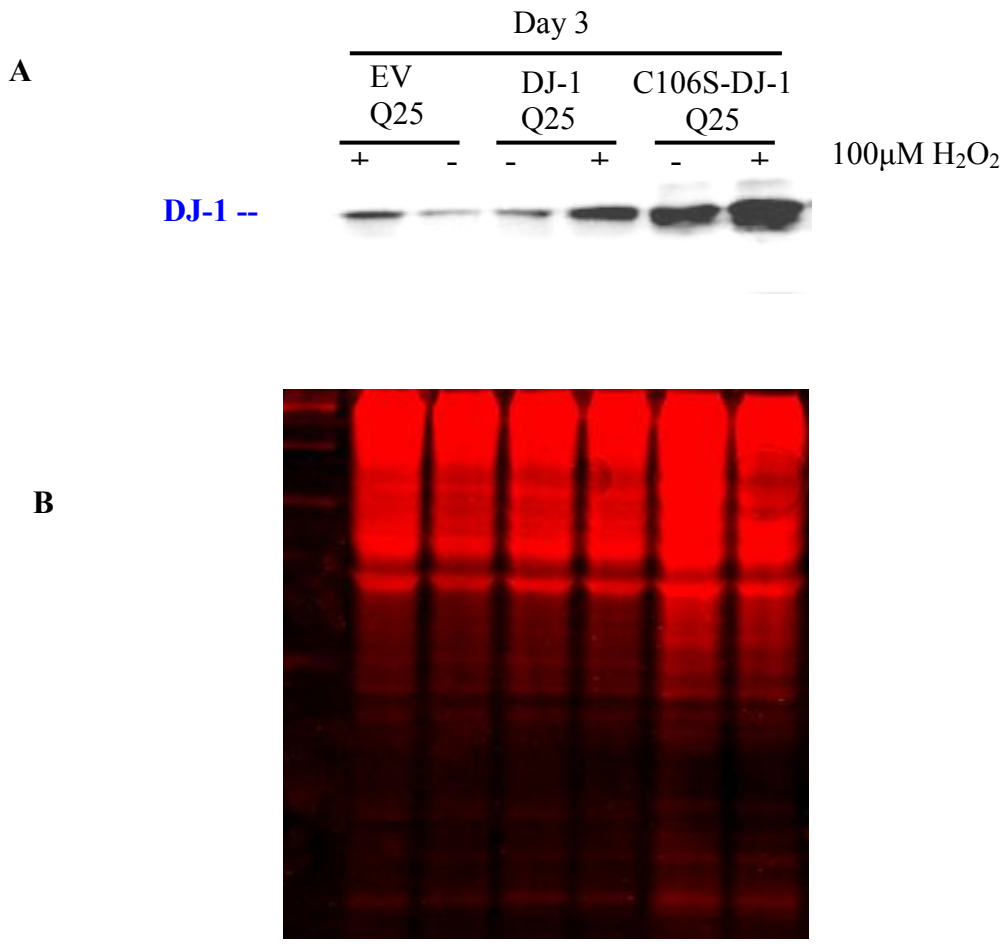

Figure A10. Mild oxidative stress enhances DJ-1 expression levels in HeLa cells 20μg of soluble protein from cells co-transfected with EV or DJ-1 or C106S-DJ-1 and httEx1Q25-mRFP treated with/without H_2O_2 were resolved on SDS-PAGE followed by incubation with primary anti-DJ-1 (Neuromics) polyclonal antibody and a fluorescent secondary antibody which was imaged by using an infrared fluorescent scanner. **(A)** Cells co-transfected with EV or DJ-1or C106S-DJ-1 with httEx1Q25-mRFP show enhance endogenous or exogenously expressed DJ-1 expression level when treated with H_2O_2. **(B)** Coomassie gel was used as a loading control.

Appendix 13

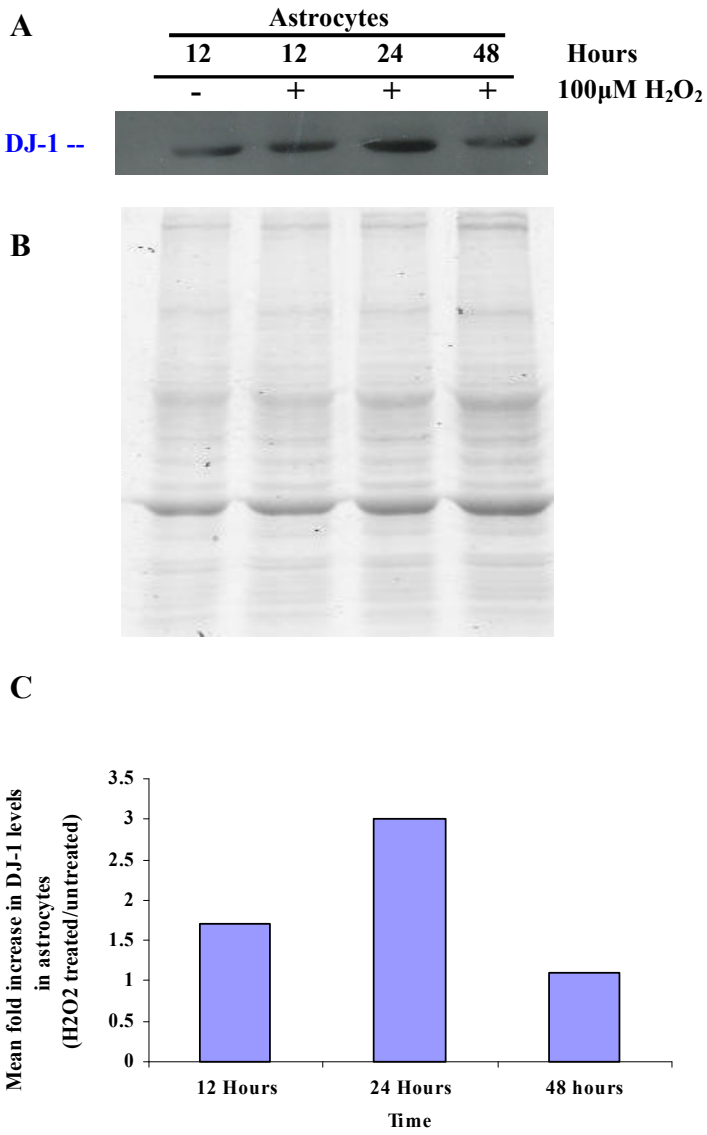

Figure A11. 100µM of H_2O_2 treatment upregulates DJ-1 expression levels in astrocytes. (A) 20µg of solubilised protein samples from astrocytes treated with/without 100µM of H_2O_2 and resolved on SDS-PAGE followed by incubation with anti-DJ-1 primary antibody and a fluorescent secondary antibody which was detected by an infrared fluorescence scanner. **(B)** Coomassie gel was used as a loading control. **(C)** Quantification of Western blot analysis shows upregulation of DJ-1 within the first 24 hours of H_2O_2 treatment whereas no change was observed at the 48 hour time point.

Appendix 14

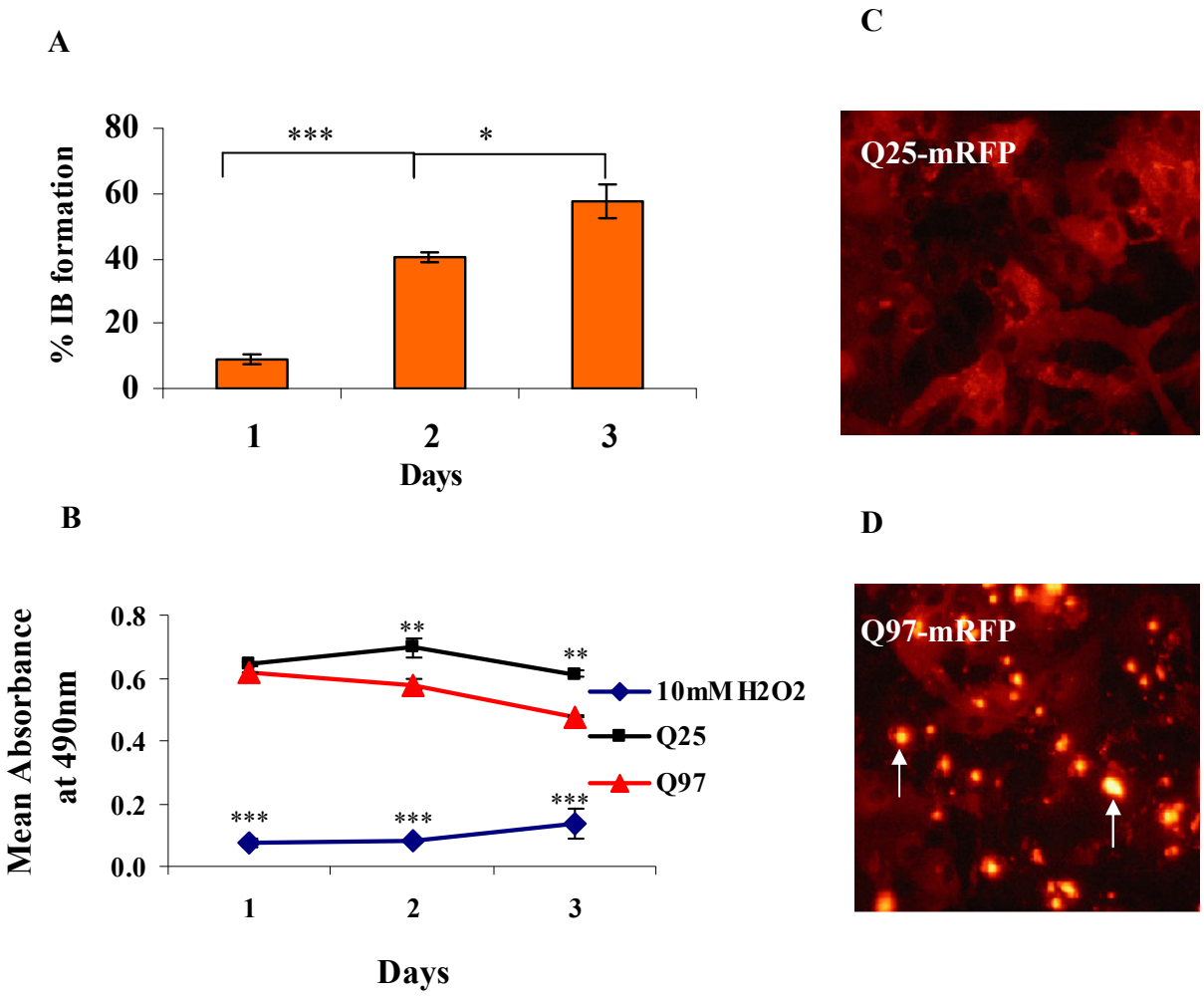

Figure A12. Astrocytes cell model of HD shows polyQ length dependant aggregation and toxicity over time. Astrocytes were infected with MOI of 10 and % IB formation and cell death was scored over time. **(A)** Astrocytes infected with httEx1Q97-mRFP show a time dependant increase in IB formation. **(B)** MTS assay was performed to study cellular toxicity over time. Cells expressing httEx1Q97-mRFP show a significant increase in cell death at day 2-3 compared to cells expressing httEx1Q25-mRFP. **(C-D)** Examples of cells infected with httEx1Q25/Q97-mRFP. Cells infected with httEx1Q25-mRFP did not form IBs whereas cells infected with httEx1Q97-mRFP show bright red IBs (white arrows). Two-way repeat measure ANOVA and Bonferroni post tests were used for toxicity analysis whereas the unpaired t-test was used for IB formation analysis. Error bars represents standard deviations (n=2).

Appendix 15

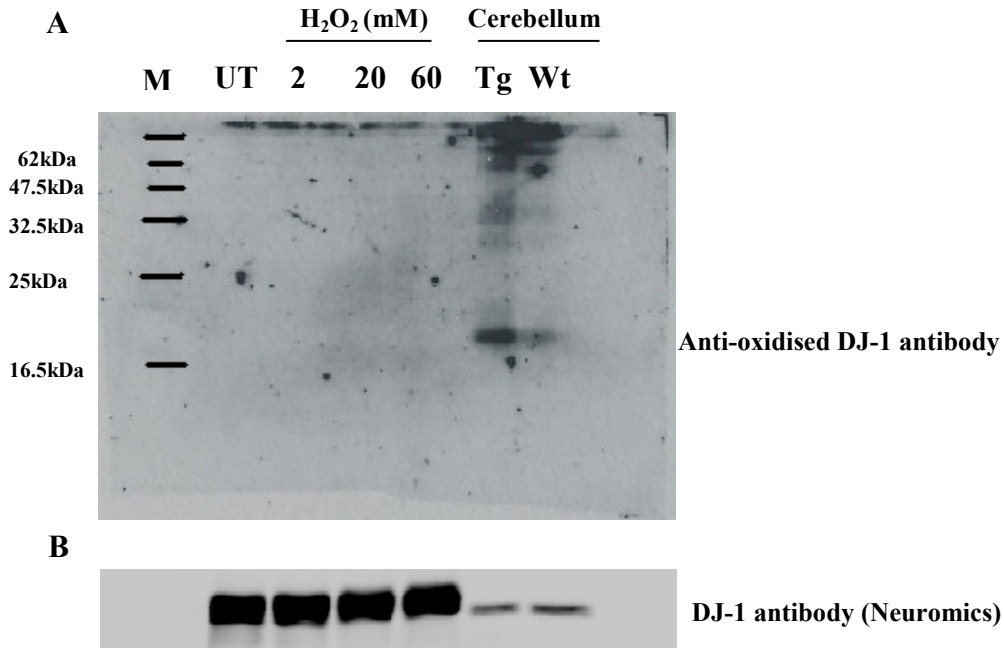

Figure A13. An antibody recognising oxidised DJ-1 did not detect H_2O_2 treated recombinant DJ-1 protein. 2µg of commercial recombinant DJ-1 protein was treated with 2, 20 and 60mM of H_2O_2 for 1 hour at room temperature. 20µg of 2% SDS solubilised protein from the cerebellum of the 17 weeks old R6/2 and age controlled animal as a positive control were resolved on SDS-PAGE followed by incubation with anti-oxidised DJ-1 primary antibody (Serotec) and HRP labelled secondary antibody which was detected by ECL. **(A)** Anti oxidised DJ-1 antibody did not detect any oxidation of recombinant DJ-1 protein when treated with H_2O_2 whereas it detected oxidised DJ-1 protein in the cerebellum of R6/2 and control animal. **(B)** Nitrocellulose membrane re-probed with polyclonal DJ-1 antibody (Neuromics) confirms that recombinant protein is indeed DJ-1 (M = marker, UT= untreated, Tg = R6/2 transgenic and Wt= wild-type).

Appendix 16

A

KDRWGSMASKRALVILAKGAEEMETVIPVDVMRRAGIKVTVAGLAGKDPVQ**C**SRDVVI**C**P
DASLEDAKKEGPYDVVVLPGGNLGAQNLSESAAVKEILKEQENRKGLIAAI**C**AGPTALLA
HEIGFGSKVTTHPLAKDKMMNGGHYTYSENRVEKDGLILTSRGPGTSFEFALAIVEALNG
KEVAAQVKAPLVLK **(Mass: 20492 Daltons)**

B

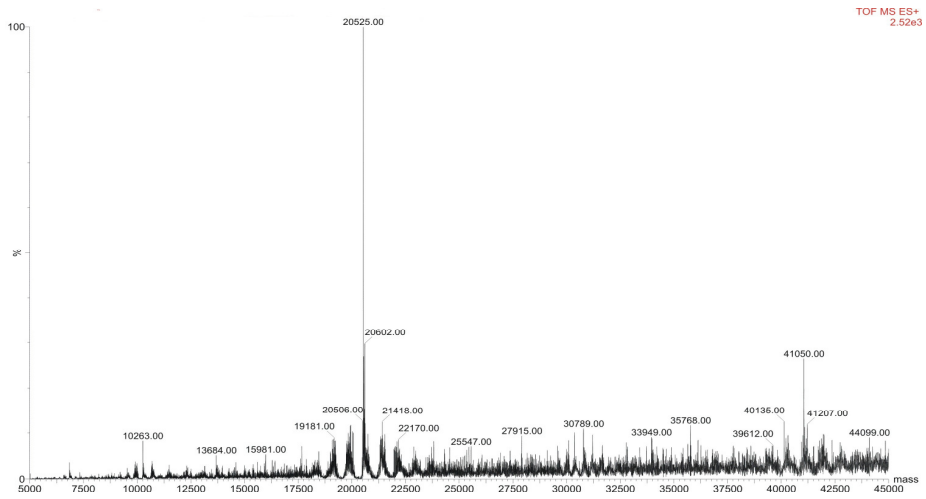

C

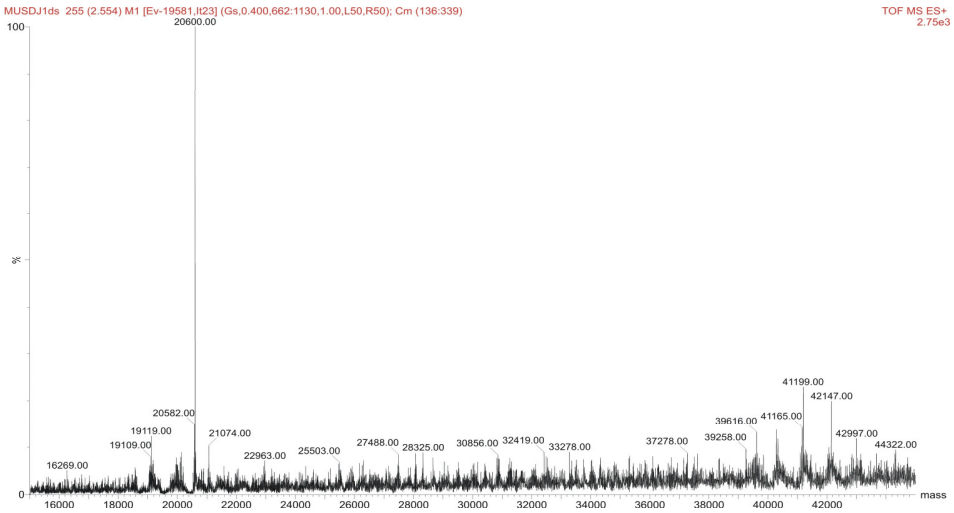

D

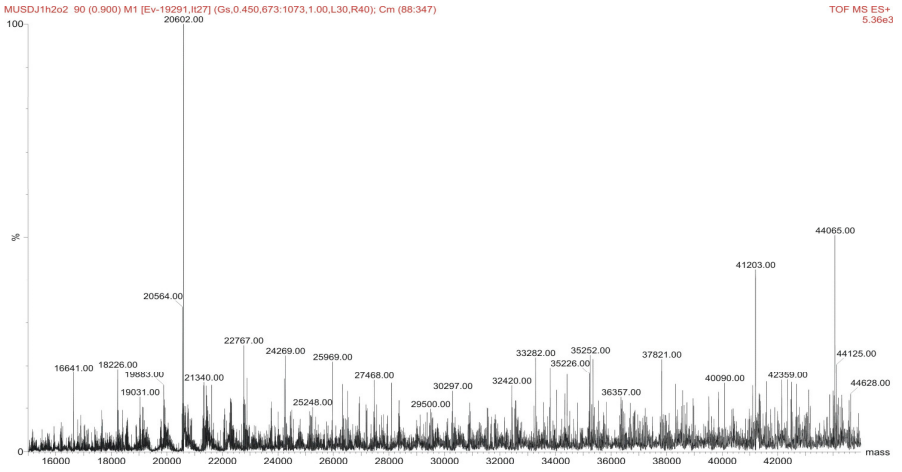

Figure A14 Characterization of recombinant human DJ-1 protein using ElectrosprayIonisation Mass Spectrometry (ES-MS). (A) DJ-1 protein sequence (Mass: 20492). (B) ES-MS spectrum of reduced DJ-1 protein with 2mM DTT (Mass: 20525, suggests a mass difference which is consistent with protein oxidation before oxidant treatment (oxidised by addition of 2 oxygen), (C) DJ-1 without DTT treatment also shows a mass difference that is consistent with a ß-Mercaptoethanol adduct as well as protein oxidation (Mass: 20600) and (C) non-reduced DJ-1 treated with 2mM H2O2 for 1 hour at room temperature shows no further oxidation of DJ-1 protein hence, no difference in DJ-1 mass is observed (Mass: 20602).

Appendix 17

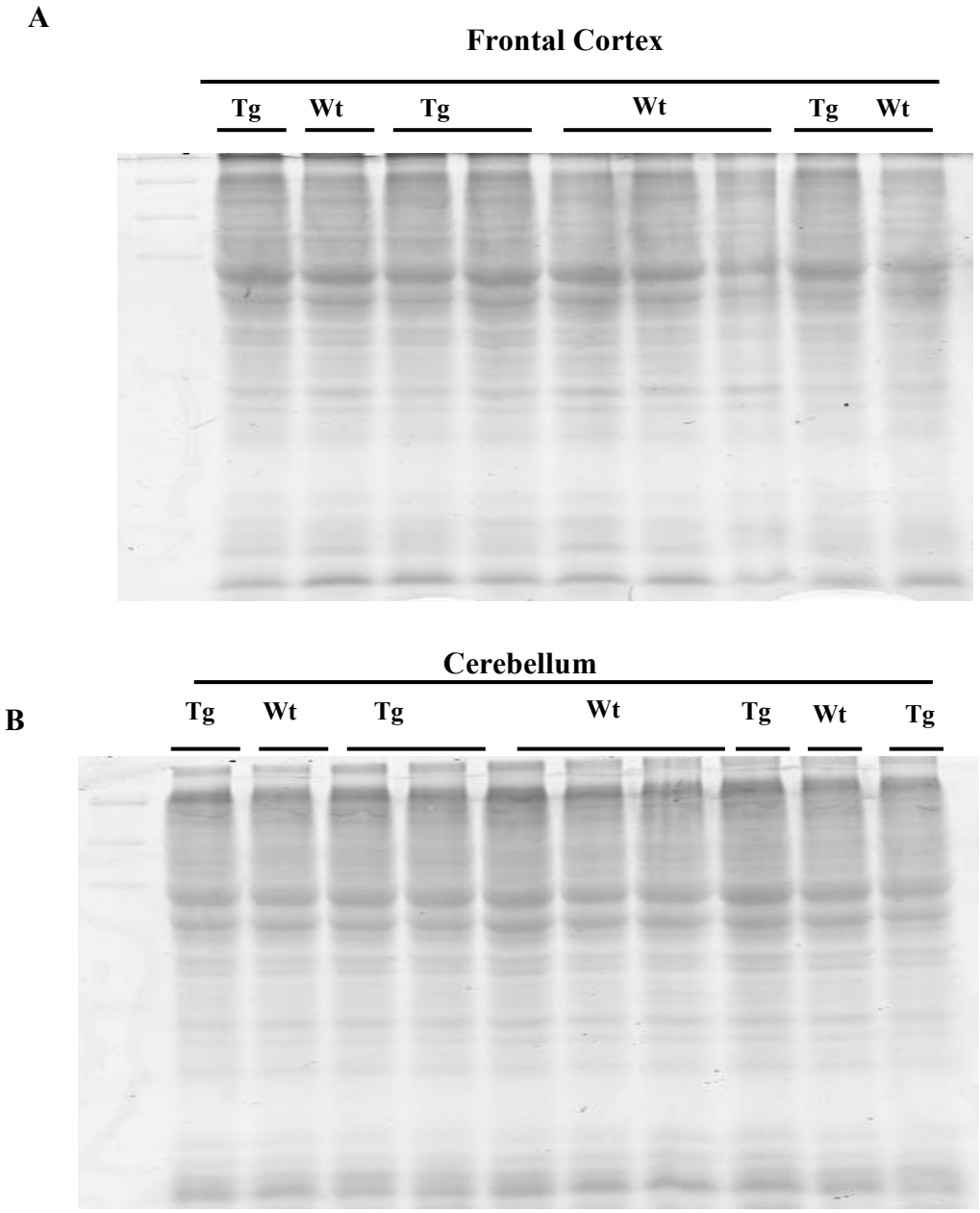

Figure A15 Coomassie gels used as a loading control for 17 weeks old R6/2 (Tg) and age control wild-type animals.
(A) Frontal cortex
(B) Cerebellum

References

Abid,M.R., Schoots,I.G., Spokes,K.C., Wu,S.Q., Mawhinney,C., and Aird,W.C. (2004). Vascular endothelial growth factor-mediated induction of manganese superoxide dismutase occurs through redox-dependent regulation of forkhead and IkappaB/NF-kappaB. J. Biol. Chem. *279*, 44030-44038.

Agostinho,P. and Oliveira,C.R. (2003). Involvement of calcineurin in the neurotoxic effects induced by amyloid-beta and prion peptides. Eur. J. Neurosci. *17*, 1189-1196.

Aguzzi,A. and Polymenidou,M. (2004). Mammalian prion biology: one century of evolving concepts. Cell *116*, 313-327.

Ahmad,M.F., Singh,D., Taiyab,A., Ramakrishna,T., Raman,B., and Rao,C. (2008). Selective Cu2+ binding, redox silencing, and cytoprotective effects of the small heat shock proteins alphaA- and alphaB-crystallin. J. Mol. Biol. *382*, 812-824.

Aikawa,R., Komuro,I., Yamazaki,T., Zou,Y., Kudoh,S., Tanaka,M., Shiojima,I., Hiroi,Y., and Yazaki,Y. (1997). Oxidative stress activates extracellular signal-regulated kinases through Src and Ras in cultured cardiac myocytes of neonatal rats. J. Clin. Invest *100*, 1813-1821.

Aiken,C.T., Tobin,A.J., and Schweitzer,E.S. (2004). A cell-based screen for drugs to treat Huntington's disease. Neurobiol. Dis. *16*, 546-555.

Alam,Z.I., Daniel,S.E., Lees,A.J., Marsden,D.C., Jenner,P., and Halliwell,B. (1997a). A generalised increase in protein carbonyls in the brain in Parkinson's but not incidental Lewy body disease. J. Neurochem. *69*, 1326-1329.

Alam,Z.I., Halliwell,B., and Jenner,P. (2000). No evidence for increased oxidative damage to lipids, proteins, or DNA in Huntington's disease. J. Neurochem. *75*, 840-846.

Alam,Z.I., Jenner,A., Daniel,S.E., Lees,A.J., Cairns,N., Marsden,C.D., Jenner,P., and Halliwell,B. (1997b). Oxidative DNA damage in the parkinsonian brain: an apparent selective increase in 8-hydroxyguanine levels in substantia nigra. J. Neurochem. *69*, 1196-1203.

Albin,R.L., Reiner,A., Anderson,K.D., Dure,L.S., Handelin,B., Balfour,R., Whetsell,W.O., Jr., Penney,J.B., and Young,A.B. (1992). Preferential loss of striato-external pallidal projection neurons in presymptomatic Huntington's disease. Ann. Neurol. *31*, 425-430.

Aleyasin,H., Rousseaux,M.W., Marcogliese,P.C., Hewitt,S.J., Irrcher,I., Joselin,A.P., Parsanejad,M., Kim,R.H., Rizzu,P., Callaghan,S.M., Slack,R.S., Mak,T.W., and Park,D.S. (2010). DJ-1 protects the nigrostriatal axis from the neurotoxin MPTP by modulation of the AKT pathway. Proc. Natl. Acad. Sci. U. S. A *107*, 3186-3191.

Alge,C.S., Priglinger,S.G., Neubauer,A.S., Kampik,A., Zillig,M., Bloemendal,H., and Welge-Lussen,U. (2002). Retinal pigment epithelium is protected against apoptosis by alphaB-crystallin. Invest Ophthalmol. Vis. Sci. *43*, 3575-3582.

Allard,L., Burkhard,P.R., Lescuyer,P., Burgess,J.A., Walter,N., Hochstrasser,D.F., and Sanchez,J.C. (2005). PARK7 and nucleoside diphosphate kinase A as plasma markers for the early diagnosis of stroke. Clin. Chem. *51*, 2043-2051.

Allen,R.G. and Tresini,M. (2000). Oxidative stress and gene regulation. Free Radic. Biol. Med. *28*, 463-499.

Allsop,D., Mayes,J., Moore,S., Masad,A., and Tabner,B.J. (2008). Metal-dependent generation of reactive oxygen species from amyloid proteins implicated in neurodegenerative disease. Biochem. Soc. Trans. *36*, 1293-1298.

Altar,C.A., Cai,N., Bliven,T., Juhasz,M., Conner,J.M., Acheson,A.L., Lindsay,R.M., and Wiegand,S.J. (1997). Anterograde transport of brain-derived neurotrophic factor and its role in the brain. Nature *389*, 856-860.

Ames,B.N. (1983). Dietary carcinogens and anticarcinogens. Oxygen radicals and degenerative diseases. Science *221*, 1256-1264.

Anderson,P.C. and Daggett,V. (2008). Molecular basis for the structural instability of human DJ-1 induced by the L166P mutation associated with Parkinson's disease. Biochemistry *47*, 9380-9393.

Andres-Mateos,E., Perier,C., Zhang,L., Blanchard-Fillion,B., Greco,T.M., Thomas,B., Ko,H.S., Sasaki,M., Ischiropoulos,H., Przedborski,S., Dawson,T.M., and Dawson,V.L. (2007). DJ-1 gene deletion reveals that DJ-1 is an atypical peroxiredoxin-like peroxidase. Proc. Natl. Acad. Sci. U. S. A *104*, 14807-14812.

Andrew,S.E., Goldberg,Y.P., Kremer,B., Telenius,H., Theilmann,J., Adam,S., Starr,E., Squitieri,F., Lin,B., Kalchman,M.A., and . (1993). The relationship between trinucleotide (CAG) repeat length and clinical features of Huntington's disease. Nat. Genet. *4*, 398-403.

Andrews,T.C. and Brooks,D.J. (1998). Advances in the understanding of early Huntington's disease using the functional imaging techniques of PET and SPET. Mol. Med. Today *4*, 532-539.

Apostol,B.L., Illes,K., Pallos,J., Bodai,L., Wu,J., Strand,A., Schweitzer,E.S., Olson,J.M., Kazantsev,A., Marsh,J.L., and Thompson,L.M. (2006). Mutant huntingtin alters MAPK signaling pathways in PC12 and striatal cells: ERK1/2 protects against mutant huntingtin-associated toxicity. Hum. Mol. Genet. *15*, 273-285.

Apostol,B.L., Kazantsev,A., Raffioni,S., Illes,K., Pallos,J., Bodai,L., Slepko,N., Bear,J.E., Gertler,F.B., Hersch,S., Housman,D.E., Marsh,J.L., and Thompson,L.M. (2003). A cell-based assay for aggregation inhibitors as therapeutics of polyglutamine-repeat disease and validation in Drosophila. Proc. Natl. Acad. Sci. U. S. A *100*, 5950-5955.

Arenas,J., Campos,Y., Ribacoba,R., Martin,M.A., Rubio,J.C., Ablanedo,P., and Cabello,A. (1998). Complex I defect in muscle from patients with Huntington's disease. Ann. Neurol. *43*, 397-400.

Arrasate,M., Mitra,S., Schweitzer,E.S., Segal,M.R., and Finkbeiner,S. (2004). Inclusion body formation reduces levels of mutant huntingtin and the risk of neuronal death. Nature *431*, 805-810.

Arrigo,A.P. (1998). Small stress proteins: chaperones that act as regulators of intracellular redox state and programmed cell death. Biol. Chem. *379*, 19-26.

Arrigo,A.P. (2001). Hsp27: novel regulator of intracellular redox state. IUBMB. Life *52*, 303-307.

Arrigo,A.P., Simon,S., Gibert,B., Kretz-Remy,C., Nivon,M., Czekalla,A., Guillet,D., Moulin,M., Diaz-Latoud,C., and Vicart,P. (2007). Hsp27 (HspB1) and alphaB-crystallin (HspB5) as therapeutic targets. FEBS Lett. *581*, 3665-3674.

Arsenijevic,D., Onuma,H., Pecqueur,C., Raimbault,S., Manning,B.S., Miroux,B., Couplan,E., ves-Guerra,M.C., Goubern,M., Surwit,R., Bouillaud,F., Richard,D., Collins,S., and Ricquier,D. (2000). Disruption of the uncoupling protein-2 gene in mice reveals a role in immunity and reactive oxygen species production. Nat. Genet. *26*, 435-439.

Aziz,N.A., van der Burg,J.M., Landwehrmeyer,G.B., Brundin,P., Stijnen,T., and Roos,R.A. (2008). Weight loss in Huntington disease increases with higher CAG repeat number. Neurology *71*, 1506-1513.

Bahadorani,S. and Hilliker,A.J. (2008). Antioxidants cannot suppress the lethal phenotype of a Drosophila melanogaster model of Huntington's disease. Genome *51*, 392-395.

Bandopadhyay,R., Kingsbury,A.E., Cookson,M.R., Reid,A.R., Evans,I.M., Hope,A.D., Pittman,A.M., Lashley,T., Canet-Aviles,R., Miller,D.W., McLendon,C., Strand,C., Leonard,A.J., Abou-Sleiman,P.M., Healy,D.G., Ariga,H., Wood,N.W., de,S.R., Revesz,T., Hardy,J.A., and Lees,A.J. (2004). The expression of DJ-1 (PARK7) in normal human CNS and idiopathic Parkinson's disease. Brain *127*, 420-430.

Barnham,K.J., Masters,C.L., and Bush,A.I. (2004). Neurodegenerative diseases and oxidative stress. Nat. Rev. Drug Discov. *3*, 205-214.

Barral,J.M., Broadley,S.A., Schaffar,G., and Hartl,F.U. (2004). Roles of molecular chaperones in protein misfolding diseases. Semin. Cell Dev. Biol. *15*, 17-29.

Barsoum,M.J., Yuan,H., Gerencser,A.A., Liot,G., Kushnareva,Y., Graber,S., Kovacs,I., Lee,W.D., Waggoner,J., Cui,J., White,A.D., Bossy,B., Martinou,J.C., Youle,R.J., Lipton,S.A., Ellisman,M.H., Perkins,G.A., and Bossy-Wetzel,E. (2006). Nitric oxide-induced mitochondrial fission is regulated by dynamin-related GTPases in neurons. EMBO J. *25*, 3900-3911.

Batelli,S., Albani,D., Rametta,R., Polito,L., Prato,F., Pesaresi,M., Negro,A., and Forloni,G. (2008). DJ-1 modulates alpha-synuclein aggregation state in a cellular model of oxidative stress: relevance for Parkinson's disease and involvement of HSP70. PLoS. One. *3*, e1884.

Bauer,P.O., Goswami,A., Wong,H.K., Okuno,M., Kurosawa,M., Yamada,M., Miyazaki,H., Matsumoto,G., Kino,Y., Nagai,Y., and Nukina,N. (2010). Harnessing chaperone-mediated autophagy for the selective degradation of mutant huntingtin protein. Nat. Biotechnol. *28*, 256-263.

Baulac,S., Lu,H., Strahle,J., Yang,T., Goldberg,M.S., Shen,J., Schlossmacher,M.G., Lemere,C.A., Lu,Q., and Xia,W. (2009). Increased DJ-1 expression under oxidative stress and in Alzheimer's disease brains. Mol. Neurodegener. *4*, 12.

Beal,M.F. (2004). Mitochondrial dysfunction and oxidative damage in Alzheimer's and Parkinson's diseases and coenzyme Q10 as a potential treatment. J. Bioenerg. Biomembr. *36*, 381-386.

Beal,M.F. (2005). Mitochondria take center stage in aging and neurodegeneration. Ann. Neurol. *58*, 495-505.

Beal,M.F., Kowall,N.W., Ellison,D.W., Mazurek,M.F., Swartz,K.J., and Martin,J.B. (1986). Replication of the neurochemical characteristics of Huntington's disease by quinolinic acid. Nature *321*, 168-171.

Becher,M.W., Kotzuk,J.A., Sharp,A.H., Davies,S.W., Bates,G.P., Price,D.L., and Ross,C.A. (1998). Intranuclear neuronal inclusions in Huntington's disease and dentatorubral and pallidoluysian atrophy: correlation between the density of inclusions and IT15 CAG triplet repeat length. Neurobiol. Dis. *4*, 387-397.

Belanger,M. and Magistretti,P.J. (2009). The role of astroglia in neuroprotection. Dialogues. Clin. Neurosci. *11*, 281-295.

Bence,N.F., Sampat,R.M., and Kopito,R.R. (2001). Impairment of the ubiquitin-proteasome system by protein aggregation. Science *292*, 1552-1555.

Benchoua,A., Trioulier,Y., Zala,D., Gaillard,M.C., Lefort,N., Dufour,N., Saudou,F., Elalouf,J.M., Hirsch,E., Hantraye,P., Deglon,N., and Brouillet,E. (2006). Involvement of mitochondrial complex II defects in neuronal death produced by N-terminus fragment of mutated huntingtin. Mol. Biol. Cell *17*, 1652-1663.

Bennett,E.J., Bence,N.F., Jayakumar,R., and Kopito,R.R. (2005). Global impairment of the ubiquitin-proteasome system by nuclear or cytoplasmic protein aggregates precedes inclusion body formation. Mol. Cell *17*, 351-365.

Bennett,E.J., Shaler,T.A., Woodman,B., Ryu,K.Y., Zaitseva,T.S., Becker,C.H., Bates,G.P., Schulman,H., and Kopito,R.R. (2007). Global changes to the ubiquitin system in Huntington's disease. Nature *448*, 704-708.

Bett,J.S., Cook,C., Petrucelli,L., and Bates,G.P. (2009). The ubiquitin-proteasome reporter GFPu does not accumulate in neurons of the R6/2 transgenic mouse model of Huntington's disease. PLoS. One. *4*, e5128.

Bett,J.S., Goellner,G.M., Woodman,B., Pratt,G., Rechsteiner,M., and Bates,G.P. (2006). Proteasome impairment does not contribute to pathogenesis in R6/2 Huntington's disease mice: exclusion of proteasome activator REGgamma as a therapeutic target. Hum. Mol. Genet. *15*, 33-44.

Bhutani,N., Venkatraman,P., and Goldberg,A.L. (2007). Puromycin-sensitive aminopeptidase is the major peptidase responsible for digesting polyglutamine sequences released by proteasomes during protein degradation. EMBO J. *26*, 1385-1396.

Blackinton,J., Kumaran,R., van der Brug,M.P., Ahmad,R., Olson,L., Galter,D., Lees,A., Bandopadhyay,R., and Cookson,M.R. (2009a). Post-transcriptional regulation of mRNA associated with DJ-1 in sporadic Parkinson disease. Neurosci. Lett. *452*, 8-11.

Blackinton,J., Lakshminarasimhan,M., Thomas,K.J., Ahmad,R., Greggio,E., Raza,A.S., Cookson,M.R., and Wilson,M.A. (2009b). Formation of a stabilized cysteine sulfinic acid is critical for the mitochondrial function of the parkinsonism protein DJ-1. J. Biol. Chem. *284*, 6476-6485.

Block,M.L., Zecca,L., and Hong,J.S. (2007). Microglia-mediated neurotoxicity: uncovering the molecular mechanisms. Nat. Rev. Neurosci. *8*, 57-69.

Bogdanov,M., Matson,W.R., Wang,L., Matson,T., Saunders-Pullman,R., Bressman,S.S., and Flint,B.M. (2008). Metabolomic profiling to develop blood biomarkers for Parkinson's disease. Brain *131*, 389-396.

Bogdanov,M.B., Andreassen,O.A., Dedeoglu,A., Ferrante,R.J., and Beal,M.F. (2001). Increased oxidative damage to DNA in a transgenic mouse model of Huntington's disease. J. Neurochem. *79*, 1246-1249.

Boillee,S., Vande,V.C., and Cleveland,D.W. (2006). ALS: a disease of motor neurons and their nonneuronal neighbors. Neuron *52*, 39-59.

Bonda,D.J., Wang,X., Perry,G., Nunomura,A., Tabaton,M., Zhu,X., and Smith,M.A. (2010). Oxidative stress in Alzheimer disease: A possibility for prevention. Neuropharmacology.

Bonifati,V., Breedveld,G.J., Squitieri,F., Vanacore,N., Brustenghi,P., Harhangi,B.S., Montagna,P., Cannella,M., Fabbrini,G., Rizzu,P., van Duijn,C.M., Oostra,B.A., Meco,G., and Heutink,P. (2002). Localization of autosomal recessive early-onset parkinsonism to chromosome 1p36 (PARK7) in an independent dataset. Ann. Neurol. *51*, 253-256.

Bonifati,V., Rizzu,P., Squitieri,F., Krieger,E., Vanacore,N., van Swieten,J.C., Brice,A., van Duijn,C.M., Oostra,B., Meco,G., and Heutink,P. (2003a). DJ-1(PARK7), a novel gene for autosomal recessive, early onset parkinsonism. Neurol. Sci. *24*, 159-160.

Bonifati,V., Rizzu,P., van Baren,M.J., Schaap,O., Breedveld,G.J., Krieger,E., Dekker,M.C., Squitieri,F., Ibanez,P., Joosse,M., van Dongen,J.W., Vanacore,N., van Swieten,J.C., Brice,A., Meco,G., van Duijn,C.M., Oostra,B.A., and Heutink,P. (2003b). Mutations in the DJ-1 gene associated with autosomal recessive early-onset parkinsonism. Science *299*, 256-259.

Bossy-Wetzel,E., Schwarzenbacher,R., and Lipton,S.A. (2004). Molecular pathways to neurodegeneration. Nat. Med. *10 Suppl*, S2-S9.

Bradford,J., Shin,J.Y., Roberts,M., Wang,C.E., Li,X.J., and Li,S. (2009). Expression of mutant huntingtin in mouse brain astrocytes causes age-dependent neurological symptoms. Proc. Natl. Acad. Sci. U. S. A *106*, 22480-22485.

Brookes,P.S., Land,J.M., Clark,J.B., and Heales,S.J. (1998). Peroxynitrite and brain mitochondria: evidence for increased proton leak. J. Neurochem. *70*, 2195-2202.

Browne,S.E. and Beal,M.F. (2004). The energetics of Huntington's disease. Neurochem. Res. *29*, 531-546.

Browne,S.E. and Beal,M.F. (2006a). Oxidative damage in Huntington's disease pathogenesis. Antioxid. Redox. Signal. *8*, 2061-2073.

Browne,S.E. and Beal,M.F. (2006b). Oxidative damage in Huntington's disease pathogenesis. Antioxid. Redox. Signal. *8*, 2061-2073.

Browne,S.E., Bowling,A.C., MacGarvey,U., Baik,M.J., Berger,S.C., Muqit,M.M., Bird,E.D., and Beal,M.F. (1997). Oxidative damage and metabolic dysfunction in Huntington's disease: selective vulnerability of the basal ganglia. Ann. Neurol. *41*, 646-653.

Browne,S.E., Ferrante,R.J., and Beal,M.F. (1999). Oxidative stress in Huntington's disease. Brain Pathol. *9*, 147-163.

Bruijn,L.I., Becher,M.W., Lee,M.K., Anderson,K.L., Jenkins,N.A., Copeland,N.G., Sisodia,S.S., Rothstein,J.D., Borchelt,D.R., Price,D.L., and Cleveland,D.W. (1997). ALS-linked SOD1 mutant G85R mediates damage to astrocytes and promotes rapidly progressive disease with SOD1-containing inclusions. Neuron *18*, 327-338.

Butterworth,J., Yates,C.M., and Reynolds,G.P. (1985). Distribution of phosphate-activated glutaminase, succinic dehydrogenase, pyruvate dehydrogenase and gamma-glutamyl transpeptidase in post-mortem brain from Huntington's disease and agonal cases. J. Neurol. Sci. *67*, 161-171.

Byers,R.K., Gilles,F.H., and Fung,C. (1973). Huntington's disease in children. Neuropathologic study of four cases. Neurology *23*, 561-569.

Canet-Aviles,R.M., Wilson,M.A., Miller,D.W., Ahmad,R., McLendon,C., Bandyopadhyay,S., Baptista,M.J., Ringe,D., Petsko,G.A., and Cookson,M.R. (2004). The Parkinson's disease protein DJ-1 is neuroprotective due to cysteine-sulfinic acid-driven mitochondrial localization. Proc. Natl. Acad. Sci. U. S. A *101*, 9103-9108.

Cannon,M.B. and Remington,S.J. (2006). Re-engineering redox-sensitive green fluorescent protein for improved response rate. Protein Sci. *15*, 45-57.

Carmichael,J., Chatellier,J., Woolfson,A., Milstein,C., Fersht,A.R., and Rubinsztein,D.C. (2000). Bacterial and yeast chaperones reduce both aggregate formation and cell death in mammalian cell models of Huntington's disease. Proc. Natl. Acad. Sci. U. S. A *97*, 9701-9705.

Carra,S., Seguin,S.J., Lambert,H., and Landry,J. (2008). HspB8 chaperone activity toward poly(Q)-containing proteins depends on its association with Bag3, a stimulator of macroautophagy. J. Biol. Chem. *283*, 1437-1444.

Carreras,M.C., Riobo,N.A., Pargament,G.A., Boveris,A., and Poderoso,J.J. (1997). Effects of respiratory burst inhibitors on nitric oxide production by human neutrophils. Free Radic. Res. *26*, 325-334.

Caspersen,C., Wang,N., Yao,J., Sosunov,A., Chen,X., Lustbader,J.W., Xu,H.W., Stern,D., McKhann,G., and Yan,S.D. (2005). Mitochondrial Abeta: a potential focal point for neuronal metabolic dysfunction in Alzheimer's disease. FASEB J. *19*, 2040-2041.

Caviston,J.P., Ross,J.L., Antony,S.M., Tokito,M., and Holzbaur,E.L. (2007). Huntingtin facilitates dynein/dynactin-mediated vesicle transport. Proc. Natl. Acad. Sci. U. S. A *104*, 10045-10050.

Ceconi,C., Curello,S., Cargnoni,A., Ferrari,R., Albertini,A., and Visioli,O. (1988). The role of glutathione status in the protection against ischaemic and reperfusion damage: effects of N-acetyl cysteine. J. Mol. Cell Cardiol. *20*, 5-13.

Cente,M., Filipcik,P., Pevalova,M., and Novak,M. (2006). Expression of a truncated tau protein induces oxidative stress in a rodent model of tauopathy. Eur. J. Neurosci. *24*, 1085-1090.

cevedo-Torres,K., Berrios,L., Rosario,N., Dufault,V., Skatchkov,S., Eaton,M.J., Torres-Ramos,C.A., and yala-Torres,S. (2009). Mitochondrial DNA damage is a hallmark of chemically induced and the R6/2 transgenic model of Huntington's disease. DNA Repair (Amst) *8*, 126-136.

Chandel,N.S. and Schumacker,P.T. (1999). Cells depleted of mitochondrial DNA (rho0) yield insight into physiological mechanisms. FEBS Lett. *454*, 173-176.

Chang,L.K., Putcha,G.V., Deshmukh,M., and Johnson,E.M., Jr. (2002). Mitochondrial involvement in the point of no return in neuronal apoptosis. Biochimie *84*, 223-231.

Charvin,D., Vanhoutte,P., Pages,C., Borrelli,E., and Caboche,J. (2005). Unraveling a role for dopamine in Huntington's disease: the dual role of reactive oxygen species and D2 receptor stimulation. Proc. Natl. Acad. Sci. U. S. A *102*, 12218-12223.

Chattopadhyay,M. and Valentine,J.S. (2009). Aggregation of copper-zinc superoxide dismutase in familial and sporadic ALS. Antioxid. Redox. Signal. *11*, 1603-1614.

Chen,L., Cagniard,B., Mathews,T., Jones,S., Koh,H.C., Ding,Y., Carvey,P.M., Ling,Z., Kang,U.J., and Zhuang,X. (2005). Age-dependent motor deficits and dopaminergic dysfunction in DJ-1 null mice. J. Biol. Chem. *280*, 21418-21426.

Chen,S., Berthelier,V., Hamilton,J.B., O'Nuallain,B., and Wetzel,R. (2002). Amyloid-like features of polyglutamine aggregates and their assembly kinetics. Biochemistry *41*, 7391-7399.

Cheng,K.C., Cahill,D.S., Kasai,H., Nishimura,S., and Loeb,L.A. (1992). 8-Hydroxyguanine, an abundant form of oxidative DNA damage, causes G----T and A----C substitutions. J. Biol. Chem. *267*, 166-172.

Chinta,S.J. and Andersen,J.K. (2008). Redox imbalance in Parkinson's disease. Biochim. Biophys. Acta *1780*, 1362-1367.

Choi,J., Levey,A.I., Weintraub,S.T., Rees,H.D., Gearing,M., Chin,L.S., and Li,L. (2004). Oxidative modifications and down-regulation of ubiquitin carboxyl-terminal hydrolase L1 associated with idiopathic Parkinson's and Alzheimer's diseases. J. Biol. Chem. *279*, 13256-13264.

Choi,J., Sullards,M.C., Olzmann,J.A., Rees,H.D., Weintraub,S.T., Bostwick,D.E., Gearing,M., Levey,A.I., Chin,L.S., and Li,L. (2006). Oxidative damage of DJ-1 is linked to sporadic Parkinson and Alzheimer diseases. J. Biol. Chem. *281*, 10816-10824.

Choo,Y.S., Mao,Z., Johnson,G.V., and Lesort,M. (2005). Increased glutathione levels in cortical and striatal mitochondria of the R6/2 Huntington's disease mouse model. Neurosci. Lett. *386*, 63-68.

Christman,M.F., Morgan,R.W., Jacobson,F.S., and Ames,B.N. (1985). Positive control of a regulon for defenses against oxidative stress and some heat-shock proteins in Salmonella typhimurium. Cell *41*, 753-762.

Chung,K.K., Thomas,B., Li,X., Pletnikova,O., Troncoso,J.C., Marsh,L., Dawson,V.L., and Dawson,T.M. (2004). S-nitrosylation of parkin regulates ubiquitination and compromises parkin's protective function. Science *304*, 1328-1331.

Ciammola,A., Sassone,J., Alberti,L., Meola,G., Mancinelli,E., Russo,M.A., Squitieri,F., and Silani,V. (2006). Increased apoptosis, Huntingtin inclusions and altered differentiation in muscle cell cultures from Huntington's disease subjects. Cell Death. Differ. *13*, 2068-2078.

Ciechanover,A. and Brundin,P. (2003). The ubiquitin proteasome system in neurodegenerative diseases: sometimes the chicken, sometimes the egg. Neuron *40*, 427-446.

Cleveland,D.W. and Rothstein,J.D. (2001). From Charcot to Lou Gehrig: deciphering selective motor neuron death in ALS. Nat. Rev. Neurosci. *2*, 806-819.

Cohen,G. and Kesler,N. (1999). Monoamine oxidase and mitochondrial respiration. J. Neurochem. *73*, 2310-2315.

Concannon,C.G., Gorman,A.M., and Samali,A. (2003). On the role of Hsp27 in regulating apoptosis. Apoptosis. *8*, 61-70.

Cookson,M.R. (2003). Crystallizing ideas about Parkinson's disease. Proc. Natl. Acad. Sci. U. S. A *100*, 9111-9113.

Coppede,F., Migheli,F., Ceravolo,R., Bregant,E., Rocchi,A., Petrozzi,L., Unti,E., Lonigro,R., Siciliano,G., and Migliore,L. (2009). The hOGG1 Ser326Cys polymorphism and Huntington's disease. Toxicology.

Cortesi,R. and Privett,O.S. (1972). Toxicity of fatty ozonides and peroxides. Lipids *7*, 715-721.

Crotzer,V.L. and Blum,J.S. (2005). Autophagy and intracellular surveillance: Modulating MHC class II antigen presentation with stress. Proc. Natl. Acad. Sci. U. S. A *102*, 7779-7780.

Cui,L., Jeong,H., Borovecki,F., Parkhurst,C.N., Tanese,N., and Krainc,D. (2006). Transcriptional repression of PGC-1alpha by mutant huntingtin leads to mitochondrial dysfunction and neurodegeneration. Cell *127*, 59-69.

Cui,X.L. and Douglas,J.G. (1997). Arachidonic acid activates c-jun N-terminal kinase through NADPH oxidase in rabbit proximal tubular epithelial cells. Proc. Natl. Acad. Sci. U. S. A *94*, 3771-3776.

Cummings,C.J., Mancini,M.A., Antalffy,B., DeFranco,D.B., Orr,H.T., and Zoghbi,H.Y. (1998). Chaperone suppression of aggregation and altered subcellular proteasome localization imply protein misfolding in SCA1. Nat. Genet. *19*, 148-154.

Cummings,C.J., Sun,Y., Opal,P., Antalffy,B., Mestril,R., Orr,H.T., Dillmann,W.H., and Zoghbi,H.Y. (2001). Over-expression of inducible HSP70 chaperone suppresses neuropathology and improves motor function in SCA1 mice. Hum. Mol. Genet. *10*, 1511-1518.

Curtin,J.F., Donovan,M., and Cotter,T.G. (2002). Regulation and measurement of oxidative stress in apoptosis. J. Immunol. Methods *265*, 49-72.

D'Autreaux,B. and Toledano,M.B. (2007). ROS as signalling molecules: mechanisms that generate specificity in ROS homeostasis. Nat. Rev. Mol. Cell Biol. *8*, 813-824.

da Costa,C.A. (2007). DJ-1: a newcomer in Parkinson's disease pathology. Curr. Mol. Med. *7*, 650-657.

Dalle-Donne,I., Aldini,G., Carini,M., Colombo,R., Rossi,R., and Milzani,A. (2006). Protein carbonylation, cellular dysfunction, and disease progression. J. Cell Mol. Med. *10*, 389-406.

Dalle-Donne,I., Giustarini,D., Colombo,R., Milzani,A., and Rossi,R. (2005a). S-glutathionylation in human platelets by a thiol-disulfide exchange-independent mechanism. Free Radic. Biol. Med. *38*, 1501-1510.

Dalle-Donne,I., Scaloni,A., Giustarini,D., Cavarra,E., Tell,G., Lungarella,G., Colombo,R., Rossi,R., and Milzani,A. (2005b). Proteins as biomarkers of oxidative/nitrosative stress in diseases: the contribution of redox proteomics. Mass Spectrom. Rev. *24*, 55-99.

Davies,S.W., Turmaine,M., Cozens,B.A., DiFiglia,M., Sharp,A.H., Ross,C.A., Scherzinger,E., Wanker,E.E., Mangiarini,L., and Bates,G.P. (1997). Formation of

neuronal intranuclear inclusions underlies the neurological dysfunction in mice transgenic for the HD mutation. Cell *90*, 537-548.

Dawson,T.M. and Dawson,V.L. (2003). Molecular pathways of neurodegeneration in Parkinson's disease. Science *302*, 819-822.

De Vos,K.J., Grierson,A.J., Ackerley,S., and Miller,C.C. (2008). Role of axonal transport in neurodegenerative diseases. Annu. Rev. Neurosci. *31*, 151-173.

de,S.R., Lashley,T., Gibb,G., Hanger,D., Hope,A., Reid,A., Bandopadhyay,R., Utton,M., Strand,C., Jowett,T., Khan,N., Anderton,B., Wood,N., Holton,J., Revesz,T., and Lees,A. (2003). Pathological inclusion bodies in tauopathies contain distinct complements of tau with three or four microtubule-binding repeat domains as demonstrated by new specific monoclonal antibodies. Neuropathol. Appl. Neurobiol. *29*, 288-302.

Dehay,B., Weber,C., Trottier,Y., and Bertolotti,A. (2007). Mapping of the epitope of monoclonal antibody 2B4 to the proline-rich region of human Huntingtin, a region critical for aggregation and toxicity. Biotechnol. J. *2*, 559-564.

Demple,B. and Harrison,L. (1994). Repair of oxidative damage to DNA: enzymology and biology. Annu. Rev. Biochem. *63*, 915-948.

Diaz-Hernandez,M., Hernandez,F., Martin-Aparicio,E., Gomez-Ramos,P., Moran,M.A., Castano,J.G., Ferrer,I., Avila,J., and Lucas,J.J. (2003). Neuronal induction of the immunoproteasome in Huntington's disease. J. Neurosci. *23*, 11653-11661.

Diaz-Hernandez,M., Valera,A.G., Moran,M.A., Gomez-Ramos,P., Alvarez-Castelao,B., Castano,J.G., Hernandez,F., and Lucas,J.J. (2006). Inhibition of 26S proteasome activity by huntingtin filaments but not inclusion bodies isolated from mouse and human brain. J. Neurochem. *98*, 1585-1596.

DiFiglia,M., Sapp,E., Chase,K., Schwarz,C., Meloni,A., Young,C., Martin,E., Vonsattel,J.P., Carraway,R., Reeves,S.A., and . (1995). Huntingtin is a cytoplasmic protein associated with vesicles in human and rat brain neurons. Neuron *14*, 1075-1081.

DiFiglia,M., Sapp,E., Chase,K.O., Davies,S.W., Bates,G.P., Vonsattel,J.P., and Aronin,N. (1997). Aggregation of huntingtin in neuronal intranuclear inclusions and dystrophic neurites in brain. Science *277*, 1990-1993.

Ding,Q., Lewis,J.J., Strum,K.M., Dimayuga,E., Bruce-Keller,A.J., Dunn,J.C., and Keller,J.N. (2002). Polyglutamine expansion, protein aggregation, proteasome activity, and neural survival. J. Biol. Chem. *277*, 13935-13942.

Distelmaier,F., Visch,H.J., Smeitink,J.A., Mayatepek,E., Koopman,W.J., and Willems,P.H. (2009). The antioxidant Trolox restores mitochondrial membrane potential and Ca2+ -stimulated ATP production in human complex I deficiency. J. Mol. Med. *87*, 515-522.

Dugan,L.L., Creedon,D.J., Johnson,E.M., Jr., and Holtzman,D.M. (1997). Rapid suppression of free radical formation by nerve growth factor involves the mitogen-activated protein kinase pathway. Proc. Natl. Acad. Sci. U. S. A *94*, 4086-4091.

Dunah,A.W., Jeong,H., Griffin,A., Kim,Y.M., Standaert,D.G., Hersch,S.M., Mouradian,M.M., Young,A.B., Tanese,N., and Krainc,D. (2002). Sp1 and TAFII130 transcriptional activity disrupted in early Huntington's disease. Science *296*, 2238-2243.

Echtay,K.S., Roussel,D., St-Pierre,J., Jekabsons,M.B., Cadenas,S., Stuart,J.A., Harper,J.A., Roebuck,S.J., Morrison,A., Pickering,S., Clapham,J.C., and Brand,M.D. (2002). Superoxide activates mitochondrial uncoupling proteins. Nature *415*, 96-99.

Engqvist-Goldstein,A.E., Kessels,M.M., Chopra,V.S., Hayden,M.R., and Drubin,D.G. (1999). An actin-binding protein of the Sla2/Huntingtin interacting protein 1 family is a novel component of clathrin-coated pits and vesicles. J. Cell Biol. *147*, 1503-1518.

Evgrafov,O.V., Mersiyanova,I., Irobi,J., Van Den Bosch,L., Dierick,I., Leung,C.L., Schagina,O., Verpoorten,N., Van,I.K., Fedotov,V., Dadali,E., Auer-Grumbach,M., Windpassinger,C., Wagner,K., Mitrovic,Z., Hilton-Jones,D., Talbot,K., Martin,J.J., Vasserman,N., Tverskaya,S., Polyakov,A., Liem,R.K., Gettemans,J., Robberecht,W., De,J.P., and Timmerman,V. (2004). Mutant small heat-shock protein 27 causes axonal Charcot-Marie-Tooth disease and distal hereditary motor neuropathy. Nat. Genet. *36*, 602-606.

Faber,P.W., Alter,J.R., MacDonald,M.E., and Hart,A.C. (1999). Polyglutamine-mediated dysfunction and apoptotic death of a Caenorhabditis elegans sensory neuron. Proc. Natl. Acad. Sci. U. S. A *96*, 179-184.

Faideau,M., Kim,J., Cormier,K., Gilmore,R., Welch,M., Auregan,G., Dufour,N., Guillermier,M., Brouillet,E., Hantraye,P., Deglon,N., Ferrante,R.J., and Bonvento,G. (2010). In vivo expression of polyglutamine-expanded huntingtin by mouse striatal astrocytes impairs glutamate transport: a correlation with Huntington's disease subjects. Hum. Mol. Genet. *19*, 3053-3067.

Fan,J., Ren,H., Jia,N., Fei,E., Zhou,T., Jiang,P., Wu,M., and Wang,G. (2008). DJ-1 decreases Bax expression through repressing p53 transcriptional activity. J. Biol. Chem. *283*, 4022-4030.

Fayazi,Z., Ghosh,S., Marion,S., Bao,X., Shero,M., and Kazemi-Esfarjani,P. (2006). A Drosophila ortholog of the human MRJ modulates polyglutamine toxicity and aggregation. Neurobiol. Dis. *24*, 226-244.

Fearnley,J.M. and Lees,A.J. (1991). Ageing and Parkinson's disease: substantia nigra regional selectivity. Brain *114 (Pt 5)*, 2283-2301.

Ferrante,R.J., Browne,S.E., Shinobu,L.A., Bowling,A.C., Baik,M.J., MacGarvey,U., Kowall,N.W., Brown,R.H., Jr., and Beal,M.F. (1997). Evidence of increased oxidative damage in both sporadic and familial amyotrophic lateral sclerosis. J. Neurochem. *69*, 2064-2074.

Ferrante,R.J., Kowall,N.W., Cipolloni,P.B., Storey,E., and Beal,M.F. (1993). Excitotoxin lesions in primates as a model for Huntington's disease: histopathologic and neurochemical characterization. Exp. Neurol. *119*, 46-71.

Firdaus,W.J., Wyttenbach,A., az-Latoud,C., Currie,R.W., and Arrigo,A.P. (2006a). Analysis of oxidative events induced by expanded polyglutamine huntingtin exon 1 that are differentially restored by expression of heat shock proteins or treatment with an antioxidant. FEBS J. *273*, 3076-3093.

Firdaus,W.J., Wyttenbach,A., Giuliano,P., Kretz-Remy,C., Currie,R.W., and Arrigo,A.P. (2006b). Huntingtin inclusion bodies are iron-dependent centers of oxidative events. FEBS J. *273*, 5428-5441.

Fitzmaurice,P.S., Shaw,I.C., Kleiner,H.E., Miller,R.T., Monks,T.J., Lau,S.S., Mitchell,J.D., and Lynch,P.G. (1996). Evidence for DNA damage in amyotrophic lateral sclerosis. Muscle Nerve *19*, 797-798.

Floor,E. and Wetzel,M.G. (1998). Increased protein oxidation in human substantia nigra pars compacta in comparison with basal ganglia and prefrontal cortex measured with an improved dinitrophenylhydrazine assay. J. Neurochem. *70*, 268-275.

Gaestel,M. (2002). sHsp-phosphorylation: enzymes, signaling pathways and functional implications. Prog. Mol. Subcell. Biol. *28*, 151-169.

Gafni,J. and Ellerby,L.M. (2002). Calpain activation in Huntington's disease. J. Neurosci. *22*, 4842-4849.

Gafni,J., Hermel,E., Young,J.E., Wellington,C.L., Hayden,M.R., and Ellerby,L.M. (2004). Inhibition of calpain cleavage of huntingtin reduces toxicity: accumulation of calpain/caspase fragments in the nucleus. J. Biol. Chem. *279*, 20211-20220.

Gauthier,L.R., Charrin,B.C., Borrell-Pages,M., Dompierre,J.P., Rangone,H., Cordelieres,F.P., De,M.J., MacDonald,M.E., Lessmann,V., Humbert,S., and Saudou,F. (2004). Huntingtin controls neurotrophic support and survival of neurons by enhancing BDNF vesicular transport along microtubules. Cell *118*, 127-138.

Gerfen,C.R., McGinty,J.F., and Young,W.S., III (1991). Dopamine differentially regulates dynorphin, substance P, and enkephalin expression in striatal neurons: in situ hybridization histochemical analysis. J. Neurosci. *11*, 1016-1031.

Gething,M.J. and Sambrook,J. (1992). Protein folding in the cell. Nature *355*, 33-45.

Giorgini,F., Guidetti,P., Nguyen,Q., Bennett,S.C., and Muchowski,P.J. (2005). A genomic screen in yeast implicates kynurenine 3-monooxygenase as a therapeutic target for Huntington disease. Nat. Genet. *37*, 526-531.

Giuliano,P., De,C.T., Affaitati,A., Pizzulo,G.M., Feliciello,A., Criscuolo,C., De,M.G., Filla,A., Avvedimento,E.V., and Varrone,S. (2003). DNA damage induced by polyglutamine-expanded proteins. Hum. Mol. Genet. *12*, 2301-2309.

Goebel,H.H., Heipertz,R., Scholz,W., Iqbal,K., and Tellez-Nagel,I. (1978). Juvenile Huntington chorea: clinical, ultrastructural, and biochemical studies. Neurology *28*, 23-31.

Goehler,H., Lalowski,M., Stelzl,U., Waelter,S., Stroedicke,M., Worm,U., Droege,A., Lindenberg,K.S., Knoblich,M., Haenig,C., Herbst,M., Suopanki,J., Scherzinger,E., Abraham,C., Bauer,B., Hasenbank,R., Fritzsche,A., Ludewig,A.H., Bussow,K., Coleman,S.H., Gutekunst,C.A., Landwehrmeyer,B.G., Lehrach,H., and Wanker,E.E. (2004). A protein interaction network links GIT1, an enhancer of huntingtin aggregation, to Huntington's disease. Mol. Cell *15*, 853-865.

Goldberg,M.S., Pisani,A., Haburcak,M., Vortherms,T.A., Kitada,T., Costa,C., Tong,Y., Martella,G., Tscherter,A., Martins,A., Bernardi,G., Roth,B.L., Pothos,E.N., Calabresi,P., and Shen,J. (2005). Nigrostriatal dopaminergic deficits and hypokinesia caused by inactivation of the familial Parkinsonism-linked gene DJ-1. Neuron *45*, 489-496.

Gong,B., Lim,M.C., Wanderer,J., Wyttenbach,A., and Morton,A.J. (2008). Time-lapse analysis of aggregate formation in an inducible PC12 cell model of Huntington's disease reveals time-dependent aggregate formation that transiently delays cell death. Brain Res. Bull. *75*, 146-157.

Goodall,E.F. and Morrison,K.E. (2006). Amyotrophic lateral sclerosis (motor neuron disease): proposed mechanisms and pathways to treatment. Expert. Rev. Mol. Med. *8*, 1-22.

Gourfinkel-An,I., Cancel,G., Duyckaerts,C., Faucheux,B., Hauw,J.J., Trottier,Y., Brice,A., Agid,Y., and Hirsch,E.C. (1998). Neuronal distribution of intranuclear inclusions in Huntington's disease with adult onset. Neuroreport *9*, 1823-1826.

Graf,P.C. and Jakob,U. (2002). Redox-regulated molecular chaperones. Cell Mol. Life Sci. *59*, 1624-1631.

Graham,R.K., Deng,Y., Slow,E.J., Haigh,B., Bissada,N., Lu,G., Pearson,J., Shehadeh,J., Bertram,L., Murphy,Z., Warby,S.C., Doty,C.N., Roy,S., Wellington,C.L., Leavitt,B.R., Raymond,L.A., Nicholson,D.W., and Hayden,M.R. (2006). Cleavage at the caspase-6 site is required for neuronal dysfunction and degeneration due to mutant huntingtin. Cell *125*, 1179-1191.

Graumann,J., Lilie,H., Tang,X., Tucker,K.A., Hoffmann,J.H., Vijayalakshmi,J., Saper,M., Bardwell,J.C., and Jakob,U. (2001). Activation of the redox-regulated molecular chaperone Hsp33--a two-step mechanism. Structure. *9*, 377-387.

Gray,B.C., Siskova,Z., Perry,V.H., and O'Connor,V. (2009). Selective presynaptic degeneration in the synaptopathy associated with ME7-induced hippocampal pathology. Neurobiol. Dis. *35*, 63-74.

Greenlund,L.J., Deckwerth,T.L., and Johnson,E.M., Jr. (1995). Superoxide dismutase delays neuronal apoptosis: a role for reactive oxygen species in programmed neuronal death. Neuron *14*, 303-315.

Groeger,G., Quiney,C., and Cotter,T.G. (2009). Hydrogen peroxide as a cell-survival signaling molecule. Antioxid. Redox. Signal. *11*, 2655-2671.

Grundke-Iqbal,I., Iqbal,K., Quinlan,M., Tung,Y.C., Zaidi,M.S., and Wisniewski,H.M. (1986). Microtubule-associated protein tau. A component of Alzheimer paired helical filaments. J. Biol. Chem. *261*, 6084-6089.

Guentchev,M., Siedlak,S.L., Jarius,C., Tagliavini,F., Castellani,R.J., Perry,G., Smith,M.A., and Budka,H. (2002). Oxidative damage to nucleic acids in human prion disease. Neurobiol. Dis. *9*, 275-281.

Guentchev,M., Voigtlander,T., Haberler,C., Groschup,M.H., and Budka,H. (2000). Evidence for oxidative stress in experimental prion disease. Neurobiol. Dis. *7*, 270-273.

Gunawardena,S., Her,L.S., Brusch,R.G., Laymon,R.A., Niesman,I.R., Gordesky-Gold,B., Sintasath,L., Bonini,N.M., and Goldstein,L.S. (2003). Disruption of axonal transport by loss of huntingtin or expression of pathogenic polyQ proteins in Drosophila. Neuron *40*, 25-40.

Gusella,J.F. and MacDonald,M.E. (1995). Huntington's disease: CAG genetics expands neurobiology. Curr. Opin. Neurobiol. *5*, 656-662.

Gusella,J.F. and MacDonald,M.E. (2009). Huntington's disease: the case for genetic modifiers. Genome Med. *1*, 80.

Gutekunst,C.A., Levey,A.I., Heilman,C.J., Whaley,W.L., Yi,H., Nash,N.R., Rees,H.D., Madden,J.J., and Hersch,S.M. (1995). Identification and localization of huntingtin in brain and human lymphoblastoid cell lines with anti-fusion protein antibodies. Proc. Natl. Acad. Sci. U. S. A *92*, 8710-8714.

Gutekunst,C.A., Li,S.H., Yi,H., Ferrante,R.J., Li,X.J., and Hersch,S.M. (1998). The cellular and subcellular localization of huntingtin-associated protein 1 (HAP1): comparison with huntingtin in rat and human. J. Neurosci. *18*, 7674-7686.

Gutekunst,C.A., Li,S.H., Yi,H., Mulroy,J.S., Kuemmerle,S., Jones,R., Rye,D., Ferrante,R.J., Hersch,S.M., and Li,X.J. (1999). Nuclear and neuropil aggregates in Huntington's disease: relationship to neuropathology. J. Neurosci. *19*, 2522-2534.

Guyton A.C. and Hall J.E. (1996). Transport of oxygen and carbon dioxide in the blood and body fluids. In Textbook of medical physiology, (Philadelphia: Saunders), pp. 513-523.

Guyton,K.Z., Liu,Y., Gorospe,M., Xu,Q., and Holbrook,N.J. (1996). Activation of mitogen-activated protein kinase by H2O2. Role in cell survival following oxidant injury. J. Biol. Chem. *271*, 4138-4142.

Hackam,A.S., Singaraja,R., Wellington,C.L., Metzler,M., McCutcheon,K., Zhang,T., Kalchman,M., and Hayden,M.R. (1998). The influence of huntingtin protein size on nuclear localization and cellular toxicity. J. Cell Biol. *141*, 1097-1105.

Hailey,D.W., Rambold,A.S., Satpute-Krishnan,P., Mitra,K., Sougrat,R., Kim,P.K., and Lippincott-Schwartz,J. (2010). Mitochondria supply membranes for autophagosome biogenesis during starvation. Cell *141*, 656-667.

Halliwell,B. (1992). Reactive oxygen species and the central nervous system. J. Neurochem. *59*, 1609-1623.

Halliwell,B. and Gutteridge,J. (2007). Free Radicals in Biology and Medicine. Oxford University Press Inc).

Halliwell,B. and Whiteman,M. (2004). Measuring reactive species and oxidative damage in vivo and in cell culture: how should you do it and what do the results mean? Br. J. Pharmacol. *142*, 231-255.

Hamanaka,R.B. and Chandel,N.S. (2010). Mitochondrial reactive oxygen species regulate cellular signaling and dictate biological outcomes. Trends Biochem. Sci.

Han,S.J., Choi,K.Y., Brey,P.T., and Lee,W.J. (1998). Molecular cloning and characterization of a Drosophila p38 mitogen-activated protein kinase. J. Biol. Chem. *273*, 369-374.

Hands, S., Sajjad, M. U., and Wyttenbach, A. Polyglutamine aggregation causes free radical production *in vitro* and *in vivo*. 2010a.
Ref Type: Unpublished Work

Hands,S.L., Mason,R., Sajjad,M.U., Giorgini,F., and Wyttenbach,A. (2010b). Metallothioneins and copper metabolism are candidate therapeutic targets in Huntington's disease. Biochem. Soc. Trans. *38*, 552-558.

Hands,S.L., Proud,C.G., and Wyttenbach,A. (2009). mTOR's role in ageing: protein synthesis or autophagy? Aging (Albany. NY) *1*, 586-597.

Hands,S.L. and Wyttenbach,A. (2010). Neurotoxic protein oligomerisation associated with polyglutamine diseases. Acta Neuropathol.

Hanson,G.T., Aggeler,R., Oglesbee,D., Cannon,M., Capaldi,R.A., Tsien,R.Y., and Remington,S.J. (2004). Investigating mitochondrial redox potential with redox-sensitive green fluorescent protein indicators. J. Biol. Chem. *279*, 13044-13053.

Harman,D. (1981). The aging process. Proc. Natl. Acad. Sci. U. S. A *78*, 7124-7128.

Hartl,F.U. (1996). Molecular chaperones in cellular protein folding. Nature *381*, 571-579.

Hayashi,T., Ishimori,C., Takahashi-Niki,K., Taira,T., Kim,Y.C., Maita,H., Maita,C., Ariga,H., and Iguchi-Ariga,S.M. (2009). DJ-1 binds to mitochondrial complex I and maintains its activity. Biochem. Biophys. Res. Commun. *390*, 667-672.

Hefti,F., Melamed,E., and Wurtman,R.J. (1980). The decarboxylation of DOPA in the parkinsonian brain: in vivo studies on an animal model. J. Neural Transm. Suppl 95-101.

Hermel,E., Gafni,J., Propp,S.S., Leavitt,B.R., Wellington,C.L., Young,J.E., Hackam,A.S., Logvinova,A.V., Peel,A.L., Chen,S.F., Hook,V., Singaraja,R., Krajewski,S., Goldsmith,P.C., Ellerby,H.M., Hayden,M.R., Bredesen,D.E., and Ellerby,L.M. (2004). Specific caspase interactions and amplification are involved in selective neuronal vulnerability in Huntington's disease. Cell Death. Differ. *11*, 424-438.

Herzig,S., Long,F., Jhala,U.S., Hedrick,S., Quinn,R., Bauer,A., Rudolph,D., Schutz,G., Yoon,C., Puigserver,P., Spiegelman,B., and Montminy,M. (2001). CREB regulates hepatic gluconeogenesis through the coactivator PGC-1. Nature *413*, 179-183.

Ho,L.W., Carmichael,J., Swartz,J., Wyttenbach,A., Rankin,J., and Rubinsztein,D.C. (2001). The molecular biology of Huntington's disease. Psychol. Med. *31*, 3-14.

Hod,Y., Pentyala,S.N., Whyard,T.C., and El-Maghrabi,M.R. (1999). Identification and characterization of a novel protein that regulates RNA-protein interaction. J. Cell Biochem. *72*, 435-444.

Hodgson,J.G., Agopyan,N., Gutekunst,C.A., Leavitt,B.R., LePiane,F., Singaraja,R., Smith,D.J., Bissada,N., McCutcheon,K., Nasir,J., Jamot,L., Li,X.J., Stevens,M.E., Rosemond,E., Roder,J.C., Phillips,A.G., Rubin,E.M., Hersch,S.M., and Hayden,M.R. (1999). A YAC mouse model for Huntington's disease with full-length mutant huntingtin, cytoplasmic toxicity, and selective striatal neurodegeneration. Neuron *23*, 181-192.

Honbou,K., Suzuki,N.N., Horiuchi,M., Niki,T., Taira,T., Ariga,H., and Inagaki,F. (2003). The crystal structure of DJ-1, a protein related to male fertility and Parkinson's disease. J. Biol. Chem. *278*, 31380-31384.

Hong,Z., Shi,M., Chung,K.A., Quinn,J.F., Peskind,E.R., Galasko,D., Jankovic,J., Zabetian,C.P., Leverenz,J.B., Baird,G., Montine,T.J., Hancock,A.M., Hwang,H., Pan,C., Bradner,J., Kang,U.J., Jensen,P.H., and Zhang,J. (2010). DJ-1 and alpha-synuclein in human cerebrospinal fluid as biomarkers of Parkinson's disease. Brain *133*, 713-726.

Horvath,M.M. and Grishin,N.V. (2001). The C-terminal domain of HPII catalase is a member of the type I glutamine amidotransferase superfamily. Proteins *42*, 230-236.

Horwitz,J. (2003). Alpha-crystallin. Exp. Eye Res. *76*, 145-153.

Howarth,J.L., Kelly,S., Keasey,M.P., Glover,C.P., Lee,Y.B., Mitrophanous,K., Chapple,J.P., Gallo,J.M., Cheetham,M.E., and Uney,J.B. (2007). Hsp40 molecules that target to the ubiquitin-proteasome system decrease inclusion formation in models of polyglutamine disease. Mol. Ther. *15*, 1100-1105.

Hsieh,C.C. and Papaconstantinou,J. (2006). Thioredoxin-ASK1 complex levels regulate ROS-mediated p38 MAPK pathway activity in livers of aged and long-lived Snell dwarf mice. FASEB J. *20*, 259-268.

Huai,Q., Sun,Y., Wang,H., Chin,L.S., Li,L., Robinson,H., and Ke,H. (2003). Crystal structure of DJ-1/RS and implication on familial Parkinson's disease. FEBS Lett. *549*, 171-175.

Huntington Study Group (2001). A randomized, placebo-controlled trial of coenzyme Q10 and remacemide in Huntington's disease. Neurology *57*, 397-404.

Huot,J., Houle,F., Marceau,F., and Landry,J. (1997). Oxidative stress-induced actin reorganization mediated by the p38 mitogen-activated protein kinase/heat shock protein 27 pathway in vascular endothelial cells. Circ. Res. *80*, 383-392.

Hyun,T.S. and Ross,T.S. (2004). HIP1: trafficking roles and regulation of tumorigenesis. Trends Mol. Med. *10*, 194-199.

Ichijo,H., Nishida,E., Irie,K., ten,D.P., Saitoh,M., Moriguchi,T., Takagi,M., Matsumoto,K., Miyazono,K., and Gotoh,Y. (1997). Induction of apoptosis by ASK1, a mammalian MAPKKK that activates SAPK/JNK and p38 signaling pathways. Science *275*, 90-94.

Im,J.Y., Lee,K.W., Junn,E., and Mouradian,M.M. (2010). DJ-1 protects against oxidative damage by regulating the thioredoxin/ASK1 complex. Neurosci. Res. *67*, 203-208.

Ito,G., Ariga,H., Nakagawa,Y., and Iwatsubo,T. (2006). Roles of distinct cysteine residues in S-nitrosylation and dimerization of DJ-1. Biochem. Biophys. Res. Commun. *339*, 667-672.

Jacobsen,J.C., Bawden,C.S., Rudiger,S.R., McLaughlan,C.J., Reid,S.J., Waldvogel,H.J., MacDonald,M.E., Gusella,J.F., Walker,S.K., Kelly,J.M., Webb,G.C., Faull,R.L., Rees,M.I., and Snell,R.G. (2010). An ovine transgenic Huntington's disease model. Hum. Mol. Genet. *19*, 1873-1882.

Jakob,U., Muse,W., Eser,M., and Bardwell,J.C. (1999). Chaperone activity with a redox switch. Cell *96*, 341-352.

James,A.M., Sharpley,M.S., Manas,A.R., Frerman,F.E., Hirst,J., Smith,R.A., and Murphy,M.P. (2007). Interaction of the mitochondria-targeted antioxidant MitoQ with phospholipid bilayers and ubiquinone oxidoreductases. J. Biol. Chem. *282*, 14708-14718.

Jana,N.R., Tanaka,M., Wang,G., and Nukina,N. (2000). Polyglutamine length-dependent interaction of Hsp40 and Hsp70 family chaperones with truncated N-terminal huntingtin: their role in suppression of aggregation and cellular toxicity. Hum. Mol. Genet. *9*, 2009-2018.

Jauslin,M.L., Meier,T., Smith,R.A., and Murphy,M.P. (2003). Mitochondria-targeted antioxidants protect Friedreich Ataxia fibroblasts from endogenous oxidative stress more effectively than untargeted antioxidants. FASEB J. *17*, 1972-1974.

Jellinger,K.A. (2006). Alzheimer. J. Neural Transm. *113*, 1603-1623.

Jenkins,B.G., Koroshetz,W.J., Beal,M.F., and Rosen,B.R. (1993). Evidence for impairment of energy metabolism in vivo in Huntington's disease using localized 1H NMR spectroscopy. Neurology *43*, 2689-2695.

Jin,H., Randazzo,J., Zhang,P., and Kador,P.F. (2010). Multifunctional antioxidants for the treatment of age-related diseases. J. Med. Chem. *53*, 1117-1127.

Jones,A.L. (1999). The localization and interactions of huntingtin. Philos. Trans. R. Soc. Lond B Biol. Sci. *354*, 1021-1027.

Jorm,A.F., Korten,A.E., and Henderson,A.S. (1987). The prevalence of dementia: a quantitative integration of the literature. Acta Psychiatr. Scand. *76*, 465-479.

Junn,E., Taniguchi,H., Jeong,B.S., Zhao,X., Ichijo,H., and Mouradian,M.M. (2005). Interaction of DJ-1 with Daxx inhibits apoptosis signal-regulating kinase 1 activity and cell death. Proc. Natl. Acad. Sci. U. S. A *102*, 9691-9696.

Kadowaki,H., Nishitoh,H., Urano,F., Sadamitsu,C., Matsuzawa,A., Takeda,K., Masutani,H., Yodoi,J., Urano,Y., Nagano,T., and Ichijo,H. (2005). Amyloid beta induces neuronal cell death through ROS-mediated ASK1 activation. Cell Death. Differ. *12*, 19-24.

Kahle,P.J., Waak,J., and Gasser,T. (2009). DJ-1 and prevention of oxidative stress in Parkinson's disease and other age-related disorders. Free Radic. Biol. Med. *47*, 1354-1361.

Kalchman,M.A., Koide,H.B., McCutcheon,K., Graham,R.K., Nichol,K., Nishiyama,K., Kazemi-Esfarjani,P., Lynn,F.C., Wellington,C., Metzler,M., Goldberg,Y.P., Kanazawa,I., Gietz,R.D., and Hayden,M.R. (1997). HIP1, a human homologue of S. cerevisiae Sla2p, interacts with membrane-associated huntingtin in the brain. Nat. Genet. *16*, 44-53.

Kamata,H. and Hirata,H. (1999). Redox regulation of cellular signalling. Cell Signal. *11*, 1-14.

Karbowski,M., Arnoult,D., Chen,H., Chan,D.C., Smith,C.L., and Youle,R.J. (2004). Quantitation of mitochondrial dynamics by photolabeling of individual organelles shows that mitochondrial fusion is blocked during the Bax activation phase of apoptosis. J. Cell Biol. *164*, 493-499.

Kasparova,S., Sumbalova,Z., Bystricky,P., Kucharska,J., Liptaj,T., Mlynarik,V., and Gvozdjakova,A. (2006). Effect of coenzyme Q10 and vitamin E on brain energy metabolism in the animal model of Huntington's disease. Neurochem. Int. *48*, 93-99.

Kass-Eisler,A., Falck-Pedersen,E., Alvira,M., Rivera,J., Buttrick,P.M., Wittenberg,B.A., Cipriani,L., and Leinwand,L.A. (1993). Quantitative determination of adenovirus-mediated gene delivery to rat cardiac myocytes in vitro and in vivo. Proc. Natl. Acad. Sci. U. S. A *90*, 11498-11502.

Kazantsev,A., Preisinger,E., Dranovsky,A., Goldgaber,D., and Housman,D. (1999). Insoluble detergent-resistant aggregates form between pathological and

nonpathological lengths of polyglutamine in mammalian cells. Proc. Natl. Acad. Sci. U. S. A *96*, 11404-11409.

Kelly,D.P. and Scarpulla,R.C. (2004). Transcriptional regulatory circuits controlling mitochondrial biogenesis and function. Genes Dev. *18*, 357-368.

Kelso,G.F., Porteous,C.M., Coulter,C.V., Hughes,G., Porteous,W.K., Ledgerwood,E.C., Smith,R.A., and Murphy,M.P. (2001). Selective targeting of a redox-active ubiquinone to mitochondria within cells: antioxidant and antiapoptotic properties. J. Biol. Chem. *276*, 4588-4596.

Khoshnan,A., Ko,J., Watkin,E.E., Paige,L.A., Reinhart,P.H., and Patterson,P.H. (2004). Activation of the IkappaB kinase complex and nuclear factor-kappaB contributes to mutant huntingtin neurotoxicity. J. Neurosci. *24*, 7999-8008.

Kiechle,T., Dedeoglu,A., Kubilus,J., Kowall,N.W., Beal,M.F., Friedlander,R.M., Hersch,S.M., and Ferrante,R.J. (2002). Cytochrome C and caspase-9 expression in Huntington's disease. Neuromolecular. Med. *1*, 183-195.

Kim,M.W., Chelliah,Y., Kim,S.W., Otwinowski,Z., and Bezprozvanny,I. (2009). Secondary structure of Huntingtin amino-terminal region. Structure. *17*, 1205-1212.

Kim,M., Lee,H.S., LaForet,G., McIntyre,C., Martin,E.J., Chang,P., Kim,T.W., Williams,M., Reddy,P.H., Tagle,D., Boyce,F.M., Won,L., Heller,A., Aronin,N., and DiFiglia,M. (1999). Mutant huntingtin expression in clonal striatal cells: dissociation of inclusion formation and neuronal survival by caspase inhibition. J. Neurosci. *19*, 964-973.

Kim,R.H., Smith,P.D., Aleyasin,H., Hayley,S., Mount,M.P., Pownall,S., Wakeham,A., You-Ten,A.J., Kalia,S.K., Horne,P., Westaway,D., Lozano,A.M., Anisman,H., Park,D.S., and Mak,T.W. (2005). Hypersensitivity of DJ-1-deficient mice to 1-methyl-4-phenyl-1,2,3,6-tetrahydropyrindine (MPTP) and oxidative stress. Proc. Natl. Acad. Sci. U. S. A *102*, 5215-5220.

Kim,Y.J., Yi,Y., Sapp,E., Wang,Y., Cuiffo,B., Kegel,K.B., Qin,Z.H., Aronin,N., and DiFiglia,M. (2001). Caspase 3-cleaved N-terminal fragments of wild-type and mutant huntingtin are present in normal and Huntington's disease brains, associate with membranes, and undergo calpain-dependent proteolysis. Proc. Natl. Acad. Sci. U. S. A *98*, 12784-12789.

King,M.A., Goemans,C.G., Hafiz,F., Prehn,J.H., Wyttenbach,A., and Tolkovsky,A.M. (2008a). Cytoplasmic inclusions of Htt exon1 containing an expanded polyglutamine tract suppress execution of apoptosis in sympathetic neurons. J. Neurosci. *28*, 14401-14415.

King,M.A., Hands,S., Hafiz,F., Mizushima,N., Tolkovsky,A.M., and Wyttenbach,A. (2008b). Rapamycin inhibits polyglutamine aggregation independently of autophagy by reducing protein synthesis. Mol. Pharmacol. *73*, 1052-1063.

King,M.P. and Attardi,G. (1989). Human cells lacking mtDNA: repopulation with exogenous mitochondria by complementation. Science *246*, 500-503.

King,M.P. and Attardi,G. (1996). Isolation of human cell lines lacking mitochondrial DNA. Methods Enzymol. *264*, 304-313.

Kinumi,T., Kimata,J., Taira,T., Ariga,H., and Niki,E. (2004). Cysteine-106 of DJ-1 is the most sensitive cysteine residue to hydrogen peroxide-mediated oxidation in vivo in human umbilical vein endothelial cells. Biochem. Biophys. Res. Commun. *317*, 722-728.

Kirkland,R.A. and Franklin,J.L. (2007). Bax affects production of reactive oxygen by the mitochondria of non-apoptotic neurons. Exp. Neurol. *204*, 458-461.

Kirkland,R.A., Windelborn,J.A., Kasprzak,J.M., and Franklin,J.L. (2002). A Bax-induced pro-oxidant state is critical for cytochrome c release during programmed neuronal death. J. Neurosci. *22*, 6480-6490.

Kirshenbaum,L.A., MacLellan,W.R., Mazur,W., French,B.A., and Schneider,M.D. (1993). Highly efficient gene transfer into adult ventricular myocytes by recombinant adenovirus. J. Clin. Invest *92*, 381-387.

Kita,H., Carmichael,J., Swartz,J., Muro,S., Wyttenbach,A., Matsubara,K., Rubinsztein,D.C., and Kato,K. (2002). Modulation of polyglutamine-induced cell death by genes identified by expression profiling. Hum. Mol. Genet. *11*, 2279-2287.

Klemenz,R., Frohli,E., Steiger,R.H., Schafer,R., and Aoyama,A. (1991). Alpha B-crystallin is a small heat shock protein. Proc. Natl. Acad. Sci. U. S. A *88*, 3652-3656.

Klepac,N., Relja,M., Klepac,R., Hecimovic,S., Babic,T., and Trkulja,V. (2007). Oxidative stress parameters in plasma of Huntington's disease patients, asymptomatic Huntington's disease gene carriers and healthy subjects : a cross-sectional study. J. Neurol. *254*, 1676-1683.

Klinefelter,G.R., Welch,J.E., Perreault,S.D., Moore,H.D., Zucker,R.M., Suarez,J.D., Roberts,N.L., Bobseine,K., and Jeffay,S. (2002). Localization of the sperm protein SP22 and inhibition of fertility in vivo and in vitro. J. Androl *23*, 48-63.

Kondoh,H., Lleonart,M.E., Gil,J., Wang,J., Degan,P., Peters,G., Martinez,D., Carnero,A., and Beach,D. (2005). Glycolytic enzymes can modulate cellular life span. Cancer Res. *65*, 177-185.

Korhonen,L. and Lindholm,D. (2004). The ubiquitin proteasome system in synaptic and axonal degeneration: a new twist to an old cycle. J. Cell Biol. *165*, 27-30.

Koroshetz,W.J., Jenkins,B.G., Rosen,B.R., and Beal,M.F. (1997). Energy metabolism defects in Huntington's disease and effects of coenzyme Q10. Ann. Neurol. *41*, 160-165.

Kotaria,N., Hinz,U., Zechel,S., and von Bohlen Und,H.O. (2005). Localization of DJ-1 protein in the murine brain. Cell Tissue Res. *322*, 503-507.

Kovtun,I.V., Liu,Y., Bjoras,M., Klungland,A., Wilson,S.H., and McMurray,C.T. (2007). OGG1 initiates age-dependent CAG trinucleotide expansion in somatic cells. Nature *447*, 447-452.

Krebiehl,G., Ruckerbauer,S., Burbulla,L.F., Kieper,N., Maurer,B., Waak,J., Wolburg,H., Gizatullina,Z., Gellerich,F.N., Woitalla,D., Riess,O., Kahle,P.J., Proikas-Cezanne,T., and Kruger,R. (2010). Reduced basal autophagy and impaired mitochondrial dynamics due to loss of Parkinson's disease-associated protein DJ-1. PLoS. One. *5*, e9367.

Kremer,H.P., Roos,R.A., Dingjan,G., Marani,E., and Bots,G.T. (1990). Atrophy of the hypothalamic lateral tuberal nucleus in Huntington's disease. J. Neuropathol. Exp. Neurol. *49*, 371-382.

Krobitsch,S. and Lindquist,S. (2000). Aggregation of huntingtin in yeast varies with the length of the polyglutamine expansion and the expression of chaperone proteins. Proc. Natl. Acad. Sci. U. S. A *97*, 1589-1594.

Kuemmerle,S., Gutekunst,C.A., Klein,A.M., Li,X.J., Li,S.H., Beal,M.F., Hersch,S.M., and Ferrante,R.J. (1999). Huntington aggregates may not predict neuronal death in Huntington's disease. Ann. Neurol. *46*, 842-849.

Kuhl,D.E., Markham,C.H., Metter,E.J., Riege,W.H., Phelps,M.E., and Mazziotta,J.C. (1985). Local cerebral glucose utilization in symptomatic and presymptomatic Huntington's disease. Res. Publ. Assoc. Res. Nerv. Ment. Dis. *63*, 199-209.

Kullik,I., Toledano,M.B., Tartaglia,L.A., and Storz,G. (1995). Mutational analysis of the redox-sensitive transcriptional regulator OxyR: regions important for oxidation and transcriptional activation. J. Bacteriol. *177*, 1275-1284.

Kuwert,T., Lange,H.W., Langen,K.J., Herzog,H., Aulich,A., and Feinendegen,L.E. (1990). Cortical and subcortical glucose consumption measured by PET in patients with Huntington's disease. Brain *113 (Pt 5)*, 1405-1423.

Laferla,F.M. and Oddo,S. (2005). Alzheimer's disease: Abeta, tau and synaptic dysfunction. Trends Mol. Med. *11*, 170-176.

Landles,C. and Bates,G.P. (2004). Huntingtin and the molecular pathogenesis of Huntington's disease. Fourth in molecular medicine review series. EMBO Rep. *5*, 958-963.

Landles,C., Sathasivam,K., Weiss,A., Woodman,B., Moffitt,H., Finkbeiner,S., Sun,B., Gafni,J., Ellerby,L.M., Trottier,Y., Richards,W.G., Osmand,A., Paganetti,P., and Bates,G.P. (2010). Proteolysis of mutant huntingtin produces an exon 1 fragment that accumulates as an aggregated protein in neuronal nuclei in Huntington disease. J. Biol. Chem. *285*, 8808-8823.

Lathrop,R.H., Casale,M., Tobias,D.J., Marsh,J.L., and Thompson,L.M. (1998). Modeling protein homopolymeric repeats: possible polyglutamine structural motifs for Huntington's disease. Proc. Int. Conf. Intell. Syst. Mol. Biol. *6*, 105-114.

LaVoie,M.J., Cortese,G.P., Ostaszewski,B.L., and Schlossmacher,M.G. (2007). The effects of oxidative stress on parkin and other E3 ligases. J. Neurochem. *103*, 2354-2368.

Lecker,S.H., Goldberg,A.L., and Mitch,W.E. (2006). Protein degradation by the ubiquitin-proteasome pathway in normal and disease states. J. Am. Soc. Nephrol. *17*, 1807-1819.

Lee,G. and Rook,S.L. (1992). Expression of tau protein in non-neuronal cells: microtubule binding and stabilization. J. Cell Sci. *102 (Pt 2)*, 227-237.

Lee,S., Jeong,S.Y., Lim,W.C., Kim,S., Park,Y.Y., Sun,X., Youle,R.J., and Cho,H. (2007). Mitochondrial fission and fusion mediators, hFis1 and OPA1, modulate cellular senescence. J. Biol. Chem. *282*, 22977-22983.

Lee,S.J., Kim,S.J., Kim,I.K., Ko,J., Jeong,C.S., Kim,G.H., Park,C., Kang,S.O., Suh,P.G., Lee,H.S., and Cha,S.S. (2003). Crystal structures of human DJ-1 and Escherichia coli Hsp31, which share an evolutionarily conserved domain. J. Biol. Chem. *278*, 44552-44559.

Legendre-Guillemin,V., Metzler,M., Charbonneau,M., Gan,L., Chopra,V., Philie,J., Hayden,M.R., and McPherson,P.S. (2002). HIP1 and HIP12 display differential binding to F-actin, AP2, and clathrin. Identification of a novel interaction with clathrin light chain. J. Biol. Chem. *277*, 19897-19904.

Legleiter,J., Mitchell,E., Lotz,G.P., Sapp,E., Ng,C., DiFiglia,M., Thompson,L.M., and Muchowski,P.J. (2010). Mutant huntingtin fragments form oligomers in a polyglutamine length-dependent manner in vitro and in vivo. J. Biol. Chem. *285*, 14777-14790.

Lev,N., Ickowicz,D., Barhum,Y., Blondheim,N., Melamed,E., and Offen,D. (2006). Experimental encephalomyelitis induces changes in DJ-1: implications for oxidative stress in multiple sclerosis. Antioxid. Redox. Signal. *8*, 1987-1995.

Levine,R.L., Moskovitz,J., and Stadtman,E.R. (2000). Oxidation of methionine in proteins: roles in antioxidant defense and cellular regulation. IUBMB. Life *50*, 301-307.

Li,H., Li,S.H., Yu,Z.X., Shelbourne,P., and Li,X.J. (2001). Huntingtin aggregate-associated axonal degeneration is an early pathological event in Huntington's disease mice. J. Neurosci. *21*, 8473-8481.

Li,J.Y., Popovic,N., and Brundin,P. (2005). The use of the R6 transgenic mouse models of Huntington's disease in attempts to develop novel therapeutic strategies. NeuroRx. *2*, 447-464.

Li,P., Nijhawan,D., Budihardjo,I., Srinivasula,S.M., Ahmad,M., Alnemri,E.S., and Wang,X. (1997). Cytochrome c and dATP-dependent formation of Apaf-1/caspase-9 complex initiates an apoptotic protease cascade. Cell *91*, 479-489.

Li,R.C., Pouranfar,F., Lee,S.K., Morris,M.W., Wang,Y., and Gozal,D. (2008). Neuroglobin protects PC12 cells against beta-amyloid-induced cell injury. Neurobiol. Aging *29*, 1815-1822.

Li,S.H. and Li,X.J. (1998). Aggregation of N-terminal huntingtin is dependent on the length of its glutamine repeats. Hum. Mol. Genet. *7*, 777-782.

Li,S.H. and Li,X.J. (2004a). Huntingtin and its role in neuronal degeneration. Neuroscientist. *10*, 467-475.

Li,S.H. and Li,X.J. (2004b). Huntingtin-protein interactions and the pathogenesis of Huntington's disease. Trends Genet. *20*, 146-154.

Li,X., Standley,C., Sapp,E., Valencia,A., Qin,Z.H., Kegel,K.B., Yoder,J., Comer-Tierney,L.A., Esteves,M., Chase,K., Alexander,J., Masso,N., Sobin,L., Bellve,K., Tuft,R., Lifshitz,L., Fogarty,K., Aronin,N., and DiFiglia,M. (2009). Mutant huntingtin impairs vesicle formation from recycling endosomes by interfering with Rab11 activity. Mol. Cell Biol. *29*, 6106-6116.

Li,X., Valencia,A., Sapp,E., Masso,N., Alexander,J., Reeves,P., Kegel,K.B., Aronin,N., and DiFiglia,M. (2010). Aberrant Rab11-dependent trafficking of the neuronal glutamate transporter EAAC1 causes oxidative stress and cell death in Huntington's disease. J. Neurosci. *30*, 4552-4561.

Li,X.J., Li,S.H., Sharp,A.H., Nucifora,F.C., Jr., Schilling,G., Lanahan,A., Worley,P., Snyder,S.H., and Ross,C.A. (1995). A huntingtin-associated protein enriched in brain with implications for pathology. Nature *378*, 398-402.

Lin,J., Handschin,C., and Spiegelman,B.M. (2005). Metabolic control through the PGC-1 family of transcription coactivators. Cell Metab *1*, 361-370.

Lin,J., Wu,H., Tarr,P.T., Zhang,C.Y., Wu,Z., Boss,O., Michael,L.F., Puigserver,P., Isotani,E., Olson,E.N., Lowell,B.B., Bassel-Duby,R., and Spiegelman,B.M. (2002). Transcriptional co-activator PGC-1 alpha drives the formation of slow-twitch muscle fibres. Nature *418*, 797-801.

Lin,J., Wu,P.H., Tarr,P.T., Lindenberg,K.S., St-Pierre,J., Zhang,C.Y., Mootha,V.K., Jager,S., Vianna,C.R., Reznick,R.M., Cui,L., Manieri,M., Donovan,M.X., Wu,Z., Cooper,M.P., Fan,M.C., Rohas,L.M., Zavacki,A.M., Cinti,S., Shulman,G.I., Lowell,B.B., Krainc,D., and Spiegelman,B.M. (2004). Defects in adaptive energy metabolism with CNS-linked hyperactivity in PGC-1alpha null mice. Cell *119*, 121-135.

Lin,M.T. and Beal,M.F. (2006). Mitochondrial dysfunction and oxidative stress in neurodegenerative diseases. Nature *443*, 787-795.

Liu,S., Li,J., Tao,Y., and Xiao,X. (2007). Small heat shock protein alphaB-crystallin binds to p53 to sequester its translocation to mitochondria during hydrogen peroxide-induced apoptosis. Biochem. Biophys. Res. Commun. *354*, 109-114.

Lo,Y.Y., Wong,J.M., and Cruz,T.F. (1996). Reactive oxygen species mediate cytokine activation of c-Jun NH2-terminal kinases. J. Biol. Chem. *271*, 15703-15707.

Logan,T., Clark,L., and Ray,S.S. (2010). Engineered disulfide bonds restores chaperone like function of DJ-1 mutants linked to familial Parkinson's disease. Biochemistry.

Lonze,B.E. and Ginty,D.D. (2002). Function and regulation of CREB family transcription factors in the nervous system. Neuron *35*, 605-623.

Lu,T.Z., Quan,Y., and Feng,Z.P. (2010). Multifaceted Role of Heat Shock Protein 70 in Neurons. Mol. Neurobiol.

Lukosz,M., Jakob,S., Buchner,N., Zschauer,T.C., Altschmied,J., and Haendeler,J. (2010). Nuclear redox signaling. Antioxid. Redox. Signal. *12*, 713-742.

Lunkes,A., Lindenberg,K.S., Ben-Haiem,L., Weber,C., Devys,D., Landwehrmeyer,G.B., Mandel,J.L., and Trottier,Y. (2002). Proteases acting on mutant huntingtin generate cleaved products that differentially build up cytoplasmic and nuclear inclusions. Mol. Cell *10*, 259-269.

Lunkes,A. and Mandel,J.L. (1998). A cellular model that recapitulates major pathogenic steps of Huntington's disease. Hum. Mol. Genet. *7*, 1355-1361.

Luthi-Carter,R., Strand,A., Peters,N.L., Solano,S.M., Hollingsworth,Z.R., Menon,A.S., Frey,A.S., Spektor,B.S., Penney,E.B., Schilling,G., Ross,C.A., Borchelt,D.R., Tapscott,S.J., Young,A.B., Cha,J.H., and Olson,J.M. (2000). Decreased expression of striatal signaling genes in a mouse model of Huntington's disease. Hum. Mol. Genet. *9*, 1259-1271.

Luthi-Carter,R., Strand,A.D., Hanson,S.A., Kooperberg,C., Schilling,G., La Spada,A.R., Merry,D.E., Young,A.B., Ross,C.A., Borchelt,D.R., and Olson,J.M. (2002). Polyglutamine and transcription: gene expression changes shared by DRPLA and Huntington's disease mouse models reveal context-independent effects. Hum. Mol. Genet. *11*, 1927-1937.

Ma,J. and Lindquist,S. (2002). Conversion of PrP to a self-perpetuating PrPSc-like conformation in the cytosol. Science *298*, 1785-1788.

Ma,J., Wollmann,R., and Lindquist,S. (2002). Neurotoxicity and neurodegeneration when PrP accumulates in the cytosol. Science *298*, 1781-1785.

Macedo,M.G., Anar,B., Bronner,I.F., Cannella,M., Squitieri,F., Bonifati,V., Hoogeveen,A., Heutink,P., and Rizzu,P. (2003). The DJ-1L166P mutant protein associated with early onset Parkinson's disease is unstable and forms higher-order protein complexes. Hum. Mol. Genet. *12*, 2807-2816.

Majoor-Krakauer,D., Willems,P.J., and Hofman,A. (2003). Genetic epidemiology of amyotrophic lateral sclerosis. Clin. Genet. *63*, 83-101.

Mancuso,M., Orsucci,D., Volpi,L., Calsolaro,V., and Siciliano,G. (2010). Coenzyme Q10 in neuromuscular and neurodegenerative disorders. Curr. Drug Targets. *11*, 111-121.

Manczak,M., Anekonda,T.S., Henson,E., Park,B.S., Quinn,J., and Reddy,P.H. (2006). Mitochondria are a direct site of A beta accumulation in Alzheimer's disease neurons: implications for free radical generation and oxidative damage in disease progression. Hum. Mol. Genet. *15*, 1437-1449.

Manczak,M., Park,B.S., Jung,Y., and Reddy,P.H. (2004). Differential expression of oxidative phosphorylation genes in patients with Alzheimer's disease: implications for

early mitochondrial dysfunction and oxidative damage. Neuromolecular. Med. *5*, 147-162.

Manev,H., Cagnoli,C.M., Atabay,C., Kharlamov,E., Ikonomovic,M.D., and Grayson,D.R. (1995). Neuronal apoptosis in an in vitro model of photochemically induced oxidative stress. Exp. Neurol. *133*, 198-206.

Mangiarini,L., Sathasivam,K., Seller,M., Cozens,B., Harper,A., Hetherington,C., Lawton,M., Trottier,Y., Lehrach,H., Davies,S.W., and Bates,G.P. (1996). Exon 1 of the HD gene with an expanded CAG repeat is sufficient to cause a progressive neurological phenotype in transgenic mice. Cell *87*, 493-506.

Mariani,E., Polidori,M.C., Cherubini,A., and Mecocci,P. (2005). Oxidative stress in brain aging, neurodegenerative and vascular diseases: an overview. J. Chromatogr. B Analyt. Technol. Biomed. Life Sci. *827*, 65-75.

Marsh,J.L., Pallos,J., and Thompson,L.M. (2003). Fly models of Huntington's disease. Hum. Mol. Genet. *12 Spec No 2*, R187-R193.

Martin,L.J., Liu,Z., Chen,K., Price,A.C., Pan,Y., Swaby,J.A., and Golden,W.C. (2007). Motor neuron degeneration in amyotrophic lateral sclerosis mutant superoxide dismutase-1 transgenic mice: mechanisms of mitochondriopathy and cell death. J. Comp Neurol. *500*, 20-46.

Martinat,C., Shendelman,S., Jonason,A., Leete,T., Beal,M.F., Yang,L., Floss,T., and Abeliovich,A. (2004). Sensitivity to oxidative stress in DJ-1-deficient dopamine neurons: an ES- derived cell model of primary Parkinsonism. PLoS. Biol. *2*, e327.

Martindale,D., Hackam,A., Wieczorek,A., Ellerby,L., Wellington,C., McCutcheon,K., Singaraja,R., Kazemi-Esfarjani,P., Devon,R., Kim,S.U., Bredesen,D.E., Tufaro,F., and Hayden,M.R. (1998). Length of huntingtin and its polyglutamine tract influences localization and frequency of intracellular aggregates. Nat. Genet. *18*, 150-154.

Martinon,F. (2010). Signaling by ROS drives inflammasome activation. Eur. J. Immunol. *40*, 616-619.

Mates,J.M., Perez-Gomez,C., and Nunez,d.C., I (1999). Antioxidant enzymes and human diseases. Clin. Biochem. *32*, 595-603.

Matsuzawa,A. and Ichijo,H. (2005). Stress-responsive protein kinases in redox-regulated apoptosis signaling. Antioxid. Redox. Signal. *7*, 472-481.

Matthews,R.T., Yang,L., Jenkins,B.G., Ferrante,R.J., Rosen,B.R., Kaddurah-Daouk,R., and Beal,M.F. (1998). Neuroprotective effects of creatine and cyclocreatine in animal models of Huntington's disease. J. Neurosci. *18*, 156-163.

Maynard,C.J., Bottcher,C., Ortega,Z., Smith,R., Florea,B.I., Diaz-Hernandez,M., Brundin,P., Overkleeft,H.S., Li,J.Y., Lucas,J.J., and Dantuma,N.P. (2009). Accumulation of ubiquitin conjugates in a polyglutamine disease model occurs without global ubiquitin/proteasome system impairment. Proc. Natl. Acad. Sci. U. S. A *106*, 13986-13991.

Mazzola,J.L. and Sirover,M.A. (2001). Reduction of glyceraldehyde-3-phosphate dehydrogenase activity in Alzheimer's disease and in Huntington's disease fibroblasts. J. Neurochem. *76*, 442-449.

McGill,J.K. and Beal,M.F. (2006). PGC-1alpha, a new therapeutic target in Huntington's disease? Cell *127*, 465-468.

Mead,S. (2006). Prion disease genetics. Eur. J. Hum. Genet. *14*, 273-281.

Mecocci,P., MacGarvey,U., and Beal,M.F. (1994). Oxidative damage to mitochondrial DNA is increased in Alzheimer's disease. Ann. Neurol. *36*, 747-751.

Mehlen,P., Hickey,E., Weber,L.A., and Arrigo,A.P. (1997). Large unphosphorylated aggregates as the active form of hsp27 which controls intracellular reactive oxygen species and glutathione levels and generates a protection against TNFalpha in NIH-3T3-ras cells. Biochem. Biophys. Res. Commun. *241*, 187-192.

Mehlen,P., Kretz-Remy,C., Preville,X., and Arrigo,A.P. (1996). Human hsp27, Drosophila hsp27 and human alphaB-crystallin expression-mediated increase in glutathione is essential for the protective activity of these proteins against TNFalpha-induced cell death. EMBO J. *15*, 2695-2706.

Melo,J.B., Agostinho,P., and Oliveira,C.R. (2007). Prion protein aggregation and neurotoxicity in cortical neurons. Ann. N. Y. Acad. Sci. *1096*, 220-229.

Mende-Mueller,L.M., Toneff,T., Hwang,S.R., Chesselet,M.F., and Hook,V.Y. (2001). Tissue-specific proteolysis of Huntingtin (htt) in human brain: evidence of enhanced levels of N- and C-terminal htt fragments in Huntington's disease striatum. J. Neurosci. *21*, 1830-1837.

Meriin,A.B., Mabuchi,K., Gabai,V.L., Yaglom,J.A., Kazantsev,A., and Sherman,M.Y. (2001). Intracellular aggregation of polypeptides with expanded polyglutamine domain is stimulated by stress-activated kinase MEKK1. J. Cell Biol. *153*, 851-864.

Meulener,M., Whitworth,A.J., rmstrong-Gold,C.E., Rizzu,P., Heutink,P., Wes,P.D., Pallanck,L.J., and Bonini,N.M. (2005a). Drosophila DJ-1 mutants are selectively sensitive to environmental toxins associated with Parkinson's disease. Curr. Biol. *15*, 1572-1577.

Meulener,M.C., Graves,C.L., Sampathu,D.M., Armstrong-Gold,C.E., Bonini,N.M., and Giasson,B.I. (2005b). DJ-1 is present in a large molecular complex in human brain tissue and interacts with alpha-synuclein. J. Neurochem. *93*, 1524-1532.

Miller,D.W., Ahmad,R., Hague,S., Baptista,M.J., Canet-Aviles,R., McLendon,C., Carter,D.M., Zhu,P.P., Stadler,J., Chandran,J., Klinefelter,G.R., Blackstone,C., and Cookson,M.R. (2003). L166P mutant DJ-1, causative for recessive Parkinson's disease, is degraded through the ubiquitin-proteasome system. J. Biol. Chem. *278*, 36588-36595.

Mitra,S., Tsvetkov,A.S., and Finkbeiner,S. (2009). Protein turnover and inclusion body formation. Autophagy. *5*, 1037-1038.

Mitsumoto,A. and Nakagawa,Y. (2001). DJ-1 is an indicator for endogenous reactive oxygen species elicited by endotoxin. Free Radic. Res. *35*, 885-893.

Mitsumoto,A., Nakagawa,Y., Takeuchi,A., Okawa,K., Iwamatsu,A., and Takanezawa,Y. (2001). Oxidized forms of peroxiredoxins and DJ-1 on two-dimensional gels increased in response to sublethal levels of paraquat. Free Radic. Res. *35*, 301-310.

Miyazaki,S., Yanagida,T., Nunome,K., Ishikawa,S., Inden,M., Kitamura,Y., Nakagawa,S., Taira,T., Hirota,K., Niwa,M., Iguchi-Ariga,S.M., and Ariga,H. (2008). DJ-1-binding compounds prevent oxidative stress-induced cell death and movement defect in Parkinson's disease model rats. J. Neurochem. *105*, 2418-2434.

Mizuno,Y., Ohta,S., Tanaka,M., Takamiya,S., Suzuki,K., Sato,T., Oya,H., Ozawa,T., and Kagawa,Y. (1989). Deficiencies in complex I subunits of the respiratory chain in Parkinson's disease. Biochem. Biophys. Res. Commun. *163*, 1450-1455.

Mizushima,N. and Klionsky,D.J. (2007). Protein turnover via autophagy: implications for metabolism. Annu. Rev. Nutr. *27*, 19-40.

Mo,J.S., Kim,M.Y., Ann,E.J., Hong,J.A., and Park,H.S. (2008). DJ-1 modulates UV-induced oxidative stress signaling through the suppression of MEKK1 and cell death. Cell Death. Differ. *15*, 1030-1041.

Moncada,S. and Erusalimsky,J.D. (2002). Does nitric oxide modulate mitochondrial energy generation and apoptosis? Nat. Rev. Mol. Cell Biol. *3*, 214-220.

Moreau,K., Luo,S., and Rubinsztein,D.C. (2010). Cytoprotective roles for autophagy. Curr. Opin. Cell Biol. *22*, 206-211.

Moriguchi,T., Toyoshima,F., Gotoh,Y., Iwamatsu,A., Irie,K., Mori,E., Kuroyanagi,N., Hagiwara,M., Matsumoto,K., and Nishida,E. (1996). Purification and identification of a major activator for p38 from osmotically shocked cells. Activation of mitogen-activated protein kinase kinase 6 by osmotic shock, tumor necrosis factor-alpha, and H2O2. J. Biol. Chem. *271*, 26981-26988.

Morimoto,N., Nagai,M., Miyazaki,K., Ohta,Y., Kurata,T., Takehisa,Y., Ikeda,Y., Matsuura,T., Asanuma,M., and Abe,K. (2010). Induction of parkinsonism-related proteins in the spinal motor neurons of transgenic mouse carrying a mutant SOD1 gene. J. Neurosci. Res. *88*, 1804-1811.

Morrow,G., Inaguma,Y., Kato,K., and Tanguay,R.M. (2000). The small heat shock protein Hsp22 of Drosophila melanogaster is a mitochondrial protein displaying oligomeric organization. J. Biol. Chem. *275*, 31204-31210.

Mronga,T., Stahnke,T., Goldbaum,O., and Richter-Landsberg,C. (2004). Mitochondrial pathway is involved in hydrogen-peroxide-induced apoptotic cell death of oligodendrocytes. Glia *46*, 446-455.

Muchowski,P.J., Schaffar,G., Sittler,A., Wanker,E.E., Hayer-Hartl,M.K., and Hartl,F.U. (2000). Hsp70 and hsp40 chaperones can inhibit self-assembly of

polyglutamine proteins into amyloid-like fibrils. Proc. Natl. Acad. Sci. U. S. A *97*, 7841-7846.

Nagakubo,D., Taira,T., Kitaura,H., Ikeda,M., Tamai,K., Iguchi-Ariga,S.M., and Ariga,H. (1997). DJ-1, a novel oncogene which transforms mouse NIH3T3 cells in cooperation with ras. Biochem. Biophys. Res. Commun. *231*, 509-513.

Nance,M.A. and Myers,R.H. (2001). Juvenile onset Huntington's disease--clinical and research perspectives. Ment. Retard. Dev. Disabil. Res. Rev. *7*, 153-157.

Neumann,M., Muller,V., Gorner,K., Kretzschmar,H.A., Haass,C., and Kahle,P.J. (2004). Pathological properties of the Parkinson's disease-associated protein DJ-1 in alpha-synucleinopathies and tauopathies: relevance for multiple system atrophy and Pick's disease. Acta Neuropathol. *107*, 489-496.

Nicoli,F., Vion-Dury,J., Maloteaux,J.M., Delwaide,C., Confort-Gouny,S., Sciaky,M., and Cozzone,P.J. (1993). CSF and serum metabolic profile of patients with Huntington's chorea: a study by high resolution proton NMR spectroscopy and HPLC. Neurosci. Lett. *154*, 47-51.

Nishikawa,K., Li,H., Kawamura,R., Osaka,H., Wang,Y.L., Hara,Y., Hirokawa,T., Manago,Y., Amano,T., Noda,M., Aoki,S., and Wada,K. (2003). Alterations of structure and hydrolase activity of parkinsonism-associated human ubiquitin carboxyl-terminal hydrolase L1 variants. Biochem. Biophys. Res. Commun. *304*, 176-183.

Nishitoh,H., Saitoh,M., Mochida,Y., Takeda,K., Nakano,H., Rothe,M., Miyazono,K., and Ichijo,H. (1998). ASK1 is essential for JNK/SAPK activation by TRAF2. Mol. Cell *2*, 389-395.

Nixon,R.A. (2005). Endosome function and dysfunction in Alzheimer's disease and other neurodegenerative diseases. Neurobiol. Aging *26*, 373-382.

Noguchi,T., Takeda,K., Matsuzawa,A., Saegusa,K., Nakano,H., Gohda,J., Inoue,J., and Ichijo,H. (2005). Recruitment of tumor necrosis factor receptor-associated factor family proteins to apoptosis signal-regulating kinase 1 signalosome is essential for oxidative stress-induced cell death. J. Biol. Chem. *280*, 37033-37040.

Nucifora,F.C., Jr., Sasaki,M., Peters,M.F., Huang,H., Cooper,J.K., Yamada,M., Takahashi,H., Tsuji,S., Troncoso,J., Dawson,V.L., Dawson,T.M., and Ross,C.A. (2001). Interference by huntingtin and atrophin-1 with cbp-mediated transcription leading to cellular toxicity. Science *291*, 2423-2428.

Nural,H., He,P., Beach,T., Sue,L., Xia,W., and Shen,Y. (2009). Dissembled DJ-1 high molecular weight complex in cortex mitochondria from Parkinson's disease patients. Mol. Neurodegener. *4*, 23.

Olanow,C.W., Perl,D.P., DeMartino,G.N., and McNaught,K.S. (2004). Lewy-body formation is an aggresome-related process: a hypothesis. Lancet Neurol. *3*, 496-503.

Olshina,M.A., Angley,L.M., Ramdzan,Y.M., Tang,J., Bailey,M.F., Hill,A.F., and Hatters,D.M. (2010). Tracking mutant huntingtin aggregation kinetics in cells reveals

three major populations that include an invariant oligomer pool. J. Biol. Chem. *285*, 21807-21816.

Olzmann,J.A., Bordelon,J.R., Muly,E.C., Rees,H.D., Levey,A.I., Li,L., and Chin,L.S. (2007). Selective enrichment of DJ-1 protein in primate striatal neuronal processes: implications for Parkinson's disease. J. Comp Neurol. *500*, 585-599.

Olzmann,J.A., Brown,K., Wilkinson,K.D., Rees,H.D., Huai,Q., Ke,H., Levey,A.I., Li,L., and Chin,L.S. (2004). Familial Parkinson's disease-associated L166P mutation disrupts DJ-1 protein folding and function. J. Biol. Chem. *279*, 8506-8515.

Ona,V.O., Li,M., Vonsattel,J.P., Andrews,L.J., Khan,S.Q., Chung,W.M., Frey,A.S., Menon,A.S., Li,X.J., Stieg,P.E., Yuan,J., Penney,J.B., Young,A.B., Cha,J.H., and Friedlander,R.M. (1999). Inhibition of caspase-1 slows disease progression in a mouse model of Huntington's disease. Nature *399*, 263-267.

Ooe,H., Iguchi-Ariga,S.M., and Ariga,H. (2006). Establishment of specific antibodies that recognize C106-oxidized DJ-1. Neurosci. Lett. *404*, 166-169.

Pamplona,R., Naudi,A., Gavin,R., Pastrana,M.A., Sajnani,G., Ilieva,E.V., Del Rio,J.A., Portero-Otin,M., Ferrer,I., and Requena,J.R. (2008). Increased oxidation, glycoxidation, and lipoxidation of brain proteins in prion disease. Free Radic. Biol. Med. *45*, 1159-1166.

Panov,A.V., Gutekunst,C.A., Leavitt,B.R., Hayden,M.R., Burke,J.R., Strittmatter,W.J., and Greenamyre,J.T. (2002). Early mitochondrial calcium defects in Huntington's disease are a direct effect of polyglutamines. Nat. Neurosci. *5*, 731-736.

Parker,W.D., Jr., Boyson,S.J., Luder,A.S., and Parks,J.K. (1990). Evidence for a defect in NADH: ubiquinone oxidoreductase (complex I) in Huntington's disease. Neurology *40*, 1231-1234.

Parone,P.A., Da,C.S., Tondera,D., Mattenberger,Y., James,D.I., Maechler,P., Barja,F., and Martinou,J.C. (2008). Preventing mitochondrial fission impairs mitochondrial function and leads to loss of mitochondrial DNA. PLoS. One. *3*, e3257.

Patel,J.R. and Brewer,G.J. (2008). Age-related changes to tumor necrosis factor receptors affect neuron survival in the presence of beta-amyloid. J. Neurosci. Res. *86*, 2303-2313.

Pellerin,L. (2005). How astrocytes feed hungry neurons. Mol. Neurobiol. *32*, 59-72.

Perez-Severiano,F., Rios,C., and Segovia,J. (2000). Striatal oxidative damage parallels the expression of a neurological phenotype in mice transgenic for the mutation of Huntington's disease. Brain Res. *862*, 234-237.

Perez-Severiano,F., Santamaria,A., Pedraza-Chaverri,J., Medina-Campos,O.N., Rios,C., and Segovia,J. (2004). Increased formation of reactive oxygen species, but no changes in glutathione peroxidase activity, in striata of mice transgenic for the Huntington's disease mutation. Neurochem. Res. *29*, 729-733.

Perluigi,M., Poon,H.F., Maragos,W., Pierce,W.M., Klein,J.B., Calabrese,V., Cini,C., De,M.C., and Butterfield,D.A. (2005). Proteomic analysis of protein expression and oxidative modification in r6/2 transgenic mice: a model of Huntington disease. Mol. Cell Proteomics. *4*, 1849-1861.

Perrin,V., Regulier,E., Abbas-Terki,T., Hassig,R., Brouillet,E., Aebischer,P., Luthi-Carter,R., and Deglon,N. (2007). Neuroprotection by Hsp104 and Hsp27 in lentiviral-based rat models of Huntington's disease. Mol. Ther. *15*, 903-911.

Perutz,M. (1994). Polar zippers: their role in human disease. Protein Sci. *3*, 1629-1637.

Perutz,M.F. (1999). Glutamine repeats and neurodegenerative diseases: molecular aspects. Trends Biochem. Sci. *24*, 58-63.

Perutz,M.F., Finch,J.T., Berriman,J., and Lesk,A. (2002a). Amyloid fibers are water-filled nanotubes. Proc. Natl. Acad. Sci. U. S. A *99*, 5591-5595.

Perutz,M.F., Pope,B.J., Owen,D., Wanker,E.E., and Scherzinger,E. (2002b). Aggregation of proteins with expanded glutamine and alanine repeats of the glutamine-rich and asparagine-rich domains of Sup35 and of the amyloid beta-peptide of amyloid plaques. Proc. Natl. Acad. Sci. U. S. A *99*, 5596-5600.

Pletjushkina,O.Y., Lyamzaev,K.G., Popova,E.N., Nepryakhina,O.K., Ivanova,O.Y., Domnina,L.V., Chernyak,B.V., and Skulachev,V.P. (2006). Effect of oxidative stress on dynamics of mitochondrial reticulum. Biochim. Biophys. Acta *1757*, 518-524.

Polidori,M.C., Mecocci,P., Browne,S.E., Senin,U., and Beal,M.F. (1999). Oxidative damage to mitochondrial DNA in Huntington's disease parietal cortex. Neurosci. Lett. *272*, 53-56.

Pratico,D., MY,L., V, Trojanowski,J.Q., Rokach,J., and FitzGerald,G.A. (1998). Increased F2-isoprostanes in Alzheimer's disease: evidence for enhanced lipid peroxidation in vivo. FASEB J. *12*, 1777-1783.

Pratico,D., Uryu,K., Leight,S., Trojanoswki,J.Q., and Lee,V.M. (2001). Increased lipid peroxidation precedes amyloid plaque formation in an animal model of Alzheimer amyloidosis. J. Neurosci. *21*, 4183-4187.

Preisinger,E., Jordan,B.M., Kazantsev,A., and Housman,D. (1999). Evidence for a recruitment and sequestration mechanism in Huntington's disease. Philos. Trans. R. Soc. Lond B Biol. Sci. *354*, 1029-1034.

Prusiner,S.B. (1982). Novel proteinaceous infectious particles cause scrapie. Science *216*, 136-144.

Prusiner,S.B. (1998). Prions. Proc. Natl. Acad. Sci. U. S. A *95*, 13363-13383.

Puigserver,P., Wu,Z., Park,C.W., Graves,R., Wright,M., and Spiegelman,B.M. (1998). A cold-inducible coactivator of nuclear receptors linked to adaptive thermogenesis. Cell *92*, 829-839.

Purdom,S. and Chen,Q.M. (2005). Epidermal growth factor receptor-dependent and -independent pathways in hydrogen peroxide-induced mitogen-activated protein kinase activation in cardiomyocytes and heart fibroblasts. J. Pharmacol. Exp. Ther. *312*, 1179-1186.

Quintanilla,R.A. and Johnson,G.V. (2009). Role of mitochondrial dysfunction in the pathogenesis of Huntington's disease. Brain Res. Bull. *80*, 242-247.

Radesater,A.C., Johansson,S., Oberg,C., and Luthman,J. (2003). The vitamin-E analog trolox and the NMDA antagonist MK-801 protect pyramidal neurons in hippocampal slice cultures from IL-1beta-induced neurodegeneration. Neurotox. Res. *5*, 433-442.

Rajasekaran,N.S., Connell,P., Christians,E.S., Yan,L.J., Taylor,R.P., Orosz,A., Zhang,X.Q., Stevenson,T.J., Peshock,R.M., Leopold,J.A., Barry,W.H., Loscalzo,J., Odelberg,S.J., and Benjamin,I.J. (2007). Human alpha B-crystallin mutation causes oxido-reductive stress and protein aggregation cardiomyopathy in mice. Cell *130*, 427-439.

Ramsey,C.P. and Giasson,B.I. (2008). The E163K DJ-1 mutant shows specific antioxidant deficiency. Brain Res. *1239*, 1-11.

Ranen,N.G., Stine,O.C., Abbott,M.H., Sherr,M., Codori,A.M., Franz,M.L., Chao,N.I., Chung,A.S., Pleasant,N., Callahan,C., and . (1995). Anticipation and instability of IT-15 (CAG)n repeats in parent-offspring pairs with Huntington disease. Am. J. Hum. Genet. *57*, 593-602.

Ranganathan,S., Harmison,G.G., Meyertholen,K., Pennuto,M., Burnett,B.G., and Fischbeck,K.H. (2009). Mitochondrial abnormalities in spinal and bulbar muscular atrophy. Hum. Mol. Genet. *18*, 27-42.

Ratovitski,T., Nakamura,M., D'Ambola,J., Chighladze,E., Liang,Y., Wang,W., Graham,R., Hayden,M.R., Borchelt,D.R., Hirschhorn,R.R., and Ross,C.A. (2007). N-terminal proteolysis of full-length mutant huntingtin in an inducible PC12 cell model of Huntington's disease. Cell Cycle *6*, 2970-2981.

Ravikumar,B., Duden,R., and Rubinsztein,D.C. (2002). Aggregate-prone proteins with polyglutamine and polyalanine expansions are degraded by autophagy. Hum. Mol. Genet. *11*, 1107-1117.

Ravikumar,B. and Rubinsztein,D.C. (2006). Role of autophagy in the clearance of mutant huntingtin: a step towards therapy? Mol. Aspects Med. *27*, 520-527.

Reiner,A., Albin,R.L., Anderson,K.D., D'Amato,C.J., Penney,J.B., and Young,A.B. (1988). Differential loss of striatal projection neurons in Huntington disease. Proc. Natl. Acad. Sci. U. S. A *85*, 5733-5737.

Rhee,J., Inoue,Y., Yoon,J.C., Puigserver,P., Fan,M., Gonzalez,F.J., and Spiegelman,B.M. (2003). Regulation of hepatic fasting response by PPARgamma coactivator-1alpha (PGC-1): requirement for hepatocyte nuclear factor 4alpha in gluconeogenesis. Proc. Natl. Acad. Sci. U. S. A *100*, 4012-4017.

Ricci,J.E., Munoz-Pinedo,C., Fitzgerald,P., Bailly-Maitre,B., Perkins,G.A., Yadava,N., Scheffler,I.E., Ellisman,M.H., and Green,D.R. (2004). Disruption of mitochondrial function during apoptosis is mediated by caspase cleavage of the p75 subunit of complex I of the electron transport chain. Cell *117*, 773-786.

Richfield,E.K., Maguire-Zeiss,K.A., Vonkeman,H.E., and Voorn,P. (1995). Preferential loss of preproenkephalin versus preprotachykinin neurons from the striatum of Huntington's disease patients. Ann. Neurol. *38*, 852-861.

Richter,C., Park,J.W., and Ames,B.N. (1988). Normal oxidative damage to mitochondrial and nuclear DNA is extensive. Proc. Natl. Acad. Sci. U. S. A *85*, 6465-6467.

Riley,B.E. and Orr,H.T. (2006). Polyglutamine neurodegenerative diseases and regulation of transcription: assembling the puzzle. Genes Dev. *20*, 2183-2192.

Rizzardini,M., Lupi,M., Mangolini,A., Babetto,E., Ubezio,P., and Cantoni,L. (2006). Neurodegeneration induced by complex I inhibition in a cellular model of familial amyotrophic lateral sclerosis. Brain Res. Bull. *69*, 465-474.

Rizzu,P., Hinkle,D.A., Zhukareva,V., Bonifati,V., Severijnen,L.A., Martinez,D., Ravid,R., Kamphorst,W., Eberwine,J.H., Lee,V.M., Trojanowski,J.Q., and Heutink,P. (2004). DJ-1 colocalizes with tau inclusions: a link between parkinsonism and dementia. Ann. Neurol. *55*, 113-118.

Ross,C.A. (2002). Polyglutamine pathogenesis: emergence of unifying mechanisms for Huntington's disease and related disorders. Neuron *35*, 819-822.

Ross,C.A. and Poirier,M.A. (2004). Protein aggregation and neurodegenerative disease. Nat. Med. *10 Suppl*, S10-S17.

Ross,C.A. and Poirier,M.A. (2005). Opinion: What is the role of protein aggregation in neurodegeneration? Nat. Rev. Mol. Cell Biol. *6*, 891-898.

Ross,C.A., Poirier,M.A., Wanker,E.E., and Amzel,M. (2003). Polyglutamine fibrillogenesis: the pathway unfolds. Proc. Natl. Acad. Sci. U. S. A *100*, 1-3.

Rousset,S., Alves-Guerra,M.C., Mozo,J., Miroux,B., Cassard-Doulcier,A.M., Bouillaud,F., and Ricquier,D. (2004). The biology of mitochondrial uncoupling proteins. Diabetes *53 Suppl 1*, S130-S135.

Rubinsztein,D.C. (2006). The roles of intracellular protein-degradation pathways in neurodegeneration. Nature *443*, 780-786.

Ryu,J.K., Nagai,A., Kim,J., Lee,M.C., McLarnon,J.G., and Kim,S.U. (2003). Microglial activation and cell death induced by the mitochondrial toxin 3-nitropropionic acid: in vitro and in vivo studies. Neurobiol. Dis. *12*, 121-132.

Sagach,V.F., Scrosati,M., Fielding,J., Rossoni,G., Galli,C., and Visioli,F. (2002). The water-soluble vitamin E analogue Trolox protects against ischaemia/reperfusion damage in vitro and ex vivo. A comparison with vitamin E. Pharmacol. Res. *45*, 435-439.

Saito,Y., Hamakubo,T., Yoshida,Y., Ogawa,Y., Hara,Y., Fujimura,H., Imai,Y., Iwanari,H., Mochizuki,Y., Shichiri,M., Nishio,K., Kinumi,T., Noguchi,N., Kodama,T., and Niki,E. (2009). Preparation and application of monoclonal antibodies against oxidized DJ-1. Significant elevation of oxidized DJ-1 in erythrocytes of early-stage Parkinson disease patients. Neurosci. Lett. *465*, 1-5.

Saitoh,M., Nishitoh,H., Fujii,M., Takeda,K., Tobiume,K., Sawada,Y., Kawabata,M., Miyazono,K., and Ichijo,H. (1998). Mammalian thioredoxin is a direct inhibitor of apoptosis signal-regulating kinase (ASK) 1. EMBO J. *17*, 2596-2606.

Sajjad,M.U., Samson,B., and Wyttenbach,A. (2010). Heat shock proteins: therapeutic drug targets for chronic neurodegeneration? Curr. Pharm. Biotechnol. *11*, 198-215.

Sanchez Mejia,R.O. and Friedlander,R.M. (2001). Caspases in Huntington's disease. Neuroscientist. *7*, 480-489.

Santamaria,A., Perez-Severiano,F., Rodriguez-Martinez,E., Maldonado,P.D., Pedraza-Chaverri,J., Rios,C., and Segovia,J. (2001). Comparative analysis of superoxide dismutase activity between acute pharmacological models and a transgenic mouse model of Huntington's disease. Neurochem. Res. *26*, 419-424.

Santamaria,G., Martinez-Diez,M., Fabregat,I., and Cuezva,J.M. (2006). Efficient execution of cell death in non-glycolytic cells requires the generation of ROS controlled by the activity of mitochondrial H+-ATP synthase. Carcinogenesis *27*, 925-935.

Sapp,E., Schwarz,C., Chase,K., Bhide,P.G., Young,A.B., Penney,J., Vonsattel,J.P., Aronin,N., and DiFiglia,M. (1997). Huntingtin localization in brains of normal and Huntington's disease patients. Ann. Neurol. *42*, 604-612.

Sarkar,S., Ravikumar,B., Floto,R.A., and Rubinsztein,D.C. (2009). Rapamycin and mTOR-independent autophagy inducers ameliorate toxicity of polyglutamine-expanded huntingtin and related proteinopathies. Cell Death. Differ. *16*, 46-56.

Saudou,F., Finkbeiner,S., Devys,D., and Greenberg,M.E. (1998). Huntingtin acts in the nucleus to induce apoptosis but death does not correlate with the formation of intranuclear inclusions. Cell *95*, 55-66.

Sawa,A., Nagata,E., Sutcliffe,S., Dulloor,P., Cascio,M.B., Ozeki,Y., Roy,S., Ross,C.A., and Snyder,S.H. (2005). Huntingtin is cleaved by caspases in the cytoplasm and translocated to the nucleus via perinuclear sites in Huntington's disease patient lymphoblasts. Neurobiol. Dis. *20*, 267-274.

Schapira,A.H., Cooper,J.M., Dexter,D., Jenner,P., Clark,J.B., and Marsden,C.D. (1989). Mitochondrial complex I deficiency in Parkinson's disease. Lancet *1*, 1269.

Scherzinger,E., Lurz,R., Turmaine,M., Mangiarini,L., Hollenbach,B., Hasenbank,R., Bates,G.P., Davies,S.W., Lehrach,H., and Wanker,E.E. (1997). Huntingtin-encoded polyglutamine expansions form amyloid-like protein aggregates in vitro and in vivo. Cell *90*, 549-558.

Scheuner,D., Eckman,C., Jensen,M., Song,X., Citron,M., Suzuki,N., Bird,T.D., Hardy,J., Hutton,M., Kukull,W., Larson,E., Levy-Lahad,E., Viitanen,M., Peskind,E., Poorkaj,P., Schellenberg,G., Tanzi,R., Wasco,W., Lannfelt,L., Selkoe,D., and Younkin,S. (1996). Secreted amyloid beta-protein similar to that in the senile plaques of Alzheimer's disease is increased in vivo by the presenilin 1 and 2 and APP mutations linked to familial Alzheimer's disease. Nat. Med. *2*, 864-870.

Schilling,G., Coonfield,M.L., Ross,C.A., and Borchelt,D.R. (2001). Coenzyme Q10 and remacemide hydrochloride ameliorate motor deficits in a Huntington's disease transgenic mouse model. Neurosci. Lett. *315*, 149-153.

Schilling,G., Klevytska,A., Tebbenkamp,A.T., Juenemann,K., Cooper,J., Gonzales,V., Slunt,H., Poirer,M., Ross,C.A., and Borchelt,D.R. (2007). Characterization of huntingtin pathologic fragments in human Huntington disease, transgenic mice, and cell models. J. Neuropathol. Exp. Neurol. *66*, 313-320.

Schwarcz,R., Whetsell,W.O., Jr., and Mangano,R.M. (1983). Quinolinic acid: an endogenous metabolite that produces axon-sparing lesions in rat brain. Science *219*, 316-318.

Sekito,A., Koide-Yoshida,S., Niki,T., Taira,T., Iguchi-Ariga,S.M., and Ariga,H. (2006). DJ-1 interacts with HIPK1 and affects H2O2-induced cell death. Free Radic. Res. *40*, 155-165.

Seo,H., Kim,W., and Isacson,O. (2008). Compensatory changes in the ubiquitin-proteasome system, brain-derived neurotrophic factor and mitochondrial complex II/III in YAC72 and R6/2 transgenic mice partially model Huntington's disease patients. Hum. Mol. Genet. *17*, 3144-3153.

Seo,H., Sonntag,K.C., and Isacson,O. (2004). Generalized brain and skin proteasome inhibition in Huntington's disease. Ann. Neurol. *56*, 319-328.

Shendelman,S., Jonason,A., Martinat,C., Leete,T., and Abeliovich,A. (2004). DJ-1 is a redox-dependent molecular chaperone that inhibits alpha-synuclein aggregate formation. PLoS. Biol. *2*, e362.

Sheu,S.S., Nauduri,D., and Anders,M.W. (2006). Targeting antioxidants to mitochondria: a new therapeutic direction. Biochim. Biophys. Acta *1762*, 256-265.

Shibata,N., Nagai,R., Uchida,K., Horiuchi,S., Yamada,S., Hirano,A., Kawaguchi,M., Yamamoto,T., Sasaki,S., and Kobayashi,M. (2001). Morphological evidence for lipid peroxidation and protein glycoxidation in spinal cords from sporadic amyotrophic lateral sclerosis patients. Brain Res. *917*, 97-104.

Shimohata,T., Nakajima,T., Yamada,M., Uchida,C., Onodera,O., Naruse,S., Kimura,T., Koide,R., Nozaki,K., Sano,Y., Ishiguro,H., Sakoe,K., Ooshima,T., Sato,A., Ikeuchi,T., Oyake,M., Sato,T., Aoyagi,Y., Hozumi,I., Nagatsu,T., Takiyama,Y., Nishizawa,M., Goto,J., Kanazawa,I., Davidson,I., Tanese,N., Takahashi,H., and Tsuji,S. (2000). Expanded polyglutamine stretches interact with TAFII130, interfering with CREB-dependent transcription. Nat. Genet. *26*, 29-36.

Shimojo,M. (2008). Huntingtin regulates RE1-silencing transcription factor/neuron-restrictive silencer factor (REST/NRSF) nuclear trafficking indirectly through a complex with REST/NRSF-interacting LIM domain protein (RILP) and dynactin p150 Glued. J. Biol. Chem. *283*, 34880-34886.

Sigaud,S., Evelson,P., and Gonzalez-Flecha,B. (2005). H2O2-induced proliferation of primary alveolar epithelial cells is mediated by MAP kinases. Antioxid. Redox. Signal. *7*, 6-13.

Simonsen,A., Cumming,R.C., Brech,A., Isakson,P., Schubert,D.R., and Finley,K.D. (2008). Promoting basal levels of autophagy in the nervous system enhances longevity and oxidant resistance in adult Drosophila. Autophagy. *4*, 176-184.

Sinadinos,C., Burbidge-King,T., Soh,D., Thompson,L.M., Marsh,J.L., Wyttenbach,A., and Mudher,A.K. (2009). Live axonal transport disruption by mutant huntingtin fragments in Drosophila motor neuron axons. Neurobiol. Dis. *34*, 389-395.

Smith,K.M., Matson,S., Matson,W.R., Cormier,K., Del Signore,S.J., Hagerty,S.W., Stack,E.C., Ryu,H., and Ferrante,R.J. (2006). Dose ranging and efficacy study of high-dose coenzyme Q10 formulations in Huntington's disease mice. Biochim. Biophys. Acta *1762*, 616-626.

Smith,M.A., Hirai,K., Hsiao,K., Pappolla,M.A., Harris,P.L., Siedlak,S.L., Tabaton,M., and Perry,G. (1998). Amyloid-beta deposition in Alzheimer transgenic mice is associated with oxidative stress. J. Neurochem. *70*, 2212-2215.

Smith,R., Bacos,K., Fedele,V., Soulet,D., Walz,H.A., Obermuller,S., Lindqvist,A., Bjorkqvist,M., Klein,P., Onnerfjord,P., Brundin,P., Mulder,H., and Li,J.Y. (2009). Mutant huntingtin interacts with {beta}-tubulin and disrupts vesicular transport and insulin secretion. Hum. Mol. Genet. *18*, 3942-3954.

Smith,R., Brundin,P., and Li,J.Y. (2005). Synaptic dysfunction in Huntington's disease: a new perspective. Cell Mol. Life Sci. *62*, 1901-1912.

Soo,E.T., Ng,Y.K., Bay,B.H., and Yip,G.W. (2008). Heat shock proteins and neurodegenerative disorders. ScientificWorldJournal. *8*, 270-274.

Sorbi,S., Bird,E.D., and Blass,J.P. (1983). Decreased pyruvate dehydrogenase complex activity in Huntington and Alzheimer brain. Ann. Neurol. *13*, 72-78.

Soto,C. and Castilla,J. (2004). The controversial protein-only hypothesis of prion propagation. Nat. Med. *10 Suppl*, S63-S67.

Spitkovsky,D., Sasse,P., Kolossov,E., Bottinger,C., Fleischmann,B.K., Hescheler,J., and Wiesner,R.J. (2004). Activity of complex III of the mitochondrial electron transport chain is essential for early heart muscle cell differentiation. FASEB J. *18*, 1300-1302.

Squitieri,F., Frati,L., Ciarmiello,A., Lastoria,S., and Quarrell,O. (2006). Juvenile Huntington's disease: does a dosage-effect pathogenic mechanism differ from the classical adult disease? Mech. Ageing Dev. *127*, 208-212.

St-Pierre,J., Drori,S., Uldry,M., Silvaggi,J.M., Rhee,J., Jager,S., Handschin,C., Zheng,K., Lin,J., Yang,W., Simon,D.K., Bachoo,R., and Spiegelman,B.M. (2006). Suppression of reactive oxygen species and neurodegeneration by the PGC-1 transcriptional coactivators. Cell *127*, 397-408.

Stack,E.C., Smith,K.M., Ryu,H., Cormier,K., Chen,M., Hagerty,S.W., Del Signore,S.J., Cudkowicz,M.E., Friedlander,R.M., and Ferrante,R.J. (2006). Combination therapy using minocycline and coenzyme Q10 in R6/2 transgenic Huntington's disease mice. Biochim. Biophys. Acta *1762*, 373-380.

Stadtman,E.R. (1990). Metal ion-catalyzed oxidation of proteins: biochemical mechanism and biological consequences. Free Radic. Biol. Med. *9*, 315-325.

Starikov,E.B., Lehrach,H., and Wanker,E.E. (1999). Folding of oligoglutamines: a theoretical approach based upon thermodynamics and molecular mechanics. J. Biomol. Struct. Dyn. *17*, 409-427.

Starkov,A.A., Fiskum,G., Chinopoulos,C., Lorenzo,B.J., Browne,S.E., Patel,M.S., and Beal,M.F. (2004). Mitochondrial alpha-ketoglutarate dehydrogenase complex generates reactive oxygen species. J. Neurosci. *24*, 7779-7788.

Steffan,J.S., Bodai,L., Pallos,J., Poelman,M., McCampbell,A., Apostol,B.L., Kazantsev,A., Schmidt,E., Zhu,Y.Z., Greenwald,M., Kurokawa,R., Housman,D.E., Jackson,G.R., Marsh,J.L., and Thompson,L.M. (2001). Histone deacetylase inhibitors arrest polyglutamine-dependent neurodegeneration in Drosophila. Nature *413*, 739-743.

Steffan,J.S., Kazantsev,A., Spasic-Boskovic,O., Greenwald,M., Zhu,Y.Z., Gohler,H., Wanker,E.E., Bates,G.P., Housman,D.E., and Thompson,L.M. (2000). The Huntington's disease protein interacts with p53 and CREB-binding protein and represses transcription. Proc. Natl. Acad. Sci. U. S. A *97*, 6763-6768.

Sugars,K.L. and Rubinsztein,D.C. (2003). Transcriptional abnormalities in Huntington disease. Trends Genet. *19*, 233-238.

Swerdlow,R.H., Parks,J.K., Miller,S.W., Tuttle,J.B., Trimmer,P.A., Sheehan,J.P., Bennett,J.P., Jr., Davis,R.E., and Parker,W.D., Jr. (1996). Origin and functional consequences of the complex I defect in Parkinson's disease. Ann. Neurol. *40*, 663-671.

Tabner,B.J., El-Agnaf,O.M., Turnbull,S., German,M.J., Paleologou,K.E., Hayashi,Y., Cooper,L.J., Fullwood,N.J., and Allsop,D. (2005). Hydrogen peroxide is generated during the very early stages of aggregation of the amyloid peptides implicated in Alzheimer disease and familial British dementia. J. Biol. Chem. *280*, 35789-35792.

Tabrizi,S.J., Cleeter,M.W., Xuereb,J., Taanman,J.W., Cooper,J.M., and Schapira,A.H. (1999). Biochemical abnormalities and excitotoxicity in Huntington's disease brain. Ann. Neurol. *45*, 25-32.

Tabrizi,S.J., Workman,J., Hart,P.E., Mangiarini,L., Mahal,A., Bates,G., Cooper,J.M., and Schapira,A.H. (2000). Mitochondrial dysfunction and free radical damage in the Huntington R6/2 transgenic mouse. Ann. Neurol. *47*, 80-86.

Tagawa,K., Marubuchi,S., Qi,M.L., Enokido,Y., Tamura,T., Inagaki,R., Murata,M., Kanazawa,I., Wanker,E.E., and Okazawa,H. (2007). The induction levels of heat shock protein 70 differentiate the vulnerabilities to mutant huntingtin among neuronal subtypes. J. Neurosci. *27*, 868-880.

Taherzadeh-Fard,E., Saft,C., Andrich,J., Wieczorek,S., and Arning,L. (2009). PGC-1alpha as modifier of onset age in Huntington disease. Mol. Neurodegener. *4*, 10.

Taira,T., Saito,Y., Niki,T., Iguchi-Ariga,S.M., Takahashi,K., and Ariga,H. (2004). DJ-1 has a role in antioxidative stress to prevent cell death. EMBO Rep. *5*, 213-218.

Takahashi,K., Taira,T., Niki,T., Seino,C., Iguchi-Ariga,S.M., and Ariga,H. (2001). DJ-1 positively regulates the androgen receptor by impairing the binding of PIASx alpha to the receptor. J. Biol. Chem. *276*, 37556-37563.

Takahashi-Niki,K., Niki,T., Taira,T., Iguchi-Ariga,S.M., and Ariga,H. (2004). Reduced anti-oxidative stress activities of DJ-1 mutants found in Parkinson's disease patients. Biochem. Biophys. Res. Commun. *320*, 389-397.

Tam,S., Spiess,C., Auyeung,W., Joachimiak,L., Chen,B., Poirier,M.A., and Frydman,J. (2009). The chaperonin TRiC blocks a huntingtin sequence element that promotes the conformational switch to aggregation. Nat. Struct. Mol. Biol. *16*, 1279-1285.

Tang,T.S., Tu,H., Chan,E.Y., Maximov,A., Wang,Z., Wellington,C.L., Hayden,M.R., and Bezprozvanny,I. (2003). Huntingtin and huntingtin-associated protein 1 influence neuronal calcium signaling mediated by inositol-(1,4,5) triphosphate receptor type 1. Neuron *39*, 227-239.

Tao,X. and Tong,L. (2003). Crystal structure of human DJ-1, a protein associated with early onset Parkinson's disease. J. Biol. Chem. *278*, 31372-31379.

Tarlac,V. and Storey,E. (2003). Role of proteolysis in polyglutamine disorders. J. Neurosci. Res. *74*, 406-416.

Thannickal,V.J. and Fanburg,B.L. (2000). Reactive oxygen species in cell signaling. Am. J. Physiol Lung Cell Mol. Physiol *279*, L1005-L1028.

The Huntington's Disease Collaborative Research Group (1993). A novel gene containing a trinucleotide repeat that is expanded and unstable on Huntington's disease chromosomes. The Huntington's Disease Collaborative Research Group. Cell *72*, 971-983.

Thompson,L.M., Aiken,C.T., Kaltenbach,L.S., Agrawal,N., Illes,K., Khoshnan,A., Martinez-Vincente,M., Arrasate,M., O'Rourke,J.G., Khashwji,H., Lukacsovich,T., Zhu,Y.Z., Lau,A.L., Massey,A., Hayden,M.R., Zeitlin,S.O., Finkbeiner,S., Green,K.N., Laferla,F.M., Bates,G., Huang,L., Patterson,P.H., Lo,D.C., Cuervo,A.M., Marsh,J.L., and Steffan,J.S. (2009). IKK phosphorylates Huntingtin and targets it for degradation by the proteasome and lysosome. J. Cell Biol. *187*, 1083-1099.

Trejo,A., Tarrats,R.M., Alonso,M.E., Boll,M.C., Ochoa,A., and Velasquez,L. (2004). Assessment of the nutrition status of patients with Huntington's disease. Nutrition *20*, 192-196.

Trettel,F., Rigamonti,D., Hilditch-Maguire,P., Wheeler,V.C., Sharp,A.H., Persichetti,F., Cattaneo,E., and MacDonald,M.E. (2000). Dominant phenotypes produced by the HD mutation in STHdh(Q111) striatal cells. Hum. Mol. Genet. *9*, 2799-2809.

Trottier,Y., Lutz,Y., Stevanin,G., Imbert,G., Devys,D., Cancel,G., Saudou,F., Weber,C., David,G., Tora,L., and . (1995). Polyglutamine expansion as a pathological epitope in Huntington's disease and four dominant cerebellar ataxias. Nature *378*, 403-406.

Truant,R., Raymond,L.A., Xia,J., Pinchev,D., Burtnik,A., and Atwal,R.S. (2006). Canadian Association of Neurosciences Review: polyglutamine expansion neurodegenerative diseases. Can. J. Neurol. Sci. *33*, 278-291.

Trushina,E., Dyer,R.B., Badger,J.D., Ure,D., Eide,L., Tran,D.D., Vrieze,B.T., Legendre-Guillemin,V., McPherson,P.S., Mandavilli,B.S., Van,H.B., Zeitlin,S., McNiven,M., Aebersold,R., Hayden,M., Parisi,J.E., Seeberg,E., Dragatsis,I., Doyle,K., Bender,A., Chacko,C., and McMurray,C.T. (2004). Mutant huntingtin impairs axonal trafficking in mammalian neurons in vivo and in vitro. Mol. Cell Biol. *24*, 8195-8209.

Trushina,E. and McMurray,C.T. (2007). Oxidative stress and mitochondrial dysfunction in neurodegenerative diseases. Neuroscience *145*, 1233-1248.

Trushina,E., Singh,R.D., Dyer,R.B., Cao,S., Shah,V.H., Parton,R.G., Pagano,R.E., and McMurray,C.T. (2006). Mutant huntingtin inhibits clathrin-independent endocytosis and causes accumulation of cholesterol in vitro and in vivo. Hum. Mol. Genet. *15*, 3578-3591.

Tsai,B., Rodighiero,C., Lencer,W.I., and Rapoport,T.A. (2001). Protein disulfide isomerase acts as a redox-dependent chaperone to unfold cholera toxin. Cell *104*, 937-948.

Tunez,I., Drucker-Colin,R., Jimena,I., Medina,F.J., Munoz,M.C., Pena,J., and Montilla,P. (2006). Transcranial magnetic stimulation attenuates cell loss and oxidative damage in the striatum induced in the 3-nitropropionic model of Huntington's disease. J. Neurochem. *97*, 619-630.

Turnbull,S., Tabner,B.J., Brown,D.R., and Allsop,D. (2003). Copper-dependent generation of hydrogen peroxide from the toxic prion protein fragment PrP106-126. Neurosci. Lett. *336*, 159-162.

Underwood,B.R., Imarisio,S., Fleming,A., Rose,C., Krishna,G., Heard,P., Quick,M., Korolchuk,V.I., Renna,M., Sarkar,S., Garcia-Arencibia,M., O'Kane,C.J., Murphy,M.P., and Rubinsztein,D.C. (2010). Antioxidants can inhibit basal autophagy and enhance neurodegeneration in models of polyglutamine disease. Hum. Mol. Genet. *19*, 3413-3429.

Valencia,A. and Moran,J. (2004). Reactive oxygen species induce different cell death mechanisms in cultured neurons. Free Radic. Biol. Med. *36*, 1112-1125.

van Duijn,C.M., Dekker,M.C., Bonifati,V., Galjaard,R.J., Houwing-Duistermaat,J.J., Snijders,P.J., Testers,L., Breedveld,G.J., Horstink,M., Sandkuijl,L.A., van Swieten,J.C., Oostra,B.A., and Heutink,P. (2001). Park7, a novel locus for autosomal recessive early-onset parkinsonism, on chromosome 1p36. Am. J. Hum. Genet. *69*, 629-634.

van Roon-Mom,W.M., Pepers,B.A., 't Hoen,P.A., Verwijmeren,C.A., den Dunnen,J.T., Dorsman,J.C., and van Ommen,G.B. (2008). Mutant huntingtin activates Nrf2-responsive genes and impairs dopamine synthesis in a PC12 model of Huntington's disease. BMC. Mol. Biol. *9*, 84.

van Roon-Mom,W.M., Reid,S.J., Jones,A.L., MacDonald,M.E., Faull,R.L., and Snell,R.G. (2002). Insoluble TATA-binding protein accumulation in Huntington's disease cortex. Brain Res. Mol. Brain Res. *109*, 1-10.

Vargas,M.R. and Johnson,J.A. (2009). The Nrf2-ARE cytoprotective pathway in astrocytes. Expert. Rev. Mol. Med. *11*, e17.

Varshney,A. and Ehrlich,B.E. (2003). Intracellular Ca2+ signaling and human disease: the hunt begins with Huntington's. Neuron *39*, 195-197.

Venkatraman,P., Wetzel,R., Tanaka,M., Nukina,N., and Goldberg,A.L. (2004). Eukaryotic proteasomes cannot digest polyglutamine sequences and release them during degradation of polyglutamine-containing proteins. Mol. Cell *14*, 95-104.

Verheij,M., Bose,R., Lin,X.H., Yao,B., Jarvis,W.D., Grant,S., Birrer,M.J., Szabo,E., Zon,L.I., Kyriakis,J.M., Haimovitz-Friedman,A., Fuks,Z., and Kolesnick,R.N. (1996). Requirement for ceramide-initiated SAPK/JNK signalling in stress-induced apoptosis. Nature *380*, 75-79.

Verhoef,L.G., Lindsten,K., Masucci,M.G., and Dantuma,N.P. (2002). Aggregate formation inhibits proteasomal degradation of polyglutamine proteins. Hum. Mol. Genet. *11*, 2689-2700.

von,H.S., Schmitt,I., Nguyen,H.P., Holzmann,C., Schmidt,T., Walther,T., Bader,M., Pabst,R., Kobbe,P., Krotova,J., Stiller,D., Kask,A., Vaarmann,A., Rathke-Hartlieb,S., Schulz,J.B., Grasshoff,U., Bauer,I., Vieira-Saecker,A.M., Paul,M., Jones,L., Lindenberg,K.S., Landwehrmeyer,B., Bauer,A., Li,X.J., and Riess,O. (2003). Transgenic rat model of Huntington's disease. Hum. Mol. Genet. *12*, 617-624.

Wacker,J.L., Zareie,M.H., Fong,H., Sarikaya,M., and Muchowski,P.J. (2004). Hsp70 and Hsp40 attenuate formation of spherical and annular polyglutamine oligomers by partitioning monomer. Nat. Struct. Mol. Biol. *11*, 1215-1222.

Walling,A.D. (1999). Amyotrophic lateral sclerosis: Lou Gehrig's disease. Am. Fam. Physician *59*, 1489-1496.

Wang,C.W. and Klionsky,D.J. (2003). The molecular mechanism of autophagy. Mol. Med. *9*, 65-76.

Wang,G.H., Mitsui,K., Kotliarova,S., Yamashita,A., Nagao,Y., Tokuhiro,S., Iwatsubo,T., Kanazawa,I., and Nukina,N. (1999). Caspase activation during apoptotic cell death induced by expanded polyglutamine in N2a cells. Neuroreport *10*, 2435-2438.

Wang,H., Lim,P.J., Karbowski,M., and Monteiro,M.J. (2009). Effects of overexpression of huntingtin proteins on mitochondrial integrity. Hum. Mol. Genet. *18*, 737-752.

Wang,J., Wang,C.E., Orr,A., Tydlacka,S., Li,S.H., and Li,X.J. (2008). Impaired ubiquitin-proteasome system activity in the synapses of Huntington's disease mice. J. Cell Biol. *180*, 1177-1189.

Wang,J., Xiong,S., Xie,C., Markesbery,W.R., and Lovell,M.A. (2005). Increased oxidative damage in nuclear and mitochondrial DNA in Alzheimer's disease. J. Neurochem. *93*, 953-962.

Wanker,E.E., Rovira,C., Scherzinger,E., Hasenbank,R., Walter,S., Tait,D., Colicelli,J., and Lehrach,H. (1997). HIP-I: a huntingtin interacting protein isolated by the yeast two-hybrid system. Hum. Mol. Genet. *6*, 487-495.

Waragai,M., Nakai,M., Wei,J., Fujita,M., Mizuno,H., Ho,G., Masliah,E., Akatsu,H., Yokochi,F., and Hashimoto,M. (2007). Plasma levels of DJ-1 as a possible marker for progression of sporadic Parkinson's disease. Neurosci. Lett. *425*, 18-22.

Waragai,M., Wei,J., Fujita,M., Nakai,M., Ho,G.J., Masliah,E., Akatsu,H., Yamada,T., and Hashimoto,M. (2006). Increased level of DJ-1 in the cerebrospinal fluids of sporadic Parkinson's disease. Biochem. Biophys. Res. Commun. *345*, 967-972.

Wardman,P. and Candeias,L.P. (1996). Fenton chemistry: an introduction. Radiat. Res. *145*, 523-531.

Warita,H., Hayashi,T., Murakami,T., Manabe,Y., and Abe,K. (2001). Oxidative damage to mitochondrial DNA in spinal motoneurons of transgenic ALS mice. Brain Res. Mol. Brain Res. *89*, 147-152.

Warner,B.B., Stuart,L., Gebb,S., and Wispe,J.R. (1996). Redox regulation of manganese superoxide dismutase. Am. J. Physiol *271*, L150-L158.

Weiss,A., Roscic,A., and Paganetti,P. (2009). Inducible mutant huntingtin expression in HN10 cells reproduces Huntington's disease-like neuronal dysfunction. Mol. Neurodegener. *4*, 11.

Wellington,C.L., Ellerby,L.M., Gutekunst,C.A., Rogers,D., Warby,S., Graham,R.K., Loubser,O., van,R.J., Singaraja,R., Yang,Y.Z., Gafni,J., Bredesen,D., Hersch,S.M., Leavitt,B.R., Roy,S., Nicholson,D.W., and Hayden,M.R. (2002). Caspase cleavage of mutant huntingtin precedes neurodegeneration in Huntington's disease. J. Neurosci. *22*, 7862-7872.

Wellington,C.L., Ellerby,L.M., Hackam,A.S., Margolis,R.L., Trifiro,M.A., Singaraja,R., McCutcheon,K., Salvesen,G.S., Propp,S.S., Bromm,M., Rowland,K.J.,

Zhang,T., Rasper,D., Roy,S., Thornberry,N., Pinsky,L., Kakizuka,A., Ross,C.A., Nicholson,D.W., Bredesen,D.E., and Hayden,M.R. (1998). Caspase cleavage of gene products associated with triplet expansion disorders generates truncated fragments containing the polyglutamine tract. J. Biol. Chem. *273*, 9158-9167.

Wellington,C.L., Leavitt,B.R., and Hayden,M.R. (2000). Huntington disease: new insights on the role of huntingtin cleavage. J. Neural Transm. Suppl 1-17.

Wexler,N.S., Lorimer,J., Porter,J., Gomez,F., Moskowitz,C., Shackell,E., Marder,K., Penchaszadeh,G., Roberts,S.A., Gayan,J., Brocklebank,D., Cherny,S.S., Cardon,L.R., Gray,J., Dlouhy,S.R., Wiktorski,S., Hodes,M.E., Conneally,P.M., Penney,J.B., Gusella,J., Cha,J.H., Irizarry,M., Rosas,D., Hersch,S., Hollingsworth,Z., MacDonald,M., Young,A.B., Andresen,J.M., Housman,D.E., De Young,M.M., Bonilla,E., Stillings,T., Negrette,A., Snodgrass,S.R., Martinez-Jaurrieta,M.D., Ramos-Arroyo,M.A., Bickham,J., Ramos,J.S., Marshall,F., Shoulson,I., Rey,G.J., Feigin,A., Arnheim,N., cevedo-Cruz,A., Acosta,L., Alvir,J., Fischbeck,K., Thompson,L.M., Young,A., Dure,L., O'Brien,C.J., Paulsen,J., Brickman,A., Krch,D., Peery,S., Hogarth,P., Higgins,D.S., Jr., and Landwehrmeyer,B. (2004). Venezuelan kindreds reveal that genetic and environmental factors modulate Huntington's disease age of onset. Proc. Natl. Acad. Sci. U. S. A *101*, 3498-3503.

Weydt,P., Pineda,V.V., Torrence,A.E., Libby,R.T., Satterfield,T.F., Lazarowski,E.R., Gilbert,M.L., Morton,G.J., Bammler,T.K., Strand,A.D., Cui,L., Beyer,R.P., Easley,C.N., Smith,A.C., Krainc,D., Luquet,S., Sweet,I.R., Schwartz,M.W., and La Spada,A.R. (2006). Thermoregulatory and metabolic defects in Huntington's disease transgenic mice implicate PGC-1alpha in Huntington's disease neurodegeneration. Cell Metab *4*, 349-362.

Wiedemann,F.R., Manfredi,G., Mawrin,C., Beal,M.F., and Schon,E.A. (2002). Mitochondrial DNA and respiratory chain function in spinal cords of ALS patients. J. Neurochem. *80*, 616-625.

Wilhelm,J., Vytasek,R., Ostadalova,I., and Vajner,L. (2009). Evaluation of different methods detecting intracellular generation of free radicals. Mol. Cell Biochem. *328*, 167-176.

Wilmer,W.A., Tan,L.C., Dickerson,J.A., Danne,M., and Rovin,B.H. (1997). Interleukin-1beta induction of mitogen-activated protein kinases in human mesangial cells. Role of oxidation. J. Biol. Chem. *272*, 10877-10881.

Wilson,J.X. (1997). Antioxidant defense of the brain: a role for astrocytes. Can. J. Physiol Pharmacol. *75*, 1149-1163.

Wilson,M.A., Collins,J.L., Hod,Y., Ringe,D., and Petsko,G.A. (2003). The 1.1-A resolution crystal structure of DJ-1, the protein mutated in autosomal recessive early onset Parkinson's disease. Proc. Natl. Acad. Sci. U. S. A *100*, 9256-9261.

Witt,A.C., Lakshminarasimhan,M., Remington,B.C., Hasim,S., Pozharski,E., and Wilson,M.A. (2008). Cysteine pKa depression by a protonated glutamic acid in human DJ-1. Biochemistry *47*, 7430-7440.

Wong,C.M., Cheema,A.K., Zhang,L., and Suzuki,Y.J. (2008). Protein carbonylation as a novel mechanism in redox signaling. Circ. Res. *102*, 310-318.

Wu,D.C., Teismann,P., Tieu,K., Vila,M., Jackson-Lewis,V., Ischiropoulos,H., and Przedborski,S. (2003). NADPH oxidase mediates oxidative stress in the 1-methyl-4-phenyl-1,2,3,6-tetrahydropyridine model of Parkinson's disease. Proc. Natl. Acad. Sci. U. S. A *100*, 6145-6150.

Wu,M., Neilson,A., Swift,A.L., Moran,R., Tamagnine,J., Parslow,D., Armistead,S., Lemire,K., Orrell,J., Teich,J., Chomicz,S., and Ferrick,D.A. (2007). Multiparameter metabolic analysis reveals a close link between attenuated mitochondrial bioenergetic function and enhanced glycolysis dependency in human tumor cells. Am. J. Physiol Cell Physiol *292*, C125-C136.

Wyttenbach,A. (2004). Role of heat shock proteins during polyglutamine neurodegeneration: mechanisms and hypothesis. J. Mol. Neurosci. *23*, 69-96.

Wyttenbach,A., Carmichael,J., Swartz,J., Furlong,R.A., Narain,Y., Rankin,J., and Rubinsztein,D.C. (2000). Effects of heat shock, heat shock protein 40 (HDJ-2), and proteasome inhibition on protein aggregation in cellular models of Huntington's disease. Proc. Natl. Acad. Sci. U. S. A *97*, 2898-2903.

Wyttenbach,A., Hands,S., King,M.A., Lipkow,K., and Tolkovsky,A.M. (2008). Amelioration of protein misfolding disease by rapamycin: translation or autophagy? Autophagy. *4*, 542-545.

Wyttenbach,A., Sauvageot,O., Carmichael,J., az-Latoud,C., Arrigo,A.P., and Rubinsztein,D.C. (2002). Heat shock protein 27 prevents cellular polyglutamine toxicity and suppresses the increase of reactive oxygen species caused by huntingtin. Hum. Mol. Genet. *11*, 1137-1151.

Wyttenbach,A., Swartz,J., Kita,H., Thykjaer,T., Carmichael,J., Bradley,J., Brown,R., Maxwell,M., Schapira,A., Orntoft,T.F., Kato,K., and Rubinsztein,D.C. (2001). Polyglutamine expansions cause decreased CRE-mediated transcription and early gene expression changes prior to cell death in an inducible cell model of Huntington's disease. Hum. Mol. Genet. *10*, 1829-1845.

Xia,Z., Dickens,M., Raingeaud,J., Davis,R.J., and Greenberg,M.E. (1995). Opposing effects of ERK and JNK-p38 MAP kinases on apoptosis. Science *270*, 1326-1331.

Xu,J., Zhong,N., Wang,H., Elias,J.E., Kim,C.Y., Woldman,I., Pifl,C., Gygi,S.P., Geula,C., and Yankner,B.A. (2005). The Parkinson's disease-associated DJ-1 protein is a transcriptional co-activator that protects against neuronal apoptosis. Hum. Mol. Genet. *14*, 1231-1241.

Yamane,K., Kitamura,Y., Yanagida,T., Takata,K., Yanagisawa,D., Taniguchi,T., Taira,T., and Ariga,H. (2009). Oxidative neurodegeneration is prevented by UCP0045037, an allosteric modulator for the reduced form of DJ-1, a wild-type of familial Parkinson's disease-linked PARK7. Int. J. Mol. Sci. *10*, 4789-4804.

Yamashita,S., Mori,A., Kimura,E., Mita,S., Maeda,Y., Hirano,T., and Uchino,M. (2010). DJ-1 forms complexes with mutant SOD1 and ameliorates its toxicity. J. Neurochem. *113*, 860-870.

Yanagida,T., Tsushima,J., Kitamura,Y., Yanagisawa,D., Takata,K., Shibaike,T., Yamamoto,A., Taniguchi,T., Yasui,H., Taira,T., Morikawa,S., Inubushi,T., Tooyama,I., and Ariga,H. (2009). Oxidative stress induction of DJ-1 protein in reactive astrocytes scavenges free radicals and reduces cell injury. Oxid. Med. Cell Longev. *2*, 36-42.

Yang,L., Calingasan,N.Y., Wille,E.J., Cormier,K., Smith,K., Ferrante,R.J., and Beal,M.F. (2009). Combination therapy with coenzyme Q10 and creatine produces additive neuroprotective effects in models of Parkinson's and Huntington's diseases. J. Neurochem. *109*, 1427-1439.

Yang,W., Dunlap,J.R., Andrews,R.B., and Wetzel,R. (2002). Aggregated polyglutamine peptides delivered to nuclei are toxic to mammalian cells. Hum. Mol. Genet. *11*, 2905-2917.

Yao,D., Gu,Z., Nakamura,T., Shi,Z.Q., Ma,Y., Gaston,B., Palmer,L.A., Rockenstein,E.M., Zhang,Z., Masliah,E., Uehara,T., and Lipton,S.A. (2004). Nitrosative stress linked to sporadic Parkinson's disease: S-nitrosylation of parkin regulates its E3 ubiquitin ligase activity. Proc. Natl. Acad. Sci. U. S. A *101*, 10810-10814.

Yaung,J., Jin,M., Barron,E., Spee,C., Wawrousek,E.F., Kannan,R., and Hinton,D.R. (2007). alpha-Crystallin distribution in retinal pigment epithelium and effect of gene knockouts on sensitivity to oxidative stress. Mol. Vis. *13*, 566-577.

Yokota,T., Sugawara,K., Ito,K., Takahashi,R., Ariga,H., and Mizusawa,H. (2003). Down regulation of DJ-1 enhances cell death by oxidative stress, ER stress, and proteasome inhibition. Biochem. Biophys. Res. Commun. *312*, 1342-1348.

Yoon,J.C., Puigserver,P., Chen,G., Donovan,J., Wu,Z., Rhee,J., Adelmant,G., Stafford,J., Kahn,C.R., Granner,D.K., Newgard,C.B., and Spiegelman,B.M. (2001). Control of hepatic gluconeogenesis through the transcriptional coactivator PGC-1. Nature *413*, 131-138.

Young,A.B., Greenamyre,J.T., Hollingsworth,Z., Albin,R., D'Amato,C., Shoulson,I., and Penney,J.B. (1988). NMDA receptor losses in putamen from patients with Huntington's disease. Science *241*, 981-983.

Zhang,F., Strom,A.L., Fukada,K., Lee,S., Hayward,L.J., and Zhu,H. (2007). Interaction between familial ALS-linked SOD1 mutants and the dynein complex: Implications of retrograde axonal transport in ALS. J. Biol. Chem.

Zhang,J., Perry,G., Smith,M.A., Robertson,D., Olson,S.J., Graham,D.G., and Montine,T.J. (1999). Parkinson's disease is associated with oxidative damage to cytoplasmic DNA and RNA in substantia nigra neurons. Am. J. Pathol. *154*, 1423-1429.

Zhang,W., Chen,C., Dong,B., Lu,D., and Chen,D. (2002). [The role of taurine as hydroxyl radical inhibitor and its effect on lipid peroxidation in selenite cataract]. Zhonghua Yan. Ke. Za Zhi. *38*, 157-160.

Zhang,Y., Li,M., Drozda,M., Chen,M., Ren,S., Mejia Sanchez,R.O., Leavitt,B.R., Cattaneo,E., Ferrante,R.J., Hayden,M.R., and Friedlander,R.M. (2003). Depletion of wild-type huntingtin in mouse models of neurologic diseases. J. Neurochem. *87*, 101-106.

Zheng,M., Aslund,F., and Storz,G. (1998). Activation of the OxyR transcription factor by reversible disulfide bond formation. Science *279*, 1718-1721.

Zhou,W. and Freed,C.R. (2004). Tyrosine-to-cysteine modification of human alpha-synuclein enhances protein aggregation and cellular toxicity. J. Biol. Chem. *279*, 10128-10135.

Zhou,W. and Freed,C.R. (2005). DJ-1 up-regulates glutathione synthesis during oxidative stress and inhibits A53T alpha-synuclein toxicity. J. Biol. Chem. *280*, 43150-43158.

Zhou,W., Zhu,M., Wilson,M.A., Petsko,G.A., and Fink,A.L. (2006). The oxidation state of DJ-1 regulates its chaperone activity toward alpha-synuclein. J. Mol. Biol. *356*, 1036-1048.

Zuccato,C., Ciammola,A., Rigamonti,D., Leavitt,B.R., Goffredo,D., Conti,L., MacDonald,M.E., Friedlander,R.M., Silani,V., Hayden,M.R., Timmusk,T., Sipione,S., and Cattaneo,E. (2001). Loss of huntingtin-mediated BDNF gene transcription in Huntington's disease. Science *293*, 493-498.

Zuccato,C., Tartari,M., Crotti,A., Goffredo,D., Valenza,M., Conti,L., Cataudella,T., Leavitt,B.R., Hayden,M.R., Timmusk,T., Rigamonti,D., and Cattaneo,E. (2003). Huntingtin interacts with REST/NRSF to modulate the transcription of NRSE-controlled neuronal genes. Nat. Genet. *35*, 76-83.

}}